ISSUED
2008/04/23

911117
Revision 0

Engineering Services For The Next Generation Nuclear Plant (NGNP) With Hydrogen Production

NGNP Contamination Control Study

Prepared by General Atomics
For the Battelle Energy Alliance, LLC

Subcontract No. 00060845
Uniform Filing Code UFC:8201.3.1.2

GA Project 30283

GENERAL ATOMICS

Rolls-Royce

URS
Washington Division

TOSHIBA
Leading Innovation >>>

OKBM

Korea Atomic Energy Research Institute

GENERAL ATOMICS

GA 1485 (REV. 08/06E)

ISSUE/RELEASE SUMMARY

☐ R & D ☐ DV&S ☒ DESIGN ☐ T&E ☐ NA	APPVL LEVEL	DISC	QA LEVEL	SYS	DOC. TYPE	PROJECT	DOCUMENT NO.	REV
	5	N	I	N/A	RGE	30283	911117	0

TITLE:
NGNP Contamination Control Study

CM APPROVAL/ DATE	REV	PREPARED BY	APPROVAL(S) ENGINEERING	APPROVAL(S) QA	APPROVAL(S) PROJECT	REVISION DESCRIPTION/ W.O. NO.
7 ISSUED APR 23 2008	0	D. Hanson	A. Shenoy	K. Partain	J. Saurwein	Initial Issue A30283.0340

CONTINUE ON GA FORM 1485-1

NEXT INDENTURED DOCUMENT(S)

N/A

COMPUTER PROGRAM PIN(S)

N/A

☐ **GA PROPRIETARY INFORMATION**

THIS DOCUMENT IS THE PROPERTY OF GENERAL ATOMICS. ANY TRANSMITTAL OF THIS DOCUMENT OUTSIDE GA WILL BE IN CONFIDENCE. EXCEPT WITH THE WRITTEN CONSENT OF GA, (1) THIS DOCUMENT MAY NOT BE COPIED IN WHOLE OR IN PART AND WILL BE RETURNED UPON REQUEST OR WHEN NO LONGER NEEDED BY RECIPIENT AND (2) INFORMATION CONTAINED HEREIN MAY NOT BE COMMUNICATED TO OTHERS AND MAY BE USED BY RECIPIENT ONLY FOR THE PURPOSE FOR WHICH IT WAS TRANSMITTED.

☒ **NO GA PROPRIETARY INFORMATION**

LIST OF CONTRIBUTORS

Name	Organization
David Hanson	GA
Richard Luu	GA
Jong-Hwa Park	KAERI
Paul Reichert	URS-WD
Harold Rothstein	URS-WD

LIST OF EFFECTIVE PAGES

Page Number	Page Count	Revision
Cover page	1	0
ii through xiv	13	0
1 through 200	200	0
A-1 through A-37	37	0
B-1 through B-18	18	0
Back page	1	0
Total Pages	270	

TABLE OF CONTENTS

LIST OF FIGURES

LIST OF TABLES

ACRONYMS AND ABBREVIATIONS

ALARA	as low as reasonably achievable [radiation exposure][1]
AVR	Arbeitsgemeinschaft Versuchs Reactor [German pebble-bed HTR]
BET	Brunauer, Emmett and Teller [a standard analytical technique for measuring the internal surface area of a porous solid]
BISO	Bi-ISOtropic coated-fuel particle design with three materials in coating system (low-density PyC, high-density PyC)
BWXT	[The Babcock & Wilcox Company]
CFR	Code of Federal Regulations
D&D	decontamination and decommissioning
DBA	design basis accident
DDN	Design Data Need
DOE	[United States] Department of Energy
EAB	exclusion area boundary
EFPD	effective full-power days
EPA	Environmental Protection Agency
EPRI	Electric Power Research Institute
EOL	end-of-life
EPZ	emergency planning zone
FDDM/F	Fuel Design Data Manual, Issue F [GA Proprietary Information]
FES	Fuji Electric Systems
FFF	fuel fabrication facility
FIMA	fissions per initial metal atom
FOAK	first-of-a-kind
FRG	Federal Republic of Germany
FSV	Fort St. Vrain [US prismatic HTGR]
GA	General Atomics

[1] In this report, text in [square brackets] is explanatory; numbers in [square brackets] are tentative values that are likely to change as the design matures.

GT-MHR	Gas Turbine – Modular Helium Reactor
HLW	high-level waste
HEU	high enriched uranium [typically 93% U-235]
HHT	Hochtemperaturreaktor mit Helium Turbine [German direct-cycle HTR]
HM	heavy metal [contamination]
HPS	helium purification system
HTA	High Temperature Absorber
HTE	High temperature electrolysis
HTGR	High Temperature Gas-Cooled Reactor
HTR	High Temperature Reactor [pebble bed HTGR]
H2-MHR	Hydrogen [Production]-Modular Helium Reactor
HTTR	[Japanese] High Temperature Test Reactor
IAEA	International Atomic Energy Agency
IHX	intermediate heat exchanger
INL	Idaho National Laboratory
ITRG	Independent Technology Review Group
ISI	in-service inspection
JAEA	Japan Atomic Energy Agency [formerly JAERI]
KAERI	Korean Atomic Energy Research Institute
LBP	lumped burnable poison
LBE	Licensing Basis Event
LEU	low enriched uranium [<20% U-235]
LLW	low-level waste
LOCA	loss of coolant accident
LTA	Low Temperature Absorber
LWR	light water reactor
MHR	Modular Helium Reactor
MHTGR	[steam-cycle] Modular High Temperature Gas-cooled Reactor
NEA	Nuclear Energy Agency [OECD organization]

NERI	Nuclear Energy Research Initiative
NFI	Nuclear Fuel Industries
NGNP	Next Generation Nuclear Plant
NHI	National Hydrogen Initiative
NP-MHTGR	New Production-Modular Helium Reactor
NPR	New Production Reactor
NRC	[United States] Nuclear Regulatory Commission
O&M	operation and maintenance
ORNL	Oak Ridge National Laboratory
PAG	Protective Action Guide
PB	Peach Bottom
PBMR	Pebble Bed Modular Reactor [South Africa]
PC-MHR	Plutonium Consumption-Modular Helium Reactor
PCS	power-conversion system
PCDSR	pre-conceptual design studies report
PCHE	printed circuit heat exchanger
PCRV	prestressed concrete reactor vessel
PNP	Prototype Nuclear Process [Heat Project – FRG]
PPMP	[NGNP] Preliminary Project Management Plan
PSCo	Public Service Company [FSV plant owner/operator]
PWC	pressurized water cooler
PWR	pressurized water reactor
PyC	pyrolytic carbon
QA	quality assurance
SI	sulfur-iodine [process for thermo chemical water splitting]
R/B	release rate-to-birth rate ratio
RN	radionuclide
SG	steam generator
SRM	System Requirements Manual

STP	standard temperature and pressure [273 K, 1 atm]
TBD	to be determined
THOR	[treatment technology for sodium-bearing radioactive waste]
THTR	Thorium Hochtemperatur Reaktor [German pebble-bed HTR]
TRISO	TRI-material, ISOtropic with the materials being low-density PyC (buffer), high-density IPyC and OPyC, and SiC.
UCNI	Unclassified Controlled Nuclear Information
U/U	user/utility [requirements]
VHTR	Very High Temperature Reactor
VLPC	Vented Low-Pressure Containment

1. SUMMARY

The U.S Department of Energy (DOE) has chosen the Very High Temperature Reactor (VHTR) for the Next Generation Nuclear Plant (NGNP) Project. The reactor design will be a helium-cooled, graphite-moderated thermal reactor that will be designed to produce electricity and hydrogen as required by the Energy Policy Act of 2005. DOE has contracted with three industrial teams, including a team led by General Atomics (GA), for conceptual design studies in support of NGNP design and licensing. As part of the contractual work scope, GA has performed a contamination control study to establish provisional limits on radionuclide (RN) contamination throughout the NGNP with particular emphasis on tritium.

The NGNP is still in the pre-conceptual design phase with major design selections (e.g., reactor core type, core outlet temperature, etc.) yet to be made. Consequently, the “provisional limits" recommended herein will likely require optimization once there is a conceptual plant design and an assessment has been made of whether or not all top-level radionuclide control requirements (e.g., off-site doses) are met with source terms based upon these provisional limits.

The programmatic benefits of performing the subject contamination control study during pre-conceptual design are threefold: (1) Design Data Needs (DDNs) can be identified and the on-going, generic NGNP technology development programs can be modified or supplemented as required; (2) inadequacies in the current analytical tools to support preliminary and final NGNP design can be identified such that these deficiencies can be remedied during the conceptual design phase; and (3) significant design issues that need to be addressed during conceptual and preliminary design can be identified early.

The above programmatic benefits of the current study were clearly demonstrated with regard to tritium contamination of the product hydrogen in the NGNP hydrogen production plant. The DDNs with regard to H-3 transport, especially the need for better characterization of H-3 sorption on irradiated core graphites, were confirmed. The substantial inadequacies of the current tritium mass balance code TRITGO and the need for a replacement code to support NGNP design and licensing were clearly demonstrated. The expectation that tritium contamination of the product hydrogen in the NGNP will be a significant design issue for the NGNP was confirmed, and design options for resolving the issue were identified.

1.1 Radionuclide Source Terms and Limits

Stringent, top-level radionuclide control requirements are anticipated for the NGNP (e.g., meet EPA Protective Action Guides (PAGs) at a 425-m Exclusion Area Boundary (EAB), etc.). Limits on RN release from the core that are consistent with these top-level RN control requirements

are needed in order to derive allowable in-service fuel failure and as-manufactured fuel quality requirements (e.g., allowable heavy-metal contamination, SiC coating defects, etc). The requirement for a 950 ^{o}C core outlet temperature will likely result in fuel temperatures during normal operation that may push the TRISO fuel to near its performance limit.

The dominant source of radioactive contamination in an MHR will be relatively modest quantities of radionuclide release from the core. *In situ* activation of structural materials will be limited, and these activation products will be fixed. There will be no analog in the NGNP to radioactive "crud" in water-cooled reactors since the helium coolant is chemically inert.

The two dominant sources of fission product release from the core are: (1) as-manufactured, heavy-metal (HM) contamination (i.e., heavy metal outside the coated particles) and (2) particles whose coatings are defective or fail in service. In addition, the volatile metals (e.g., Cs, Ag, Sr) can, at sufficiently high temperatures for sufficiently long times, diffuse through the SiC coating and be released from intact TRISO particles; however, diffusive release from intact particles during normal operation is only significant compared to other sources for silver and tritium release.

The radionuclide containment system for the commercial GT-MHR (and, presumably, for the NGNP as well) is comprised of multiple barriers to limit radionuclide release from the core to the environment to insignificant levels during normal operation and a spectrum of postulated accidents. The five principal release barriers are: (1) the fuel kernel; (2) the particle coatings, particularly the SiC coating; (3) the fuel-element structural graphite; (4) the primary coolant pressure boundary; and (5) the Vented Low-Pressure Containment (VLPC) building.

As part of the design process, performance requirements must be derived for each of the above release barriers. Of these barriers, the particle coatings are the most important. Moreover, the in-reactor performance characteristics of the coated-particle fuel are strongly influenced by its as-manufactured attributes. Consequently, the fuel performance requirements and fuel quality requirements must be systematically defined and controlled.

When the fuel requirements presented herein were derived, credit was taken for radionuclide retention by each of the release barriers. Barrier performance requirements are specified such that only the particle coatings are needed to meet 10CFR100 off-site dose limits; however, credit for the additional barriers is taken to meet the PAG dose limits. The alternative would be to set fuel failure limits sufficiently low that the PAG dose limits could be met even if it were assumed that 100% of the fission product inventories of failed particles were released to the environment. This approach is considered impractical. For perspective, for the 350 MW(t) steam-cycle MHTGR with a 425-m EAB, the allowable I-131 release limits to meet the PAG thyroid dose limit of 5 rem were 2.6 Ci for short-term events, such a rapid depressurization, and

29 Ci for long-term events, such as a depressurized core conduction cooldown. Converting these Curie limits to allowable fuel failure fractions for a 600 MW(t) NGNP gives failure limits of ~10^{-7} during normal operation and ~10^{-6} during core heatup events, respectively.

The irradiation and postirradiation experimental programs to justify such low failure fractions for TRISO fuel would be massive, and the QC costs to verify the corresponding as-manufactured fuel quality requirements during mass production would likely be prohibitively expensive (at least with destructive QC methods). Consequently, credit is taken for iodine retention in the kernels of failed particles $(10x)^2$ and for iodine retention in the VLPC (10x) during core heatup accidents. If no credit is taken for retention in the VLPC, the allowable fuel failure fraction would have to be reduced by an order of magnitude (to ~10^{-6} during normal operation and ~10^{-5} during core heatup accidents).

Overall, the most constraining radionuclide control requirement for the steam-cycle MHTGR was to comply with the dose limits specified in the EPA PAGs at the 425-m EAB so that the Emergency Planning Zone (EPZ) could be located at the EAB to preclude the need for public evacuation plans. The PAGs limit both whole body and thyroid doses; these dose limits were used to derive allowable environmental releases of noble gases and iodines, respectively, during Licensing Basis Events (LBEs). The limit on iodine-131 (the dominant iodine isotope) release from the plant was used to derive the limit on I-131 release from the core which, in turn, was used to set the limit on in-service fuel failure. Finally, this limit on in-service coating failure was used to derive the limits on certain as-manufactured defects, including the missing-buffer layer fraction.

The second, most constraining, top-level radionuclide control requirement for the steam-cycle MHTGR was to limit the occupational exposure to ≤10% of 10CFR20 (i.e., a factor of 10 ALARA margin was imposed on the design). A detailed occupational exposure assessment has not been performed for the GT-MHR (or for the NGNP). Hence, in deriving limits on plateout activity consistent with the subject goal, it was necessary to rely heavily upon previous occupational exposure assessments for earlier steam-cycle HTGR designs and upon engineering judgment. On that basis, it was projected that the ≤10% of 10CFR20 goal would be met if the radiation fields around the primary circuit due to fission product plateout were limited to ≤10 mR/hr for scheduled maintenance activities (e.g., IHX and circulator ISI, etc.) and to ≤100 mR/hr for unscheduled maintenance activities (e.g., steam-generator tube plugging, etc.). These limits on

---

[2] This assumption that the core-average, fractional release of I-131 from exposed kernels is only 10% is highly uncertain. If higher release fractions are determined experimentally for high-burnup UCO kernels, then there will be an incentive to take even more credit for holdup in the VLPC.

dose rates were in turn used to set limits on the primary circuit plateout inventories, in particular, limits on the releases of metallic fission products from the core, including Ag-110m, Cs-134, and Cs-137. Finally, the limits on Cs release from the core were used to derive limits on as-manufactured SiC defects.

It is anticipated that off-site dose limits and occupational exposure limits will again be the most constraining, top-level radionuclide control requirements for both the NGNP and commercial H2-MHR designs. It remains to be determined which of these requirements will be the more constraining with respect to in-service fuel failure and as-manufactured fuel quality for the for the NGNP.

For the NGNP conceptual design phase, it is recommended herein that the allowable in-service fuel failure limit and as-manufactured fuel quality requirements be maintained at the commercial GT-MHR limits despite the anticipated higher core outlet temperature for the NGNP (900-950 ^{o}C versus 850 ^{o}C). The primary reason for this recommendation is the necessity to limit the release of I-131 in order the meet the PAGs during rapid depressurization accidents. However, it is recommended to increase the allowable Ag-110m fractional release by a factor of 2.5 back to the steam-cycle MHTGR limit of 5.0×10^{-4}. The latter recommendation is based upon review of the available data on Ag release (e.g., the R2 K13 test) and the predicted Ag-110m release from a direct-cycle GT-MHR with Pu fuel and a 850 ^{o}C core outlet temperature. The preliminary NGNP radionuclide design criteria, which are summarized in Table 1-1, are presented in Section 7 of this report incorporate these two recommendations.

Table 1-1. Provisional NGNP Radionuclide Design Criteria

Parameter	Commercial GT-MHR		VHTR	
	≥50% Confidence	≥95% Confidence	≥50% Confidence	≥95% Confidence
As-Manufactured Fuel Quality				
HM contamination	$\leq 1.0 \times 10^{-5}$	$\leq 2.0 \times 10^{-5}$	$[\leq 1.0 \times 10^{-5}]$	$[\leq 2.0 \times 10^{-5}]$
Missing or defective buffer	$\leq 1.0 \times 10^{-5}$	$\leq 2.0 \times 10^{-5}$	$[\leq 1.0 \times 10^{-5}]$	$[\leq 2.0 \times 10^{-5}]$
Defective SiC	$\leq 5.0 \times 10^{-5}$	$\leq 1.0 \times 10^{-4}$	$[\leq 5.0 \times 10^{-5}]$	$[\leq 1.0 \times 10^{-4}]$
In-Service Fuel Performance				
Normal operation	$\leq 5.0 \times 10^{-5}$	$\leq 2.0 \times 10^{-4}$	$[\leq 1.0 \times 10^{-4}]$	$[\leq 4.0 \times 10^{-4}]$
Core heatup accidents	$[\leq 1.5 \times 10^{-4}]$	$[\leq 6.0 \times 10^{-4}]$	$[\leq 3.0 \times 10^{-4}]$	$[\leq 1.2 \times 10^{-3}]$
Metallic Core Release Limits				
Cs-137 core fractional release	1.0×10^{-5}	1.0×10^{-4}	$[1.0 \times 10^{-5}]$	$[1.0 \times 10^{-4}]$
Ag-110m core fractional release	2.0×10^{-4}	2.0×10^{-3}	$[5.0 \times 10^{-4}]$	$[5.0 \times 10^{-3}]$

1.2 Plant Tritium Source Term and Limits

A radionuclide containment issue of special interest for the NGNP is the containment of tritium. Tritium will be produced in an HTGR by various nuclear reactions. Given its high mobility, especially at high temperatures, some tritium will permeate through the intermediate heat exchanger and hydrogen process vessels, contaminating the product hydrogen and process steam. This tritium contamination will contribute to public and occupational radiation exposures; consequently, stringent limits on tritium contamination in the product hydrogen are anticipated to be imposed by regulatory authorities. Design options are available to control tritium in an HTGR, but they can be expensive so an optimal combination of mitigating features must be implemented in the design.

The following sources of tritium production have been identified, primarily from early surveillance programs at operating HTGRs (steam-cycle plants), and they can be reasonably well quantified for an H2-MHR: (1) ternary fission, (2) neutron activation of He-3 in the primary He coolant, (3) neutron activation of lithium impurities in fuel-compact matrix and core graphite, and (4) neutron capture reactions in boron used in control materials. Ternary fission will be the dominant source of tritium production, but this tritium should be largely retained in the TRISO-coated fuel particles. He-3 activation will generate a relatively modest fraction of the total tritium

produced in the reactor; however, since it is born in the primary coolant, it will likely be an important source of tritium in the primary helium and, hence, of product contamination as well.

Tritium strongly chemisorbs on irradiated nuclear graphite at elevated temperatures. Consequently, a large fraction of the tritium entering the primary helium will be absorbed on the huge mass of graphite in the core. In operating HTGRs, including Fort St. Vrain, the core graphite was a far more important sink for tritium removal than the helium purification system (HPS). However, a large fraction of this stored tritium can be released if water is introduced into the primary coolant (a low-probability event for a VHTR with an IHX).

Tritium will permeate through the heat exchangers and process piping in the NGNP and will contaminate the product hydrogen and process steam. Surface films will play a critically important role in establishing the in-reactor, tritium permeation rates. Oxide films can reduce H-3 permeability by orders of magnitude; however, normal plant operating transients (e.g., startup/shutdown, etc.) may compromise film integrity and result in increased H-3 permeation rates.

A perplexing challenge at this stage of the NGNP Project is to set a provisional limit on the allowable tritium contamination in the product hydrogen and/or process steam when there is no conceptual plant design. The international regulatory standards for allowable tritium contamination in air and drinking water vary remarkably. For example, the regulatory limits on tritium in drinking water vary from a low of 2.7 pCi/g in France to 2057 pCi/g in Australia to no tritium-specific regulatory limits in Japan and Korea (although the public exposure from all sources of artificial radiation is controlled); the US EPA standard is 20 pCi/g (0.74 Bq/g). Traditional exposure pathway analysis for specific assumed release and transport scenarios appears inappropriate for this immature stage of NGNP design definition. Consequently, it is recommended that the US EPA drinking water standard of 20 pCi/g be provisionally adopted as the goal for allowable tritium contamination in the product hydrogen and/or process steam for NGNP preconceptual design.

This recommendation can be compared with the previous German goal of ≤10 pCi/g of tritium in synthetic “natural” gas produced by coal gasification with a pebble-bed HTR (the so-called PNP Project). It is fully expected that when the NGNP conceptual design is defined and a traditional exposure pathway analysis is performed, it will be demonstrated that this 20 pCi/g limit on tritium contamination is excessively conservative and that it can be relaxed by at least two orders of magnitude (as was the case for the PNP Project). Consequently, this recommended limit should not be considered a formal requirement for the NGNP Project but an early and extremely ambitious figure-of-merit for use until the conceptual design is defined.

1.3 Limits On Dust Production in the Primary Circuit

Some level of particulate matter ("dust") will be present in the primary coolant circuit of a VHTR. Based upon past HTGR operating experience, the levels of dust in the primary circuit of a VHTR with a prismatic core are expected to be much lower than with a pebble-bed core. Nevertheless, the NGNP will be a first-of-a-kind plant, and limits need to be established on the allowable levels of dust accumulation in the primary circuit in order to avoid possible deleterious effects on the mechanical integrity of primary circuit components (e.g., erosion) and/or on system performance (e.g., heat exchanger fouling).

The potential deleterious effects of dust include: (1) erosion of primary system surfaces due to abrasion or impaction; (2) fouling of primary system heat transfer surfaces due to poorly conducting layering effects and possible flow blockages, especially with printed circuit-type heat exchangers; (3) instrument and sample line plugging; and (4) possible contribution to carburization of primary circuit metals at high service temperatures (carburization is the addition of carbon to a metal, generally at temperatures between 850 and 950 °C).

Potential sources of dust in an HTGR primary coolant system are: (1) foreign material introduced into the system during initial construction or refueling; (2) graphite or carbonaceous dust resulting from abrasion and/or erosion of prismatic fuel- or reflector element surfaces exposed to the helium coolant; (3) foreign material introduced from interfacing systems; (4) corrosion or erosion products from metallic surfaces of the coolant system; and (5) carbon deposition as a result of CO decomposition.

Primary sinks for these dust products are deposition onto reactor coolant system surfaces and removal by the high-temperature filter/absorber in the helium purification system.

Both the Peach Bottom (PB) and Fort St. Vrain (FSV) experience with respect to dust composition and concentrations are expected to be atypical for the NGNP (and a commercial VHTR). The Peach Bottom primary circuit was coated with a carbonaceous deposit from the cracking of lubricating oil that leaked in from a purified He transfer compressor in the He purification system. Oil bearings will not be used in the NGNP. The dust concentrations in FSV were quite low and consisted primarily of ferritic metal oxides (rust) from the chronic water ingress from the circulator water bearings. The NGNP will not use water bearings. The dust data from the German AVR and THTR pebble-bed reactors are almost certainly even more atypical for a prismatic-core NGNP because of the abrasion-induced dust production within the pebble bed (60 kg of carbon dust accumulated in the 45 MW(t) AVR during its 20-year operation).

The most prototypical dust data for a prismatic-core NGNP are expected to be from the Japanese 30 MW(t) HTTR which has a prismatic core, a 10 MW intermediate heat exchanger, and 20 MW pressurized water cooler in the primary circuit. The HTTR has never experienced either oil or water ingress.

The HTTR has full-flow, sintered-metal filters upstream of each of the primary circuit circulators. The pressure drops across these filters increased early in plant operation indicating that a significant quantity of dust had been collected by the filters. The filters were replaced, and the contaminated dust was characterized to determine its nature and possible sources. The results of this dust investigation have not been published in the open literature to date.

As part of the current NGNP workscope, Fuji Electric Systems (FES) contracted with the Japan Atomic Energy Agency (JAEA) for them to provide a report summarizing their experience with characterizing the dust in the HTTR primary circuit. This JAEA report has been provided to the NGNP program as JAEA proprietary information which cannot be distributed beyond GA and Idaho National Laboratory (INL).[3] The major conclusions of the report are summarized below:

1. The dominant source of dust collected on the HTTR circulator pre-filters is the abrasion of the graphite piston rings in the purified He compressors. Construction debris (e.g., filaments of Kaowool insulation) may have contributed to a lesser extent.

2. The graphite components of the HTTR prismatic core do not appear to contribute significantly to the circulating dust in the primary circuit.

3. The dust is primarily carbonaceous. Both graphite and amorphous carbon are present.

4. The particles collected on the filters have effective diameters of 1 - 3 μm; the particle size distribution was not determined.

5. JAEA does not believe that full-flow dust filters will be necessary in future VHTRs with prismatic cores.

A review of dust behavior in non-HTGR, high-temperature gas systems was also conducted, including the following:

- Blade erosion phenomena in combustion turbines.

---

[3] The JAEA report has been provided to INL for their use with appropriate restrictions to safeguard the JAEA proprietary information contained therein.

- Fly ash erosion effects in fossil-fired power plants, including those with ultra-supercritical boilers.
- The THOR nuclear waste solidification project that turns liquid waste (such as INL sodium-bearing waste) into a carbonate suitable for disposal in the DOE Waste Isolation Pilot Plant.
- Chemical demilitarization projects that incinerate chemical weapons such as mustard gas and nerve agents.
- Heat exchanger fouling in refineries and in plants processing organic chemicals that are subject to coke formation.

In general, this non-HTGR experience appears to be of limited applicability to the NGNP dust issue for following reasons: (1) the service temperatures are generally much lower than 900-950 ^{o}C; (2) the particulate loadings are orders of magnitude higher; (3) the coolant chemistry is much different (e.g., oxygen potential is typically many orders of magnitude higher); and (4) the surface loadings required to cause significant degradation in heat exchanger performance are orders of magnitude higher.

For the present, the “best estimate” and “conservative” dust attributes given in Section 6.3 should be considered the “Maximum Expected” and “Design” criteria for NGNP preconceptual design. These recommendations, which are summarized in Table 1-2, are based primarily upon Peach Bottom and FSV dust data and engineering judgment; the HTTR dust data are not inconsistent with the “Maximum Expected” gas concentration.

Table 1-2. Provisional NGNP Dust Design Criteria

Attribute	“Maximum Expected”	“Design”
Composition	graphite	graphite, metal oxides
Particle size distribution	0.1 - 5 μm	0. 01 - 10 μm
Gas concentration	<10 μg/m^3	<3 mg/m^3
Surface loading	<0.5 g/m^2	<5 g/m^2

1.4 Plant Mass Balance for Radionuclides

A broad spectrum of radionuclides, including tritium, will be produced by various nuclear reactions (principally fission) in a VHTR. These radionuclides represent a potential radiation hazard to plant personnel, product consumers, and the general public. Consequently, the plant must be designed to assure these radionuclides are controlled to meet all regulatory requirements with sufficient margin to account for the uncertainties in the predicted source

terms for a first-of-a-kind (FOAK) plant. An important consideration for plant design and optimization is to determine an overall plant mass balance for these radionuclides.

Radionuclide design criteria, or the allowable levels of radionuclide accumulation in the primary coolant circuit during normal plant operation, are defined for a 600 MW(t) NGNP consistent with the fuel quality and performance requirements outlined in Section 1.1. However, there is an unresolved issue at this writing. The allowable core release fractions derived in Section 4 are for a 350 MW(t) plant, but the NGNP thermal power may be as high as 600 MW(t), a factor of 1.7 higher. Consequently, to achieve the same Curie releases from a 600 MW(t) plant, the allowable fractional releases would have to be a factor of 1.7 lower. Conceptually, the most obvious means to accomplish that would be to reduce the allowable in-service fuel failure and as-manufactured HM contamination by a corresponding factor of 1.7.

Such a recommendation was considered here but judged to be premature. First and foremost, the power level of the NGNP has not yet been selected, and power levels less than 600 MW(t) are under active consideration. Moreover, while the results of the on-going AGR-1 fuel irradiation test are certainly encouraging to date, the fuel has not yet reached full burnup and postirradiation heating tests are well in the future. Until compliance with the current, already stringent, fuel performance requirements is convincingly demonstrated, it seems imprudent to tighten them further. Once the AGR fuel qualification program is complete and the NGNP source terms have been validated, a determination can be made whether or not further tightening of the fuel requirements would be necessary – and practical – for future commercial VHTR plants.

A two-tier set of radionuclide design criteria, referred to as the "Maximum Expected" and "Design" criteria, are presented in Appendix A. In principle, the "Design" criteria are derived from externally imposed requirements, such as site-boundary dose limits and ALARA requirements (Section 1.1). The "Maximum Expected" criteria are then derived by dividing the "Design" criteria by an uncertainty factor, or design margin, to account for uncertainties in the design methods. This uncertainty factor is a factor of four for the release of fission gases from the core and a factor of 10 for the release of fission metals. The fuel and core are to be designed such that there is at least a 50% probability that the fission product releases will be less than the "Maximum Expected" criteria and at least a 95% probability that the releases will be less than the "Design" criteria (elaborated in Section 2.3.3).

The "Maximum Expected" criteria are to be used for Environmental Impact Reports, for planning component removal and maintenance procedures, and for other applications where "best-estimate" results are appropriate. The "Design" criteria represent upper limits for all normal operating conditions. They are to be used for safety analyses, sizing of the helium purification

and radwaste systems, the design of plant hardware including service and shipping casks, and the specification of the associated shielding requirements.

The computer program RADC was used to calculate the RN design criteria. Since the NGNP is still in the pre-conceptual design phase, many basic plant parameters have not yet been selected. Consequently, for this scoping study, the point of departure was the previous RADC analysis for the 350 MW(t) steam-cycle MHTGR. Required input parameters for RADC were taken from the 600 MW(t) commercial GT-MHR conceptual design as available, or the 350 MW(t) MHTGR parameters were used (scaled up by power level if appropriate). The assumed as-manufactured HM contamination and in-service fuel failure fraction were consistent with the values recommended for the NGNP in Section 1.1 (essentially the same as for the commercial GT-MHR).

With the base case results described above, a sensitivity study was performed to identify the dominant variables for defining radionuclide mass balances to provide guidance to plant design and optimization studies. This study investigated the effects of various parameters on the circulating RN inventories and plateout inventories in the primary circuit at the end of plant life (60 yr). Variables investigated included core and system design parameters such as HM contamination fraction, fuel failure fraction, helium purification constant, plateout removal constant, and silver diffusive release fraction from the core. These parameters were varied by a factor of 10.

The coolant activity is dominated by noble gases and is most affected with the change of the HM contamination fraction and fuel failure fraction. The coolant inventories of I-131, Xe-133 and total circulating activity change by ~5x or by ~0.5x when the HM contamination and fuel failure fraction parameters are changed by an order of magnitude above or below the base case, respectively. The He purification constant parameter has a large effect on the circulating activity of 5.3-day Xe-133, but it has little effect on the I-131 circulating activity which preferentially plates out. The total circulating activity, which is dominated by relatively short-lived noble gases, is only modestly affected by the He purification rate.

In general, the plateout activity is not affected in the study range of the purification removal constant and plateout removal constants (i.e., the plateout removal rate far exceeds the purification rate). The plateout activity is most affected by a change of fuel failure fraction and the diffusive release fraction in the case of Ag-110m. The plateout activity is also affected by a change in the HM contamination fraction but to a lesser degree than by a change in the fuel failure fraction.

1.5 Plant Mass Balance for Tritium

Plant mass balances for H-3 were calculated with the TRITGO code for three different notional plant configurations: (1) a single two-stage intermediate heat exchanger (IHX) supplying a small hydrogen production plant and a steam generator (SG) in the secondary circuit, (2) a small IHX supplying a hydrogen plant and a large IHX coupled to a steam generator in the secondary heat transport system, and (3) a small IHX supplying a hydrogen production plant and a large steam generator in the primary heat transport system,

For a typical application of TRITGO, the reactor core is divided into a number of tritium source regions such as the active core, the inner reflector, the outer reflector, the top reflector, the bottom reflector, and the control rods. The user inputs characteristic parameters for each region, including the average neutron flux, average temperature, impurity concentrations, and total mass. TRITGO determines the amount of tritium present in each region due to ternary fission, neutron reactions with graphite impurities, neutron capture in boron control materials, and He-3 activation in the coolant. The TRITGO output includes the amount of tritium bound in solids, sorbed on graphite surfaces, in the primary coolant, in the helium purification system, in the steam generator, and lost to the environment through condenser blowdown or steam generator leakage (the latter for a steam-cycle plant).

TRITGO was originally written at ORNL in the mid-1970s for the analysis of steam-cycle HTGRs, and a number of material properties were built into the code. Subsequently, GA acquired the code and modified it for use on the MHTGR and NP-MHTGR programs. The H-3 transport models currently in use at GA, and supplied to KAERI for this analysis, are contained and controlled in the GA Fuel Design Data Manual. Some of these component models have not yet been incorporated into the TRITGO code. It is anticipated that they would be incorporated into an improved version of TRITGO or into a new code written for NGNP preliminary and final designs.

As indicated in Section 1.2, ternary fission will be the dominant source of tritium production, and some fraction of this tritium will be diffusively released from the intact, TRISO-coated fuel particles, given the high average fuel temperatures in a VHTR core. Using the available information on H-3 release rates from TRISO-coated particles, especially target particles, models were developed at GA for predicting H-3 release from failed and intact TRISO fuel particles. An approximate core volume temperature distribution for the NGNP with a 950 ^{o}C outlet temperature was available, based upon the scoping core design work performed by KAERI and GA under the earlier Phase 1 NGNP engineering services contract. Using this approximate volume temperature distribution and the GA H-3 release correlation, it was conservatively estimated that 30% of the tritium produced in the fuel by ternary fission would be

released into the He coolant; and this release fraction was used in the TRITGO base-case analysis. It is likely to be excessively conservative.

Irradiated graphite is known to have a high sorptivity for tritium, but the sorptivities of modern nuclear graphites have not been well characterized. The original graphite sorption isotherm built into TRITGO was clearly unsatisfactory in that it had no temperature or fast fluence dependence. In 1986, Myers derived a new isotherm which includes crude temperature dependence and a fast fluence, and this new isotherm has also been added as an option in the TRITGO code. Presumably, the Myers isotherm is an improvement over the original isotherm in that it includes a temperature- and fast fluence dependence that the available experimental data indicate; however, the uncertainties in the Myers isotherm are clearly quite large and unquantified.

In 1991, the then-available data for H-3 permeation through Alloy 800 was reevaluated and a new formulation for tritium permeation through metals was constructed in support of the NPR Project. This so-called “CEGA” H-3 permeation correlation is based primarily upon the H-3 permeation rates measured for Incoloy 800 tube specimens removed from the Peach Bottom steam generator at end-of-life. The TRITGO code was modified to accommodate this new correlation whose functional form is different from the traditional permeation correlation.

The leading candidate material for the IHX and for the superheater section of the steam generator is IN 617. While the tritium permeability of IN 617 has not been as well characterized as that of some other metals, including Alloy 800H, there are several German comparative studies that indicate the tritium permeabilities of IN 617 and Alloy 800H are quite comparable at the service temperatures anticipated for the NGNP IHX and steam generator. Consequently, the CEGA correlation was used for IN 617 as well as for Alloy 800H.

In addition to the performing a best-estimate TRITGO analysis for the three plant configurations described above, a sensitivity study was also performed for Configuration 1 (a single two-stage IHX supplying a small hydrogen production plant and a steam generator).

The reactor system design is identical for each of the three plant configurations analyzed; consequently, the production of tritium is the same for each configuration. As expected, the dominant source of tritium production is ternary fission. However, the activation of He-3 in the primary helium and activation of Li in the core graphite contribute significantly to the predicted amount of tritium in the primary coolant. The sorption of tritium on the core graphite is predicted to be the most important sink for tritium in the primary circuit, much more important than either helium purification or permeation through the heat exchangers (in fact, this behavior was observed in Fort St. Vrain).

The predicted amount of tritium permeation through the heat exchangers was highest for Configuration 1 and lowest for Configuration 3. The amount of H-3 permeation was lowest for Configuration 3 with the steam generator in the primary circuit because the average metal temperatures were somewhat lower for that configuration. For all three configurations, the predicted amount of tritium permeation into the secondary circuit would be problematic if it were allowed to transport further into the hydrogen production plants. Since there is no other major sink for tritium in the secondary heat transport, it can be reasonably assumed that most of it would eventually permeate into the process streams and contaminate the product hydrogen. Consequently, the anticipated need for a helium purification system in the secondary coolant circuit is confirmed. The required size and exact configuration of this secondary HPS (e.g., the need for liquid nitrogen-cooled charcoal beds required) are still under review.

While the uncertainties in these H-3 mass balance predictions are large and the limitations of the TRITGO code are substantial, the results do convincingly demonstrate that significant tritium permeation through the heat exchangers should be expected for all three configurations. This expectation that tritium contamination will be a design issue for the NGNP is supported by the observed tritium behavior in operating HTGRs. It is of particular interest to consider the implications for judging the relative merits of locating a steam generator in a primary- or secondary coolant loop (i.e., the relative merits of Configuration 2 versus Configuration 3).

Based upon the surveillance data from FSV and other steam-cycle HTGRs, tritium will contaminate the process steam to some degree regardless of the location of the steam generator in the NGNP. However, it is noteworthy that for these earlier steam-cycle plants, all of which had their steam generators located in the primary circuit, tritium contamination control was not a significant operational or compliance issue.

Without engineered mitigating design features, the relative amount of tritium permeation through the heat exchangers of the NGNP will likely be higher than through the steam generators of previous operating HTGRs because of higher operating temperatures in the core and in the steam generator in the NGNP. Tritium control would be relatively easier if the steam generator were located in the secondary circuit because that configuration allows for the inclusion of a second purification system in the secondary coolant circuit. With the steam generator in the primary circuit, the size of the primary He purification system can be increased, but the dominant tritium sink in the primary circuit is expected to be the core graphite. Consequently, very large increases in the He purification system would be required to significantly reduce the amount of permeation into the secondary steam.

While locating the steam generator in the secondary circuit would facilitate tritium control, the cost penalty for the inclusion of an extra loop with a large IHX and another large circulator is judged to be excessive. Consequently, it is expected that any steam generator will be located in the primary circuit of the NGNP and that tritium control will prove manageable for that configuration as it did for all previous operating steam-cycle HTGRs

1.6 Design Options for Radionuclide Control In HTGRs

There are two effective approaches for reducing the release of radionuclides from the core into the primary coolant circuit. The most effective approach would be to improve the as-manufactured fuel quality and to reduce the allowable in-service fuel failure. While conceptually attractive, this approach is not considered practical at the current time. While the results of the AGR-1 fuel irradiation test to date are certainly encouraging, the fuel has not yet reached full design burnup and fast fluence. Moreover, it has yet to be demonstrated that TRISO fuel of that quality, much less of a significantly higher quality fuel, can be economically mass produced. The second approach is to optimize the core nuclear and thermal designs to minimize fuel temperatures. Such core optimization should be a top priority during the conceptual and preliminary design phases. In addition, fuel temperature minimization is the only effective means to reduce the diffusive releases of Ag-110m and tritium from intact TRISO particles.

Once programmatic limits on the allowable tritium contamination levels in the product hydrogen are adopted and a comparison with the expected H-3 contamination levels has been made, trade studies can be conducted to determine which design option for H-3 control, or combinations thereof, is optimal for the reference plant design. At this point, the addition of a large helium purification system to the secondary coolant loop for tritium removal appears to be essential. Also, as indicated above, the allowable Li impurity in core graphite should be reduced to the fullest extent practical, and the B_4C granules in the lumped burnable poison and in the control rods should be coated to improve tritium retention (and resistance to hydrolysis). Tritium permeation barrier coatings, especially Al-based coatings, have the potential to dramatically reduce product contamination levels if a practical means can be identified for applying them to a printed circuit-type IHX.

In addition, ceramic heat exchangers, especially those fabricated of SiC, should have far lower tritium permeabilities than metallic heat exchangers (e.g., see Figure 2-4). The issue has been whether or not industrial-scale ceramic heat exchangers could reasonably be expected to be available in the timeframe required for the NGNP. Sandia has estimated that a 100 MW bayonet-type sulfuric acid decomposer could be constructed of Hexoloy© SiC tubes currently available from Saint-Gobain Ceramics. It is not known at this writing whether the corrosion rates of this material in decomposing sulfuric acid at temperatures >850 ^{o}C and elevated pressures have been determined.

1.7 Adequacy of Current NGNP Technology Programs

The adequacy of the current NGNP technology programs to support the preconceptual design recommended by the GA NGNP team, which included a direct-cycle, gas-turbine, power conversion system(PCS), was assessed in the NGNP Umbrella Technology Development Plan, including those aspects of contamination control in a VHTR where the current technology was judged to be inadequate to support NGNP design and licensing. The NGNP Project rejected the inclusion of a direct-cycle PCS in the NGNP conceptual design and mandated the inclusion of a steam generator in either the primary- or secondary heat transport system.

Now that the current contamination control study has been completed for three different plant configurations described above, the NGNP DDNs have been reassessed. With the exception of those DDNs that specifically applied to a direct-cycle PCS, the earlier critique still applies (see Section 10). The DDNs will need to be revisited again when the NGNP conceptual design is completed.

It is noteworthy that the current AGR fuel development plan does not address tritium transport. However, a test plan to characterize tritium transport behavior in VHTRs was prepared in 2007. It is anticipated that this tritium characterization plan will be incorporated into the on-going AGR program. The tritium transport issues addressed in this test plan are generic to all HTGRs, but the test program priorities and test articles are design specific. The NGNP is still in the preconceptual design phase at this writing; consequently, this test plan will need to be reviewed and revised as appropriate when the conceptual design of the NGNP is finalized. In particular, the inclusion of a steam generator in the primary coolant circuit of the NGNP would increase the priority of the tests to determine the effects of water on tritium transport behavior.

The design methods that are available to estimate H-3 production, distribution, and release, are rather rudimentary and characterized by large uncertainties (see Section 8). They will need to be upgraded for preliminary design and independently validated prior to completion of final design. Some technology development will be necessary to provide the bases for these design methods improvements and validation. Four DDNs related to tritium behavior have been identified at this writing (and more may be identified as the NGNP design matures): (1) measurement of H-3 release from irradiated intact TRISO particles, (2) measurement of the H-3 sorptivities of irradiated core graphites, (3) measurement of H-3 release from irradiated, bare and coated B_4C granules, and (4) measurement of H-3 permeation rates through candidate IHX and steam generator metals. A test program has recently been initiated at INL to address the latter permeation DDN, and it is anticipated that the other three H-3 DDNs will be addressed in a future update of the AGR fuel plan.

1.8 Adequacy of Current Design Methods

Both the TRITGO and RADC codes used in this study are GA legacy codes that need to be upgraded for conceptual design and replaced by modern codes for preliminary and final design.

The current limitations with TRITGO have proven to be particularly problematic. As indicated above, TRITGO was written in the mid-1970s for predicting the tritium mass balance in a steam-cycle HTGR which is represented by a collection of coupled compartments (e.g., active core, primary He coolant, He purification system, secondary water coolant, etc.). A differential mass balance is formulated for each compartment, including the various H-3 sources and sinks described in Section 1.2, are modeled in each compartment as appropriate. The H-3 concentration in each compartment is determined by solving analytically a coupled set of linear first-order differential equations. The fundamental limitation with TRITGO is this analytical solution technique which necessitates that the H-3 concentrations be linear functions of the various material properties, such as the H-3 permeability of metals, and independent of time. The current version of TRITGO can also only model a plant configuration with a single primary and second coolant circuit (steam cycle). Consequently, it cannot simultaneously analyze a plant configuration that contains dissimilar parallel loops (e.g., an IHX in one primary loop and a steam generator in a second primary loop).

In principle, the TRITGO code could be extensively modified to include an arbitrary number of parallel and coupled serial loops; however, the fundamental limitation (i.e., the analytical solution technique) is so restrictive that it would be far better to write a new code that is solved numerically and that allows non-linear and time-dependent functionalities. TRITGO is only marginally adequate for conceptual design, and it should be replaced as soon as practical with a new tritium mass balance code which employs a numerical solution technique.

The RADC code is a zero-dimensional, radionuclide inventory code that is a modification of the RAD2 code that was written in the mid-1960s to predict a radionuclide mass balance for the Peach Bottom HTGR. RADC has a number of significant limitations. In particular, it does not calculate neutron activation products from neutron reactions with fission products [e.g., $Ag^{109}(n,\gamma)Ag^{110m}$, $Cs^{133}(n,\gamma)Cs^{134}$, etc.], neutron reactions with core impurities [$N^{14}(n,p)C^{14}$, $Li^{6}(n,\alpha)H^{3}$, etc.], or neutron reactions with control materials [e.g., $B^{10}(n,2\alpha)H^{3}$, etc.]. It also does not calculate heavy-metal buildup and decay chains; instead, the core inventories of important activation products have to be calculated externally and effective fission yields supplied to RADC.

The above limitations, as well as other limitations, in RADC have long been recognized, and a replacement code called RANDI was written by GA in 1977 which in principle eliminated them.

However, RANDI requires extensive automated input from other codes. As written, RANDI cannot be conveniently used in a stand-alone mode to generate radionuclide design criteria, independent of a core nuclear design and full-core fuel performance and fission product release analyses (which provide fuel failure fractions, fission product release fractions, etc.).

RADC is adequate for conceptual design, but it should be replaced for preliminary and final design. The possibility of modifying and simplifying the RANDI code so that it can be used in a stand-alone mode should be investigated before committing to writing an entirely new code. In particular, the utility of modifying RANDI so that the core inventories could be automatically input from a general purpose, radionuclide generation and depletion code, such as the industry standard ORIGIN2 code or the GA GARGOYLE code, should be determined.

2. INTRODUCTION AND BACKGROUND

The U.S Department of Energy (DOE) has chosen the Very High Temperature Reactor (VHTR) for the Next Generation Nuclear Plant (NGNP) Project. The reactor design will be a helium-cooled, graphite-moderated thermal reactor that will be designed to produce electricity and hydrogen as required by the Energy Policy Act of 2005. DOE has contracted with three industrial teams, including a team led by General Atomics, for conceptual design studies in support of NGNP design and licensing [Work Plan 2007]. As part of the contractual work scope, GA has performed a contamination control study to establish provisional limits on RN contamination throughout the NGNP with particular emphasis on tritium.

2.1 Purpose

The primary purpose of this study was to establish provisional limits on RN contamination throughout the NGNP with particular emphasis on tritium since it can permeate through heat exchangers and contaminate the product hydrogen in a H2-MHR and the process steam in a steam-cycle plant.

As elaborated in the next subsection, the NGNP is still in the pre-conceptual design phase with major design selections (e.g., reactor core type, core outlet temperature, etc.) yet to be made. Consequently, the “provisional limits" recommended herein will likely require optimization once there is a conceptual plant design and an assessment has been made of whether or not all top-level radionuclide control requirements (e.g., off-site dose limits, etc.) are met with source terms based upon these provisional limits.

The programmatic benefits of performing the subject contamination control study during pre-conceptual design are threefold: (1) Design Data Needs (DDNs) can be identified and the on-going, generic NGNP technology development programs modified or supplemented as required (e.g., the need to characterize tritium transport in the hydrogen production plants); (2) inadequacies in the current analytical tools to support preliminary and final NGNP design can be identified such that these deficiencies can be remedied during the conceptual design phase (e.g., the need for an improved plant tritium mass balance code to replace TRITGO); and (3) significant design issues that need to be addressed during conceptual design can be identified early (e.g., the necessity for a large helium purification system in the secondary heat transport circuit to control tritium migration into the hydrogen process plants).

2.2 NGNP Design Status

Of the advanced reactor concepts, the VHTR is especially well suited for producing hydrogen because of its high-temperature capability, advanced stage of development relative to other

high-temperature reactor concepts, and passive-safety features. The VHTR can provide the high-temperature process heat required to produce hydrogen by either thermochemical water splitting or by high temperature electrolysis [e.g., Richards 2004]. A leading conceptual design for nuclear hydrogen production is a Modular Helium Reactor (MHR) coupled via an intermediate heat exchanger[4] (IHX) to a hydrogen production plant using the sulfur-iodine (SI) thermochemical process or high temperature electrolysis (HTE); this plant concept is referred to herein as the H2-MHR.

At this writing, the NGNP is still in the pre-conceptual design phase with major design selections yet to be made. During the previous phase of the NGNP Project, a preconceptual design was recommended by the GA NGNP team which included a direct-cycle, gas-turbine, power conversion system (PCS) [GA PCDSR 2007]. A complete set of DDNs was also identified for this preconceptual design [NGNP TDP 2007], including those aspects of contamination control in a VHTR where the current technology was judged to be inadequate to support NGNP design and licensing.

The NGNP Project rejected the inclusion of a direct-cycle PCS in the NGNP conceptual design and mandated the inclusion of a steam generator in either the primary- or secondary heat transport system [NGNP PCD 2007]. Consequently, the issue of NGNP DDNs will need to be revisited once the conceptual design is determined. The DDNs related to radionuclide transport, including tritium transport, are anticipated to be largely unaffected since they are mostly generic.

For this task the NGNP Reactor System was assumed to employ a 600 MW(t) prismatic core and to operate with a 950 ^{o}C core outlet temperature. Three plant configurations were considered: (1) a single two-stage IHX supplying a small hydrogen production plant and a steam generator, (2) a small IHX to supply a hydrogen production plant and a large steam generator in the primary heat transport system, and (3) a small IHX to supply a hydrogen plan and large IHX coupled to a steam generator in the secondary heat transport system. These conceptual plant configurations and their thermal/fluid dynamic performance characteristics are described in detail in [Labar 2008].

[4] The IHX design for the NGNP may be either a conventional helical-coil design or more developmental compact heat exchanger designs, such as a printed circuit heat exchanger (PCHE) design.

2.3 Radionuclide Control in MHRs

A fundamental requirement in the design of any nuclear power plant is the containment and control of the radionuclides produced by the various nuclear reactions; in response, different radionuclide containment systems have been designed and employed for different reactor designs.

2.3.1 Radionuclide Control Philosophy

The most effective means of minimizing radioactive contamination in a nuclear power plant is source reduction. The dominant source of radionuclides in an MHR is the fission product inventory in the reactor core. For modular HTGR designs, a hallmark philosophy has been adopted since the early 1980s to design the plant such that the radionuclides would be retained in the core during normal operation and postulated accidents [e.g., PSID 1992]. The key to achieving this safety goal is the reliance on TRISO-coated fuel particles for primary fission product containment at their source, along with passive cooling to assure that the integrity of the coated particles is maintained even if the normal cooling systems were permanently disrupted.

2.3.2 Radionuclide Containment System

In response to the above goal, a radionuclide containment system for an MHR, which reflects a defense-in-depth philosophy, has been designed to limit radionuclide release from the core to the environment to insignificant levels during normal operation and a spectrum of postulated accidents. Nevertheless, a small fraction of TRISO fuel particles have as-manufactured defects and these particles may experience in-service coating failure [e.g., PSID 1992], resulting in fission product release from the core and attendant contamination of the primary coolant circuit. A fundamental design requirement is to establish allowable limits on core releases during normal operation and postulated accidents.

As shown schematically in Figure 2-1, the five principal release barriers in an MHR radionuclide containment system are: (1) the fuel kernel, (2) the particle coatings, particularly the SiC coating, (3) the fuel element structural graphite, (4) the primary coolant pressure boundary; and (5) the VLPC. The effectiveness of these individual barriers in containing radionuclides depends upon a number of fundamental factors including the chemistry and half-lives of the various radionuclides, the service conditions, and irradiation effects. The effectiveness of these release barriers is also event specific.

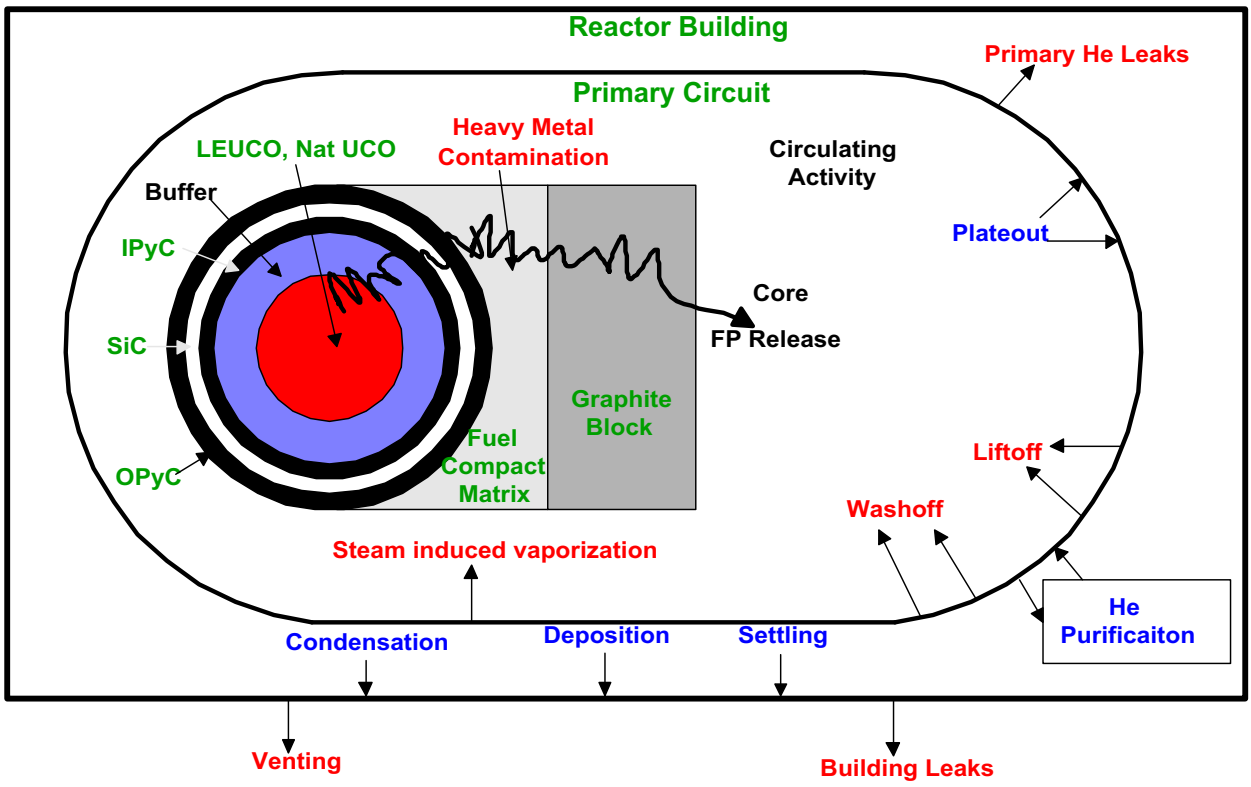

Figure 2-1. MHR Radionuclide Containment System

The first barrier to fission product release is the fuel kernel itself. Under normal operating conditions, the kernel retains >95% of the radiologically important, short-lived fission gases such as Kr-88 and I-131. However, the effectiveness of a UCO kernel for retaining gases can be reduced at elevated temperatures or if an exposed kernel is hydrolyzed by reaction with trace amounts of water vapor which may be present in the helium coolant (the UO_2 kernel used in PBMR fuel is somewhat less susceptible to hydrolysis effects than is UCO). The retentivity of oxidic fuel kernels for long-lived, volatile fission metals such as Cs, Ag, and Sr is strongly dependent upon the temperature and the burnup.

The second - and most important - barrier to fission product release from the core is the silicon carbide and pyrocarbon coatings of each fuel particle. Both the SiC and PyC coatings provide a barrier to the release of fission gases. The SiC coating acts as the primary barrier to the release of metallic fission products because of the low solubilities and diffusion coefficients of fission metals in SiC; the PyC coatings are partially retentive of Cs at lower temperatures but provide little holdup of Ag and Sr.

With a prismatic core, the fuel-compact matrix and the fuel-block graphite collectively are the third release barrier (with a pebble-bed core, the analog is the pebble matrix, including the unfueled outer shell). The fuel-compact matrix is relatively porous and provides little holdup of the fission gases which are released from the fuel particles. However, the matrix is a composite

material which has a high content of amorphous carbon, and this constituent of the matrix is highly sorptive of metallic fission products, especially Sr. While the matrix is highly sorptive of metals, it provides little diffusional resistance to the release of fission metals because of its high interconnected porosity.

The fuel-element graphite, which is denser and has a more ordered structure than the fuel-compact matrix, is somewhat less sorptive of the fission metals than the matrix, but it is more effective as a diffusion barrier than the latter. The effectiveness of the graphite as a release barrier decreases as the temperature increases. Under typical core conditions, the fuel element graphite attenuates the release of Cs from the core by an order of magnitude, and the Sr is essentially completely retained. The extent to which the graphite attenuates Ag release is not nearly as well characterized, and there is some evidence that the retention of Ag by graphite increases as the total system pressure increases (implying gas-phase transport through the interconnected pore structure of the graphite).

Typically, the two dominant sources of fission product release from the core are (1) as-manufactured, HM contamination (i.e., heavy metal outside the coated particles) and (2) particles whose coatings are defective or fail in service. In addition, the volatile metals (e.g., Cs, Ag, Sr) can, at sufficiently high temperatures for sufficiently long times, diffuse through the SiC coating and be released from intact TRISO particles; however, diffusive release from intact particles during normal operation is only significant compared to other sources for silver and tritium release. Fission products resulting from fissions in HM contamination outside of the particles are obviously not attenuated by the kernels or coatings, nor are the fission products produced in the kernels of failed particles appreciably attenuated by the failed coatings. In these cases, the fission products must be controlled by limiting the respective sources and by the fuel-element graphite in the case of the fission metals and actinides.

The fourth release barrier is the primary coolant pressure boundary. Once the fission products have been released from the core into the coolant, they are transported throughout the primary circuit by the helium coolant. The helium purification system efficiently removes both gaseous and metallic fission products from the primary coolant at a rate determined by the gas flow rate through the purification system (the primary purpose of the HPS is to control chemical impurities in the primary coolant). However, for the condensable fission products, the dominant removal mechanism is deposition (“plateout”) on the various helium-wetted surfaces in the primary circuit (i.e., the deposition rate far exceeds the purification rate).

The plateout rate is determined by the mass transfer rates from the coolant to the fixed surfaces and by the sorptivities of the various materials of construction for the volatile fission products and by their service temperatures. Condensable radionuclides may also be transported throughout the primary circuit sorbed on particulates (“dust”) which may be present in the

primary coolant; the plateout distribution of these contaminated particulates may be considerably different than the distribution of radionuclides transported as atomic species.

The circulating and plateout activities in the primary coolant circuit are potential sources of environmental release in the event of primary coolant leaks or as a result of the venting of primary coolant in response to overpressuring of the primary circuit (e.g., in response to significant water ingress in a steam-cycle plant). The fraction of the circulating activity lost during such events is essentially the same as the fraction of the primary coolant that is released, although the radionuclide release can be mitigated by pump down through the HPS if the leak rate is sufficiently slow.

A small fraction of the plateout may also be reentrained, or "lifted off," if the rate of depressurization is sufficiently rapid. The amount of fission product liftoff is expected to be strongly influenced by the amount of dust in the primary circuit as well as by the presence of friable surface films on primary circuit components which could possibly spall off during a rapid depressurization.

Other mechanisms which can potentially result in the removal and subsequent environmental release of primary circuit plateout activity are "steam-induced vaporization" and "washoff." In both cases, the vehicle for radionuclide release from the primary circuit is water which has entered the primary circuit. In principle, both water vapor and liquid water could partially remove plateout activity. However, even if a fraction of the plateout activity were removed from the fixed surfaces, there would be environmental release only in the case of venting of helium/steam from the primary circuit. For all but the largest water ingress events the pressure relief valve does not lift. Moreover, the radiologically important nuclides, such as iodine and cesium, are expected to remain preferentially in the liquid water which remains inside the primary circuit. The probability of large water ingress with a gas-turbine plant or a plant with an IHX is much lower than for a conventional steam-cycle plant because with the former the secondary water pressures are lower than the primary He pressures.

The vented low-pressure containment is the fifth barrier to the release of radionuclides to the environment. Its effectiveness as a release barrier is highly event-specific. The VLPC may be of limited value during rapid depressurization transients; however, it is of major importance during longer term, core conduction cool-down transients during which forced cooling is unavailable. Under such conditions, the natural removal mechanisms occurring in the VLPC, including condensation, fallout and plateout, serve to attenuate the release of condensable radionuclides, including radiologically important iodines, by at least an order of magnitude.

2.3.3 Radionuclide Design Criteria

Standard GA design practice is to define a two-tier set of radionuclide design criteria, - referred to as “Maximum Expected” and “Design” criteria, - (or allowable core releases for normal operation and Anticipated Operational Occurrences); this practice has been followed since the design of the Peach Bottom 1 prototype U.S. HTGR up through the current commercial GT-MHR [e.g., Hanson 2002b]. The “Design” criteria are derived from externally imposed requirements, such as site-boundary dose limits, occupational exposure limits, etc.; in principle, any of these radionuclide control requirements could be the most constraining for a given reactor design. The off-site PAG dose limits proved to be the most constraining for the 350 MW(t) steam-cycle MHTGR, and they will probably be the most constraining for the commercial H2-MHR as well although occupational exposures are anticipated to take on added importance for a direct-cycle plant compared to a steam-cycle plant.

Once the “Design” criteria have been derived from the radionuclide control requirements, the corresponding “Maximum Expected,” criteria are derived by dividing the “Design” criteria by an uncertainty factor, or design margin, to account for uncertainties in the design methods. This uncertainty factor is typically a factor of four for the release of fission gases from the core and a factor of 10 for the release of fission metals. The fuel and core are to be designed such that there is at least a 50% probability that the fission product release will be less than the “Maximum Expected” criteria and at least a 95% probability that the release will be less than the “Design” criteria. The GA approach to implementing such radionuclide design criteria is illustrated in Figure 2-2. (No particular scale is implied in this figure; it is simply a conceptual illustration of the approach.)

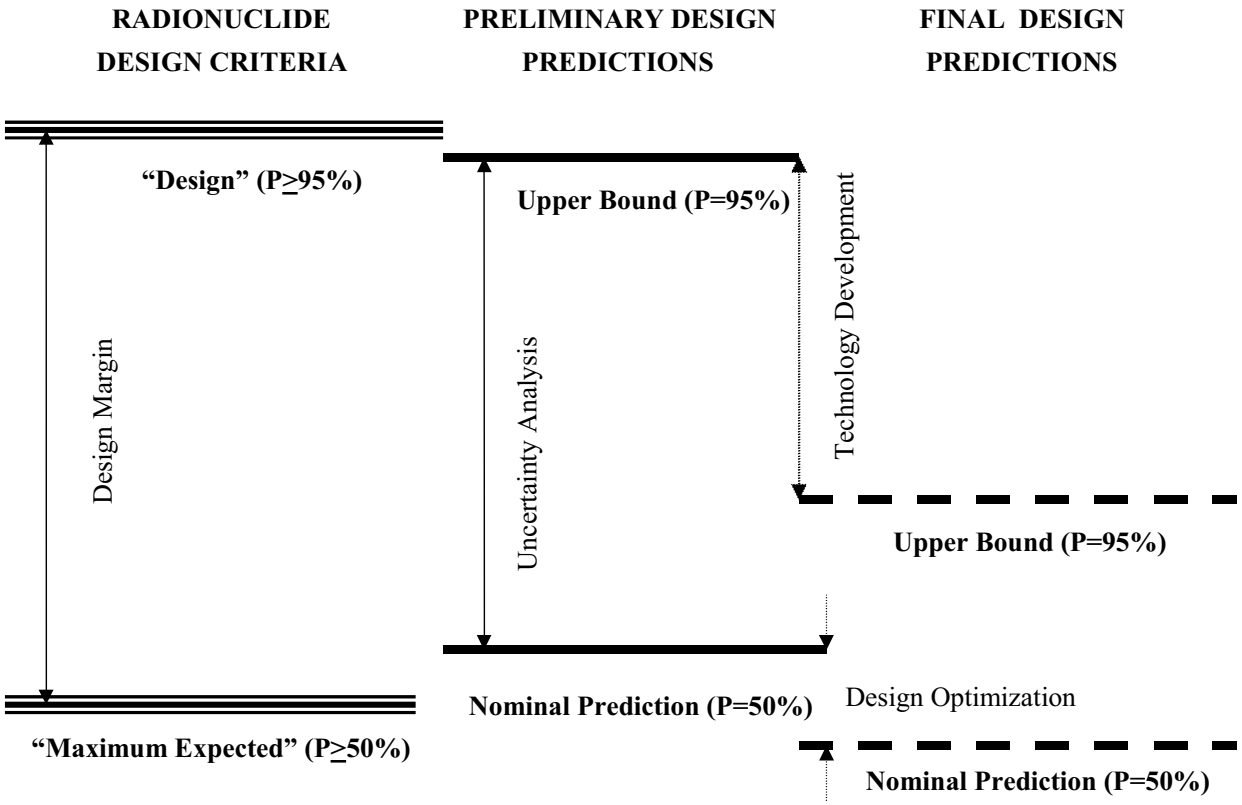

Figure 2-2. Radionuclide Design Criteria

In the example given in Figure 2-2, the Preliminary Design predictions (solid lines) slightly exceed the criteria (triple lines) at the 50% confidence level: i.e., the nominal (50% confidence) prediction is slightly higher than the "Maximum Expected" criterion, but 95% confidence prediction meets the "Design" criterion, primarily because a large design margin was chosen to accommodate the considerable uncertainties in the current design methods at the Preliminary Design stage. This example was chosen because it is anticipated to roughly reflect the current prediction of Ag-110m release from a GT-MHR core, based upon previous GA analysis of the PC-MHR operating with a 850 ^{o}C core outlet temperature. Silver release is of particular concern for a direct-cycle MHR because it can be diffusively released from intact TRISO particles at high temperatures and preferentially deposit on the turbine, where it is predicted to be a dominant contributor to operation and maintenance (O&M) dose rates (it is only a minor contributor to off-site dose rates because of its low effectivity).

There are several candidate options for resolving this design issue. The first option is simply to relax the "Maximum Expected" criterion and to design the plant to accommodate the currently predicted levels of 250-day Ag-110m release and the large uncertainties in the predictive methods; however, this option implies high O&M dose rates and the attendant requirements for

fully remote turbine maintenance, etc. Another option is to develop and qualify efficient decontamination protocols to reduce the dose rates from the turbine prior to refurbishment to levels permitting hands-on maintenance. A third option (dashed lines) is to reduce the predicted Ag release and the uncertainties therein by a combination of design optimization (primarily to reduce the nominal prediction) and technology development (primarily to reduce the uncertainty in the prediction).

Since diffusive release from intact particles is the dominant source of Ag release, the most effective design changes to reduce Ag release are those that reduce the peak fuel temperatures in the core. Some reduction in peak temperatures can be achieved by improved fuel zoning to optimize the core power distribution for minimum Ag release, and further reductions are possible with various fuel shuffling schemes. Larger fuel temperature reductions require more dramatic changes in the fuel-block design and/or in-core operating conditions (e.g., power density); such changes have broad implications for the overall plant design and fuel cycle costs.

A comprehensive trade study would be required to identify the optimal combination of the above options to resolve the plateout issue. In any case, it might be prudent to design a first-of-a-kind, direct-cycle HTGR to permit fully remote turbomachine maintenance should the actual O&M dose rates prove to be higher than predicted. Furthermore, the option of having a spare turbomachine to permit extended delay times prior to turbomachine refurbishment should also be evaluated during conceptual design.[5]

2.4 Helium Purification System Design and Performance

In order to avoid deleterious effects on structural materials, undesirable chemical impurities present in the primary coolant must be controlled; consequently, all HTGR designs, including modern VHTR designs, include a helium purification system. Principally, the chemical impurities involved are:

1. H_2O, N_2, and O_2 from graphite outgassing;
2. H_2O, CO, CH_4, CO_2 and H_2 from water ingress and its subsequent reaction with graphite;
3. H_2 and CH_4 from reaction of oil contaminants with graphite;
4. N_2 and O_2 from air ingress during maintenance and venting operations.

---

[5]After five years, only 0.6% of 250-d Ag-110m would remain; however, 19% of 2.1-yr Cs-134 would remain, and 30-yr Cs-137 would be effectively unchanged. Nevertheless, there is reason to believe that the Cs isotopes can be efficiently removed by standard decontamination protocols [e.g., Hanson 2002b].

Source #2 will be of much less importance for direct-cycle GT-MHRs and for hydrogen-producing VHTRs with an intermediate heat exchanger because of the absence of a steam-generator in the primary circuit which is typically the primary source of water ingress for a steam-cycle HTGR (FSV with its water-bearing circulators was an exception). Source #3 has been practically eliminated for modern MHR designs wherein magnetic bearings have replaced oil-lubricated bearings.

While the primary purpose of the HPS is to control chemical impurities, it also serves to remove radionuclides from the circulating helium coolant, including noble gases and tritium. The HPS also removes condensable radionuclides, including iodine isotopes and volatile fission metals (Ag, Cs, Sr, etc.), but these condensable radionuclides typically deposit on the He-wetted surfaces in the primary coolant circuit much more rapidly than they are removed by the HPS.

Typically, the HPS consists of a number of unit operations to efficiently control the chemical and radioactive impurities in the primary coolant, including tritium. The HPS for the commercial GT-MHR is briefly described below as an example [Shenoy 1996]. It is anticipated that the HPS design for the VHTR will be quite similar to that for the GT-MHR although the mass flow rates for the two plant designs may be different.

The GT-MHR HPS operates to remove helium from the primary coolant loop, process it to remove chemical and radioactive impurities, and return the purified helium to the primary coolant loop as purge helium for turbomachinery seals, vessel seals, and vessel pressure relief piping (and possible use for reactor pressure vessel cooing). In addition, the HPS operates in conjunction with the helium transfer and storage train to pressurize, depressurize, and control the primary coolant inventory consistent with plant load.

For a four-module, commercial GT-MHR, the HPS consists of four helium purification sections and two shared regeneration sections [Shenoy 1996]. Each helium purification section purifies a side stream of primary coolant helium at a maximum rate of 0.567 kg/sec (4500 lb/hr) and the regeneration section regenerates spent absorber beds within the helium purification section. One He purification section is provided for each reactor module, while one regeneration section is shared by two reactor modules. A block diagram of the helium purification section is shown in Figure 2-3. The system is a He processing train consisting of filters, dryers, packed beds, and heat exchangers. With the exception of the He compressors and He isolation valves, there are no moving parts which assures that the system that has high reliability and availability.

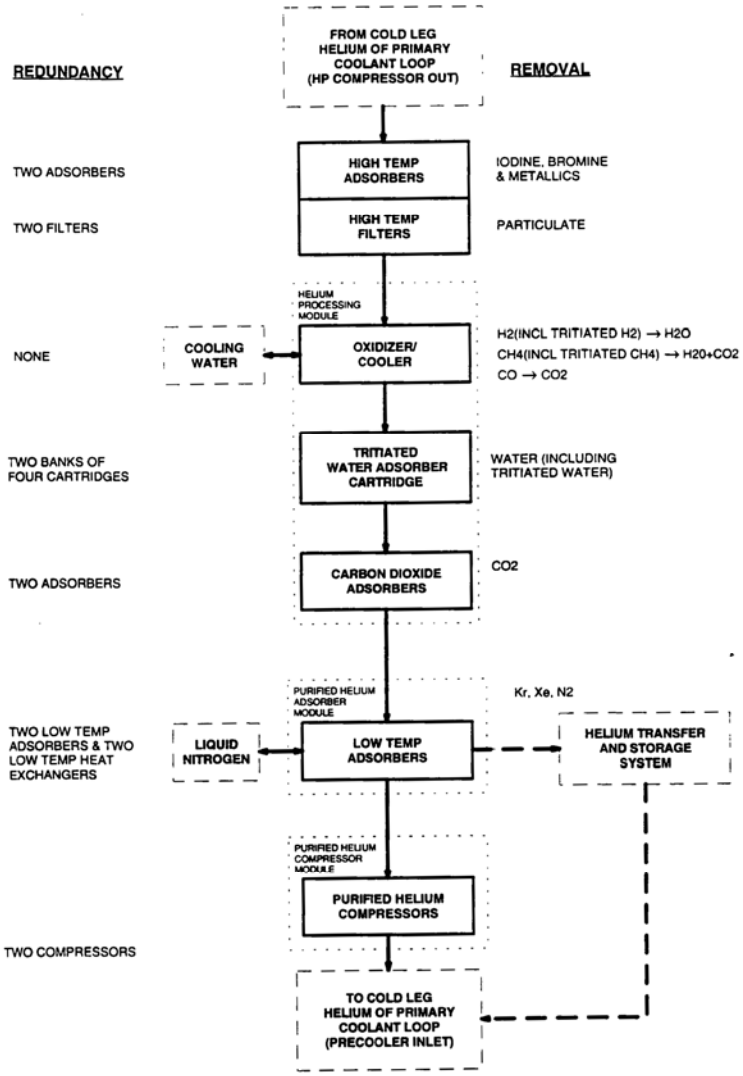

Figure 2-3. Block Diagram of HPS for GT-MHR

With such a design, control of hydrogen and tritium is accomplished by the use of copper oxide beds to oxidize the H_2 and HT to H_2O and HTO, respectively. The tritiated water is subsequently removed by molecular sieve dryers downstream of the oxidizers. Any trace amounts of HT or HTO remaining in the helium will be completely removed by the liquid nitrogen-cooled charcoal beds which are included in the train primarily to remove noble gases.

All operating HTGRs have utilized an HPS design which included oxidizer beds for the removal of hydrogen and tritium with the exception of Fort St. Vrain. Instead of oxidizer beds, the FSV HPS used titanium sponge getter beds for the removal of hydrogen and tritium. These Ti getter beds frequently became deactivated by CO and N_2 impurities present in the primary helium. However, the practical consequences for FSV operation were negligible because the core graphite proved to be a far more efficient sink than the HPS for the removal of hydrogen and

tritium from the coolant. Nevertheless, all subsequent GA HPS designs have utilized oxidizer beds and dryers for controlling hydrogen and tritium, and the future use of Ti getters is not recommended based upon the FSV experience.

2.5 Tritium Transport in the NGNP

A radionuclide containment issue of special interest for the NGNP is the containment of tritium [e.g., Hanson 2006b]. Tritium will be produced in an HTGR by various nuclear reactions. Tritium is extremely mobile, especially at high temperature. It permeates and/or diffuses through most solid materials, including ceramics and metals. While tritium does permeate through most solid materials, the permeation rates can vary by many orders of magnitude as illustrated in Figure 2-4.

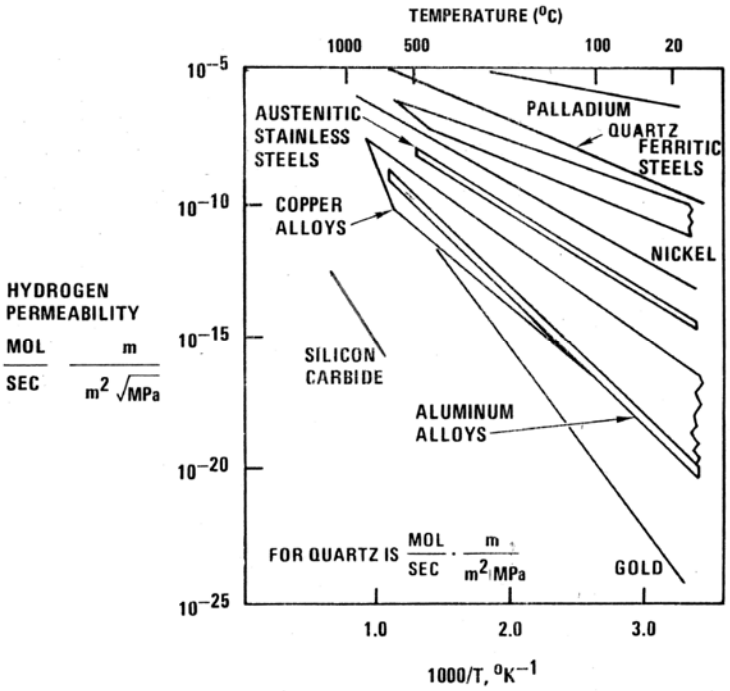

Figure 2-4. H-3 Permeabilities of Various Materials

Given its high mobility, especially at high temperatures, some tritium will permeate through the IHX and hydrogen process vessels, contaminating the product hydrogen and process steam. This tritium contamination will contribute to public and occupational radiation exposures; consequently, stringent limits on tritium contamination in the product hydrogen are anticipated to be imposed by regulatory authorities. Design options are available to control tritium in an HTGR, but they can be expensive so an optimal combination of mitigating features must be implemented in the design.

The following sources of tritium production have been identified, primarily from early surveillance programs at operating HTGRs (steam-cycle plants), and they can be reasonably quantified for the NGNP: (1) ternary fission, (2) neutron activation of He-3 in the primary He coolant, (3) neutron activation of lithium impurities in fuel-compact matrix and core graphite, and (4) neutron capture reactions in boron in control materials. Ternary fission will be the dominant source of tritium production, but much this tritium will be largely retained in the TRISO-coated fuel particles. He-3 activation will generate a relatively modest fraction of the total tritium production in the reactor; however, since it is born in the primary coolant, it will likely be an important source of tritium in the primary helium and, hence, a major source of product contamination as well.

Tritium strongly chemisorbs on irradiated nuclear graphite at elevated temperatures (the sorptivity of unirradiated graphite is much lower). Consequently, a large fraction of the tritium entering the primary helium will be sorbed on the huge mass graphite in the core. In operating HTGRs, including Fort St. Vrain, the core graphite was a far more important sink for tritium removal than the helium purification systems. However, a large fraction of this stored tritium can be released if water is introduced into the primary coolant (a low-probability event for a VHTR with an IHX).

Tritium will permeate through the heat exchangers and process piping in an H2-MHR and will contaminate the product hydrogen. Surface films will play a critically important role in establishing the in-reactor, tritium permeation rates. Oxide films can reduce H-3 permeability by orders of magnitude. However, normal plant operating transients (e.g., startup/shutdown, etc.) may compromise film integrity and result in increased H-3 permeation rates.

Design methods are available to estimate H-3 production, distribution, and release, but they are rudimentary and characterized by large uncertainties [Myers 1987, Hanson 2006a]. The current design methods appear adequate for Preconceptual and Conceptual Design, but they will need to be upgraded for Preliminary Design and independently validated prior to completion of Final Design. Some technology development will be necessary to provide the basis for these design methods improvements and validation.

2.6 Scope of Work

As defined in [Work Plan 2007], the scope of this study includes the following subtasks:

1. Plant Tritium Source Term and Limits

a. Identify the various sources of tritium production in a VHTR.
b. Identify tritium transport pathways for two plant configurations.[6]
c. Review top-level regulatory requirements.
d. Recommend allowable limits on tritium contamination in the product streams and plant waste streams to assure compliance with regulatory requirements.

2. Radionuclide Source Terms and Limits
   a. Identify the various sources of radionuclide production in a VHTR.
   b. Review top-level, radionuclide control requirements.
   c. Estimate in-service fuel service conditions from previous core design studies.
   d. Derive the allowable limits on RN contamination in product streams and plant waste streams from top-level regulatory requirements, including off-site dose limits and occupational exposure limits.
   e. Derive limits on RN release from the core during normal operation from allowable contamination limits.
   f. Derive limits on in-service fuel failure and as-manufactured fuel quality requirements from the RN release limits.

3. Limits on Dust Production
   a. Identify various sources of possible dust production in a VHTR.
   b. Review and assess past HTGR operating experience with dust production and behavior and its relevance to the NGNP.
   c. Identify potentially deleterious effects of dust on primary components (e.g., erosion, heat exchanger fouling, etc.).
   d. Evaluate the deleterious effects of particulate matter in other high-temperature gas systems (e.g., combustion turbines, coal plants, etc.) for relevance to the NGNP.
   e. Recommend conservative limits on dust production and accumulation in the primary heat transport system of the NGNP.

4. Plant Mass Balance for Tritium & Radionuclides
   a. Define the overall plant configuration and basic operating parameters (provided by the PCDSR and other Phase 2 studies).
   b. Using the source terms and limits derived in Subtask 1, calculate an overall plant mass balance for tritium with the TRITGO code (H-3 inventory in the core, in the primary coolant, in the helium purification system, and in the process and waste streams).

---

[6] Three plant configurations were actually evaluated (see Section 8).

c. Using the source terms and limits derived in Subtask 2, calculate an overall plant mass balance for radionuclides with the RADC code.
d. Perform sensitivity studies will be performed be as necessary to identify dominant variables for both the tritium and radionuclide mass balances to provide guidance to plant optimization studies.

5. Design Options for Tritium & Radionuclide Control
   a. Realistic limits on H-3 contamination of product hydrogen (while perhaps more of a prerequisite than a design option, realistic limits on allowable H-3 contamination in the product hydrogen are nevertheless critically important).
   b. Stringent limits on Li impurities in core materials.
   c. Coated B_4C granules in control materials.
   d. Increased He purification rate in primary loop.
   e. Purification system for secondary loop.
   f. Customized coolant chemistry in the secondary loop.
   g. Permeation resistant coatings on heat exchanger surfaces

6. Reporting

2.7 Assumptions

A number of key assumptions had to be made before the study could be performed; these assumptions are summarized here and repeated throughout the body of the report as they apply.

Assumptions

1. The NGNP will have a thermal power of 600 MW (i.e., full commercial scale).
2. The NGNP will employ a prismatic core.
3. The plant will be designed for periodic operation with a core outlet temperature of 950 ^{o}C; however, sustained plant operation will be at ≤900 ^{o}C
4. Both SI and HTE H_2 demonstration plants will be included in the NGNP.
5. The reference NGNP fuel will be TRISO-coated UCO particles designed for high burnup; the fuel for the initial core and first few reloads may be low burnup TRISO UO_2 particles.
6. Unprocessed, spent MHR fuel elements will be the final waste form.
7. Helium will be the coolant in the secondary heat transport circuit.
8. A upper-bound core outlet temperature of 950 ^{o}C will provide a conservative estimate of the tritium permeation rates through the plant heat exchangers.
9. H-3 contamination of the product hydrogen can be controlled to acceptable levels.
10. The NGNP plant site will have a 425-m Exclusion Area Boundary (i.e., commercial utility site characteristics).

11. Previous GT-MHR (gas turbine) and MHTGR (steam cycle) studies are applicable to NGNP.
12. The currently available design methods are adequate for pre-conceptual and conceptual design but will require significant upgrading or replacement for preliminary and final design.
13. The current NGNP technology programs will be modified and supplemented as required to address the Design Data Needs identified by plant designers and regulatory authorities.

2.8 Report Organization

As indicated in Section 2.1, the purpose of this study is to establish provisional limits on RN contamination throughout the NGNP with particular emphasis on tritium since it can permeate through heat exchangers and contaminate the product hydrogen in a H2-MHR and the process steam in a steam-cycle plant. This report is intended to be a stand-alone document although the reader is encouraged to acquire key references that are called out in the various sections.

The report is organized somewhat differently than the workscope presented in the Work Plan (see Section 2.6) to improve the logic and continuity. After the introductory and background information presented here in Section 2, the top-level regulatory and user requirements as presented in the [Systems Requirements Manual (SRM) 2007] that mandate radionuclide control are summarized in Section 3. The sources and provisional limits on radionuclide contamination, tritium contamination and particulate matter are addressed in Sections 4, 5 and 6, respectively. The calculated plant mass balances for radionuclides and for tritium are presented in Sections 7 and 8, respectively. The design options for controlling radionuclide contamination, especially tritium, are described in Section 9. The adequacy of the current NGNP technology programs to assure that the provisional limits given in Sections 4, 5 and 6 can be met to the satisfaction of future H2-MHR customers and regulatory authorities is assessed in Section 10. The adequacy of the current design methods to support NGNP design and licensing is assessed in Section 11. Finally, a series of conclusions and recommendations are presented in Section 12.

3. TOP-LEVEL RADIONUCLIDE CONTROL REQUIREMENTS

The System Requirements Manual (SRM) is intended to be the top-level design document for the NGNP. The SRM serves as the roadmap document that identifies the source of the NGNP top-level requirements (i.e., mission needs and objectives) and how these top-level requirements flow down through subordinate requirements at the plant, system, subsystem, and ultimately the component level. Design requirements for the NGNP include both institutionally imposed and functionally derived requirements. Each pre-conceptual engineering services contractor prepared an SRM as part of its Phase 1 workscope.

The System Requirements Manual prepared by GA [SRM 2007] has adopted a particular protocol for identifying requirements which is reproduced here: "If the plant-level requirement is an institutional requirement, the source of the requirement is given in brackets following the requirement. If a source is not shown following the statement of the requirement, the requirement is a functionally derived requirement. A number is assigned to each requirement for identification purposes. The identification number has the format 3.x.y where 3.x is the SRM section number and y is the requirement number. If a requirement is subordinate to a higher-level requirement (i.e., it stems from the higher-level requirement), the subordinate requirement has the format 3.x.y.z, where 3.x.y is the identification number for the higher-level requirement and z is the unique number for the subordinate requirement. Brackets { } are used herein to identify a value that is preliminary in nature because of design uncertainty or insufficient documentation, or that requires verification."

3.1 Plant-Level Requirements

The plant-level requirements given in Section 3 of the GA-prepared SRM have been reviewed, and those judged to *directly* impact contamination control reproduced in this section. Consistent with the SRM, requirements that are specific to achievement of the six NGNP high-level functions (F1 - F6 below) are grouped by function. The various references cited in the requirements are identified in Table 3-1. In some cases, the decision to include or exclude a certain requirement was rather arbitrary; in any case, the plant design will have to meet all of the requirements whether they are included here or not.

Table 3-1. SRM References Cited in Requirements

Ref. 2	"Next Generation Nuclear Plant – High Level Functions And Requirements," INEEL/EXT-03-01163, Idaho National Laboratory, September 2003
Ref. 9	"Utility/User Incentives, Policies, and Requirements for the Gas Turbine-Modular Helium Reactor," DOE-GT-MHR-100248, Rev. 0, Technology Insights, September 1995

F0. Overall Plant-Level Requirements

PLT 3.0.9 - The NGNP shall be designed for an operating life of 60 calendar years from the date of authorization to operate. Provisions shall be made for economic replacement of components that cannot be designed for 60-year operation. [Ref. 2, Section 3.1.11; U/U Requirement, Ref. 9, Section 3.1.2 and SRM Section 2.3.5, Fig. 1].

F1. Develop and Demonstrate a Commercial-Scale Prototype VHTR

PLT 3.1.1.1 – The NGNP reactor shall consist of a graphite moderated, prismatic block core. [Ref. 2, Sections 3.1.3 and 3.1.5].

PLT 3.1.1.3 – The NGNP shall use qualified TRISO-coated uranium oxycarbide (UCO) or uranium dioxide fuel. The fuel particles shall be agglomerated into cylindrical compacts. Qualified uranium dioxide fuel may be acceptable for initial fuel loading, but shall be replaced by UCO, when it is has been qualified. [Ref. 2, Sections 3.1.7 and 3.1.10]

PLT 3.1.1.6 - The NGNP shall include a helium purification system to maintain the helium coolant purity.

PLT 3.1.2.1 - The reactor shall have a nominal power level of 550 MW(t) with a stretch capability to about 600 MW(t).

PLT 3.1.8 – The NGNP shall be designed to achieve fuel burn up consistent with maximum fuel utilization while minimizing waste streams, optimizing fuel economics, and ensuring low proliferation risk. [Ref. 2, Section. 3.1.9].

PLT 3.1.9 - The NGNP shall be designed to satisfy the following top-level radionuclide control regulatory requirements:

- During normal operation, offsite radiation doses to the public shall be < limits specified in Appendix I of 10 CFR 50 and 40 CFR 190
- Occupational radiation exposures shall be ≤10% of the limits specified in 10 CFR 20
- During DBAs, offsite doses at the site EAB shall be less than those specified in the Manual of Protective Action Guides and Protective Actions for Nuclear Incidents (EPA-520/1-75-001) for sheltering and evacuation

[Ref. 9, Section 3.1.13 and U/U Requirement, SRM Section 2.3.5, Fig. 1].

PLT 3.1.10 - The design of the NGNP systems and processes shall be such that the volume of low-level radioactive dry and wet waste, as shipped off-site, shall be less than 3.6 m^3, annually (excluding replaceable reflector elements). [U/U Requirement, SRM Section 2.3.5, Fig. 1].

PLT 3.1.11.6 - The NGNP shall be designed to demonstrate a probability of $<5 \times 10^{-7}$ per plant year that offsite doses at or beyond the site EAB of 425 meters will [not] exceed the limits specified in the Manual of Protective Action Guides and Protective Actions for Nuclear Incidents (EPA-520/1-75-001) for sheltering and evacuation. [U/U Requirement, SRM Section 2.3.5, Fig. 1].

PLT 3.1.11.7 - The NGNP shall be designed to demonstrate that plant personnel exposure of <70 person-rem/GW_e-year. [U/U Requirement, SRM Section 2.3.5, Fig. 1].

PLT 3.1.11.14 - The NGNP design shall include provisions for satisfying the plant decommissioning requirements as specified in Section 3.12 of Ref. 9. [U/U Requirement, Ref. 9, Section 3.11].

F2. Develop and Demonstrate High-Efficiency Power Conversion

None identified that impact the scope of the current contamination control study.

F3. Obtain Licenses and Permits to Construct/Operate the NGNP

None identified that impact the scope of the current contamination control study.

F4. Develop and Demonstrate Hydrogen Production

PLT 3.4.1 - Hydrogen production shall be demonstrated using a thermo chemical process and a high-temperature steam electrolysis (HTE) process. [Ref. 2, Section 3.4.2]

PLT 3.4.1.1 - The thermo chemical process to be demonstrated by the NGNP shall be the sulfur-iodine (SI) process.

PLT 3.4.2.5 - Leakage of the working fluid used to transport the heat shall be less than {10%} per year. Radionuclide release associated with working fluid leakage shall be within occupational and public dose limits specified in 10 CFR 20.

PLT 3.4.5 - The interface system between the NGNP and the hydrogen production plants shall be designed to ensure that tritium migration into the hydrogen production systems will be limited, such that the maximum amount of tritium released from the integrated NGNP facilities or found in drinking water does not exceed EPA standards. [Ref. 2, Section 3.4.5].

PLT 3.4.6 - The total concentration of radioactive contaminants in the hydrogen product gas and associated hydrogen production systems shall be minimized to ensure that worker and public dose limits for the integrated NGNP and hydrogen production facilities do not exceed NRC regulatory limits. [Ref. 2, Section 3.4.6].

PLT 3.4.8.2 - Emissions from the hydrogen plant shall comply with all applicable requirements of the Clean Water Act/Water Programs (CWA), 40CFR100-149, as well as compliance with all state and local requirements. [Ref. 2, Section 4.1.2]

F5. Include Testing Provisions

PLT 3.5.8 – For demonstration of commercial plant radiological source terms, the NGNP shall be designed to experimentally determine the fission product activity that could potentially be released should there be a rupture in the primary coolant boundary. [PLT 3.1.9; PLT 3.1.11.6].

F6. Enable Demonstration of Energy Products and Processes

PLT 3.6.4.1 - Provisions shall be included in the design of the NGNP to add capability to produce ≥540°C (1000°F) steam to develop/demonstrate the production of process steam to displace coal, oil and natural gas use in process industries such as petrochemical plants, refineries, aluminum mills, and steel mills.

PLT 3.6.4.2 - The provisions made in the NGNP design to add steam production capability shall be equally adaptable to adding additional capability for high temperature process heat to develop/demonstrate production of reducing gas for steel making, substitute pipeline gas, ammonia and methanol.

PLT 3.6.4.3 - The NGNP shall include provisions to add process systems (e.g., a steam-methane reformation process for H_2 production and/or a methanol production process) to develop/demonstrate the utilization of process steam and/or process heat produced by the NGNP.

3.2 System-Level Requirements

The SRM allocates the plant-level requirements to the individual plant systems, buildings and structures. Inclusion here of system-level requirements that are obvious reproductions of plant-level requirements is not, in general, considered necessary for the purpose of this report. However, certain system-level requirements do provide a degree of specificity that is not obvious from the parent plant-level requirements, and they are reproduced below by system. In any case, the various systems will have to meet all of the requirements assigned to them in the SRM.

Reactor System (11)[7]

The reference fuel cycle shall be based on the use of a once-through uranium fuel cycle with U-235 enrichment no greater than 19.9%.[8]

The Reactor System shall achieve fuel burn up consistent with maximum fuel utilization while minimizing waste streams, optimizing fuel economics, and ensuring low proliferation risk

The Reactor System shall be capable of utilizing alternate fuel cycles (Pu fuel, deep-burn of LWR spent fuel, etc.).

Primary Helium Purification Subsystem (24)

The helium purification trains shall be designed to remove the following major chemical impurities: CO, CO_2, H_2 (including tritium), N_2, 0_2, H_2S, CH_4, and other hydrocarbons. Lesser amounts of impurities such as Br, I, H_2O, Kr, and Xe shall also be removed along with filterable particulates and certain metallic elements.

Each helium purification train shall process the primary coolant helium at a constant volumetric flow rate regardless of the primary coolant system pressure. At 100% of rated reactor power and vessel system pressure, the helium purification subsystem shall process primary coolant at a rate of (TBD) kg/s.

Each helium purification train shall be sized such that the fraction of radionuclide activity removed from the circulating primary coolant is 2.9×10^{-5} per second.

---

[7] The number in parenthesis after the system name is the system number as defined in the SRM.
[8] The system-level requirements in the SRM are not numbered at this writing.

Plant Monitoring System (35)

Analytical instrumentation shall be capable of detecting and quantifying certain specific chemical and radioactive impurities circulating in the primary coolant helium.

Condensable radionuclide analyses shall be accomplished by means of plate-out probes located in the hot circulating primary coolant flow stream.

Secondary Heat Transport System (42)

A helium purification system similar to that designed for the primary coolant helium shall be provided to maintain the purity of the secondary loop helium. This purification system shall be installed in the Reactor Service Building adjacent to the primary coolant purification system to minimize duplication of services required by the systems.

Leakage of the working fluid used to transport the heat shall be less than {10%} per year. Radionuclide release associated with working fluid leakage shall be within the occupational and public dose limits specified in 10CFR20.

SI-Based Hydrogen Production System (43)

None identified that impact the scope of the current contamination control study.

HTE- based Hydrogen Production System (44)

None identified that impact the scope of the current contamination control study.

Reactor Complex (51)

Following a reactor vessel depressurization event, and the attendant building pressure equalization, the Reactor Building shall confine and/or filter for release the gaseous contents. The release rate shall be equal to or less than one building volume/day.

4. RADIONUCLIDE SOURCE TERMS AND LIMITS

Stringent top-level radionuclide control requirements are anticipated for the NGNP (e.g., meet PAGs at the EAB, etc.). Limits on radionuclide release from the core that are consistent with these top-level RN control requirements are needed in order to derive allowable in-service fuel failure and as-manufactured fuel quality requirements (e.g., allowable SiC coating defects, etc). The requirement for a 950 ^{o}C core outlet temperatures will likely result in fuel temperatures during normal operation that will push TRISO fuel particles to near its performance limits.

4.1 Sources of Radioactive Contamination

The dominant source of radioactive contamination in an MHR will be relatively modest quantities of radionuclide release from the core [e.g., PSID 1992]. *In situ* activation of structural materials will be limited and the activation products will be fixed. There will be no analog in the NGNP to radioactive "crud" in water-cooled reactors since the helium coolant is chemically inert.

As introduced in Section 2, the two dominant sources of fission product release from the core are as-manufactured, heavy-metal contamination and failed particles. In addition, the volatile metals (e.g., Cs, Ag, Sr) can, at sufficiently high temperatures for sufficiently long times, diffuse through the SiC coating and be released from intact TRISO particles; however, diffusive release from intact particles during normal operation is only significant compared to other sources for silver and tritium release. Fission products resulting from fissions in HM contamination outside of the particles are obviously not attenuated by the kernels or coatings, nor are the fission products produced in the kernels of failed particles appreciably attenuated by the failed coatings. In these cases, the fission products must be controlled by limiting the respective sources and by the fuel-element graphite in the case of the fission metals and actinides.

Expressed in the simplest terms, the fractional release of a radionuclide from the core is given by the following relationship:

$$(f.r.)_{core} = \frac{C(f.r.)_c + F(f.r.)_F + [1-C-F](f.r.)_D}{AF_{graphite}} \qquad (4\text{-}1)$$

where:

- $(f.r.)_{core}$ = fractional release from core
- C = heavy-metal contamination fraction
- $(f.r.)_C$ = fractional release from contamination
- F = failure fraction

$(f.r.)_F$ = fractional release from failed particles
$(f.r.)_D$ = fractional diffusive release from intact particles
$AF_{graphite}$ = graphite attenuation factor[9]

In reality, the problem of calculating the full-core fractional release is much more complicated than implied by Eqn. (4-1). For example, the fissile and fertile particle failure fractions are generally different and vary in space and time, the fractional releases from contamination and failed particles and graphite attenuation factors vary in space and time, and "partially" failed particles (i.e., particles with a failed SiC coating but with intact inner and/or outer pyrocarbon coatings) must also be considered. Full-core computer codes are needed to keep track of all these effects; nevertheless, the results given by Eqn. (4-1) are quite intuitive.

4.2 Radionuclide Source Terms

The most important consideration in predicting the radionuclide release rates from an MHR core is to predict the in-service performance of the TRISO-coated fuel particles. However, it is impractical to rely exclusively on the fuel particle coatings for radionuclide containment. Consequently, the effectiveness of the other radionuclide release barriers in the RN containment system must also be quantified.

4.2.1 *Fuel Failure Mechanisms*

During the past four decades of coated-particle fuel development and demonstration, a number of mechanisms have been identified - and quantified – which can compromise the capability of the coated fuel particles to retain radionuclides (i.e., functional failure of the coated particle). A considerable number of documents have been prepared on the topic of coated particle failure mechanisms; IAEA TECDOC-978 [1997] provides a good summary along with an extensive bibliography.

The following failure mechanisms have been identified as capable of causing partial or total failure of the TRISO coating system under irradiation and during postulated accidents; these mechanisms are shown schematically in Figure 4-1. Phenomenological performance models, typically inspired by first principles and correlated with experimental data, have been developed to model each of these mechanisms. Design methods incorporating these models have been developed to predict fuel performance and fission product release from the reactor core into the primary coolant.

---

[9] Graphite attenuation factor = fission product release from fuel compact/release into coolant.

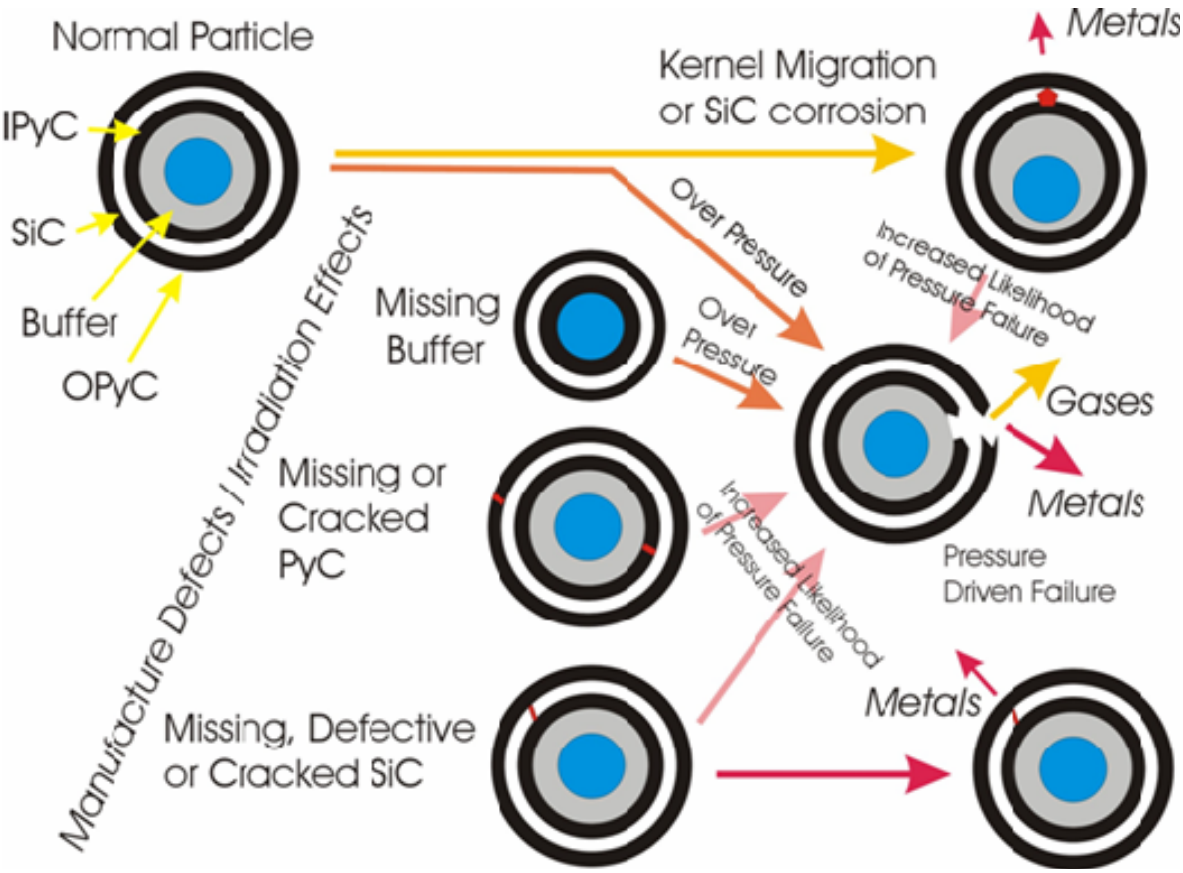

Figure 4-1. TRISO Particle Failure Mechanisms

1. Coating damage during fuel manufacture, resulting in HM contamination on coating surfaces and in the fuel compact matrix.
2. Pressure vessel failure in standard particles (i.e., particles without manufacturing defects).
3. Pressure vessel failure in particles with defective or missing coatings.
4. Irradiation induced failure of the OPyC coating;
5. Irradiation induced failure of the IPyC coating and potential SiC cracking;
6. Failure of the SiC coating due to kernel migration in the presence of a temperature gradient.
7. Failure of the SiC coating caused by fission product/SiC interactions.
8. Failure of the SiC coating by thermal decomposition.
9. Failure of the SiC coating due to heavy-metal dispersion in the IPyC coating.

These particle failure mechanisms will not be discussed in any detail here. The interested reader is encouraged to consult the large number of technical reports and journal articles on the topic. As stated previously, TECDOC-978 is a good point of departure.

4.2.2 *Radionuclide Release Mechanisms*

As with fuel particle failure, a number of mechanisms have been identified - and quantified – which govern the transport of radionuclides in HTGR core materials, and a large number of documents have been prepared on the topic. Especially notable is Dragon Project Report DP-828, Part III, which provides a comprehensive set of transport models along with analytical solutions for many bounding cases [Nabielek 1974]; this report remains as useful today as it was three decades ago despite the development of numerical methods for predicting fission product transport. Once again, TECDOC-978 [1997] provides a good summary of radionuclide transport phenomena in HTGR core materials along with an extensive bibliography.

The transport of radionuclides from the location of their birth through the various material regions of the core to their release into the helium coolant is a relatively complicated process. The principal steps and pathways are shown schematically in Figure 4-2. For a pebble-bed core, those steps related to transport across the gap between the fuel compact and the fuel-element and transport in the fuel-element graphite are eliminated. Also for certain classes of radionuclides, some steps are eliminated (e.g., noble gases are not diffusively released from intact TRISO particles, but noble gases are not significantly retarded by the compact matrix or fuel-element graphite).

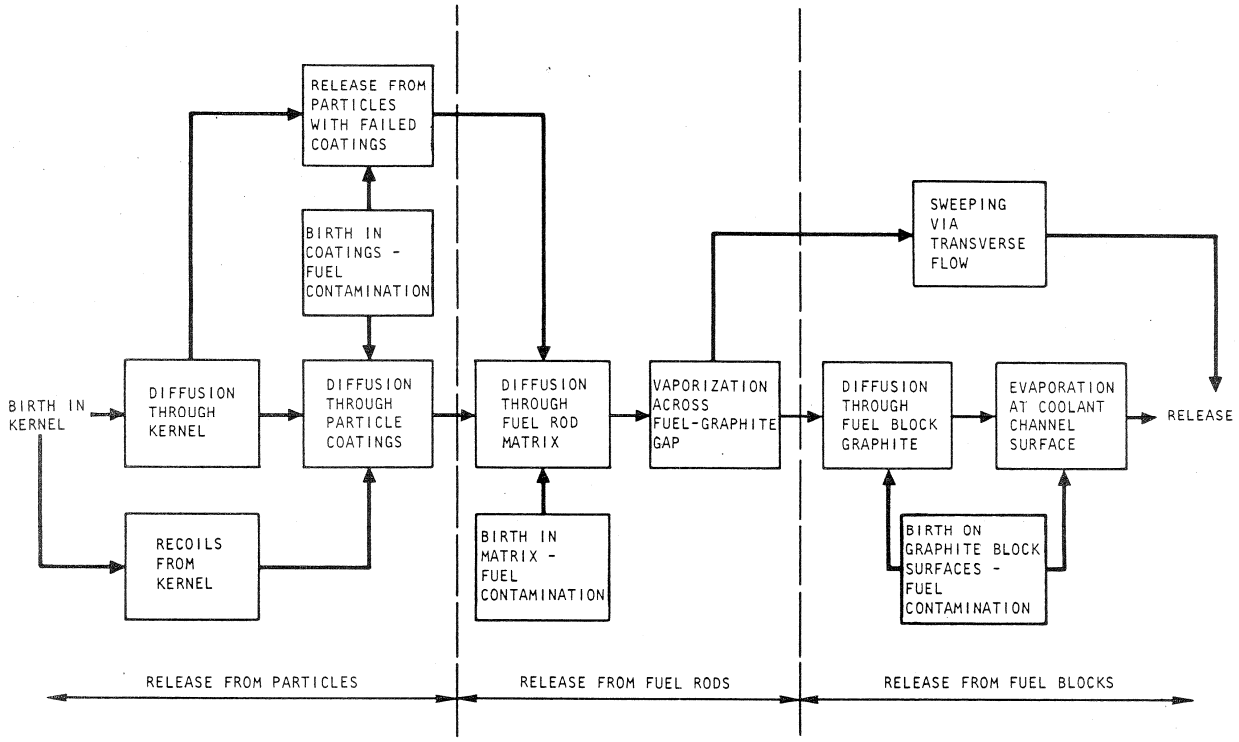

Figure 4-2. Principal Steps in Radionuclide Release from an HTGR Core

As implied by Eqn. (4-1), radionuclide transport must be modeled in the fuel kernel, in the particle coatings, in fuel-compact matrix, and fuel-element graphite. While the actual radionuclide transport phenomena in an HTGR core are complex and remain incompletely characterized after four decades of modeling efforts, the basic approach remains unchanged; radionuclide transport is essentially treated as a transient solid-state diffusion problem with various modifications and/or additions to account for the effects of irradiation and heterogeneities in the core materials. The point of departure is Fick's first law of diffusion which in slab geometry simply postulates that the diffusive flux is proportional to the negative concentration gradient with the proportionality constant being the diffusion coefficient:

$$\phi = -D\frac{\partial c}{\partial x} \quad , \tag{4-2}$$

The mass balance equation in slab geometry, ignoring for the moment source and radioactive decay, relates the difference in mass flux across a differential volume to the change in concentration in the volume:

$$\frac{\partial c}{\partial t} = -\frac{\partial \phi}{\partial x} \quad , \tag{4-3}$$

Substituting Eqn. (4-2) into Eqn. (4-3) gives the transient diffusion equation, which is usually called Fick's second law of diffusion:

$$\frac{\partial c}{\partial t} = \frac{\partial}{\partial x}\left(D\frac{\partial c}{\partial x}\right) \quad , \tag{4-4}$$

where the variables in Eqns. (4-2) through (4-4) are:

ϕ = diffusive flux of atoms (atoms/cm^2-s)
D = diffusion coefficient (cm^2-s)
c = concentration of atoms (atoms/cm^3)
x = spatial coordinate (cm)
t = time (s)

For solid-state diffusion processes, the diffusion coefficient *D* is typically observed to be exponentially dependent upon the absolute temperature, and the familiar Arrhenius equation is generally used to fit the data:

$$D = D_o \, \mathbf{exp}\left(-E/RT\right) \quad , \tag{4-5}$$

where:
D_o = preexponential factor (D for $T \rightarrow \infty$) (cm^2/s)
E = activation energy (cal/mole)
T = absolute temperature (K)
R = gas constant (= 1.987 cal-mole/K)

For the present problem, radionuclides are produced by various nuclear reactions in the core, and the radiologically significant ones decay so that the mass balance equation (4-4) is generalized to include a source term and a decay term:

$$\frac{\partial c}{\partial t} = \frac{\partial}{\partial x}\left(D \frac{\partial c}{\partial x} \right) - \lambda c + s \quad , \tag{4-6}$$

where:

λ = decay constant (s^{-1})

s = volumetric source rate (atoms/cm^3-s)

To model the radionuclide transport in an HTGR core, the balance equations become more complicated by the addition of decay chains and the appropriate boundary and interface equations; nevertheless, the essence of these models is captured in Eqn. (4-6). The transport of the various classes of radionuclides (Table 4-1) in the kernels, coatings, matrix and graphite are considered in the following subsections.

Table 4-1. Classes of Radionuclides of Interest for HTGR Design

RN Class	Key Nuclide	Breathing DCF (Sv/Bq)	Form in Fuel	In-Core Behavior
Tritium	H-3	4.3×10^{-11}	Element (gas)	Permeates intact SiC
Noble Gases	Xe-133	~ 0	Element (gas)	Retained by PyC/SiC
Halogens	I-131	2.3×10^{-7}	Element (gas)	Retained by PyC/SiC
Alkali Metals	Cs-134	1.2×10^{-8}	Oxide-Element	Retained by SiC
Tellurium Group	Te-132	6.0×10^{-8}	Complex	Retained by PyC/SiC
Alkaline Earths	Sr-90	7.3×10^{-7}	Oxide-Carbide	High graphite retention
Noble Metals	Ag-110m	1.2×10^{-7}	Element	Permeates intact SiC
Lanthanides	La-140	4.2×10^{-9}	Oxide	Retained by graphite
Actinides	Pu-239	3.2×10^{-4}	Oxide-Carbide	Retained by graphite

4.2.2.1 Radionuclide Transport in Fuel Kernels

In general, the release of fission products from the fuel kernel is treated as a transient diffusion process. In spherical geometry, the generalized continuity equation (4-6) takes the form:

$$\frac{\partial c}{\partial t} = \frac{1}{r^2}\frac{\partial}{\partial r}\left(D\frac{\partial c}{\partial r}\right) - \lambda c + s \quad , \tag{4-7}$$

where r is the radius of the sphere.

The radiologically significant fission gases (e.g., 2.8-hr Kr-88) are typically short-lived, the production rates and release rates reach equilibrium quickly, and the steady-state, core service conditions change relatively slowly by comparison; consequently, steady-state approximations are typically used in core design and analysis methods for fission gas release during normal operation [e.g., Haire 1974]; these approximations are described below. In contrast, the key fission metals (e.g., 30-yr Cs-137) are typically long-lived, and transient analysis methods are necessary.

4.2.2.1.1 Fission Gas Release from Fuel Kernels

The release of fission gases from heavy-metal contamination and from fuel kernels is typically expressed in terms of the release rate-to-birth rate ratio (R/B); at steady-state, the R/B ratio is numerically equal to the fractional release. At steady-state, the R/B for isotope *i* of element *j* is calculated from the following relationship [e.g., Haire 1974]:

$$\left(R/B\right)_{ji} = 3\left(\frac{\xi_j}{\lambda_i}\right)^{1/2}\left[\coth\left(\frac{\lambda_i}{\xi_j}\right)^{1/2} - \left(\frac{\xi_j}{\lambda_i}\right)^{1/2}\right] \quad , \tag{4-8}$$

where:

$(R/B)_{ji}$ = fractional release for isotope *i* of element *j* from as-manufactured HM contamination or failed fuel particles

λ_i = decay constant for isotope i of element j (s^{-1})

ξ_j = diffusion parameter for chemical element j (s^{-1})

Equation (4-8) has been derived and discussed by several authors, but normally it is attributed to Booth. It is the steady-state solution of the diffusion equation in spherical coordinates assuming (1) constant birth rate and (2) zero concentration at the surface of the sphere. The diffusion parameter ξ_j is defined as $\xi_j = D_j/a^2$ where D_j is a diffusion coefficient characterizing release of a fission gas and where "a" is a characteristic distance through which the fission gases diffuse before release. The values of D_j and "a" are never used directly in core analysis. Rather, the fractional release (R/B) is determined from in-pile measurements, and this value is substituted into Eqn. (4-8) from which ξ_j is calculated. The fractional release of a radioisotope of a given element is dependent on its decay constant; for fractional releases (R/Bs) less than ~0.1 (i.e., small values of ξ/λ), Equation 4-8 can be approximated by:

$$\left(R/B\right)_{ji} = 3\sqrt{\left(\frac{\xi_j}{\lambda_i}\right)} \quad , \tag{4-9}$$

The gas release models give the R/Bs from contamination and failed particles as a function of chemical element, isotope half-life, temperature, and burnup. These functional dependencies are determined experimentally. At high irradiation temperatures, experimental fission gas release measurements show that the R/B is proportional to the square root of isotope half life as required by Eqn. (4-9); an example is given in Figure 4-3 which shows the measured fission gas release from Peach Bottom Core 2 (BISO-coated HEU (Th,U)C_2 fuel) and as-manufactured Fort St. Vrain fuel (TRISO-coated HEU (Th,U)C_2 fuel).

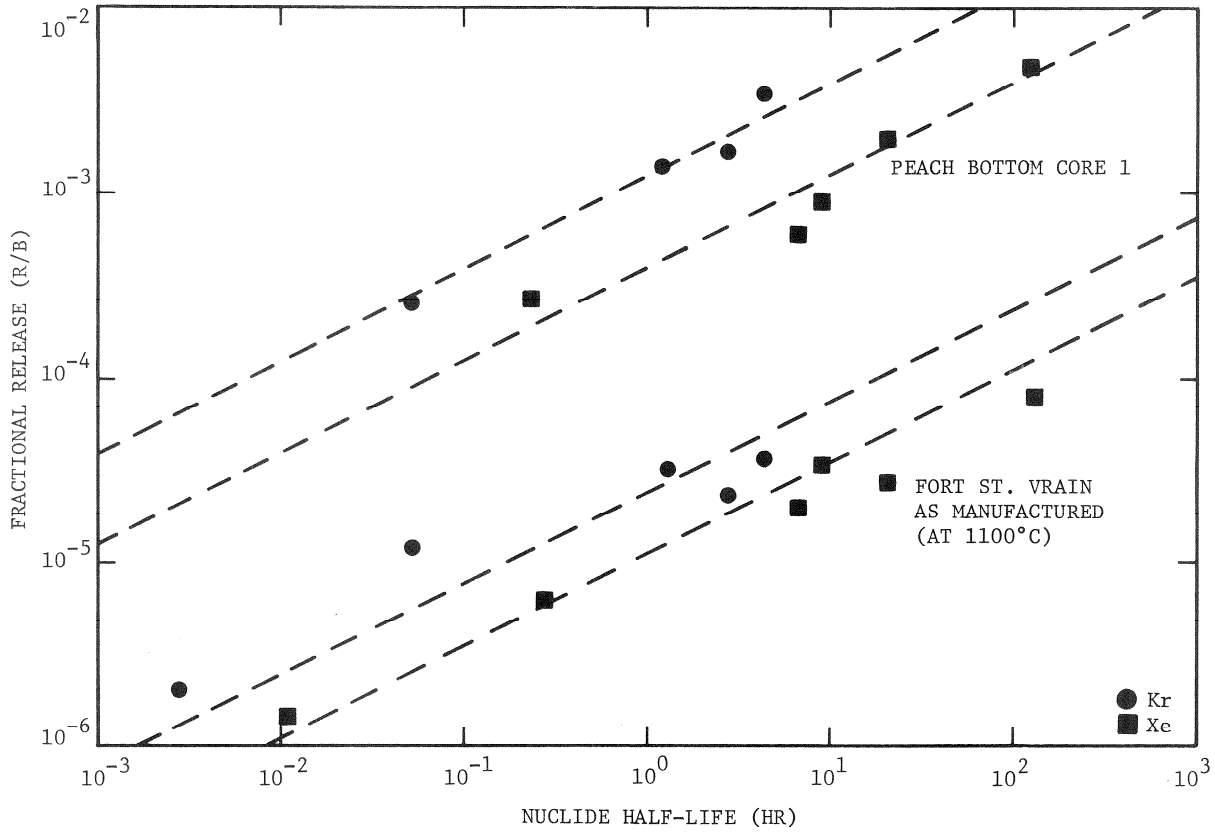

Figure 4-3. Isotopic R/Bs vs. Radioactive Half Life

While this observation is consistent with a diffusive release mechanism, the actual release mechanism is evidently much more complicated. For example, some fission fragments born near the exterior surface of the kernel are released by recoil, and high-energy neutrons produce irradiation-induced defects and other structural changes. In addition, gaseous fission products may become trapped at intrinsic or irradiation-induced defects to form bubbles which themselves migrate. In fact, at lower irradiation temperatures (say, <1000 °C) and at very high neutron fluxes, significant deviations from the square root-of-half life dependence are often

observed. Moreover, at lower temperatures, the R/Bs tend to plateau and become almost athermal as indicated in Figure 4-4; this transition is rationalized as the diffusive release component becoming small compared to the recoil component.

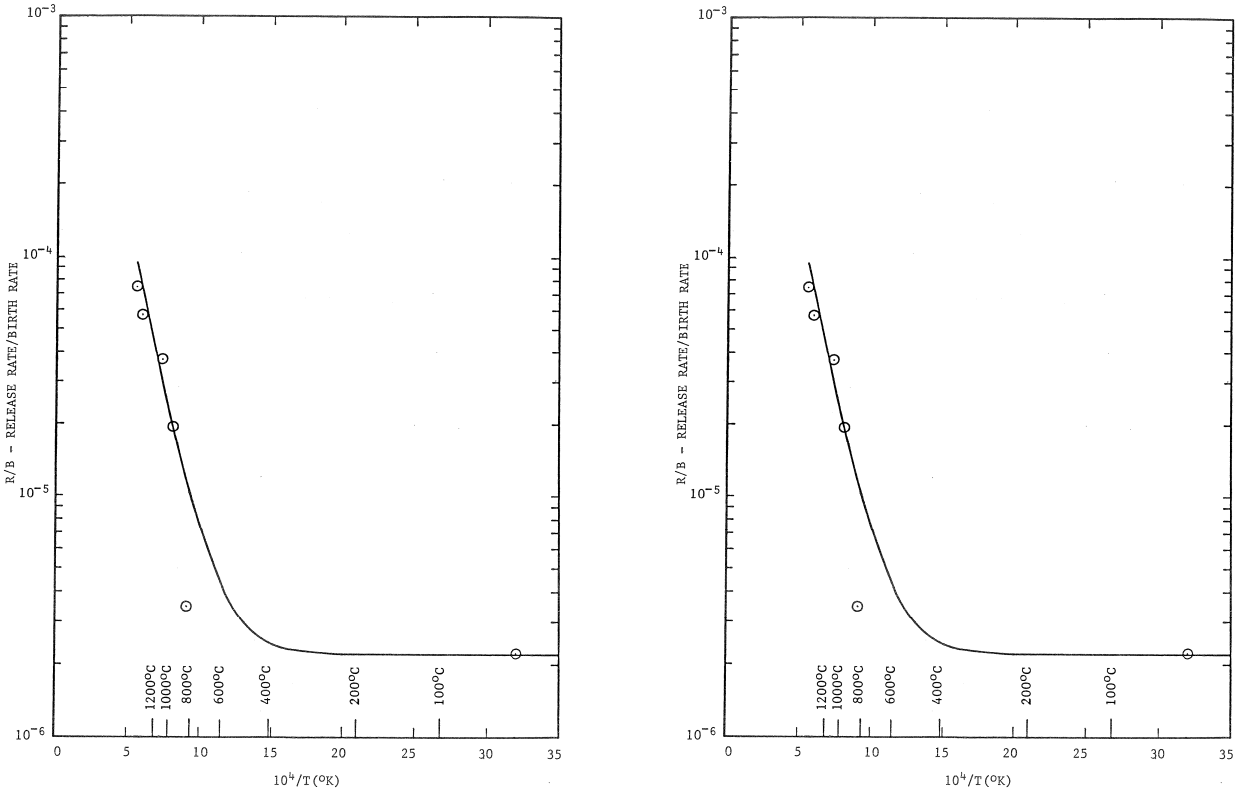

Figure 4-4. Temperature Dependence of Fission Gas Release

The modeling expedient for such complexities has typically been to add additional terms to Eqn. (4-9). For example, the reference GA gas release model [Myers 1987] starts with

$$\left(R/B\right)_{ji} = 3\sqrt{\left(\frac{\xi_j}{\lambda_i}\right)} \bullet f(T) \bullet f(Bu) \ ,$$

$$\left(R/B\right)_{ji} = 3\sqrt{\left(\frac{\xi_{o,j}}{\lambda_i}\right)} \bullet \left[A + (1-A) \bullet \exp\left\langle -\frac{E}{R}\left(\frac{1}{T}\right) - \left(\frac{1}{T_o}\right)\right\rangle\right] \bullet \left[1 + \sigma * Bu^n\right], \quad (4\text{-}10)$$

where:

Bu = burnup (% FIMA)
E = activation energy (J/mol)
R = gas constant (8.314 J/mol-K)
T = absolute temperature (K)
A, T_o, σ, n = constants

The values of the constants must be determined experimentally for each gaseous fission product element (Kr, Xe) and for each fuel kernel composition [Myers 1987].

The fractional releases of fission gases from exposed fuel kernels under irradiation can be enhanced if the kernel is hydrolyzed by reaction with trace amounts of water vapor which may be present in the helium coolant. The magnitude of the effect depends upon the kernel composition with UC_2 showing the largest enhancement and UO_2 showing the least; the effect for UCO is intermediate. With kernels containing uranium carbide, the water reacts to convert the carbide phase completely to oxide along with kernel swelling and increased porosity. With UO_2 kernels, a hyperstoichiometric uranium-oxide phase may be formed; in any case, kernel porosity is increased with enhanced gas release.

As illustrated in Figure 4-5,[10] the general response of the exposed kernel to the introduction of water vapor consists of three distinct phases: (1) a transient release of stored fission gas with a concomitant increase in the steady-state fractional release, (2) a period of constant steady-state release, and, upon removal of the water vapor, (3) a monotonic decline in the fractional release to prehydrolysis values (or nearly so) [Myers 1995]. Relatively complicated empirical models have been derived from the experimental data which reproduce these transient results [Myers 1995]; however, for design purposes, a simpler approach is taken in recognition that the transient release phase is short lived, and that a new steady-state R/B is established if the water is persistent, or the R/B returns to its original value if the water is removed. For fully hydrolyzed UCO fuel, a correlation similar to Eqn. (4-10) is used but with different fitting constants, and a "hydrolysis increase factor" of 1.7 is included [Myers 1987].

[10] In the illustration the exposed kernels were originally LEU UCO (80% UO_2 and 20% UC_2), but the UC_2 phase had already been converted to UO_2 by prior water injections so the observed response is effectively that of UO_2.

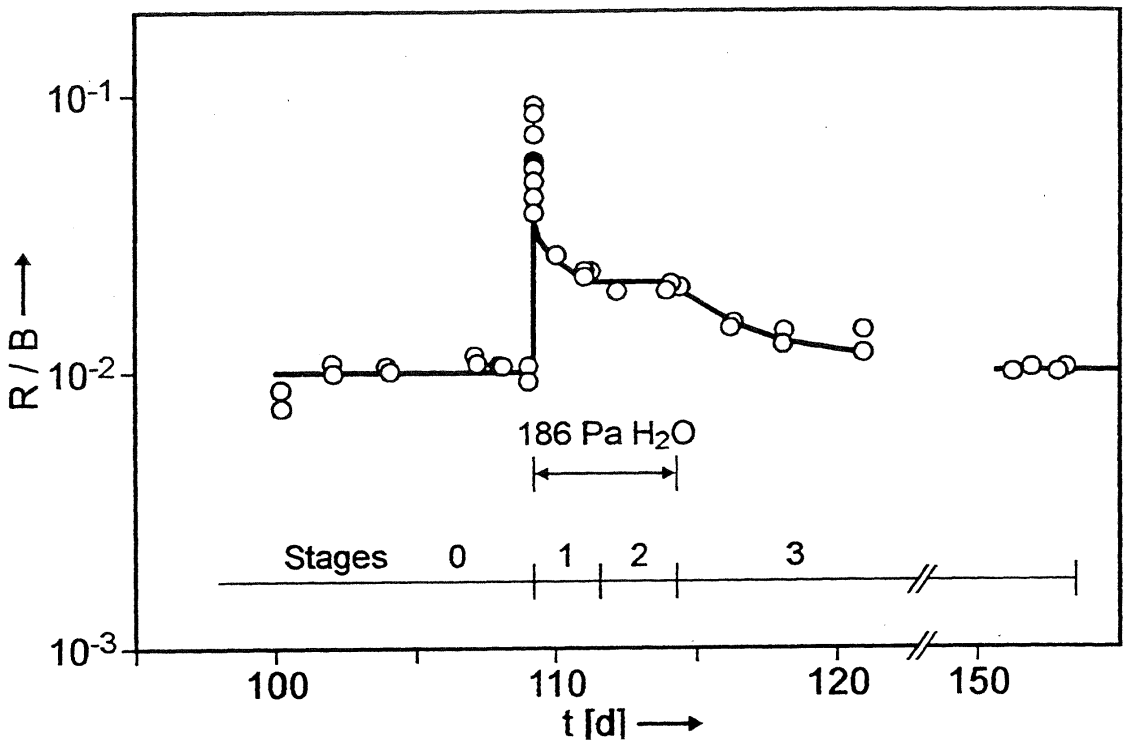

Figure 4-5. Effect of Hydrolysis on Fission Gas Release

For perspective, it is noteworthy that the technical specifications for HTGR normal plant operation will limit concentrations of oxidants in the primary coolant to very low levels (e.g., for the Fort St. Vrain HTGR the limit was <10 ppm total oxidants). If the technical specification limits are reached, corrective action must be taken, including removal of the oxidants by action of the helium purification system. Moreover, Advanced HTGR designs, including the commercial GT-MHR and the PBMR, are direct-cycle systems rather than steam-cycle systems. The probability of a large water ingress with a direct-cycle plant is much lower than for a steam-cycle plant because with the former designs, the secondary water pressures are lower than the primary He pressures, and the heat-exchanger tubes experience much lower temperatures during normal operation.

The R/B values for the radioisotopes of krypton and xenon are conveniently measured experimentally; however, the effectivities of noble gases are generally low. In contrast, the effectivities of radioisotopes of the halogens (Br, I) and chalcogens (Se, Te) produced by fission tend to be significantly higher, hence more significant to reactor design and safety analysis. Experimental measurement of the release rates of these volatile radionuclides is more difficult (e.g., they deposit in sample lines, etc.) but manageable with special techniques. Fortunately, the R/B values for iodine and tellurium have been shown to be slightly lower than that of xenon isotopes with the same half life [Haire 1974]. Consequently, it is convenient and conservative to

assume that iodine and tellurium have the same release characteristics as xenon; by analogy, it is further assumed that bromine and selenium have the same release characteristics as krypton.

4.2.2.1.2 Fission Metal Release from Fuel Kernels

The transport of fission metals through the kernel is modeled as a transient diffusion process. [Nabielek 1974] provides a number of analytical solutions for bounding conditions (e.g., constant power and constant temperature), but Eqn. (4-7) is typically solved numerically with appropriate boundary and interface conditions which vary depending upon whether a bare kernel or an encapsulated kernel in an intact coated particle is being modeled.

For fission metal transport in fuel kernels, the reference GA diffusivity is given by the following equations

$$D' = D_o \exp(-Q/RT) , \quad (4\text{-}11)$$

with

$$D_o = C_1 [1 + (1 + n) C_2 F^n] , \quad (4\text{-}12)$$

where

D' = reduced diffusion coefficient (s^{-1}),
D_o = a constant (s^{-1}),
Q = activation energy (J/mol),
T = temperature (K),
R = gas constant (8.314 J/mol-K),
F = burnup (% FIMA),
C_1, C_2, n = constants.

The release of metallic fission products is calculated with computer codes (e.g., TRAFIC-FD, [Tzung 1992a]) which assume that the kernel material is homogeneous. Therefore, it is necessary to determine an effective homogeneous diffusion coefficient. Use of an effective diffusion coefficient in code calculations will result in the same fractional release of fission products from the fuel kernel as was observed in the measurements from which the coefficient was derived. The effective diffusion coefficient is calculated according to the equation

$$D = D'r^2 , \quad (4\text{-}13)$$

where

D = effective diffusion coefficient (cm^2/s),
D' = reduced diffusion coefficient (s^{-1}) given in Eqn. 4-11,
r = kernel radius (cm).

The reference GA correlations for kernel diffusivities include a very strong burnup dependence; e.g., for Cs transport in UCO and ThO_2 kernels, the diffusivity is a function of burnup to the 4^{th}

power in Eqn. (4-12); this conclusion is derived primarily from measured Cs releases from ThO_2 with burnups from 1– 6 % FIMA. Whether this strong burnup dependence really applies to UCO kernels at burnups >20 % FIMA needs further confirmation.

As with the transport of fission gases in the kernel, the transport of mobile fission metals, including Cs, Ag, Sr and Eu isotopes, is undoubtedly much more complicated than classical Fickian diffusion. The fission product speciation in the kernel changes with burnup, especially with UCO kernels as the oxygen potential changes, and these changes in chemistry could affect the mobility of oxide-forming species, including Cs and Sr. The probable exception is silver which appears to remain in elemental form for all kernel compositions and burnups of interest.

4.2.2.2 Radionuclide Transport in Particle Coatings

Under normal operating conditions, the fission gases, including iodines, are quantitatively retained by the coatings of an intact TRISO particle. The transport of the volatile fission metals, including Ag, Cs, Sr, and Eu, in the PyC and SiC coatings is also treated as a transient Fickian diffusion process (Eqn. 4-6). In this case, the geometry is a spherical shell, and the interface conditions between the layers are assumed to be described by partition factors $p^{(i)}$:

$$p^{(i)}c^{(i)} = c^{(i+1)} \quad , \tag{4-14}$$

where $c^{(i)}$ is the concentration at the outer surface of the i^{th} coating layer, and $c^{(i+1)}$ is the concentration at the inner surface of the adjacent exterior layer. Partition factors are introduced to account for possible discontinuities in the concentration at the interface of adjacent materials with different chemical affinities for the migrating species. In fact, a constant partition factor is a gross simplification; nevertheless, there are currently no reliable data to even estimate these partition factors, and they are typically set to unity in most modeling work.

As with transport in the fuel kernel, radionuclide transport in the PyC and SiC coatings is undoubtedly more complex than homogeneous Fickian diffusion. These apparent migration coefficients are generally structure sensitive which indicates that the migration process is not a simple diffusion process but likely a combination of lattice diffusion, grain boundary diffusion, pore diffusion, etc., complicated further by effects like irradiation-enhanced trapping and adsorption. Consequently, any quoted diffusion coefficients should be called “effective” diffusion coefficients which implies that the overall migration process can be approximately described by Fick’s laws.

4.2.2.3 Radionuclide Transport in Fuel-Compact Matrix

As previously stated, the fuel-compact matrix is relatively porous and provides little holdup of the fission gases which are released from the fuel particles, and the effect is generally

neglected. However, the matrix is a composite material which has a high content of amorphous carbon, and this constituent of the matrix is highly sorptive of metallic fission products, especially Sr. While the matrix is highly sorptive of metals, it provides little diffusional resistance to the release of fission metals because of its high interconnected porosity; the matrix of a spherical fuel element is denser and partially graphitized so it does provide more diffusional resistance as discussed in the next subsection.

For prismatic designs, fission metal transport in the fuel compact matrix is again modeled as a transient Fickian diffusion process: the transient diffusion equation for cylindrical geometry is solved with an evaporative boundary condition. It is assumed that sorption equilibrium prevails in the gap between the fuel compact and the fuel hole surface of the fuel block. At equilibrium, the vapor pressure in the helium-filled gap and solid-phase concentration on the fuel-compact surface are uniquely related to one another by a sorption isotherm which is determined experimentally.

Conceptually, the partial pressure of the migrating species in the gas gap is calculated from its concentration on the surface of the fuel compact using a matrix sorption isotherm, and then the equilibrium surface concentration on the fuel-hole surface of the fuel block is calculated from the partial pressure in the gap using a graphite sorption isotherm. In general, the compact matrix material is more sorptive than the graphite so there is a discontinuity in surface concentrations across the gap (a “partition factor” using the terminology introduced above). The magnitude of the partition factor is less than the ratio of the intrinsic sorptivities of the matrix and graphite because there is also a temperature drop across the gap (say, ~30 ^{o}C), and the lower temperature increases the effective sorptivity of the graphite.

Several different sorption isotherms have been derived by making various assumptions about the potential energy distributions of the sorption sites which lead to different functional dependencies between the gas-phase partial pressure and the surface concentration; however, for the sorption of fission products on core materials, the experimental data are generally correlated with a simple Henrian isotherm (linear dependence) for low sorbate concentrations and with a Freundlich isotherm (exponential dependence) at higher sorbate concentrations.

Functionally, the partial pressure in the gap is assumed to be the sum of the pressures calculated with the two isotherms [Myers 1987]:

$$\ln P_F = \left(A + \frac{B}{T} \right) + \left(D + \frac{E}{T} \right) \ln C_{gr} \quad , \tag{4-15}$$

$$\ln P_H = \left(A + \frac{B}{T} \right) + \left(D - 1 + \frac{E}{T} \right) \ln C_t + \ln C_{gr} \quad , \tag{4-16}$$

$$P = P_F + P_H \quad , \tag{4-17}$$

$$\ln C_t = d_1 - d_2 T \quad , \tag{4-18}$$

where:

P_F = partial pressure from Freundlich isotherm (Pa)
P_H = partial pressure from Henrian isotherm (Pa)
T = absolute temperature (K)
C_{gr} = mass concentration of sorbate (mol/kg)
C_t = transition concentration (mol/kg)
A, D, d_1 = constants (dimensionless)
B, E = constants (K)
d_2 = constant (K^{-1})

Sorption isotherms for Cs, Sr and Ag have been measured for a variety of nuclear graphites and matrix materials; the data are summarized in [TECDOC-978 1997]. Measurements have been made on both unirradiated and irradiated materials. For matrix materials with a high content of amorphous carbon, irradiation has little effect; however, for highly graphitic materials, the Cs and Sr sorptivities are observed to increase with increasing neutron fluence. Apparently, neutron irradiation of the crystalline component causes damage which serves to create additional sorption sites. Consequently, the sorption isotherms have been modified to include a fast fluence dependence which is fit to the experimental data.

4.2.2.4 Radionuclide Transport in Fuel-Element Graphite

The fuel element graphite, which is denser and has a more ordered structure than the fuel-compact matrix, is somewhat less sorptive of the fission metals than the matrix, but it is much more effective as a diffusion barrier than the latter. Traditionally, the transport of fission metals in the fuel-element graphite and in the outer unfueled shell of a fuel sphere has been modeled as transient Fickian diffusion with an evaporative boundary condition at the coolant interface; the graphite web of a prismatic fuel element is treated as an equivalent slab, and the pebble is modeled in spherical coordinates.

As already discussed for transport in other core materials, the transport of fission metals, including Cs, Sr, and Ag, in nuclear graphite is more complex than simple homogeneous Fickian diffusion [e.g., Nabielek 1974]. Consequently, other more complicated models have been proposed including “a two-phase diffusion” model, a “coupled fast-slow diffusion” model, a

diffusion-trapping model, and others. Unfortunately, in all cases, there are insufficient experimental data available to derive the material property data necessary for the models or even to develop reliable empirical fits.

At the coolant boundary, the mass flux ϕ from the surface into the flowing coolant is given by the product of a convective mass transfer coefficient and a concentration driving force which is the difference between the desorption pressure (expressed as a volumetric concentration) and the "free stream" or mixed mean concentration in the coolant:

$$\phi = h(C_v - C_\infty) \quad , \tag{4-19}$$

where:

ϕ = diffusive flux of atoms (atoms/cm^2-s)
h = mass transfer coefficient (cm/s)
C_v = equilibrium desorption concentration in the boundary layer (atoms/cm^3)
C_∞ = mixed mean coolant concentration (atoms/cm^3)

The equilibrium desorption pressure in the boundary layer is calculated with a sorption isotherm as described in the previous subsection and converted to a volumetric concentration C_v using the ideal gas law. The mixed mean coolant concentration C_∞ is often conservatively set to zero; alternatively, a two-dimensional model can be used that integrates the total flux into the coolant as it passes through the fuel-element or core, thereby providing the coolant concentration at each local point.

4.3 Requirements Mandating Radionuclide Control

As described in Section 2.3.2, the radionuclide containment system for the commercial GT-MHR (and, presumably, for the NGNP as well although the design is still in the pre-conceptual phase) is comprised of multiple barriers to limit radionuclide release from the core to the environment to insignificant levels during normal operation and a spectrum of postulated accidents. To reiterate, the five principal release barriers are: (1) the fuel kernel, (2) the particle coatings, particularly the SiC coating, (3) the matrix/graphite, (4) the primary coolant pressure boundary; and (5) the VLPC. As part of the design process, performance requirements must be derived for each of these release barriers. Of these multiple release barriers, the particle coatings are the most important. Moreover, the in-reactor performance characteristics of the coated-particle fuel are strongly influenced by its as-manufactured attributes. Consequently, the fuel performance requirements and fuel quality requirements (allowable, as-manufactured HM contamination and coating defects) must be systematically defined and controlled.

The logic for deriving these fuel quality specifications is illustrated in Figure 4-6 [Hanson 2001]. Top-level requirements for an advanced HTGR design will be defined by both the regulators and the users. Lower-level requirements will then be systematically derived using a top-down functional analysis methodology. With this approach, the radionuclide control requirements for each of the release barriers can be defined. For example, starting with the allowable doses at the site boundary, limits on Curie releases from the VLPC, from the reactor vessel, and from the reactor core will be successively derived. Fuel failure criteria are in turn derived from the allowable core release limits. Finally, the required as-manufactured fuel attributes will be derived from the in-reactor fuel failure criteria, with consideration of achievable values based on existing fuel experience, thereby providing a logical basis for the fuel quality specifications.

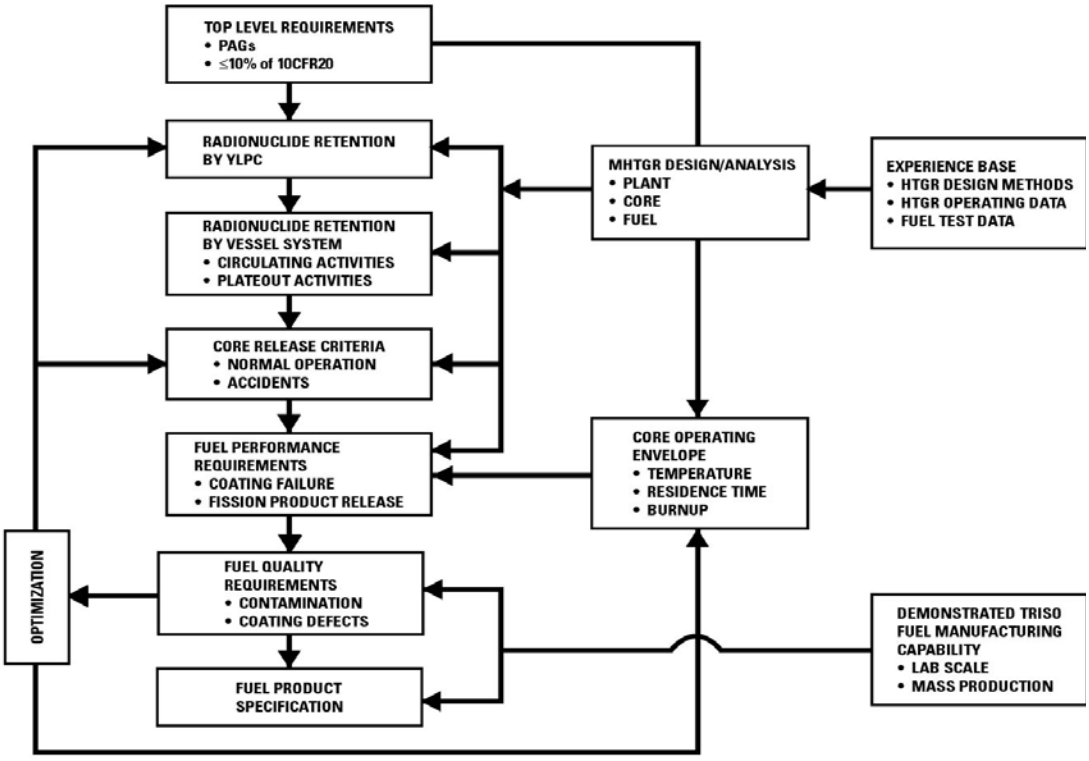

Figure 4-6. Logic for Derivation of Fuel Quality Requirements

A comprehensive top-down functional analysis to define fuel requirements has not yet been performed for either the commercial GT-MHR or the NGNP.[11] However, a preliminary fuel product specification for the GT-MHR has been prepared [Munoz 1994], based upon

[11] Since the NGNP is in a very early phase, and since representative information on fuel design criteria is available for the GT-MHR, information in this section is predominantly associated with the GT-MHR to illustrate the requirements anticipated for advanced HTGRs.

extrapolation of the functional analysis performed for the steam-cycle MHTGR. In addition, a generic fuel product specification for Advanced HTGRs [Scheffel 2003] has been prepared as input to the AGR fuel development program, which is developing a fuel product and process specification to be responsive to the evolving needs of the VHTR. In-service fuel performance requirements and as-manufactured fuel quality requirements have not yet been defined for a generic VHTR or for the NGNP. The fuel performance and quality requirements adopted for a given HTGR design along with the fuel service conditions will determine the amount of technology development that will be necessary to support the design and license the plant. Consequently, it is critically important that a comprehensive set of fuel requirements be derived for the NGNP early in the design process.

Overall, the most constraining radionuclide control requirement for the steam-cycle MHTGR was to comply with the dose limits specified in the EPA PAGs at the 425-m EAB so that the EPZ could be located at the EAB to preclude the need for public evacuation plans [Hanson 2001]. The PAGs limit both whole body and thyroid doses; these dose limits were used to derive allowable environmental releases of noble gases and iodines, respectively, during Licensing Basis Events. The limit on iodine-131 (the dominant iodine isotope) release from the plant was used to derive the limit on I-131 release from the core which, in turn, was used to set the limit on in-service fuel failure. Finally, this limit on in-service coating failure was used to derive the limits on certain as-manufactured defects, including the missing-buffer layer fraction.

The second, most constraining, top-level radionuclide control requirement for the steam-cycle MHTGR was to limit the occupational exposure to ≤10% of 10CFR20 (i.e., a factor of 10 ALARA margin was imposed on the design). A detailed occupational exposure assessment was not performed for the MHTGR. Hence, in deriving limits on plateout activity consistent with the subject goal, it was necessary to rely heavily upon previous occupational exposure assessments for earlier steam-cycle HTGR designs and upon engineering judgment. On that basis, it was projected that the ≤10% of 10CFR20 goal would be met if the gamma radiation fields around the primary circuit due to fission product plateout were limited to ≤10 mR/hr for scheduled maintenance activities (e.g., circulator ISI) and to ≤100 mR/hr for unscheduled maintenance activities (e.g., steam-generator tube plugging). These limits on gamma dose rates were in turn used to set limits on the primary circuit plateout inventories, in particular, limits on the releases of metallic fission products from the core, including Ag-110m, Cs-134, and Cs-137. Finally, the limits on Cs release from the core were used to derive limits on as-manufactured SiC defects.

It is anticipated that off-site dose limits and occupational exposure limits will again be the most constraining, top-level radionuclide control requirements for the NGNP. It remains to be

determined which of these requirements will be the more constraining with respect to in-service fuel failure and as-manufactured fuel quality for the NGNP.

4.4 Limits on Radionuclide Release from the Core

The fuel performance and quality requirements adopted for a given HTGR design along with the fuel service conditions will determine the amount of technology development that will be necessary to support the design and licensing of the plant. Consequently, it is critically important that a comprehensive set of fuel requirements be derived for the NGNP early in the design process. In-service fuel performance requirements and as-manufactured fuel quality requirements were proposed for a generic VHTR were in the Development Plan for Advanced High Temperature Coated-Particle Fuels [Hanson 2003] assuming that the top-level radionuclide control requirements would be the same as for the 350 MW(t) steam-cycle MHTGR (Section 4.3).

In this advanced fuel development plan, the fuel requirements for a generic VHTR with a 1000 ^{o}C core outlet temperature were assumed to be the same as those for the direct-cycle GT-MHR with a 850 ^{o}C core outlet temperature [Munoz 1994]. This assumption may prove to be too ambitious. It is reasonable to expect that the as-manufactured fuel quality limits can be met since the Germans met or exceeded comparable limits in the late 1970s [e.g., Hanson 2001] and the AGR fuel development program met comparable limits for the AGR-1 irradiation test [Maki 2005]. However, the in-service fuel performance limits could prove problematic; in particular, the allowable core metal release limits (Ag, Cs, etc.) may have to be increased even if the failure limits are maintained because of the higher average core temperatures which will result in less overall retention by the fuel kernels of failed particles and by the fuel-element graphite.

The provisional VHTR fuel performance and quality requirements are summarized in Table 4-2, and the provisional metal release limits are shown in Table 4-3 [Hanson 2003]. These limits are compared to the commercial GT-MHR limits in the subject tables. For perspective, the allowable metal release limits for the US steam-cycle MHTGR plant and for the German direct-cycle HHT plant are also shown in the latter table [Hanson 1995]. The VHTR limits on volatile metal release are particularly speculative at this writing (because they were developed for a direct-cycle GT-MHR rather than for a VHTR), and considerable plant design and fuel development will likely be required to optimize them.

Table 4-2. Coating Integrity Required for Generic VHTR Fuel

Parameter	Commercial GT-MHR		VHTR	
	≥50% Confidence	≥95% Confidence	≥50% Confidence	≥95% Confidence
As-Manufactured Fuel Quality				
Missing or defective buffer	$\leq 1.0 \times 10^{-5}$	$\leq 2.0 \times 10^{-5}$	$[\leq 1.0 \times 10^{-5}]$	$[\leq 2.0 \times 10^{-5}]$
Defective SiC	$\leq 5.0 \times 10^{-5}$	$\leq 1.0 \times 10^{-4}$	$[\leq 5.0 \times 10^{-5}]$	$[\leq 1.0 \times 10^{-4}]$
HM contamination	$\leq 1.0 \times 10^{-5}$	$\leq 2.0 \times 10^{-5}$	$[\leq 1.0 \times 10^{-5}]$	$[\leq 2.0 \times 10^{-5}]$
Total fraction HM outside intact SiC	$\leq 6.0 \times 10^{-5}$	$\leq 1.2 \times 10^{-4}$	$[\leq 6.0 \times 10^{-5}]$	$[\leq 1.2 \times 10^{-4}]$
In-Service Fuel Performance				
Normal operation	$\leq 5.0 \times 10^{-5}$	$\leq 2.0 \times 10^{-4}$	$[\leq 1.0 \times 10^{-4}]$	$[\leq 4.0 \times 10^{-4}]$
Core heatup accidents	$[\leq 1.5 \times 10^{-4}]$[(a)]	$[\leq 6.0 \times 10^{-4}]$	$[\leq 3.0 \times 10^{-4}]$	$[\leq 1.2 \times 10^{-3}]$

[(a)]Values in [square brackets] are provisional and subject to revision as the design evolves.

Table 4-3. Provisional Fission Metal Release Limits for a Generic VHTR

Reactor Plant	Type	COT[12] (°C)	Allowable Core Fractional Release			
			Cs-137		Ag-110m	
			"Expected"	"Design"	"Expected"	"Design"
MHTGR	Steam-cycle	700	7.0×10^{-6}	7.0×10^{-5}	5.0×10^{-4}	5.0×10^{-3}
HHT	Direct-cycle	850	2.0×10^{-5}	1.0×10^{-4}	8.6×10^{-5}	6.5×10^{-4}
GT-MHR	Direct-cycle	850	1.0×10^{-5}	1.0×10^{-4}	2.0×10^{-4}	2.0×10^{-3}
VHTR	Process heat	950	$[1.0 \times 10^{-5}]$	$[1.0 \times 10^{-4}]$	$[2.0 \times 10^{-4}]$	$[2.0 \times 10^{-3}]$

Upon further consideration for the NGNP, it is now recommended that the allowable in-service fuel failure limit be reduced by a factor of two to the GT-MHR limit of $\leq 5.0 \times 10^{-5}$ (which is also the steam-cycle MHTGR limit). The reason for this recommendation is the necessity to limit the release of I-131 in order the meet the PAGs during rapid depressurization accidents. Also, it is recommended to increase the allowable Ag-110m fractional release by a factor of 2.5 back to

[12] COT = core outlet temperature

the steam-cycle MHTGR limit of 5.0×10^{-4}. The latter recommendation is base upon review of the available data on Ag release (e.g., the R2 K13 test [Acharya 1987]) and the predicted Ag-110m release from a direct-cycle GT-MHR with Pu fuel and a 850 ^{o}C core outlet temperature [PC-MHR 1994]. The preliminary NGNP radionuclide mass balance given in Section 7 incorporates these two recommendations.

5. PLANT TRITIUM SOURCE TERM AND LIMITS

Tritium (H-3) will be produced in an H2-MHR by various nuclear reactions. Given its high mobility, especially at high temperatures, some tritium will permeate through the IHX and the hydrogen plant process heat exchangers, contaminating the product hydrogen [e.g., Gainey 1976, Hanson 2006b]. This tritium contamination will contribute to public and occupational radiation exposures; consequently, stringent limits on tritium contamination in the product hydrogen are anticipated to be imposed by regulatory authorities. Design options are available to control tritium in an H2-MHR, but they can be expensive so an optimal combination of mitigating features must be implemented in the design.

5.1 Tritium Transport in HTGRs

The following sources of tritium production have been identified, primarily from early surveillance programs at operating HTGRs (steam-cycle plants), and they can be reasonably quantified for a H2-MHR: (1) ternary fission (yield ≈ 10^{-3}), (2) neutron activation of He-3 in the primary He coolant (He-3 abundance = 2 x 10^{-7}), (3) neutron activation of lithium impurities in fuel-compact matrix and core graphite, and (4) neutron capture reactions in boron control materials. Ternary fission will be the dominant source of tritium production, but much of this tritium will be retained in the TRISO-coated fuel particles. He-3 activation will generate a relatively modest fraction of the total tritium production in the reactor; however, since it is born in the primary coolant, it will likely be a major source of tritium in the primary helium and, hence, a major source of product contamination as well.

Tritium strongly chemisorbs on irradiated nuclear graphite at elevated temperatures. Consequently, a large fraction of the tritium entering the primary helium will be sorbed on the huge mass of graphite in the core. In operating HTGRs, including Fort St. Vrain, the core graphite was a far more important sink for tritium removal than the HPS. However, a large fraction of this stored tritium can be released if water is introduced into the primary coolant (a low-probability event for an H2-MHR with an IHX and/or direct-cycle gas turbine).

Tritium will permeate through the heat exchangers and process piping in an H2-MHR and will contaminate the product hydrogen. Surface films will play a critically important role in establishing the in-reactor, tritium permeation rates. Oxide films can reduce H-3 permeability by orders of magnitude. However, normal plant operating transients (e.g., startup/shutdown, etc.) may compromise film integrity and result in increased H-3 permeation rates.

Design methods are available to estimate H-3 production, distribution, and release, but they are rudimentary and characterized by large uncertainties [Hanson 2006b]. The current design

methods appear marginally adequate for conceptual design, but they will need to be upgraded for preliminary design and independently validated prior to completion of final design. Some technology development will be necessary to provide the basis for these design methods improvements and validation.

5.2 Product Contamination

Given the behavior of tritium summarized above, tritium will be produced in an H2-MHR and will migrate, to some degree, throughout the plant, including the hydrogen production plant. Consequently, the primary helium coolant and the process streams, including the hydrogen product stream, will likely contain measurable quantities of tritium. Since tritium is a radiological hazard, especially when ingested into the human body, this tritium contamination represents a potential dose contributor for both occupational and public exposure. Of particular significance for an H2-MHR is the tritium contamination of the product hydrogen, which may be consumed by the general public (e.g., in fuel-cell powered transportation vehicles).

The fundamental issue is not whether tritium will contaminate the product hydrogen because it almost certainly will, based on past operating experience with steam-cycle HTGRs. The fundamental issues are the allowable levels of tritium contamination in the product hydrogen and the design features that will need to be implemented to assure that these limits are met with the required design margin.

The tritium production rates and its transport behavior in the primary coolant circuit of an H2-MHR can be conservatively estimated with reasonable confidence, given the available design methods for predicting tritium transport and its observed behavior in operating steam-cycle HTGRs. The unique design challenge for the H2-MHR will be predicting the rates of H-3 transport into the hydrogen production plant and its migration behavior in the various process streams. The possible H-3 contamination pathways in the SI process are shown schematically in Figure 5-1 [Richards 2006a].[13]

[13] A comparable evaluation of the tritium distribution in an HTE plant has not yet been reported.

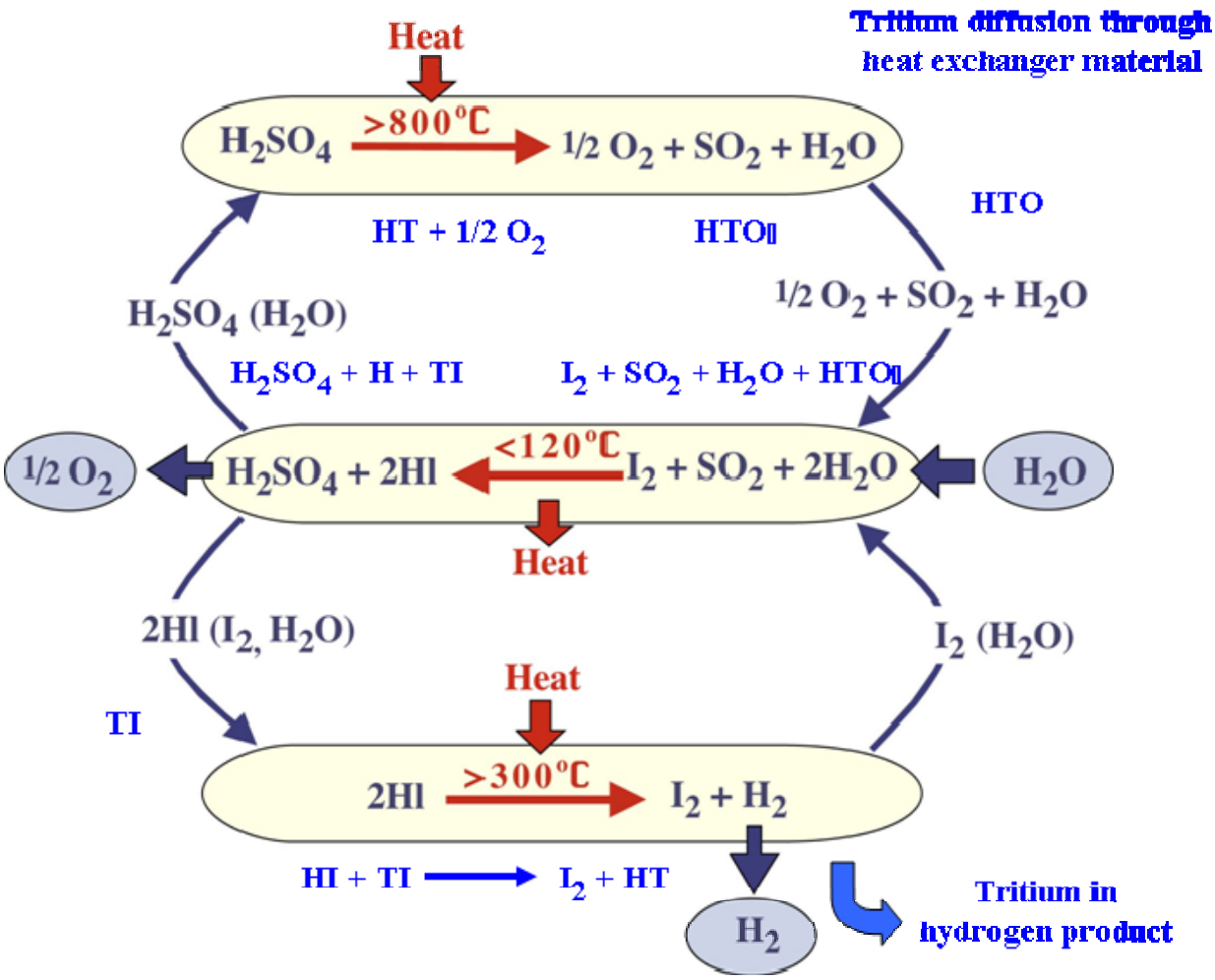

Figure 5-1. H-3 Contamination Pathways in SI Process

5.3 Contribution to Radionuclide Source Terms

In addition to contaminating the product hydrogen stream, tritium will likely be present at some concentration in the gaseous and liquid effluent streams released from the plant into the surrounding environment [Hanson 2006b]. While compliance with the various national regulations on public radiation exposure from nuclear plants (e.g., 10CFR50, Appendix I) was not a problem, tritium was nevertheless the dominant dose contributor to off-site doses during normal operation for previous steam-cycle HTGRs. Moreover, for those operating HTGRs that solidified the tritiated water removed by their HPSs, tritium was a major contributor to the total radionuclide inventories disposed of as a solid waste as well.

In contrast, tritium has consistently been predicted to be an insignificant dose contributor for postulated accidents for operating HTGRs and for proposed advanced HTGR designs. For postulated accidents in advanced HTGR designs, the dominant off-site dose contributors are

consistently predicted to be the radioiodines, especially I-131 [e.g., PSID 1992]; the H-3 inventories in an HTGR are too small to be significant compared to the radioiodines and noble gases [the exception being the tritium-producing New Production Reactor). It is anticipated that the same results will be obtained when dose assessments for normal plant operation and postulated accidents are made for the H2-MHR.

With an H2-MHR, the majority of the waste heat is rejected through evaporation of a small fraction of the circulating water. A makeup water system replenishes water lost to evaporation and is also used to control the water chemistry in the circulating water. Excess makeup water is blown down from the cooling tower basin to the receiving water body. The water released from evaporation and blow down are potential sources of tritium release to the environment and these sources are factored into the design of the HPS. Radionuclide releases, including H-3 release, via this pathway will need to be quantified for both normal operation and a spectrum of postulated accidents.

5.4 Sources of Tritium Production

There are multiple sources of H-3 production in an HTGR, including ternary fission and a variety of neutron capture reactions [Gainey 1976]. The principal neutron capture reactions are:

1. Li-6(n,α)H-3 σ (2200 m/s) = 9.53 **x** 10^{-26} m^2 (953 barns)[14]
2. He-3(n,p)H-3 σ (2200 m/s) = 5.4 x 10^{-25} m^2 (5400 barns)
3. B-10(n,α)Li-7 σ (2200 m/s) = 4.01 x 10^{-25} m^2 (4010 barns)
4. Li-7(n,nα)H-3 σ (E > 0.18 MeV) = 1.53 x 10^{-29} m^2 (153 mbarns)
5. B-10(n,2α)H-3 σ (E > 0.18 MeV) = 5.0 x 10^{-30} m^2 (50 mbarns)

Other possible neutron capture reactions include:

1. B-11(n,T)Be-9(n,α)Li-6(n,α)H-3
2. C-12(n,α)Be-9(n,α)Li-6(n,α)H-3
3. O-16(n,N-15)H-2(n, γ)H-3
4. N-14(n,C-12)H-3

These latter reactions are of negligible importance compared to the five reactions listed as the principal sources due to small concentrations of the reactive material, a low reaction cross

[14] where σ = microscopic cross section.

section, and/or high reaction threshold energy. A possible major source of tritium from fast neutrons is the reaction:

B-10(n,2α)H-3 σ (E > 0.18 MeV) = 5.0 x 10^{-30} m^2 (50 mbarns)

The fast neutron flux in HTGRs is significant, but its contribution to tritium production is largely unknown. For example, in Fort St. Vrain the calculated fast neutron flux (average) was 3.6 x 10^{13} n/cm^2-sec (E > 0.18 MeV) compared to the calculated thermal flux (average) of 6.0 x 10^{13} n/cm^2-sec (E < 0.18 MeV). In a typical HTGR core, about 10% of the total fissions are caused by fast neutrons.

Even if the nuclear properties (accurate fluxes, cross sections, etc.) are well known, a reliable knowledge of the tritium-forming impurities present in the reactor is also required. Of greatest importance is the Li-6 content of core materials, including fuel element graphite, fuel particles, fuel-compact matrix, reflector graphite, control materials, and core insulation. In general, the total lithium content of these materials is extremely low, often bordering on the detection limits for most analytical methods for Li measurement. Also of importance is the He-3 content of the helium, which is also extremely low (atom ratio He-3/He-4 of about 2 x 10^{-7} for He obtained from gas wells), and can be expected to vary depending on the source of supply. Typical impurity levels of tritium-forming materials expected to be present in HTGR core materials are given in Table 5-1.

Table 5-1. Typical H-3 Producing Impurity Levels in Reactor Components

Impurity	Expected value
Lithium	
Core graphite	0.05 ppm[(a)]
Core matrix	0.50 ppm
Reflector (temporary)	0.05 ppm
Reflector (permanent)	2 ppm
Boron	
Control rod	~30% B
Burnable poison	~1% B
Reflector	10.3% B
He-3	
Coolant	0.1 - 0.2 ppm[(b)]

[(a)]ppm by weight

[(b)]ppm by volume

Ternary fission is typically the dominant source of H-3 production in an HTGR. However, of greater importance is the dominant source(s) of H-3 release into the primary coolant. This latter topic is discussed in the next subsection.

5.4.1 Ternary Fission

Tritium is formed by ternary fission in an HTGR core with the reported yields typically ranging from about 0.8 to 2.3 x 10^{-4} atoms/fission, depending on the fissile nuclide and the neutron flux spectrum [Gainey 1976]. The available tritium yield data are summarized in Table 5-2. The H-3 yields from thermal fissioning of U-235 and Pu-239 are reasonably well known. However, the H-3 yields from fast fissioning are not well known; reported H-3 yields from the fast fissioning of U-238 are an order of magnitude greater than from the thermal fissioning of U-235 and Pu-239 and from the fast fissioning of U-235 [Buzzelli 1976]. Since about 10% of the total fissioning in an HTGR core is from fast fissioning, this uncertainty in the fast fission H-3 yields introduces a nontrivial uncertainty in the total core production of H-3 from ternary fission. A core average H-3 yield of 1.0 x 10^{-4} atoms/fission has been traditionally assumed at General Atomics for reactor design and safety analysis [Gainey 1976, Hanson 2006b].

Table 5-2. H-3 Yields from Ternary Fission

Source	Tritium Atoms/Fission (X 10^{-4})				
	U-233	**U-235**	**U-238**	**Pu-239**	**Pu-241**
Thermal Neutrons					
[Fluss 1972]	1.1	0.85 ± 0.09			
[Horrocks 1973]	0.88 ± 0.07	0.75 ± 0.08		1.51 ± 0.10	
[Albenesius 1960]		0.95 ± 0.08			
[Sloth 1962]		0.8 ± 0.01			
[Ray 1966]		0.87			
[Marshall 1966]				2.3	0.26
[Albenesius 1959]		0.5 – 1.0			
[Vorobiev 1969]		1.26			
[Dakowski, 1967]		1.24			
Fast Neutrons					
[Fluss 1972, Halpen 1971]		2.0 – 2.2			
[Buzzelli 1976]		1.4 – 1.7	10 – 20.6		

The rate of tritium production by ternary fission can be calculated from the reactor thermal power by the following expression[15]:

$$\frac{dN_T}{dt} = kPY - \lambda N_T \qquad (5\text{-}1)$$

where: N_T = the number of tritium atoms in the core (atoms),
t = time (sec),
k = fission rate per unit power (3.12 x 10^{16} fissions/MW-sec),
P = reactor thermal power (MW),
Y = fission yield (1.0 x 10^{-4} H-3 atom/fission)
λ = H-3 decay constant (1.792 x 10^{-9} sec^{-1})

[15] The nomenclature used here is essentially the same as that used in [Gainey 1976] and continued in [Hanson 2006b] since the latter is in large measure an update of the former.

Upon assumption of constant power operation and with the initial condition that $N_T = 0$ at t = 0, Equation (5-1) can be integrated to give the number of H-3 atoms after time t (sec).

$$N_T(t) = \frac{kPY}{\lambda}(1 - e^{-\lambda t}) \tag{5-2}$$

Since the H-3 activity rather than the number of H-3 atoms is typically measured and reported, it is more convenient to express Equation (5-2) and the subsequent equations in this report in terms of H-3 activity:

$$A_T(t) = \lambda N_T(t) = kPY(1 - e^{-\lambda t}) \tag{5-3}$$

where: A_T = H-3 activity (disintegration/sec, dps, Becquerel)

The H-3 activity can be expressed in the traditional unit of radioactivity, the Curie (Ci), with the conversion factor 3.7 x 10^{10} dps/Ci.

Further, an average plant availability factor f is often included by replacing the actual time t with the product (f x t). Since plant availability factors now typically range between 0.8 – 0.9, the distinction is of little practical importance.

5.4.2 Neutron Activation of Lithium

As stated above, lithium is present as a trace impurity in many core materials, including fuel element graphite, fuel particles, fuel-compact matrix, reflector graphite, control materials, and core insulation. Typical concentrations are given in Table 5-1. Li-6 with a natural abundance of 7.5% has a significant neutron capture cross section and transmutes to H-3:

Li-6(n,α)H-3 σ (2200 m/s) = 9.53 **x** 10^{-26} m^2 (953 barns)

The rate of production of H-3 from the neutron activation of Li-6 is calculated by the solution of the following differential equations where N_1 is Li-6 and N_2 is the H-3 produced from Li-6 activation:

$$\frac{dN_1}{dt} = -\phi_1 \sigma_1 N_1 \tag{5-4}$$

and

$$\frac{dN_2}{dt} = \phi_1 \sigma_1 N_1 - \lambda_2 N_2 \tag{5-5}$$

where: φ = the average flux to which the Li-6 impurity is exposed (n/cm^2-sec)
σ_i = neutron cross section of nuclide i (cm^2/n)

With $N_{1,0}$ being the initial number of Li-6 atoms and assuming a constant flux (constant power), the above equations can be solved to give [Gainey 1976]:

$$N_1 = N_{1,0} e^{-\phi_1 \sigma_1 t} \tag{5-6}$$

and

$$N_2 = \frac{\phi_1 \sigma_1 N_{1,0}}{\lambda_2 - \phi_1 \sigma_1} \left(e^{-\phi_1 \sigma_1 t} - e^{-\lambda_2 t} \right) \tag{5-7}$$

Converting to activity, the H-3 produced by Li-6 activation A_2 is:

$$A_2 = \lambda_2 N_2 = \frac{\phi_1 \sigma_1 N_{1,0}}{1 - \frac{\phi_1 \sigma_1}{\lambda_2}} \left(e^{-\phi_1 \sigma_1 t} - e^{-\lambda_2 t} \right) \tag{5-8}$$

5.4.3 Neutron Activation of He-3

The trace He-3 content of the primary He has a large cross section and will readily activate to H-3 under irradiation:

He-3(n,p)H-3 σ (2200 m/s) = 5.4 x 10^{-25} m^2 (5400 barns)

The He-3 content of the helium (atom ratio He-3/He-4) ranges from about 2 x 10^{-7} for He obtained from gas wells (the normal source of He coolant for HTGRs) to an order of magnitude higher for He obtained from the atmosphere [Wichner 1979].

The gross generation rate of tritium from He-3 is given by the following differential equations where N_3 is the H-3 produced by He-3 activation and N_4 is the He-3 content of the primary coolant [Gainey 1976].

$$\frac{dN_3}{dt} = \sigma_1 \phi_1 N_4 \tag{5-9}$$

The rate of change of He-3 content of the primary circuit coolant is:

$$\frac{dN_4}{dt} = F_H N_{4,0} - F_H N_4 - \sigma_1 \phi_3 N_4 \tag{5-10}$$

where: $N_{4,0}$ = concentration of He-3 in the makeup helium
F_H = fractional makeup rate for helium coolant
φ_3 = average neutron flux experienced by the total He inventory

or, grouping terms,

$$\frac{dN_4}{dt} = F_H N_{4,0} - (F_H + \sigma_1 \phi_3) N_4 \tag{5-11}$$

Integration of Eqn (5-11) gives the concentration of He-3 and hence the H-3 generation rate:

$$N_4 = \frac{\sigma_1 \phi_3 N_{4,0} \exp[-(F_H + \sigma_1 \phi_3) t] + F_H N_{4,0}}{F_H + \sigma_1 \phi_3} \tag{5-12}$$

Substituting for N_4 in Eqn (5-9) gives the H-3 generation rate as:

$$\frac{dN_3}{dt} = \phi_1\sigma_1\left\{\frac{\sigma_1\phi_3 N_{4,0}\exp[-(F_H+\sigma_1\phi_3)t]+F_H N_{4,0}}{(F_H+\sigma_1\phi_3)}\right\} \quad (5\text{-}13)$$

Use of this relation has shown (Forsyth 1974) that the H-3 generation rate will fall to an equilibrium value in about 40 days if the He leak rate from the primary circuit is less than 0.2% of the circulating coolant per day.

5.4.4 Neutron Capture Reactions in Control Materials

Boron-10 is used as a neutron absorber in control rods, in burnable poison in fuel elements, and often in the permanent reflectors and core support structure to reduce neutron damage. Several neutron capture reactions with these B-10 control materials in the core will produce tritium. The dominant reactions are:

B-10(n, α)Li-7	σ (2200 m/s) = 4.01 x 10^{-25} m^2 (4010 barns)
Li-7(n,nα)H-3	σ (E > 0.18 MeV) = 1.53 x 10^{-29} m^2 (153 mbarns)
B-10(n,2α)H-3	σ (E > 0.18 MeV) =5.0 x 10^{-30} m^2 (50 mbarns)

Tritium production from these two reactions can be calculated from the following equations N_5, N_6 and N_7 are the number of atoms present of B-10, Li-7, and H-3, respectively [Gainey 1976]:

$$\frac{dN_5}{dt} = -\phi\bar{\sigma}_{BL}N_5 \quad (5\text{-}14)$$

$$\frac{dN_6}{dt} = \phi\bar{\sigma}_{BL}N_5 - \hat{\phi}\bar{\sigma}_{LH}N_6 \quad (5\text{-}15)$$

$$\frac{dN_7}{dt} = \hat{\phi}\bar{\sigma}_{LH}N_6 - \hat{\phi}\bar{\sigma}_{BH}N_5 - \lambda N_7 \quad (5\text{-}16)$$

where: ϕ = total flux

$\hat{\phi}$ = flux above 3.3 Mev

$\bar{\sigma}_{BL}$ = average self-shielded cross section for B-10(n, α)Li-7 reaction

$\bar{\sigma}_{LH}$ = average self-shielded cross section for Li-7(n,nα)H-3 reaction

$\bar{\sigma}_{BH}$ = average self-shielded cross section for B-10(n,2α)H-3 reaction

$$\frac{N_7(t)}{N_{5,0}} = \frac{\hat{\phi}\bar{\sigma}_{LH}\phi\bar{\sigma}_{BL}}{\hat{\phi}\bar{\sigma}_{LH}-\phi\bar{\sigma}_{BL}}\left(\frac{\exp(-\phi\bar{\sigma}_{BL}t)}{\lambda-\phi\bar{\sigma}_{BL}}-\frac{\exp(-\hat{\phi}\bar{\sigma}_{LH}t)}{\lambda-\hat{\phi}\bar{\sigma}_{LH}}\right)+\frac{\hat{\phi}\bar{\sigma}_{BH}\exp(-\phi\bar{\sigma}_{BL}t)}{\lambda-\phi\bar{\sigma}_{BL}}$$
$$-\left[\frac{\hat{\phi}\bar{\sigma}_{LH}\phi\bar{\sigma}_{BL}}{\hat{\phi}\bar{\sigma}_{LH}-\phi\bar{\sigma}_{BL}}\left(\frac{1}{\lambda-\phi\bar{\sigma}_{BL}}-\frac{1}{\lambda-\hat{\phi}\bar{\sigma}_{LH}}\right)+\frac{\hat{\phi}\bar{\sigma}_{BH}}{\lambda-\phi\bar{\sigma}_{BL}}\right]\exp(-\lambda t) \quad (5\text{-}17)$$

In summary, the mechanisms by which H-3 is produced in an HTGR are well established (i.e., ternary fission and various neutron capture reactions with Li-6, He-3 and B-10). However, the uncertainties in the total in-reactor H-3 production rates are nontrivial because of the uncertainties in the ternary fission yields, especially for fast fissioning, and because of the uncertainties of in the concentrations of H-3 generating trace impurities, especially Li-6.

5.5 Tritium Transport Behavior

The various H-3 transport pathways in an HTGR (steam-cycle plant) are shown schematically in Figure 5-2. The transport behavior of H-3 in HTGRs has been reviewed previously [e.g., Forsyth 1974, Gainey 1976]. While these previous reviews are three decades old, the information contained therein is still largely relevant. The models used at GA to describe H-3 transport are contained and controlled in the Fuel Design Data Manual, Issue F (FDDM/F) [Myers 1987]. FDDM/F is a GA proprietary document, but the H-3 transport models contained therein are readily available in the review report prepared by Martin [1993] at Oak Ridge National Laboratory (ORNL). Both the earlier GA review of H-3 behavior [Gainey 1976] and the ORNL review of the H-3 transport models [Martin 1993] are liberally excerpted in this section.

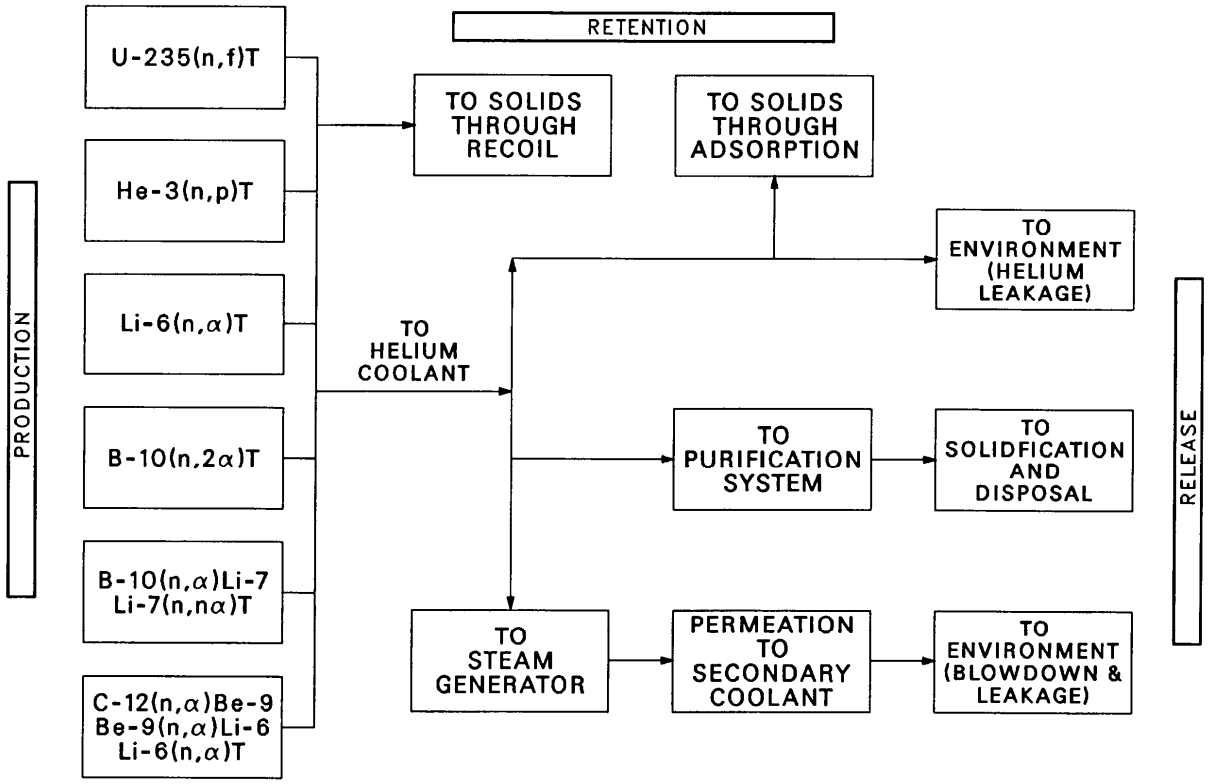

Figure 5-2. H-3 Distribution in an HTGR (Steam-Cycle Plant)

The information about H-3 transport in HTGRs can be organized in a number of ways. The tritium in the primary coolant is of greatest importance in the present context since it is most readily available for transport into the secondary loop and beyond to contaminate the product hydrogen. Consequently, this section is organized by sources of H-3 release into the primary coolant and by sinks for H-3 removal from the primary coolant.

5.5.1 Tritium Release into Primary Coolant

The most readily available source of H-3 in the primary He is obviously the neutron activation of He-3 directly in the primary coolant. The other potential sources are H-3 inventories produced by neutron capture reactions in various core materials (Section 5.4).

5.5.1.1 H-3 Release from Coated Fuel Particles

As stated previously, the largest source of H-3 production in an HTGR is typically ternary fission; hence, the largest H-3 inventory is contained within the coated fuel particles. Before this tritium can be released into the primary coolant, it must be released from the fuel kernels and permeate through the pyrocarbon (PyC) and SiC coatings of the TRISO fuel particles. The then

available data on H-3 release from failed and intact TRISO fuel particles, which was taken from [GA 1972], was summarized by Gainey [1976] as follows:

The available data on tritium retention in early TRISO particles with high enriched uranium (HEU) at the end of irradiation is summarized in [GA 1972]. Figure 5-3 shows the tritium release from UO_2 and UC_2 particles during postirradiation anneals. In general, tritium retention decreases with higher irradiation and annealing temperatures and with higher burnups, although quantitative models are difficult to derive because of the limited data available. Gainey [1976] summarizes the TRISO data base as follows:

1. UO_2 and UC_2 particles were only studied at high burnup (>60% FIMA) while $(Th,U)C_2$ particles were studied at low burnup (<25% FIMA),
2. Tritium release exhibited dependencies on burnup and irradiation temperature, and
3. Tritium retention is greatest for UO_2, intermediate for UC_2, and least for $(Th,U)C_2$

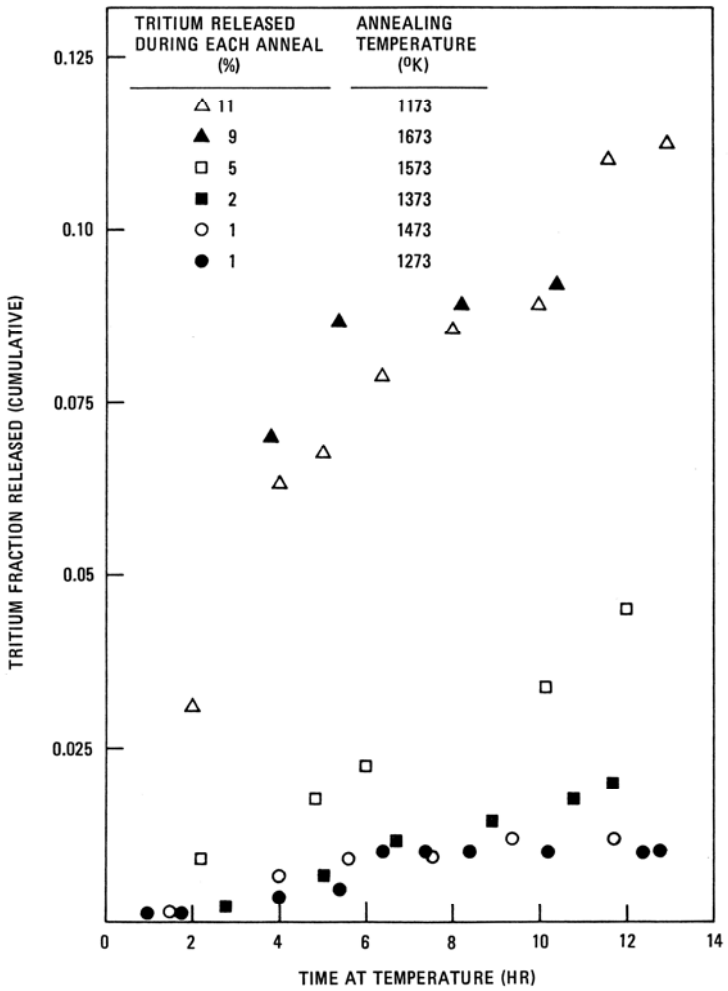

H-3 Release from Intact UO_2 TRISO Particles

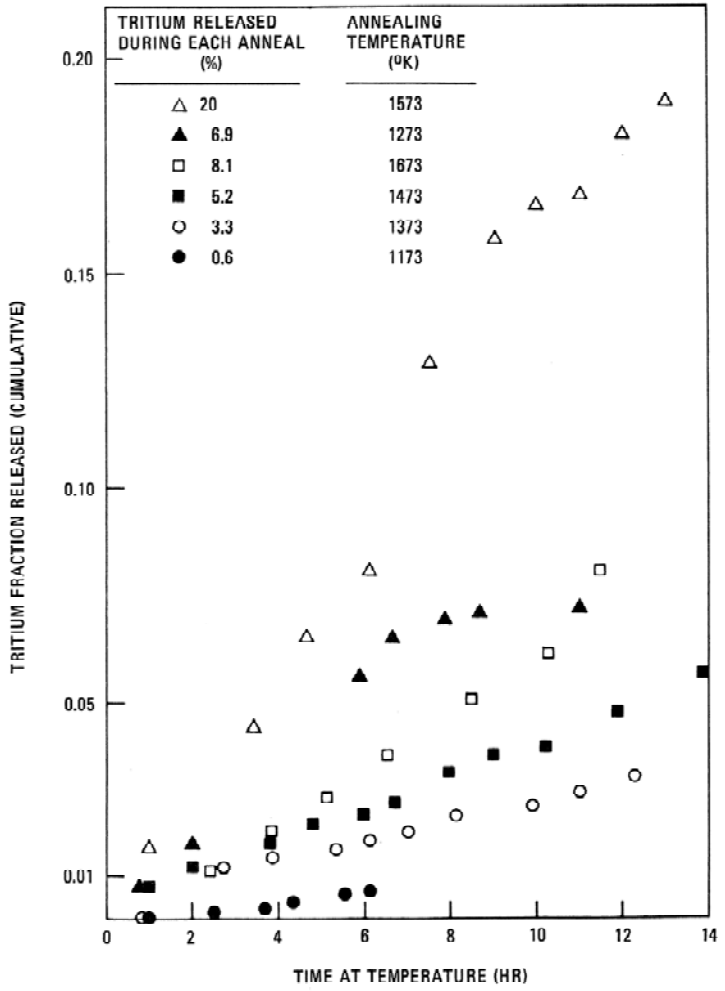

H-3 Release from Intact UC_2 TRISO Particles

Figure 5-3. H-3 Release from Intact TRISO Fuel Particles

In end-of-irradiation retention measurements, TRISO-coated $(Th,U)C_2$ particles, irradiated to 12 to 26% FIMA, retained essentially all the tritium at 950 ^oC, and the percentage of tritium retained decreased with irradiation temperature. TRISO-coated UO_2 particles, irradiated to 60 to 75% burnup, showed similar behavior, [i.e., high retention at low temperature (~900 ^oC) and decreasing retention with increasing temperature]. By comparison, the TRISO UC_2 particles appeared to be less effective in retaining tritium. In general, the data indicate that tritium is highly retained in fuel material, even in fuel compacts containing failed particles, during irradiation to high burnup for up to 450 days at temperatures around 900 ^oC and that the retention decreases with increasing temperature. The irradiation process itself, by the creation of sorption sites, may, in part, account for the high retention of tritium.

A review of both the internal GA data base and the external HTGR literature did not produce any significant information about measured H-3 release rates from modern, low enriched uranium (LEU) TRISO fuel particles. However, there is another large data base regarding H-3 release from TRISO-coated particles. TRISO-coated target particles for the production of tritium have been under development for more than two decades. These target particles have been investigated for the production of H-3 for nuclear weapons and for future fusion reactors. Typically, these target particles have a kernel composed of a lithium aluminum oxide compound with a conventional TRISO-coating system [e.g., Yang 1982]. The critical performance parameter for these target particles is the H-3 permeation rate in the TRISO coating system, especially in the SiC coating; consequently, H-3 permeabilities through TRISO coatings, especially SiC, have been investigated as part of target development programs in the USA and Japan.

There was a major target development program in the USA in the late 1980s and early 1990s to develop TRISO-coated lithium aluminates particles for use in the New Production Reactor (NPR). General Atomics, Idaho National Laboratory and Los Alamos National Laboratory were the main participants in this USDOE-funded program. Extensive data on H-3 release from target particles under irradiation and during postirradiation heating tests were developed as a result. While there are a few open-literature publications describing the NPR program, most of the technical data are in reports that are “Unclassified Controlled Nuclear Information” (UCNI) which are not publicly available.

5.5.1.2 H-3 Release from Matrix and Core Graphite

As introduced previously, tritium is produced within the graphite moderator, reflector blocks, and the compact matrix material from neutron activation of Li-6 and B-10 impurities. It appears that some tritium produced in this way is retained at its place of birth (i.e., by recoil), and some would be capable of migrating out into the helium coolant [Gainey 1976]. Tritium retention by recoil into structural solids is described in Section 5.6.1. Because of these recoil effects, tritium born

in solid graphitic structures in the core, principally the fuel and reflector graphite, may well behave differently (i.e., be more effectively retained) than tritium that is adsorbed from the coolant on to these graphitic structures; tritium chemisorption on graphitic structures is described in Section 5.6.2.

Elleman's results (cited in [Gainey 1976]) indicate that ~20% of the tritium produced could be permanently held in the graphite structure. Figure 5-4 shows the results of studies of tritium release at different temperatures from graphite containing 0.1 ppm Li irradiated at high neutron flux [Walter 1973]. The results imply that tritium release from graphite is a diffusion-limited process since the release is proportional to the square root of time.

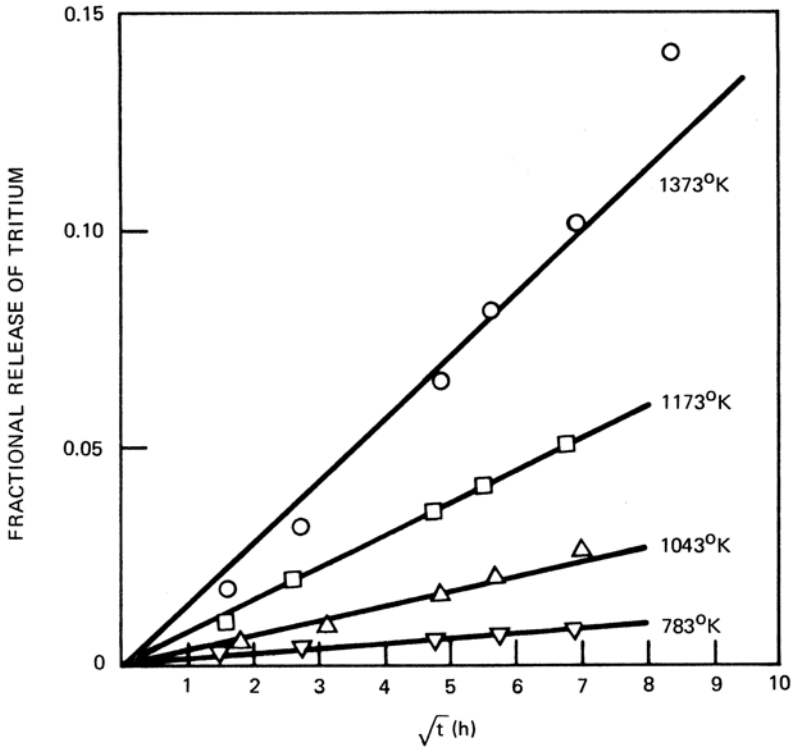

Figure 5-4. Tritium Release Isotherms from Annealed/Irradiated Graphite Probes

The results of postirradiation heating tests on irradiated graphite performed at KFA Juelich are shown in Figure 5-5 [Fischer 1974]. Although the heating times are short (a few hours), the data imply that H-3 would be very strongly retained at normal operating temperatures. KFA explained their results by assuming that a combined diffusion/desorption mechanism was responsible for the release. They considered chemisorption and molecular dissociation at the graphite surface and absorption and diffusion into the graphite bulk. Data are also available for hydrogen (protium) desorption from several graphites, including TSP nuclear graphite [e.g., Bansal 1971].

No correlations are given in FDDM/F [Myers1987] for tritium release from irradiated core graphite. The TRITGO manual [Hanson 2006a] recommends a graphite retention factor of 0.99 for H-3 born in core graphite; given the data in Figures 5-4 and 5-5, that assumption seems rather optimistic for a VHTR core. Isotherms for H-3 chemisorption on graphite are described in Section 8.1.2.3.

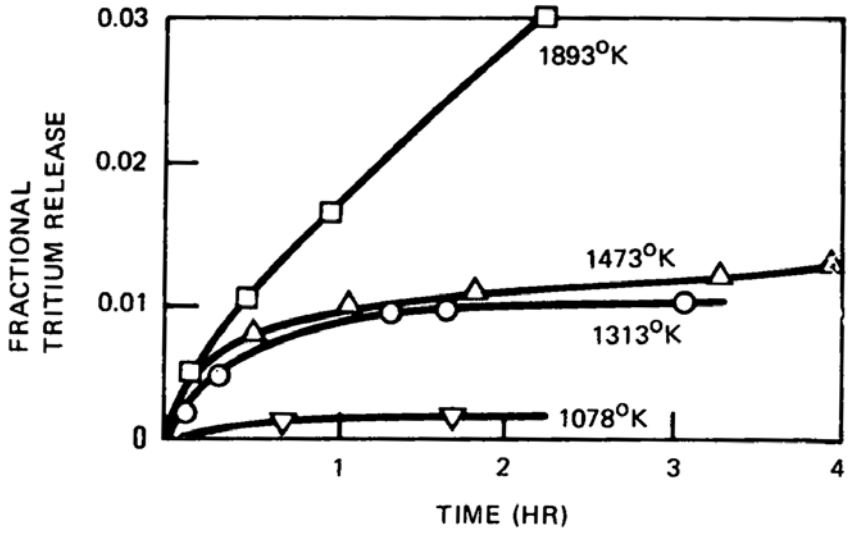

Figure 5-5. H-3 Release from Graphite during Postirradiation Heating

5.5.1.3 H-3 Release from Control Materials

Boron-10 is used as a neutron absorber in control rods, in burnable poison in fuel elements, and often in the permanent reflectors and core support structure to reduce neutron damage. Several neutron capture reactions with these B-10 control materials in the core will produce tritium (Section 5.4). The boron is typically present as B_4C granules which have been pressed into pellets with a carbonaceous binder.

There are limited data available on H-3 release from B_4C pellets. Data presented by Gainey [1976] for tritium release from B_4C pellets shows a minimum fractional release of about 20% at approximately 760 °C, with increasing release fractions at hotter and colder temperatures. Tritium release fractions between 80 and 85% were measured at temperatures of 593 and 871 °C. These H-3 release data were obtained from [Pitner 1973]; the results are shown in Figures 5-6 and 5-7. Little information was provided about the physical characteristics of the B_4C pellets used in these experiments so it is not clear how representative the samples were of the B_4C used in HTGRs. These results show the H-3 fractional release a complex function of irradiation temperature but not the burnup level. This behavior was thought to be due to the

way in which tritium combined chemically with the B_4C. Annealing at temperatures well above the irradiation temperature was necessary to release tritium from the pellets.

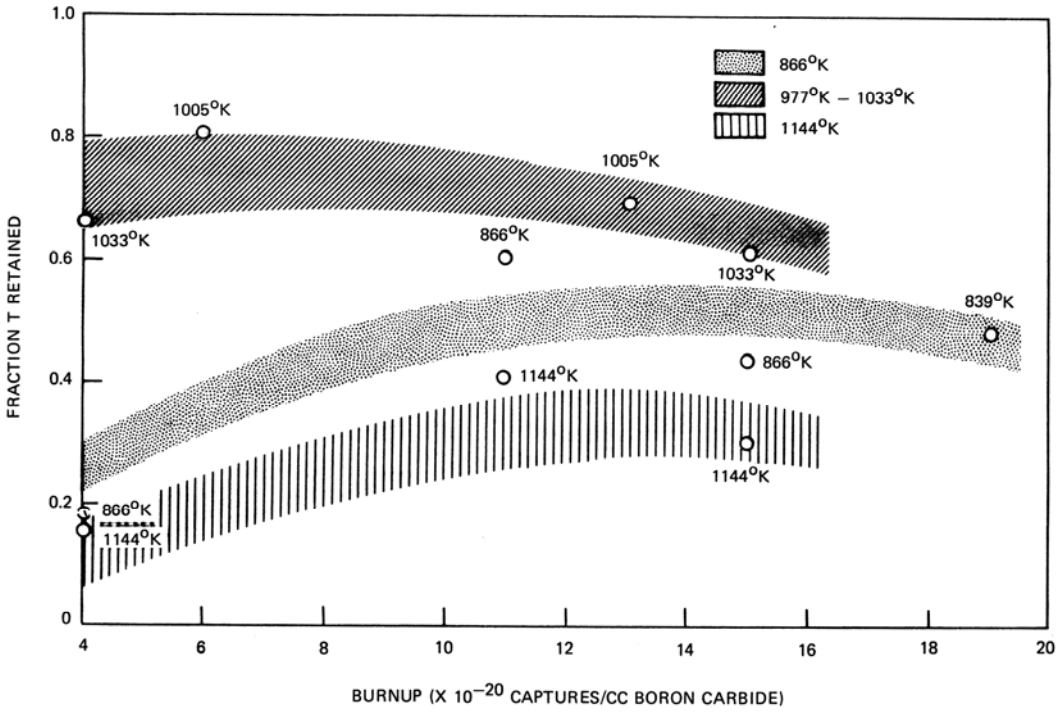

Figure 5-6. Tritium Retained in Boron Carbide

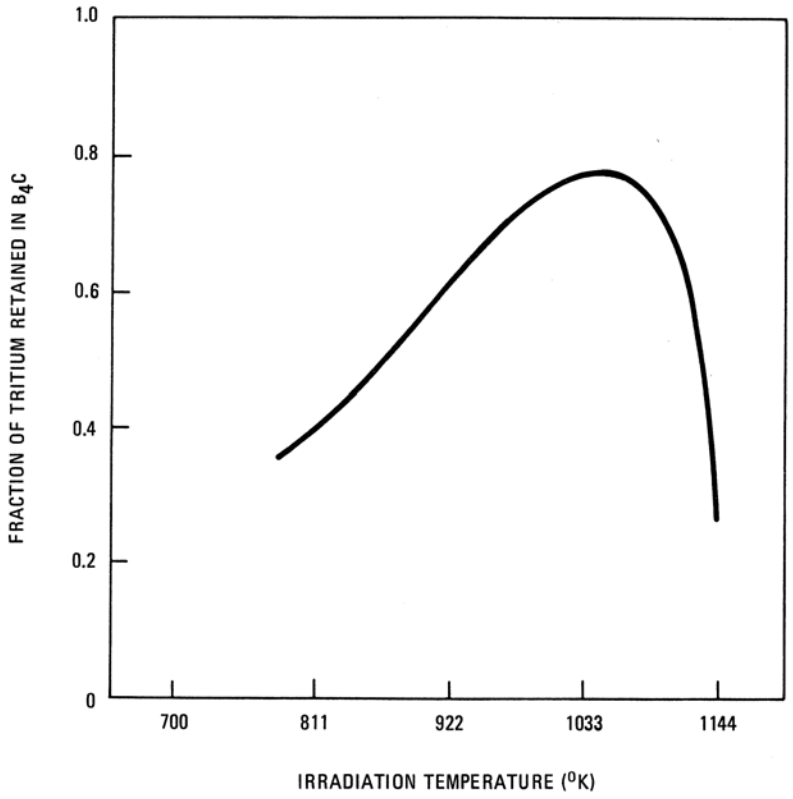

Figure 5-7. Temperature Dependence of H-3 Retention in B_4C Pellets

One of the design issues associated with the use of B_4C as a control material in HTGR cores is that it can hydrolyze if exposed to water, forming volatile boric acid which leads to the potential for migration of neutron poison within the core. In fact, hydrolysis of the B_4C in the reserve shutdown pellets with the attendant formation of boric acid did occur in Fort St. Vrain as a result of water ingress; although this occurrence presented no safety issue for FSV operation, it was nevertheless an undesirable operational event [Asmussen 1983].

One design option for mitigating the potential for B_4C hydrolysis is to apply a protective coating to the B_4C granules prior to pressing them into pellets. Such protective coatings should also increase the tritium retention. Specimens of B_4C granules coated with dense pyrocarbon and other specimens coated with SiC were prepared and irradiated as piggyback samples in fuel irradiation capsule HRB-21 [Heffernan 1991]. Unfortunately, only the structural integrity of the coated B_4C particles was examined visually during the postirradiation examination [Acharya 1995], and the tritium retention characteristics were not determined.

5.5.2 Tritium Removal from Primary Coolant

The various sinks which can remove H-3 from the primary coolant are described below. With the exception of the helium purification system, the effectiveness of these various removal mechanisms is not well quantified.

5.5.2.1 Removal by Recoil

In neutron activation reactions, tritium is generated as a triton, which is the tritium nucleus without an orbiting electron (i.e., a positively charged tritium ion); a triton is highly reactive. Tritons produced by neutron activation reactions in solids, such as graphite, could energetically recoil into graphite crystallites where they could displace hydrogen in a C-H bond or carbon in a C-C bond. This recoil action might also produce additional active sites upon which further chemisorption could occur. It is not known what fraction of tritium trapped by recoil is held irreversibly; the estimates range from a high of 99% [Compere 1974] to ~20% [Gainey 1976]. Tritons produced by neutron capture reactions in boron control materials may also react chemically with the carbon in the B_4C [Gainey 1976].

Tritons from He-3 activation in the primary coolant will come to rest in solids in fractions which vary from region to region because of the varying proportion of space associated with coolant channels and fabricated holes, clearance annuli, and pores. The recoil energy of a triton is about 0.2 MeV leading to an estimated range of 0.05 cm (500 μm) in helium at 47.6 atm and 600 ^{o}C. Because graphite pores generally are smaller than 0.05 cm, the fraction bound is generally assumed to be unity [Compere 1974].

5.5.2.2 Removal by Chemisorption on Graphite

All isotopes of hydrogen chemisorb on graphite, especially at high temperatures. Tritium entering the primary coolant becomes equilibrated with the relatively much larger concentration of ordinary hydrogen (i.e., protium) which is present in the primary coolant (~10 ppmv H_2 is a typical value for steam-cycle HTGRs), and its chemical behavior then becomes indistinguishable from that of ordinary hydrogen.

There are a limited number of old (pre-1980) measurements of hydrogen sorption on nuclear graphite. An example of these old data is the measurement of hydrogen sorption on TSP nuclear graphite shown in Figure 5-8. Note that the sorptivity increases with increasing temperature up to about 1100 ^{o}C (which is well above the peak temperatures experienced by the core reflector graphite).

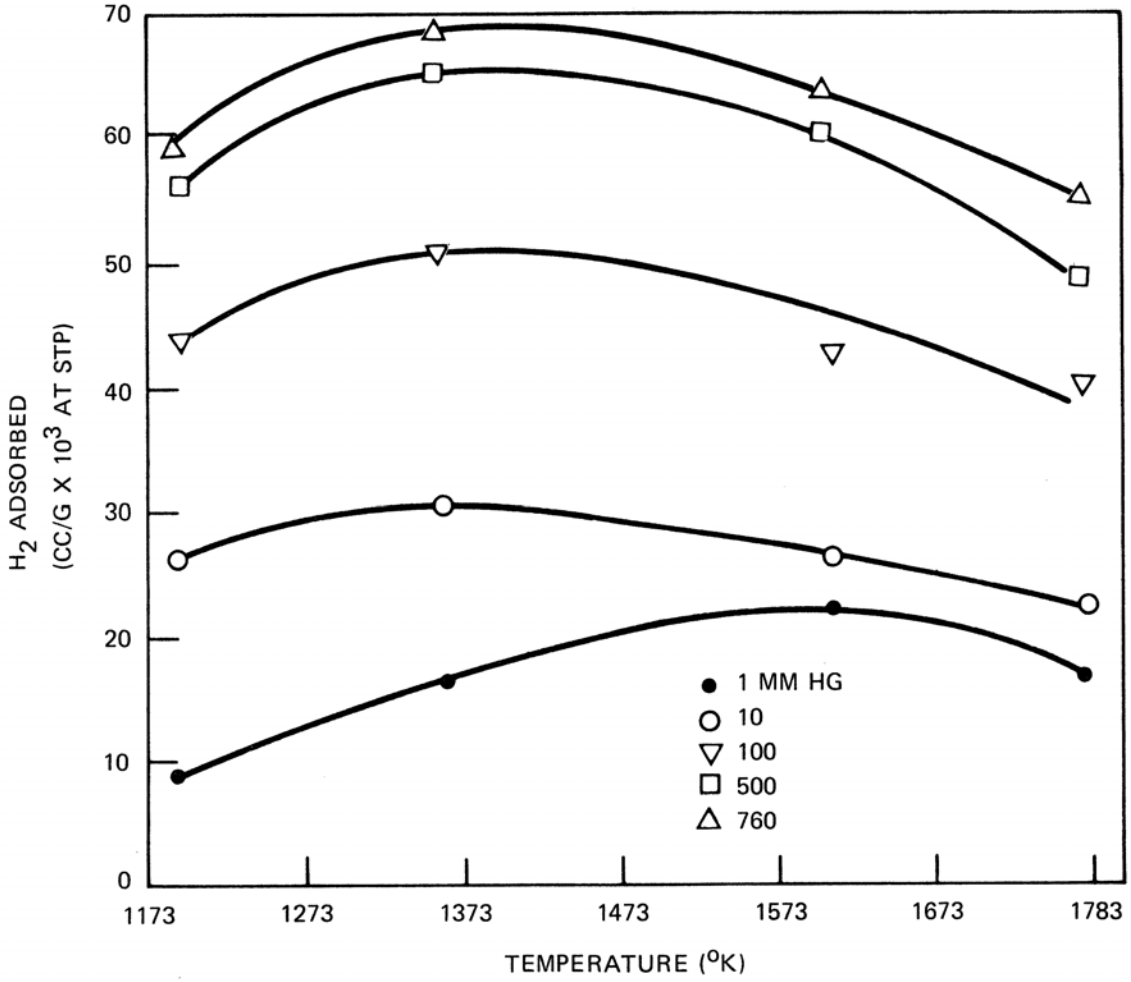

Figure 5-8. Hydrogen Sorption on TSP Nuclear Graphite

In the mid-1980s Strehlow [1985] at ORNL measured the sorptivities of several nuclear graphite, including H-327 and POCO, for tritium gas and tritium oxide at temperatures ranging from 175 to 750 °C.[16] Higher temperatures were found to result in tritium sorption at concentrations as high as 2.1×10^{13} a/cm^2. Sorbed quantities at lower temperatures after exposure to either tritium oxide or tritium gas were found to be in the range of 1×10^8 a/cm^2, some five orders of magnitude lower. Oxidized specimens showed the expected profile effects of greater penetration of the tritium into the specimens. The relationship of the BET surface area to the amount adsorbed appeared to be linear for oxidized specimens; however, the

[16] These results are reported in a brief journal article [Strehlow 1985]. Surprisingly, no detailed technical report could be located in the ORNL library.

amount of tritium sorbed by unoxidized specimens could not be simply related to the BET surface area.

High-purity graphite is also a candidate material for various applications in magnetic confinement fusion reactors, including for the first wall. Consequently, tritium sorption on graphite has also been investigated by fusion researchers [e.g., Causey 1989]. Typically, the experimental conditions investigated are not representative of the conditions in an HTGR primary circuit.

Typically, hydrogen and tritium sorption graphite is correlated using a Temkin isotherm.[17] The classical form of a Temkin isotherm is given as:

$$\frac{\theta}{1-\theta} = aP\exp[Q(1-\alpha\theta)/RT] \tag{5-18}$$

where: a = adsorption constant (atm^{-1}),
P = gas pressure (atm),
Q = heat of adsorption at zero coverage (J/mol),
R = gas constant (8.314 J/mol-K),
T = absolute temperature (K),
α = factor for change in heat of adsorption with coverage,
θ = fractional surface coverage.

During and after water ingress, the loss of tritium from the graphite by exchange with the hydrogen in the water for tritium on the graphite becomes significant [Myers 1986]. That this occurs at low temperatures is reported although experiments have been conducted in which no significant amount tritiated water has been detected below 400 °C. In FSV, water ingress occurring during startup and shutdown led to large increases in the tritium concentration in the primary coolant. As an estimate of the effect of water ingress on the release of tritium sorbed on graphite, a release of roughly 67% of the sorbed tritium is postulated on the basis of the observed tritium content of 3.7 μCi/g-graphite in FSV graphite dust samples which have experienced water ingresses and the expected content of between 10 and 15 μCi/g-graphite in the absence of water.

[17] With a Temkin isotherm, the heat of adsorption decreases as a linear function of increasing fractional surface coverage. In contrast, the heat of adsorption is constant with a Langmuir isotherm and decreases as an exponential function of increasing fractional surface coverage with a Freundlich isotherm.

5.5.2.3 Removal by the Helium Purification System

The He purification system for the GT-MHR was described in Section 2.4. With such a design, control of hydrogen and tritium is accomplished by the use of copper oxide beds to oxidize the H_2 and HT to H_2O and HTO, respectively. The tritiated water is subsequently removed by molecular sieve dryers downstream of the oxidizers. Any trace amounts of HT or HTO remaining in the helium will be completely removed by the liquid nitrogen-cooled charcoal beds which are included in the train primarily to remove noble gases.

All operating HTGRs have utilized an HPS design which included oxidizer beds for the removal of hydrogen and tritium with the exception of Fort St. Vrain (see Section 8 for details). Instead of oxidizer beds, the FSV HPS used titanium sponge getter beds for the removal of hydrogen and tritium. These Ti getter beds frequently became inactivated by CO and N_2 impurities present in the primary helium. However, the practical consequences for FSV operation were negligible because the core graphite proved to be a far more efficient sink than the HPS for the removal of hydrogen and tritium from the coolant. Nevertheless, all subsequent GA HPS designs have utilized oxidizer beds and dryers for controlling hydrogen and tritium, and the future use of Ti getters is not recommended based upon the FSV experience.

In the simplest case, the primary coolant activity of member i of a decay chain is given by [e.g., Haire 1974]:

$$\frac{dA_{i,circ}}{dt} = (R/B)_i B_i - (\lambda_i + r_{HPS} + r_{po}) A_{i,circ} \tag{5-19}$$

and

$$r_{HPS} = \frac{\dot{m}_{HPS}}{M} \tag{5-20}$$

and

$$r_{po} = -\frac{\dot{m}_{He}}{M} \ln(1-\tau) \tag{5-21}$$

where: $(R/B)_i$ = release rate-to-birth rate ratio for nuclide i (numerically equal to the steady-state fractional release),

$A_{i,circ}$ = circulating activity of nuclide i (Ci),
B_i = birth rate for nuclide i (Ci/sec),
λ_i = decay constant (sec^{-1}),
r_{HPS} = purification constant (sec^{-1}),
r_{po} = plateout removal constant (sec^{-1}),
$\dot{m}_{HPS}$ = sidestream HPS mass flow rate (kg/see),
M = total mass of circulating He in primary circuit (kg),

$\dot{m}_{He}$ = primary He mass flow rate (kg/see),

τ = "plateout per pass," the fraction of a condensable radionuclide removed during one transit through the primary circuit.

With the initial condition of $A_{i,circ} = 0$ at t = 0, Equation (5-19) is integrated to give:

$$A_{i,circ} = \frac{(R/B)_i B}{1 + \frac{r_{HPS} + r_{po}}{\lambda_i}} 1 - \left(e^{-(\lambda_i + r_{HPS} + r_{po})t} \right) \qquad (5\text{-}22)$$

5.5.2.4 H-3 Permeation through Metals

As previously discussed, tritium is of concern for hydrogen-producing VHTRs because the isotopes of hydrogen, including tritium, can permeate through most solid materials, including those metals comprising heat exchangers, and contaminate the product hydrogen. The permeation of hydrogen isotopes through metals and ceramics has been investigated for many decades. There is a vast literature on the topic and on-going research, especially in the fusion community; however, the data are limited for the specific combination of materials of construction, service temperatures, tritium and hydrogen concentrations, and oxidation potentials that are postulated for the IHX and the H_2 process plant of an H2-MHR.

The available data indicate that each of the aforementioned variables can be important. A key factor, which is discussed in more detail below, is that the hydrogen permeability of most metals is strongly influenced by the oxidation potential and the attendant surface oxide layers that are typically present on both sides of the wall material in a heat exchanger, such as the steam generator in a steam-cycle HTGR or the IHX in an H2-MHR. In general, the presence of a coherent oxide layer can reduce the effective hydrogen permeability by orders of magnitude.

While these oxide-permeation barrier phenomena could, in principle, be very beneficial in an operating H2-MHR, they are also a major complication: (1) modeling of H-3 permeation behavior must account for the effect of the oxide layers; (2) accurate prediction of H-3 behavior, including product contamination, in an H2-MHR must address the effects of coolant chemistry and oxide-layer formation; (3) extrapolation of existing hydrogen permeation data to H2-MHR service conditions becomes more uncertain; and (4) any experimental measurements of H-3 permeation rates through candidate materials of construction for the IHX should include representative coolant chemistries and surface layers on both sides of the material. At this stage of development of a first-of-a-kind facility, it is practically impossible to predict with high confidence the coolant chemistries, hence characteristic surface oxidation states, in the primary and secondary circuits of an H2-MHR.

The general approach that has been taken in modeling the permeation of hydrogen isotopes through metals and in correlating experimental permeation data is summarized below.

5.5.2.4.1 Permeation Models and Data Correlation

In the first approximation, the permeation of gases, including tritium, through metals is usually described in terms of Fick's first law of diffusion; in one dimension, the flux is proportional to the concentration gradient (after [Gainey 1976]):

$$J = -D_g \frac{dC}{dx} \tag{5-23}$$

where: J = permeation flux (atom/cm^2-sec),
D_g = gaseous diffusion coefficient (cm^2/sec),
C = concentration in the metal (atom/cm^3),
x = distance (cm).

Sievert's law states that the equilibrium concentration of a diatomic gas dissolved in a metal is given by (i.e., the gas has dissociated and is migrating in atomic form):

$$C = K_s p^{1/2} \tag{5-24}$$

where: K_s = Sievert's law constant [cm^3(STP)-mm/cm^2-torr^{½}],
p = pressure (torr),

Combining Fick's law with Sievert's law (for a small wall thickness) gives

$$J = \frac{K_p}{x}(p_1^{1/2} - p_2^{1/2}) \tag{5-25}$$

where K_p includes both the diffusion coefficient and Sievert's law constant and is called a permeability coefficient [cm^3(STP)-mm/cm^2-sec-torr^{½}]. The subscript 1 refers to upstream pressure while subscript 2 refers to downstream pressure. When the downstream pressure is low,

$$J \approx \frac{K_p}{x}(p_1^{1/2}) \tag{5-26}$$

The square-root of pressure dependence of J assumes that the diatomic gas dissociates and permeates through the metal lattice in the atomic state.

K_p may be written in the form of an Arrhenius relation:

$$K_p = K_o \exp(-Q/RT) \tag{5-27}$$

where K_o = preexponential factor [cm^3(STP)-mm/cm^2-sec-$torr^{1/2}$],
Q = activation energy for gas permeation (J/mol),
R = gas constant,
T = absolute temperature (K)

As postulated above, measured hydrogen isotope permeabilities in metals generally show exponential temperature dependence as illustrated in Figure 5-9 for Incoloy 800 [Gainey 1976]; the measured activation energies are generally less than 20,000 cal/mol and are occasionally quite small (e.g., 3430 cal/mol for niobium).

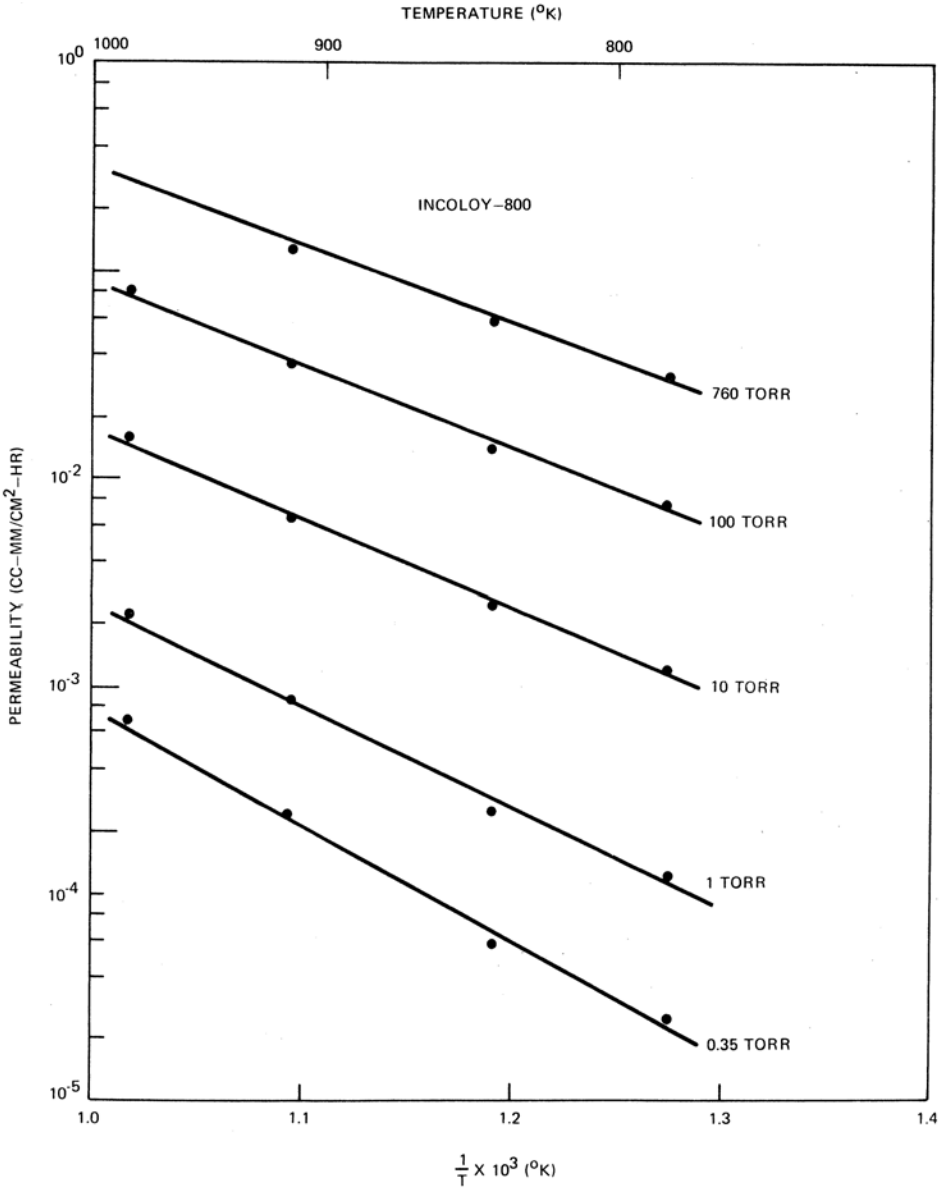

Figure 5-9. Hydrogen Permeation through Incoloy 800

However, the observed dependence of the permeation rate on hydrogen partial pressure is often different from the square-root dependence predicted by Eqns. (5-25) and (5-26), especially if the experimental data span a large partial pressure range. In fact, the data often show a square root of pressure dependence at high partial pressures; a pressure dependence between square root and linear at intermediate partial pressures; and a square root dependence again at very low partial pressures [Gainey 1976]. The first two observations are easily rationalized: diatomic gases are assumed to dissociate and permeate through metal lattices in the atomic state (square-root pressure dependence; see above), but they are assumed to permeate through oxides in the molecular state (linear pressure dependence). Since it is difficult to prevent at least a partial oxide layer from forming on most metals (exceptions being the noble metals, nickel, etc.,), pressure dependence between square root and linear suggests the presence of an oxide layer which represents a resistance to permeation of the same order of magnitude as that of the base metal.

The observation that the pressure dependence again becomes square root at very low partial pressures is more difficult to rationalize. Strehlow and Savage [1974] suggested that defects or cracks in the oxide layer could be responsible for this behavior. The expected behavior for the permeation of hydrogen through a metal coated with an oxide containing no holes or other gross imperfections is illustrated in the upper diagram of Figure 5-10. Permeation through a metal with an oxide film that contains cracks, holes, or other porosity would be expected to lead to a different asymptote when the permeation rate is low. Defects in the film constitute a path for permeation which is parallel to that through the crystalline portion of the oxide but which is in series with the path through the metal. The flux through the defects would add to that through the crystalline oxide, with the net flux expected to depend on the half power of driving pressure according to Strehlow and Savage (the basis for this conclusion is the citation of unpublished ORNL-4881). The general behavior expected for permeation through a metal with a defective oxide film is illustrated in the lower diagram of Figure 5-10.

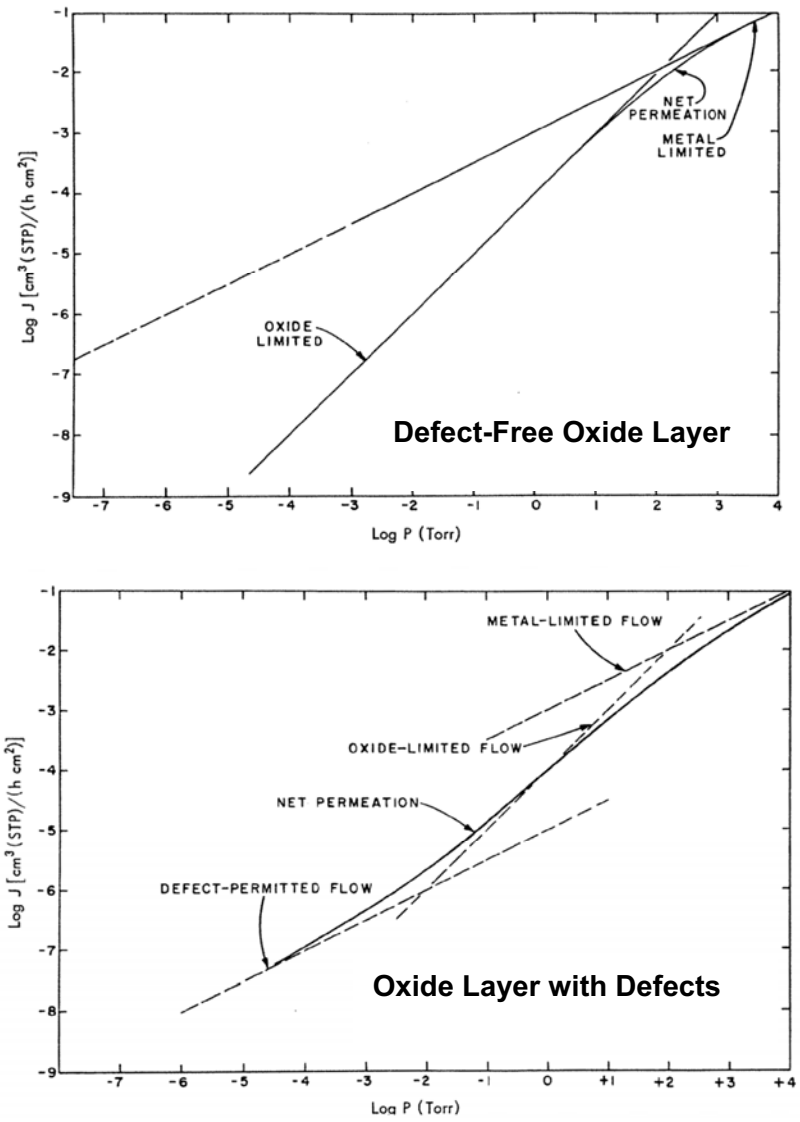

Figure 5-10. Effect of Oxide Films on Permeation Pressure Dependence

A recurring theme in the hydrogen permeation literature is that the oxidation effects must be considered in modeling and data correlation. A dramatic illustration of the effect of oxidation is given in Figure 5-11. Workers at ORNL [Bell 1975] used a mixed isotope technique to measure the permeability of tritium through Incoloy 800 with a controlled steam atmosphere on the inside of the tube. Hence, the influence of surface oxidation on tritium permeation was determined. A long-term experiment (>2000 hr) was conducted with Incoloy 800 at 930 K with the inside of the tube continuously purged with a sweep gas of Ar/H_2O with a H_2O partial pressure of 0.3 MPa. The tritium permeability of the metal dropped continuously with time (a factor of 160 in 84 days, which was attributed to the progressive oxidation of the metal to form a protective oxide coating. The permeability rapidly decreased for the first 36 hr, and then linearly decreased at a much

slower rate as a function of the square root of time, suggesting that diffusion through a growing oxide layer was the rate limiting step.

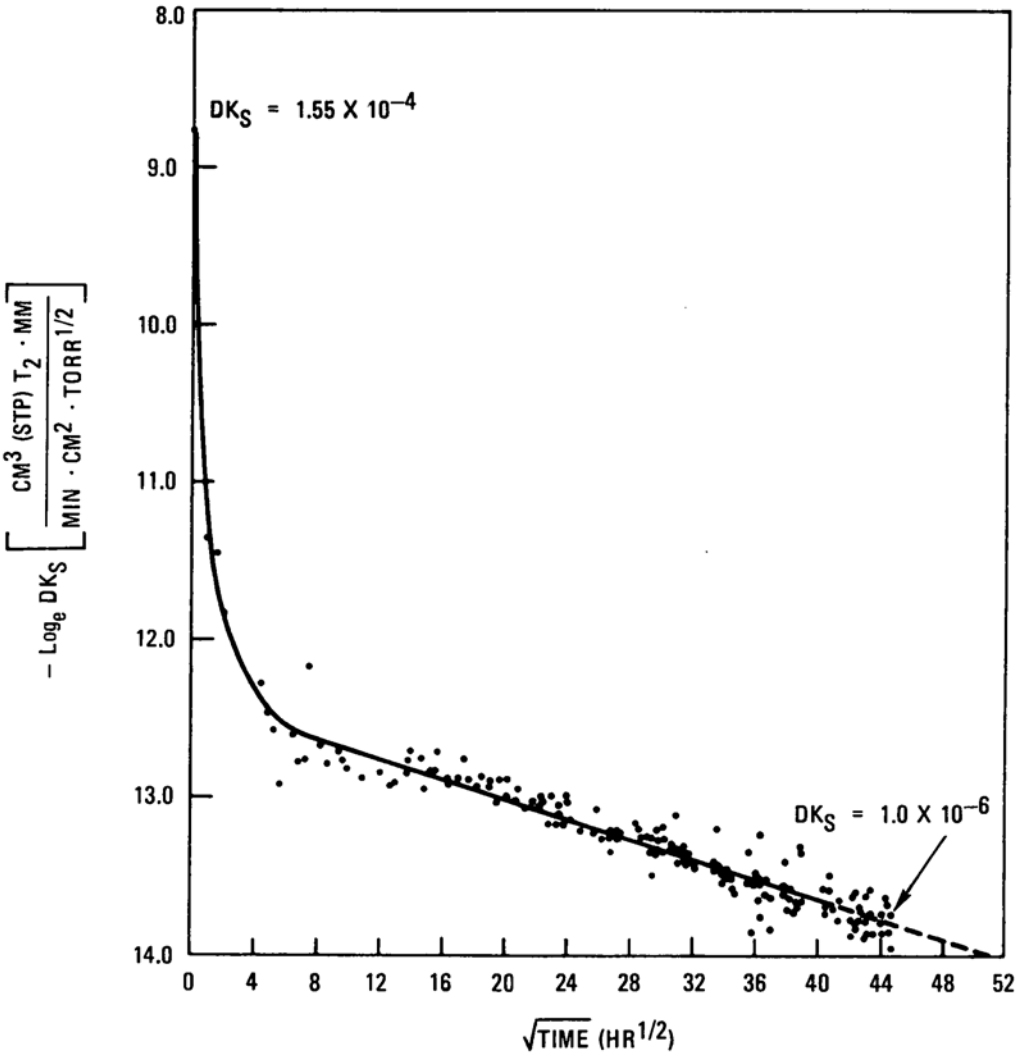

Figure 5-11. Effect of Steam Oxidation on H-3 Permeation through I-800

Given such results, it is important that the surface oxidation state be considered when developing H-3 permeation models and when performing H-3 permeation measurements.

5.5.2.4.2 H-3 Permeation Data

There is a large and growing literature regarding the permeabilities of hydrogen isotopes through a variety of metals and ceramics.[18] The topic is being actively investigated by the fusion community because possible tritium release from breeding blankets will be a design and safety issue for fusion power plants. Despite this large literature, relatively little H-3 permeation data have been identified for the exact service conditions anticipated for the IHX in an H2-MHR. Takeda [1999) has assembled the relevant hydrogen permeation data for high-temperature alloys relevant for the IHX in an H2-MHR; his efforts are summarized in Table 5-3. The greatest weakness of these data is that the coolant chemistry was often unspecified and uncontrolled in the subject tests.

Table 5-3. Hydrogen Permeabilities for High-Temperature Alloys

Alloy	Pre-exponential factor K_o [cm^3(NTP)-cm^{-1}-s^{-1}-$Pa^{-0.5}$]	Activation energy E_o [$kJ.mol^{-1}$]	Temperature T [°C]
Nickel	7.73×10^{-5}	54.84	-
Inconel-600	2.22×10^{-4}	66.14	800 - 1000
Inconel-625	1.37×10^{-4}	62.12	800 - 1000
Incoloy-600*	1.00×10^{-4}	64.05	700 - 950
Incoloy-800	2.13×10^{-4}	69.07	800 - 1000
Incoloy-800*	5.45×10^{-4}	64.05	700 - 950
Incoloy-800	2.31×10^{-4}	74.1	600 - 950
Incoloy-800**	9.77×10^{-5}	74.1	649
Incoloy-807	2.96×10^{-4}	73.18	800 - 1000
Hastelloy-N**	2.59×10^{-4}	77.99	605
Hastelloy-X	2.00×10^{-4}	66.98	800 - 1000
Hastelloy-XR	1.0×10^{-4}	67.2	570 - 820
Hastelloy-XR*	4.7×10^{-5}	70.2	800
Hastelloy-XR**	2.5×10^{-4}	76.6	670 - 820

*Some oxidation of test specimen. **Deuterium data.

The leading candidate material for the IHX and for the superheater section of the steam generator is IN 617. While the tritium permeability of IN 617 has not been as well characterized

[18] For example, a Google search in April 2008, resulted in 562,000 hits for “hydrogen permeation metals;” 58,200 hits for “tritium permeation metals;” and 641 hits for “hydrogen permeation Inconel 617.”

as that of some other metals, including Alloy 800H, there are several German comparative studies that indicate the tritium permeabilities of IN 617 and Alloy 800H are quite comparable at the service temperatures anticipated for the NGNP IHX and steam generator [Schaefer 1984, Schmidt 1985]. The permeabilities of a number of high-temperature alloys, including IN 617 and Alloy 800H, are compared in Figure 5-12 [Schmidt 1985]. At the temperatures of interest for the NGNP, the nominal differences in the H-3 permeabilities of IN 617 and Alloy 800H are small (<2x); in fact, the differences are much smaller than the variabilities for either alloy as a function of oxidation state. Consequently, in the TRITGO mass balance analysis (Section 8), the so-called "CEGA" correlation for Alloy 800H (Section 8.1.2.4.2) was used for IN 617 as well.

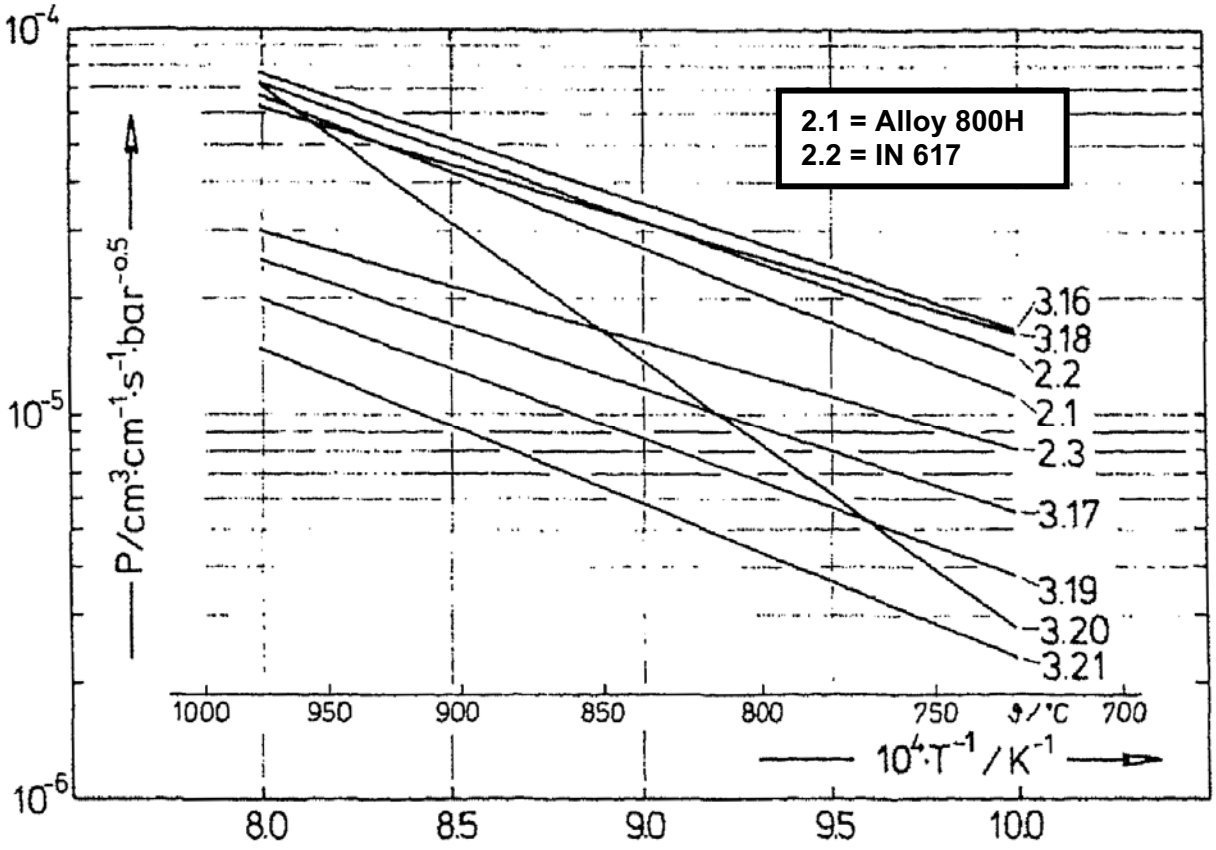

Figure 5-12. Comparison of the H-3 Permeabilities of High-Temperature Alloys

In fact, one of the greatest challenges when predicting the extent of product contamination in a H2-MHR is that the primary and secondary coolant chemistries in such a first-of-a-kind plant cannot be predicted with high confidence. As a practical matter, these uncertainties will remain until there are actual operating data from an operating H2-MHR. As mentioned previously, the first data could be available shortly after 2010 if the plans to couple a SI pilot plant to the HTTR come to fruition.

5.5.2.5 Sorption on Metal Surfaces

Hydrogen, and by inference tritium as well, chemisorbs on metals, especially noble metals and high-nickel alloys. Tests in Sweden [Gainey 1976] have also shown that tritium will sorb on metal oxide films that are in contact with tritiated water. However, the amount of metal surface area in the primary circuit of a VHTR is small compared to the huge BET surface area of the graphite structures in the reactor system. Hence, sorption on metal surfaces, especially at the high service temperatures in the primary coolant loop of a VHTR, is considered to be insignificant compared to the sorption on the core graphite.

5.6 Requirements Mandating Tritium Control

The 10CFR20 limits for occupational exposure, including a factor of 10 ALARA margin, will have to be met for all pathways that expose plant workers to tritium-contaminated hydrogen and to tritium-contaminated process steam and secondary coolant water. The 10CFR50, Appendix I, dose limits for off-site releases from nuclear power plants during normal operation will have to met, including the contributions from tritium releases via liquid, gaseous, and solid pathways. These regulatory limits will be the basis for deriving quantitative tritium release limits once a conceptual NGNP plant design is defined.

5.7 Limits on Tritium Contamination in Products

A perplexing challenge at this stage of the NGNP Project is to set a provisional limit on the allowable tritium contamination in the product hydrogen and/or process steam when there is no conceptual plant design. The international regulatory standards for allowable tritium contamination in air and drinking vary remarkably (see Table 5-4). For example, the regulatory limits on tritium in drinking water (Table 5-5) vary from a low of 2.7 pCi/g in France to 2057 pCi/g in Australia to no tritium-specific regulatory limits in Japan and Korea (although the public exposure from all sources of artificial radiation is obviously controlled); the US EPA standard is 20 pCi/g (0.74 Bq/g) [CNSC 2008]. Traditional exposure pathway analysis for specific assumed release and transport scenarios appears inappropriate for this immature stage of NGNP design definition. Consequently, it is recommended that the US EPA drinking water standard of 20 pCi/g be provisionally adopted as the goal for allowable tritium contamination in the product hydrogen and/or process steam for NGNP preconceptual design.

This recommendation can be compared with the previous German goal of ≤10 pCi/g of tritium in synthetic natural gas produced by coal gasification with a pebble-bed HTR (the so-called PNP Project). It is fully expected that when the NGNP conceptual design is defined and a traditional exposure pathway analysis is performed, it will be demonstrated that this 20 pCi/g limit on tritium contamination is excessively conservative and that it can be relaxed by at least two orders of magnitude (as was the case for the PNP Project). Consequently, this recommended

limit should not be considered a formal requirement for the NGNP Project but an early and ambitious figure-of-merit for use until the conceptual design is defined.

Table 5-4. International Limits on Tritium Contamination in Various Media

Organization	H-3 Limit	Value
Regulatory Limits		
US NRC	Air	**84 pCi/g** (100 pCi/l)
US EPA	Drinking Water	**20 pCi/g** (20,000 pCi/l)
France, Germany, UK	Drinking Water	**2.7 pCi/g** (100 Bq/l)
Canada (Ontario)	Drinking Water	**189 pCi/g** (7000 Bq/l)
Australia	Drinking Water	**2057 pCi/g** (76,103 Bq/l)
IAEA	Exemption Limits	**27 x 10^6 pCi/g** (10^6 Bq/g)
Programmatic Limits		
PNP (FRG)	H-3 in syn gas	**10 pCi/g**
KINS (Korean "ACRS")	H-3 in hydrogen (IAEA limit)	**27 x 10^6 pCi/g**
KAERI (Korea)	Air	**6284 pCi/g** (232.5 Bq/g)
KAERI (Korea)	Water	**1081 pCi/g** (40 Bq/g)
JAERI (Japan)	H-3 in hydrogen	**1510 pCi/g**
NGNP	H-3 in hydrogen/steam	[**20/20**] **pCi/g** (EPA H_20)

Table 5-5. International Limits for Tritium in Drinking Water

TABLE A1.
SUMMARY TABLE OF INTERNATIONAL LIMITS FOR TRITIUM IN DRINKING WATER

		Power reactors*		Information Obtained	Tritium Limit (Bq/L)
		CANDU	Total		
CANDU OWNERS	Canada	18	18	yes	7,000
	- Alberta	0	0	yes	7,000
	- Manitoba	0	0	yes	7,000
	- N. Brunswick	1	1	yes	none
	- Ontario	16	16	yes	7,000
	- Quebec	1	1	yes	7,000
	India	15	17	no	n/a
	Republic of Korea	4	20	partly	none
	Romania	2	2	yes	100
	China	2	10	yes	none
	Argentina	1	12	partly	none
	Pakistan	1	2	no	n/a
EU	Total	2	126	yes	100
	Belgium	0	7	yes	100
	Finland	0	4	yes	30,000
	France	0	59	yes	100
	Germany	0	17	yes	100
	Italy	0	0	yes	100
	Northern Ireland	0	0	yes	100
	Scotland	0	2	yes	100
	Spain	0	8	yes	100
	Sweden	0	10	yes	100
	United Kingdom	0	19	yes	100
OTHER	Australia	0	0	yes	76,103
	Japan	0	53	partly	none
	Norway	0	0	yes	100
	Russia	0	31	partly	7,700
	Switzerland	0	5	yes	10,000
	United States	0	103	yes	740
	- California	0	4	yes	740
	WHO	n/a	n/a	yes	10,000

* Sources:

World Nuclear Association reactor database
http://www.world-nuclear.org/reference/reactorsdb_index.php
CANDU Owners Group website
http://www.candu.org

6. LIMITS ON DUST PRODUCTION IN THE PRIMARY CIRCUIT

Some level of particulate matter (“dust”) will be present in the primary coolant circuit of a VHTR. Based upon past HTGR operating experience, the levels of dust in the primary circuit of a VHTR with a prismatic core are expected to be much lower than with a pebble core. Nevertheless, the NGNP will be a first-of-a-kind (FOAK) plant, and limits need to be established on the allowable levels of dust accumulation in the primary circuit in order to avoid possible deleterious effects on the mechanical integrity of primary circuit components (e.g., abrasion) and/or on system performance (e.g., heat exchanger fouling). Dust in the primary circuit is addressed in this section to:

1. Identify experience bases for its determinations;

2. Address the potential impacts of dust on the performance of primary circuit components (e.g., heat exchanger fouling, instrument line plugging, effects on materials, etc); and

3. To determine, based on available information, recommendations for circulating and deposited dust loading goals or limits to preclude deleterious effects, and their impact on the process flow requirements to the Helium Purification System (see Section 2.4 for an overview of the HPS design and performance).

6.1 Sources of and Sinks for Dust in an HTGR

Sources of dust in an HTGR primary coolant system are potentially from:

1. Foreign material introduced into the system during initial construction or refueling;
2. Graphite or carbonaceous dust resulting from friction or erosion of prismatic fuel or reflector surfaces exposed to the helium coolant.
3. Foreign material introduced from interfacing systems;
4. Corrosion or erosion products from metallic surfaces of the coolant system
5. Carbon deposition as a result of CO decomposition

Quantitative prediction of these sources has historically been problematic and therefore, largely experience based. This has historically been the case as well in the somewhat analogous development of activation source terms and cleanup system design for Light Water Reactors (LWRs).

Sinks for these dust products are deposition onto reactor coolant system surfaces and removal by the HPS high temperature filter.

Deposition of dust on surfaces exposed to high velocity helium flow such as coolant channels, heat transfer surfaces, and power conversion system turbine surfaces will involve deposition and resuspension effects that will likely result in an equilibrium loading. Low velocity locations may accumulate settled particulates.

6.2 Helium Purification System Performance Requirements

The NGNP System Requirements Manual [SRM 2007] identifies the following operational requirements for the HPS:

- The helium purification trains shall be designed to remove the following major chemical impurities: CO, CO_2, H_2 (including Tritium), N_2, O_2, H_2S, CH_4, and other hydrocarbons. Lesser amounts of impurities such as Br, I, H_2O, Kr, and Xe shall also be removed along with filterable particulates and certain metallic elements.
- Each helium purification train shall process the primary coolant helium at a constant volumetric flow rate regardless of the primary coolant system pressure. At 100% of rated reactor power and vessel system pressure, the helium purification subsystem shall process primary coolant at a rate of {TBD} kg/s.
- Each helium purification train shall be designed for a gross throughput sufficient to allow depressurization of the Vessel System within 24 hours following a reactor shutdown. Each helium purification train shall be sized such that the purification constant r_p = (mass flow rate through the helium purification subsystem)/(total mass of circulating helium) is ≥ 2.9 x 10^{-5} per second.

Based on a nominal GT-MHR design the total mass of circulating helium of ~10,000 lbs, the final criterion yields a minimum purification flow of ~ 500 kg/hr. NUREG/CR6824 “Materials Behavior in HTGR Environments” [2003] uses a basis of 0.5 kg/sec or 1800 kg/hour. Total circulating coolant flow is 325 kg/sec, so these cleanup flow rates represent a fraction of between 0.04% and 0.15% of coolant flow. These cleanup rates are comparable to the PWR letdown cleanup flow fraction of total reactor coolant flow. An overview of the GT-MHR HPS is given in Section 2.4.

6.3 HTGR Operating Experience with Dust Production and Behavior

A review of HTGR operating experience is necessary to establish dust production and behavior. Both the Peach Bottom and Fort St. Vrain (FSV) experience with respect to dust composition and concentrations are expected to be atypical for the NGNP (and a commercial VHTR). The dust data from the German AVR and THTR pebble-bed reactors are almost certainly even more atypical for a prismatic-core NGNP because of the pebble bed associated abrasion - induced

dust production. The most prototypical dust data for a prismatic-core NGNP are expected to be from the Japanese 30 MW(t) HTTR which has a prismatic core, a 10 MW intermediate heat exchanger, and 20 MW pressurized water cooler in the primary circuit. HTTR has never experienced oil or water ingress.

6.3.1 Peach Bottom Prismatic HTGR

Peach Bottom Unit 1 was a 115 MW(t)/40 MW(e) prototype HTGR with a two-loop primary coolant circuit comprised of a steel reactor vessel, vertical U-tube steam generators, electric motor-driven oil-lubricated compressors, and interconnecting piping. After seven years of commercial operation, the reactor was shut down for decommissioning in 1974 because of its perceived uneconomically small size. An extensive end-of-life (EOL) R&D program was conducted to validate reference GA design methods with emphasis on fission product transport and Incoloy 800 material performance [Steward 1978].

The Peach Bottom primary circuit was coated with a carbonaceous deposit from the cracking of lubricating oil that leaked in from a purified He transfer compressor in the He purification system [Dyer 1977, Wichner 1991]. The dust in Peach Bottom was characterized by the following measurements: (1) plateout probes and cascade impactors that were used to sample the primary coolant [Dyer 1977]; (2) samples of the particulate matter removed by the cyclone filters that processed a side stream of the primary coolant [Dyer 1977]; and (3) examination of the carbon deposits on the samples of steam-generator tubes and gas ducts that were removed during the EOL R&D program [Steward 1978]. The results are summarized in [Wichner 1991].

The carbon deposit in the Peach Bottom primary circuit had no deleterious effects on plant operation. Oil bearings will not be used in the NGNP.

6.3.2 Fort St. Vrain Prismatic HTGR

The Fort St. Vrain (FSV) Nuclear Generating Station was designed to produce 842 MW(t) and 330 MW(e) and had many design features common to prismatic-core MHRs (e.g., graphite moderator, helium coolant, and similar designs for fuel particles, fuel elements, and control rods) [e.g., Baxter 1994]. Unlike the MHR designs with their steel pressure vessels, the FSV primary coolant circuit was wholly contained within a prestressed concrete reactor vessel (PCRV) with the core and reflectors located in the upper part of the cavity, and the steam generators and circulators located in the lower part. No EOL R&D program was conducted at FSV, and no radiochemical examinations were reported when the primary circuit components, including the steam generators, were removed as part of the plant decommissioning which is now complete [Hanson 2005].

FSV operation was plagued with frequent water ingresses due to malfunctioning of the water bearings used in the main He circulators [Copinger 2004]. Consequently, the surfaces of the ferritic components in the primary circuit, including the steam generator evaporator and economizer tube bundles, were oxidized.

The dust in the FSV primary circuit was not as well characterized as the dust in Peach Bottom. Two plateout probes were removed from FSV and analyzed to demonstrate compliance with the technical specifications on allowable I-131 and Sr-90 plateout in the primary circuit. Quantities of particulate matter were observed on the fibrous filters contained in these two plateout probes [Burnette 1982, Akers 1991]; however, this particulate matter was not well characterized beyond measuring its radionuclide content.

Samples of deposited dust were obtained from a FSV circulator when it was changed out for repair, and the dust samples were analyzed at ORNL [Sparks 1991]. The dust concentrations were quite low and consisted primarily of ferritic metal oxides (rust) from the aforementioned chronic water ingress events. Most of the dust was Fe_3O_4 with about 10 wt% MoS_2 and 5% other oxides. It was postulated that the MoS_2 particles resulted from its use as a lubricant on the bolts used to mount the circulator in its PCRV cavity. MoS_2 was also used as a lubricant on the SS347 control rod drive cables. This MoS_2 lubricant was observed to hydrolyze producing sulfates during water ingress events [Montgomery 1985], and it is speculated that partial hydrolysis of the MoS_2 surface film on the cables could have led to the spallation of friable unhydrolyzed MoS_2 and its introduction into the primary coolant as aerosol particles. No graphite particles were detected on the circulator.

The small quantities of dust in the FSV primary circuit had no deleterious effects on plant operation. There was no evidence that the graphite core components were a significant source of dust. The NGNP circulators will not use water bearings.

6.3.3 AVR Pebble-Bed HTR

The Arbeitsgemeinschaft Versuchsreaktor (AVR) was a 46 MW_t/15 MW_e prototype pebble-bed High Temperature Reactor (HTR) which began operation in 1968 on a site adjacent to the KFA Juelich national laboratory (now called FZ Juelich) in the Federal Republic of Germany (FRG). [Marnet 1994]. A broad spectrum of coated- particle types was tested, ranging from the initial core of HEU BISO (Th,U)C_2 fuel to high-quality, LEU TRISO UO_2 reload fuel, beginning in 1982. In 1988, after 21 years of operation the AVR was permanently shut down.

Initially, the AVR operated with a core outlet temperature of 850 ^oC; in 1974, the outlet temperature was raised to 950 ^oC (Engelhard 1975); this temperature increase caused no serious operational problems, but the release rates of Sr and Cs from the older BISO-coated

carbide fuel particles increased significantly producing rather high plateout inventories in the primary circuit at EOL (these high plateout activities, especially Sr-90, have served to complicate the ongoing AVR D&D program).

Both the AVR and THTR (see Section 6.3.4 for a brief description of the THTR) contained spherical fuel elements ("pebbles"), each 6 cm in diameter. The AVR core contained ~110,000 spherical fuel elements. At various times during its operating life, the AVR fuel consisted of $(U,Th)C_2$, $(U, Th)O_2$, UO_2, ThO_2, UC_2, and UCO fuel kernels, contained in both BISO and TRISO coatings [e.g., Ziermann 1984]. The fuel element for both reactors consisted of an outer fuel-free zone of matrix graphite with a minimum thickness of 5 mm.

High concentrations of dust were observed in the AVR primary coolant circuit, primarily as a result of the mechanical interactions of the recirculating fuel spheres with one another and with the fixed graphite reflectors. A rather extensive R&D program was conducted to characterize the dust in AVR, especially its effects on radionuclide transport [TECDOC-978 1997]. The primary means of obtaining these data were: (1) the Hot Gas Sampling Tube VAMPYR-I which consisted of a 2.2-m long probe followed by a series of filters, (2) the VAMPYR-II which was essentially an out-of-pile loop which used AVR primary coolant as its fission product sources and consisted of a plateout section with pre- and post filters; and (3) the cold gas filter experimental program. The latter program provided the best characterization of the AVR dust.

The cold gas filter experiment involved 45 tests where a coolant flow of 8 m^3/hr (STP) was bypassed through filters of quartz paper which allowed retention of dust particles down to 0.3 μm diameter with an efficiency of 50%. Dust concentrations during steady-state operation were in the range of 1-2 $\mu g/m^3$; however, during transient operation dust concentrations can be higher by some orders of magnitude. The average dust concentration in the AVR over the final years of operation was about 5 $\mu g/m^3$ [Wawrzik 1987]. Particle size distributions were measured yielding an average dust particle diameter of about 0.6 μm which corresponds to a median diameter of about 5–10 μm for a particle volume-weighted distribution [Gottaut 1990]. The size distribution of AVR dust appeared to be similar for all filter experiments, suggesting a persistent source (i.e., pebble abrasion).

The operational experience with an AVR gas stream laden with carbon-dust particles indicated that at the end of its 20-year operation, 60 kg of carbon dust was collected [NUREG/CR6824 2003]. The dust in AVR is highly contaminated with 30-yr Cs-137 and 28-yr Sr-90; this contaminated dust has complicated the on-going D&D program.

6.3.4 THTR Pebble-Bed HTR

The Thorium-Hochtemperaturreactor (THTR) was a 756 MW_t/307 MW_e pebble-bed, demonstration power plant, located at Hamm-Uentrop, FRG. The plant operated for 423 EFPD, beginning in 1983, until final shutdown in 1988 [Baeumer 1991] because of a combination of factors, including anti-nuclear politics in Germany. The utility chose the German "safe enclosure" D&D option for the THTR (comparable to the US SAFESTOR). The plant will be maintained in this state for 30 years when complete dismantling is planned.

The pebble-bed core consisted of ~675,000 spherical fuel elements with BISO-coated HEU $(Th,U)O_2$ particles. Except for the distinctly different core designs, the THTR shared a number of common design features with FSV (Section 6.3.2). For example, both demonstration reactors utilized PCRVs rather than steel pressure vessels, and both reactors had helical-coil steam generators. The THTR utilized electric motor-driven circulators with oil bearings which proved far more reliable than the FSV circulators with their ill-fated water bearings. Unlike FSV, the waste heat from the THTR-300 was exhausted via a dry cooling tower.

As with the AVR, high concentrations of dust were observed in the THTR primary coolant circuit, again as a result of the mechanical interactions of the recirculating fuel spheres with one another and with the fixed graphite reflectors. However, unlike the AVR, the THTR code design included in-core control rods. An additional source of fission product release and dust developed during reactor operation as a result of mechanical damage to a relatively large number of fuel spheres from the insertion of control rods into the pebble bed. A strong correlation was found between the number of damaged fuel elements in the core and the circulating gas activity. The upper limits on the fraction of exposed fuel kernels were estimated to be 8×10^{-5} for the entire core and 5×10^{-3} for damaged fuel elements. Despite this additional source of fission gas release, the total circulating activity remained well below the licensed allowable activity (<4% of the "Design" activity [Roellig 1991]).

The radionuclide loadings on graphite dust collected in the THTR from the moisture sensors were measured after 300 EFPD as part of an effort to estimate the total dust production [Dietrich 1998]. The estimated range of dust production was 13 - 400 kg with an expected value of 25 kg. The distribution of dust within the primary circuit depended upon on particle size, coolant velocity, and geometry. The specific activity was relatively high, 2×10^8 Bq/g maximum, mainly

caused by the radionuclides Co-60, Sr-95[19], Hf-181, and Pa-235 [Baeumer 1991] due to the enhanced particle failure from fuel element fracture. The measurements for the radiologically relevant cesium and silver isotopes were 1.1 x 10^6 Bq/g for Cs-137, 5.7 x 10^5 Bq/g for Cs-134, 5.0 x 10^5 Bq/g for Ag-110m [Wahsweiler 1987]. If the Cs plateout were primarily on dust, if these loadings were characteristic, and if 25 kg is a good estimate of the total dust in the primary circuit, then the total Cs-137 plateout inventory was <1 Ci which corresponds to a fractional release from the core of <1 x 10^{-6} which seems very unlikely with BISO fuel and mechanically failed fuel spheres.

The presence of highly contaminated dust and fuel debris in the primary circuit will likely complicate the future D&D of the THTR as it has done for the D&D of the AVR.

6.3.5 HTTR Prismatic HTGR

The JAEA High Temperature Test Reactor (HTTR) is a 30 MW_t test reactor constructed at Oarai, Japan [e.g., Saito 1994]. The reactor is designed primarily to investigate nuclear process heat applications. A portion of the nuclear heat (10 MW) is transported from the prismatic core to the secondary cooling loop through an intermediate heat exchanger; the remainder of the heat is dumped to a pressurized water cooler (PWC). The plant is designed to operate initially with a core outlet temperature of 850°C and then at 950 °C for process heat applications. Hydrogen production by thermochemical water splitting (sulfur-iodine cycle) will be first investigated. The reactor achieved initial criticality in 1998, full power with a reactor outlet temperature of 850 °C in 2000, and full power with an outlet temperature of 950 °C in 2004 [Fujikawa 2004].

The HTTR fuel element is a pin-in-block design that was originally developed by the British HTGR program in the 1970s. The core consists of 30 fuel columns, and each fuel column contains five blocks for a total of 150 blocks. The initial core has design life of 660 EFPD. The TRISO-coated, 600-µm, LEU UO_2 fuel particles are contained in annular fuel compacts which are encased in a graphite sleeve. These graphite fuel pins are then placed in holes in the hexagonal graphite block.

---

[19]The presence of 25-s Sr-95 on THTR dust samples, as reported in TECDOC-978, is not credible; presumably, this is a typographical error, and the detected nuclide was 64-day Zr-95. The reported presence of 24.4-m Pa-235 is also not credible and should be taken as 27-d Pa-233. With HEU/Th fuel, the presence of nuclides such as Zr-95 and Pa-233 is a clear indication of fuel debris in the primary circuit from broken fuel spheres since these nuclides are not released from intact HTR fuel elements even at extremely high temperatures.

A major objective for installing filters upstream of the helium gas circulators, in addition to the primary helium purification system in the HTTR, is the reduction and removal of circulating dust in the primary circuit. During the initial operation of the HTTR, the differential pressure across the filter had increased excessively over the duration of operations such that the limit of the differential pressure regulated in the technical specifications of the HTTR would be expected to be exceeded. It was speculated that dust produced by either carbon deposition from CO decomposition, debris from mechanical interactions, or both of these sources had been captured by the filters and caused the increased pressure drop. JAEA replaced and inspected the filters to identify the cause to the problem of the filter differential pressure increase. The results of this dust examination have not been published in the open literature to date.

As part of the current NGNP workscope, Fuji Electric Systems contracted with the Japan Atomic Energy Agency (JAEA) for them to provide a report summarizing their experience with characterizing dust in the HTTR primary circuit. This JAEA report [Furusawa 2008] has been provided to the NGNP program as JAEA proprietary information which cannot be distributed beyond GA and INL.[20] The major conclusions of the report are summarized below:

1. The pressure drops across full-flow filters upstream of the HTTR primary circuit circulators increased early in plant operation indicating that a significant quantity of dust had been collected by the filters. The filters were replaced, and the dust characterized.

2. The dominant source of dust in the circulator pre-filters is the abrasion of the graphite piston rings in the purified He compressors. Construction debris (e.g., filaments of Kaowool insulation) may have contributed to a lesser extent.

3. The graphite core components do not appear to contribute significantly to the circulating dust in the HTTR primary circuit.

4. The dust is primarily carbonaceous. Both graphite and amorphous carbon are present.

    a. The dominant source of the graphitic carbon is the graphite piston rings in the purified He compressors.

    b. The source of the amorphous carbon is unclear. Carbon deposition (CO disproportionation) is not predicted because the calculated oxygen potential in the

[20] The JAEA report has been provided to INL for their use with appropriate restrictions to safeguard the JAEA proprietary information contained therein.

HTTR primary coolant is sufficiently high to keep the ferritic surfaces oxidized (hence, unable to catalyze CO decomposition).

5. A conservative estimate of the total quantity of dust collected on the three primary circuit circulator pre-filters is about 550 cm^3 (equivalent to about 1 kg of IG-110 graphite).

6. The particles collected on the filters have effective diameters of 1 - 3 μm. The particle size distribution was not determined.

7. The dust on the filters is contaminated, primarily with neutron activation products; the dominant dose contributors are 5.3-year Co-60 and 60-day Sb-124.

8. After filter replacement, the pressure drops across the new filters again increased indicating a persistent source of dust. The graphite piston rings in the HPS also continue to wear and to require replacement which is consistent with the conclusion that they are the dominant source of dust in the primary circuit.

9. JAEA recommends that future VHTRs employ active purification methods to not only minimize the coolant impurities but to inject trace impurities to custom tailor the chemistry in order to preclude carbon deposition and carburization/decarburization of high-temperature metals (injection of trace quantities of CO is currently favored).

10. JAEA does not believe that full-flow dust filters will be necessary in future VHTRs with prismatic cores.

6.4 Potentially Deleterious Effects of Dust on Reactor Components

The principal potential deleterious effects of dust are:

- Erosion of primary system surfaces due to abrasion.
- Fouling of primary system heat transfer surfaces due to poorly conducting layering effects and possible flow blockages.
- Instrument line plugging.
- Contribution to metallurgical problems such as carburization or scaling, especially for high temperature operation (carburization is the addition of carbon to the surface of a metal, generally at temperatures between 850 and 950°C).

Dust in the NGNP is expected to be dominated by graphite. This material typically has low hardness (NUREG/CR6824 indicates carbon dust particles have an average Vickers hardness of 20) and behaves as a lubricant, and therefore would not be expected to serve as an effective erodent of metallic surfaces. It principal effect would be deposition.

Assuming a graphite density of 2.25 g/cm^3, the best estimate surface loading of 0.5 g/m^2 would suggest an equivalent uniform film layer thickness of 0.22 microns. A rough estimate of the total surface area in a 600 MW(t) NGNP is 1.3 x 10^5 m^2 (this is a GT-MHR number where the area of the recuperator is dominant). The average deposited activity on this basis would be 65 kg. In light of AVR experience, the "best estimate" value also appears adequately conservative for evaluations herein and possibly overly conservative for surfaces exposed to high velocity coolant flow. Most of the AVR dust was collected from areas that would have had low flow to allow this accumulation.

The particle size distribution indicates that this NGNP layer would be non-uniform, as expected. In high velocity coolant flow regions, deposition and resuspension are assumed to balance at equilibrium. Since deposition is expected to be proportional to the coolant-borne concentration, which is inversely proportional to the cleanup rate, as a simplification, surface loading may be considered as inversely proportional to the cleanup rate as well. This would only apply to surfaces exposed to high velocity where resuspension can occur. Consistent with AVR experience, most of the deposited dust may be to low velocity areas where resuspension would not be expected.

It should be noted that HPS flow does not impact resuspension phenomena which are controlled by coolant flow velocity. Only deposition could be controlled by reducing helium borne dust, and in circuit deposition is expected to be the dominant removal mechanism rather than the HPS.

Heat Exchanger Fouling: Based on the above, the effective "uniform film layer" on heat transfer surfaces will likely be even lower than the 0.22 micron thickness. This is not considered to be significant for heat transfer purposes. The analogous heat exchanger surface fouling in a fossil power plant boiler results from orders of magnitude higher surface loadings of soot and fly ash, where fouling may be sufficient to require soot blowers for instance.

Regarding general fouling in typical industry heat exchanger duty, the Wolverine Tube Heat Transfer Data Book indicates that "Sedimentation fouling" from suspended solids contained in liquids which can settle out upon the heat transfer surface are usually not strongly adherent to the affected surface and are self-limiting (i.e., the thicker a deposit becomes, the more likely it is to wash off) and thus attain some asymptotic average value over a period of time. The Data Book also indicates that sedimentation fouling is strongly affected by velocity and less so by wall temperature; however, "a deposit can 'bake on' to a hot wall and become very difficult to remove." Except for this "baking on" comment (which would be accelerated by higher temperatures), this liquid experience is not considered particularly applicable to the NGNP

gaseous coolant with limited suspended solids application except as a basis for confidence in the NGNP application regarding similar sedimentation fouling effects.

Some concern has been expressed with respect to plugging of printed circuit heat exchangers (PCHE), which are more compact with much smaller flow channels than shell and tube heat exchangers. These heat exchangers tend to have high velocities that may provide a self-cleaning effect, according to some vendors. The coolant passages are of millimeter size, and while seemingly small, are large with respect to expected particle sizes and boundary layer thicknesses. However, with the anticipated zig-zag flow paths it will be necessary to perform flow passage fouling and plugging tests to validate the self-cleaning effect.

Instrument Line Plugging: This issue principally relates to sample lines, which can be designed to minimize plugging potential. Further, the anticipated dust loading is small compared to that encountered in many applications.

Dust Impact on Reactor Coolant System, PCS and IHX Surfaces: Adhesion of deposited graphite particulate on metallic surfaces materials is expected to be principally electrostatic. Because of graphite softness, erosion of metallic surfaces is not expected to be significant.

[ANL/EXT-06-46 2006] provides a relatively current summary of issues with respect to other effects that impurities in the helium coolant may potentially have on metallic components such as the IHX surfaces. This data is considered applicable to primary circuit components as well. The citation is principally related to gas contaminants, and their potential contributions to their contribution to carburization, surface scaling, or corrosion of underlying material.

Deposited graphite dust could conceivably contribute to carburization if a coherent (and thus protective) oxide surface layer is not present and, therefore, is considered here. Any effects resulting from potential carburization, scaling, or corrosion of materials such as Alloy 617 (UNS N06617, also designated as Inconel® 617) may impact circulating contaminants with large cross sections. This alloy has a 10-15% cobalt concentration. It is recognized that the components that would be constructed using Alloy 617 will not be positioned in areas with significant neutron flux and would not be activated in place, with the possible exception of the hot duct through which coolant from the reactor vessel is sent.

However, any erosion/corrosion products that were to become suspended in the helium coolant would potentially be deposited in core coolant channels where activation could occur. For these reasons it is important to assure that IN 617 not have friable surface oxide films that are expected to passivate these surfaces and prevent corrosion of underlying material.

LWRs classically, and future Advanced LWRs will, apply significant efforts to limit the use of cobalt containing materials in components outside of the reactor, such as in steam generators, for which the EPRI Advanced Light Water Reactor Utility Requirements Document states “the concentration of the cobalt in the steam generator tubes shall be less than 0.015 weight percent.”

[ANL/EXT-06-46 2006] demonstrates that Alloy 617 has high carburization resistance at the lower 850 ^{o}C core exit temperature. For the higher 950 ^{o}C design, coolant chemistry, in terms of H_2/H_20, CO/CO_2 and CH_4/H_2 may require management to control carburization.

Alloys with lower cobalt content, if otherwise mechanically suitable, would be preferable. Cobalt content should be a consideration in material selection until it can be determined that activation products will not be problematic.

6.5 Effects of Particulate Matter in other High-Temperature Gas Systems

A review of other non-HTGR systems involving relatively high temperature materials and with entrained dust was conducted, including the following:

- Fossil-fueled Power Generation, including the use of ultra-supercritical boilers
- THOR nuclear waste solidification projects that turns liquid waste (such as INL sodium-bearing waste) into a carbonate suitable for disposal in the DOE Waste Isolation Pilot Plant.
- Chemical Demilitarization projects that incinerate chemical weapons such as mustard gas and nerve agents.

In general, all of these applications are of limited applicability to the 950 C NGNP helium coolant metal exposure conditions for the following reasons:

1. Typical fossil-fueled power generation equipment operates at temperatures below 700 ^{o}C; ultra-supercritical boilers can have fire-side temperatures between 760 and 870 ^{o}C. Additionally, particulate loadings will be many orders of magnitude higher, environmental chemistry (e.g., oxygen presence) will be much different, and acceptable erosion/corrosion thresholds will be much higher. Additionally, high temperature materials such as IN 617 are only now being investigated for possible use.
2. THOR furnace maximum temperature is only 750 ^{o}C, with extreme particulate loadings since that is the product. Also, different chemistry conditions apply, and the equipment design “working life” is only for a 1-5 year mission.
3. Specialty metal selection is based on qualification to 870 ^{o}C, but operation is only at 540 ^{o}C. Effluent sampling is performed with glass samplers at operation conditions, or with quartz

samplers at the highest temperature conditions (where glass would melt), but not with metals.

As further investigations regarding item 1, the abstracts of several technical reports on fly ash erosion/corrosion were reviewed and summarized below:

A Final Technical Report on Fireside Corrosion and Fly Ash Erosion in Boilers [EPRI-CS-5071 1987]:

This report investigates methods of reducing the importance of fireside corrosion and fly ash erosion as factors responsible for tube failures in utility boilers, by evaluation of the causes and the remedial measures used in practice. Fireside corrosion and fly ash erosion are considered to be major problems only at those units burning coal that is rated as very aggressive (high sulfur, alkalis, and chlorine), or that contains a high percentage of erosion minerals such as quartz in the ash. These problems are effectively managed by extensive maintenance and the use of sacrificial, temporary measures such as pad welding and the fitting of tube shields. There are available, proven, permanent solutions for most of the fireside corrosion and fly ash erosion problems encountered, but they are not widely applied because the costs of installation are perceived to compare unfavorably with continued maintenance activities. Nevertheless, several forced outages annually are still caused by fireside corrosion or flyer erosion. It is important to note that these are typically repeat failures in the same location, and often the same tube, which indicated that the palliative solutions which have been applied have been ineffective. There are permanent solutions which could be worthwhile. An important example is the use of cold air velocity measurements for the selection and orientation of screens and baffles, which has been shown to be capable of essentially eliminating fly ash erosion as a boiler tube failure mechanism.

A Final Technical Report on Fireside Corrosion of Superheated Alloys for Advanced-cycle Steam Plants [EPRI-CS-5195 1987]:

This report addressed the coal-ash corrosion data in the following areas: (1) laboratory corrosion test data on higher strength tube materials and cast support materials, (2) discussion and interpretation of results of these data, (3) discussion of methods for avoiding corrosion, and (4) review of recent fireside corrosion studies and plant experience. Laboratory tests using synthetic ash showed severe corrosion losses for high-temperature alloys such as austenitic stainless steels containing molybdenum and Fe-Ni-Cr alloys. This corrosion loss occurs in the temperature range between 677 and 718 ^{o}C. The laboratory tests performed during this program have shown that some modified stainless steels such as Foster Wheeler-developed Alloy 4C and Sandvik 235 MA will provide substantially improved resistance to corrosion, which

will be adequate in most cases. For most steels and high alloys, the maximum corrosion rates were above 704 ^{o}C, indicating that future designs for plants operating in this region must incorporate additional material development. Alternative materials and special alloys containing silicon additions appear promising."

EPRI Sootblower Conference 2006 – "Advanced Erosion Protection Technology for Steam Boiler Superheat, Reheat and Evaporator Tubes", [2006].

One of the major causes for premature tube failure is excessive fireside boiler tube erosion caused by the impact, cutting action, and abrasive wear of fly ash entrained flue gases undercutting the area they strike. This conference discussed the results laboratory analyses comparing wear resistant materials for the protection of high erosion prone fireside boiler tubes, and verification of laboratory analysis in actual field trials. The report states:

"Erosion is caused by the impact, cutting action, or abrasive wear of small solid particles freely immersed in the direction of fluid flow that frequently undercut portions of the material they strike. Erosion is the progressive loss of original material from a solid surface due to mechanical interaction between that surface an the impinging fluid or solid particles."

Long time investigation of the effect of fouling on the super-heaters in a circulating fluidized biomass boiler. - International Journal of Energy Research, Volume 30, Issue 13 (Ref. 13)

This investigation involves measurements and theories on the mechanisms of forming deposit layers on super-heater tubes in a biomass-fired boiler, especially the deposit layer thickness and the soot-blowing frequency effect on the super-heaters heat transfer. The measurements show a deposit growth rate on the super-heater of approximately 4 g m^{-2} h^{-1}. The distribution of the deposit material varies significantly between the windward and the leeward side of the tubes, with the thickest layers on the windward side. Further down stream of the first super-heater, the fouling problem on the super-heater and re-heater tubes are not so severe. A theoretical model shows that a deposit layer of 20 mm will decrease the heat transfer rate of the first super-heater by nearly 40%. The soot-blowing system shows a strong positive effect on the heat transfer rate of the super-heater a few hours after a soot-blowing sequence has been completed. However in the long run, the varied soot-blowing frequency does not have a significant influence on the deposit layer growth rate."

With respect to this last investigation, comparing the NGNP best-estimate surface loading of 0.5 g/m^2 on heat transfer surfaces (over the 60-yr operating lifetime) to a deposit growth rate on a super-heater of approximately 4 g/m^2 per hour, it is obvious that even worst expected NGNP dust loadings are negligible by comparison. Similarly, the statement from the above

investigation “a deposit layer of 20 mm will decrease the heat transfer rate of the first super-heater by nearly 40%” can be compared to the previously stated NGNP best-estimate surface equivalent uniform film layer thickness of 0.22 microns on heat transfer surfaces, so five orders of magnitude lower decrease in heat transfer degradation resulting from the dust deposition can be anticipated for NGNP (in addition to the fact that the thermal conductivity of nuclear grade graphite is higher than that of steel).

6.6 Recommended Limits on Dust Production and Accumulation

For the present, the “best estimate” and “conservative” dust attributes given in Section 6.3 should be considered to be the “Maximum Expected” and “Design” dust attributes for NGNP conceptual design. This recommendation should be reviewed once the HTTR dust data have been evaluated.

GA conservative estimates of the dust concentrations and characteristics that might occur in the GT-MHR based upon Peach Bottom and FSV dust data are summarized below:

- Composition: amorphous carbon, ferritic metal oxide, graphite
- Particle size distribution: 0. 01 to 10 μm
- Upper bound gasborne concentration: <3 mg/m^3
- Upper bound surface loading: <5 g/m^2

For NGNP, the above gasborne concentration and surface loading (after 60 years of plant operation) would be considered very conservative upper bounds. GA “best estimates” for the NGNP are summarized below:

- Composition: graphite (dominant), metal oxides (minor)
- Particle size distribution: 0.1 to 5 μm (mass median equivalent diameter = ~0.5 μm)
- “Best estimate” gasborne concentration: <10 $\mu g/m^3$ (~ $1/300^{th}$ of the extrapolated Peach Bottom value because of the elimination of water ingress related oxide products.)
- “Best estimate” surface loading: <0.5 g/m^2 (~10% of the extrapolated Peach Bottom value)

This “best estimate” gasborne concentration is not inconsistent with the measured dust concentrations in HTTR. JAEA has not made an estimate of the quantity of dust that is deposited in the HTTR primary circuit; the quantity is expected to be small, given the inclusion of full-flow filters in the primary circuit.

Additionally, at 7 MPa and 850 ^oC temperature, the reactor coolant helium density is 0.75 kg/m^3. With a 500 kg/hr flow rate and 10 $\mu g/m^3$ dust loading, the HPS would remove 0.06 kg of dust

per year (dust will not penetrate the various HPS unit operations; the only possibility for dust to be present in the purified He would be dust generation in the LN_2-cooled charcoal beds). At the conservative 3 mg/m^3 values, 18 kg/yr would be collected which, based upon Peach Bottom, Fort St. Vrain and HTTR operating experience, is extremely conservative for a prismatic NGNP.

7. PLANT MASS BALANCE FOR RADIONUCLIDES

A broad spectrum of radionuclides, including tritium, will be produced by various nuclear reactions (principally fission) in a VHTR. Given the high service temperatures in a VHTR, some of the more volatile fission products will be released from the core and will migrate throughout the plant, and a small fraction will be released from the plant to the environment. In particular, some tritium will permeate through the intermediate heat exchanger and the hydrogen plant process vessels, contaminating the product hydrogen. These radionuclides represent a potential radiation hazard to plant personnel, product consumers, and the general public. Consequently, the plant must be designed to assure these radionuclides are controlled to meet all regulatory requirements with sufficient margin to account for the uncertainties in the predicted source terms for a FOAK plant. An important consideration for plant design and optimization is to determine an overall mass balance for these radionuclides.

7.1 Plant Configuration

Radionuclides are generated in the reactor core as a result of fissioning and other nuclear reactions in the fuel and core structural materials. The prismatic fuel elements in an MHR core contain LEU fuel made up of TRISO-coated fuel particles. As discussed in Section 4, a small fraction of these fuel particles are manufactured with defective coatings. There is also low levels of heavy-metal contamination (“tramp uranium” in LWR parlance) in the fuel compacts as well as in the graphite blocks. Radionuclides are released from fuel with defective coatings and from HM contamination, migrate through the fuel compact matrix and fuel-element graphite, and are released into the primary helium coolant. Once released to the coolant, the radionuclides accumulate in the primary coolant until they are removed by radioactive decay, the helium purification system, or, in the case of the condensable radionuclides, are deposited (“plated out”) on helium wetted surfaces in the primary circuit.

A first-order estimate of the total radionuclide inventories in the coolant, deposited in the primary circuit and resident in the HPS can be calculated provided that the RN release rates from the core into the primary coolant are quantified. The RADC code performs fuel, plateout, circulating, and HPS inventory calculations [Eichenberg 1993]. The modem version of RADC is based on the original RAD2 code developed by Vanslager [1965] for the analysis of the Peach Bottom HTGR.

The RADC code solves a modified set of the Bateman equations for serial radioactive decay chains. The classical buildup and decay equations have been extended to account for radionuclide sources that are dependent upon a specified fuel failure and contamination fraction and release fractions (R/Bs) from failed fuel and contamination that are functions of the

chemical element and radioactive half life. The effects of helium purification and plateout are accounted for by including zero-order removal constants for each in the mass balance. A Licensing Topical Report [Haire 1974] was written describing the mathematical formulations in RADC.

7.2 Radionuclide Source Terms

Radionuclide design criteria, or the allowable levels of radionuclide accumulation in the primary coolant circuit, are defined herein for the 600 MW(t) NGNP with prismatic fuel elements.

A two-tier set of radionuclide design criteria, referred to as the "Maximum Expected" and "Design" criteria, are presented here. In principle, the "Design" criteria are derived from externally imposed requirements, such as site-boundary dose limits and ALARA requirements. The "Maximum Expected" criteria are then derived by dividing the "Design" criteria by an uncertainty factor, or design margin, to account for uncertainties in the design methods. This uncertainty factor is a factor of four for the release of fission gases from the core and a factor of 10 for the release of fission metals. The fuel and core are to be designed such that there is at least a 50% probability that the fission product release will be less than the "Maximum Expected" criteria and at least a 95% probability that the release will be less than the "Design" criteria. In addition, to account for the possibility of "saturation" and circulating dustborne activity, an additional safety factor of 40 is applied to the "plateout per pass" (i.e., 40% plateout per pass for the "Maximum Expected" and 1% per pass for the "Design" criteria) when calculating the circulating activities of all condensable species except iodine. Measurements in FSV and in the CPL 2 in-pile loops suggest an iodine plateout per pass of the order of 1% to 10%; consequently, for iodine 1% per pass is assumed for both the "Maximum Expected" and "Design" calculations.

The "Maximum Expected" values are to be used for Environmental Impact Reports, for planning component removal and maintenance procedures, and for other applications where "best-estimate" results are appropriate. The "Design" values represent upper limits for all normal operating conditions. They are to be used for safety analyses, sizing of the helium purification and radwaste systems, the design of plant hardware including service and shipping casks, and the specification of the associated shielding requirements.

The as-manufactured HM contamination fraction, in-service fuel failure fractions, core release fractions, etc., assumed for calculating the plant RN mass balance that is presented in this section are consistent with the limits derived from the top-level RN control requirements (PAGs, etc.) derived in Section 4. However, there is an unresolved issue at this writing. The allowable core release fractions derived in Section 4 are for a 350 MW(t) plant, but the NGNP thermal power may be as high as 600 MW(t), a factor of 1.7 higher. Consequently, to achieve the same

Curie releases from a 600 MW(t) NGNP plant, the allowable fractional releases would have to be a factor of 1.7 lower. Conceptually, the most obvious means to accomplish that would be reduce the allowable in-service fuel failure and as-manufactured HM contamination by a corresponding factor of 1.7 (e.g., the allowable fuel failure during normal operation would be reduced from 5×10^{-5} to 3×10^{-5}, etc.).

Such a recommendation was considered here but judged to be premature for a number of reasons. First and foremost, the power level of the NGNP has not yet been selected, and power levels less than 600 MW(t) are under active consideration. Secondly, the core service conditions have not yet been determined; it is possible (but not highly likely) that the core release fractions recommended in Section 4 will be met with margin when a core design is selected, and a full-core fuel performance analysis is completed. Thirdly, while the results of the on-going AGR-1 irradiation test are certainly encouraging to date, the fuel has not yet reached full burnup and postirradiation heating tests are well in the future.

Until compliance with the current, already stringent, fuel performance requirements is convincingly demonstrated, it seems imprudent to tighten them even further. In the event that the predicted NGNP off-site doses would marginally exceed the PAGs with 425-m commercial EAB, trade studies would be performed to determine the optimal resolution. For a FOAK NGNP on a government reservation, it might appropriate to require a somewhat larger EAB and EPZ. Alternatively, a reduction in the assumed fractional liftoff of iodine plateout during depressurization accidents from 5% to 3% might prove feasible. Once the AGR fuel qualification program is complete and the NGNP source terms validated, an objective determination can be made whether or not further tightening of the fuel requirements would be necessary - and practical - for future commercial VHTR plants.

7.3 RADC Model

The computer program RADC was used to calculate fuel, circulating, plateout, and HPS inventories for the NGNP. Since the NGNP is still in the pre-conceptual design phase, many basic plant parameters have not yet been selected. Consequently, for this scoping study, the point of departure was the previous RADC analysis for the 350 MW(t) steam-cycle MHTGR [Jovanovic 1989]. Required input parameters for RADC were taken from the 600 MW(t) GT-MHR conceptual design [Shenoy 1996] if available, or the 350 MW(t) MHTGR were used (scaled up by power level if appropriate). The assumed as-manufactured HM contamination and in-service fuel failure fraction were consistent with the values recommended for the NGNP in Section 4 (essentially the same as for the commercial GT-MHR). The assumed input values for MHTGR and NGNP are compared in Table 7-1.

Table 7-1. Comparison of Assumptions for 350 MW MHTGR and 600 MW NGNP

Parameter	350 MW MHTGR	600 MW NGNP
Thermal power (MW)	350	600
Fuel cycle	LEU/Th	LEU/NatU (see note 2)
Plant lifetime (yr)	40	60
Plant capacity factor	0.8	0.94
Mass flow rate (lb/hr)	1.25×10^{6}	2.54×10^{6}
Circulating He inventory (lb)	4340	10,000
He purification rate (lb/hr)	850	See note (1)
He purification constant (sec^{-1})	5.4×10^{-5}	2.4×10^{-5}
Core power density (w/cm^3)	5.9	6.6
Fuel residence time (yr)	3.3	3
Number of fuel elements	660	1020
Design Margin		
Design/Expected – Gases	4	See note (1)
Design/Expected – Metals	10	See note (1)
HM contamination fraction		
50% confidence	1×10^{-5}	See note (1)
95% confidence	2×10^{-5}	See note (1)
SiC defect fraction		
50% confidence	5×10^{-5}	See note (1)
95% confidence	1×10^{-4}	See note (1)
Fuel failure fraction		
50% confidence	5×10^{-5}	See note (1)
95% confidence	2×10^{-4}	See note (1)
Diffusion Parameters (sec^{-1})		
As-manufactured - Kr		1.7×10^{-18}
Failed - Kr		3.9×10^{-10}
As-manufactured - Xe		1.1×10^{-19}
Failed - Xe		4.4×10^{-10}
Hydrolysis increase factor (f_H)	1.7	1.0
Kr-85m release fraction (R/B)		
50% confidence	9.3×10^{-7}	See note (1)
95% confidence	3.7×10^{-6}	See note (1)
Xe-138 release fraction (R/B)		
50% confidence	6.8×10^{-8}	See note (1)
95% confidence	2.7×10^{-7}	See note (1)
Cs release fraction		
50% confidence	6.7×10^{-6}	1.0×10^{-5}
95% confidence	6.7×10^{-5}	1.0×10^{-4}
Ag release fraction		
50% confidence	5.0×10^{-4}	2.0×10^{-4}
95% confidence	5.0×10^{-3}	2.0×10^{-3}
Sr release fraction		
50% confidence	3.0×10^{-8}	See note (1)
95% confidence	3.0×10^{-7}	See note (1)

Parameter	350 MW MHTGR	600 MW NGNP
Minimum fractional release	4.8×10^{-9}	See note (1)
Plateout/pass (%) except iodine		
50% confidence	40	See note (1)
95% confidence	1	See note (1)
Cycle average circulating gaseous activity (Ci)		
H-3	6.00E-02	See note (1)
C-14	0.00E+00	See note (1)
Plateout at end of life (Ci)		
H-3	0.00E+00	See note (1)
C-14	0.00E+00	See note (1)
Purification system activity at end of life (Ci)		
H-3	1.06E+03	See note (1)
C-14	0.00E+00	See note (1)
Total core activity after fuel reload (1.5 yr) (Ci)		
H-3	2.44E+03	See note (1)
C-14	7.86E+01	See note (1)
Total core activity after fuel reload (3.0 yr) (Ci)		
H-3	4.20E+03	See note (1)
C-14	1.58E+02	See note (1)
Macroscopic absorption cross section (1/sec)		
RH105	1.27E-06	See note (1)
PD108	3.33E-09	
PD109	2.73E-10	
AG109	1.99E-08	
PD110	1.11E-10	
PD111	2.73E-10	
AG111M	1.38E-10	
AG111	1.38E-10	
CD111	1.12E-09	
PD112	2.73E-10	
AG112	4.62E-11	
CD113	3.39E-06	
SN126	1.75E-11	
XE135	1.51E-04	
ND143	1.90E-08	
PM147	3.33E-08	
PM149	8.35E-08	
SM149	4.33E-06	
SM151	2.89E-07	
EU151	5.58E-07	
SM152	3.44E-08	
SM153	4.71E-08	
EU153	3.88E-08	

Parameter	350 MW MHTGR	600 MW NGNP
SM154	7.26E-10	
GD155	1.29E-06	
SM156	8.35E-08	
EU156	4.13E-08	
GD156	1.67E-09	
EU157	8.35E-08	
GD157	5.72E-06	

Notes:

(1): Value for 600 MW(t) NGNP is the same as 350 MW(t) MHTGR.
(2): Yields: 0 U-233; U-235; Pu-239 and 0.09 Pu-240.

7.4 Description of Analysis

The parameters, input data and assumptions used in conjunction with the RADC code to calculate an overall NGNP plant mass balance for radionuclides are described below.

7.4.1 Bases

The subject radionuclide inventories are for a 600 MW(t) NGNP operating on the low-enriched (20%) natural uranium (LEU/NatU) fuel cycle. The distribution of fissions among the fissile nuclides (U-235, U-233, Pu-239, and Pu-241) is representative of a 3.0-year, equilibrium prismatic core. "Nominal" full-power plant conditions were assumed with one exception: the core thermal power is 102% of nominal full-power per NRC Regulatory Guide 1.49 to account for uncertainties in core power measurements. The plant lifetime is 60 yr, the power density 6.6 w/cm³, the capacity factor ("equivalent availability") is 94%, and the fuel element residence time is 3.0 yr.

The circulating inventory of helium in the primary circuit was assumed to be 10,000 lb_m which is actually the total helium inventory in the commercial GT-MHR [Shenoy 1996] so the plateout removal constant and He purification constant are somewhat underestimated. The helium purification constant was calculated based upon the HPS mass flow rate of 850 lb_m/hr [Shenoy 1996] and the above value for the total helium inventory. The key assumptions used in the calculations to calculate are listed below.

1. Provisional radionuclide “Design” criteria (≥95% confident) for the NGNP were obtained as follows. The fission gas release limits were defined by limiting the I-131 and Sr-90 plateout (the latter is dominated by the release of its Kr-90 precursor) so that a <[5%] liftoff during a rapid depressurization could be tolerated.

2. Key specifications for fuel quality are ≤2.0 x 10^{-5} heavy-metal contamination and ≤1.0 x 10^{-4} SiC defects at 95% confidence. These fuel quality limits were established to meet the fission product retention requirements of the NGNP.

3. The dose rates around the primary circuit from induced radioactivity due to neutron activation will be small compared to the dose rates due to fission product plateout. This assumption implies that the cobalt content in structural materials exposed to significant neutron fluxes must be very low and/or that the graphite reflectors must be sufficiently boronated to minimize the neutron fluxes.

7.4.2 Fission Product Nuclides

The fission product nuclides included here can be circumscribed by two general criteria: only nuclides with a yield from U-233, U-235, Pu-239, or Pu-241 greater than 0.1% and with a half-life greater than 1 min are included. Exceptions are the short-lived noble gases Kr-90, Kr-91, Xe-139, and Xe-140 which have important daughters. Radionuclides with a half-life longer than 220,000 yr (1 x 10^{-13} sec^{-1}) years are treated as stable nuclides (this includes the radiologically important nuclide I-129, which has a 1.6 x 10^{7} year half-life). Fission product yields, branching ratios, and decay constants were obtained from [Rider 1978].

7.4.3 Activation Product Nuclides

The activation product nuclides produced in the reactor core that are of interest to the HTGR design are also tabulated in this document. H-3, C-14,and Ag-110m require special treatment.

The H-3 inventories in the fuel and primary coolant are taken from the TRITGO analysis in Section 8. They correspond to maximum values that occur early in reactor lifetime when the Li content in the permanent graphite structures is the highest.

The major mode of C-14 production in the fuel element is through the neutron activation of N-14, which exists as an impurity in the graphite, via a (n,p) reaction. A nitrogen impurity content of 100 ppm, was conservatively assumed. The release of C-14 into the helium coolant will be negligible and has been set to zero.

The production modes of Ag-110m are: (1) the low direct fission yield and (2) the neutron activation of stable Ag-109, a higher yield fission product nuclide, resulting primarily from Pu fissions. An effective yield for Ag-110m was calculated to give the proper core inventory from a burnup analysis done for the 600 MW(t) commercial GT-MHR.

The other activation product nuclides included are Cs-134, Cs-136, Pm-148m, Pm-148, Eu-152, Eu-154, and Eu-155. These nuclides are produced through the neutron activation of other fission products. The release of these nuclides from the core is determined on the same basis as for the fission product isotopes of that element (e.g., Cs-134 and Cs-136 are assumed to have the same fractional releases as Cs-137). The effective yields corresponding to the end-of-life inventories were used for conservatism.

7.5 Predicted Radionuclide Distribution in NGNP

The predicted “Design” and “Maximum Expected” plant distributions for 250 radionuclides are given in the following subsections.

7.5.1 "Design" Nuclide Inventories

The “Design” (≥95% confident) radionuclide inventories were calculated for the equilibrium core, primary coolant, primary circuit plateout, and He purification system were calculated for the assumed plant conditions described above.

7.5.1.1 Equilibrium Core Inventories

The "Design" inventories for the fuel elements and the total core are given in Table A-1 (see Appendix A). The "Maximum Expected" fuel inventories are given in Table A-2 (see Appendix A). The third column of Table A-1 lists the equilibrium core inventory of the fission product and activation product nuclides upon shutdown from maximum power for refueling. The radionuclide inventories are given in Curies, and the stable nuclides are given in grams. The greatest fuel exposure is assumed to be 3.0 years and the least, 1.5 years. To be conservative when calculating fuel element and total core inventories, it is assumed that the core operated at 102% of nominal power for 94% of the fuel lifetime. In addition, the maximum of the cumulative yields from U-233, U-235, Pu-239, or Pu-241 is used, and the "Maximum Expected" fractional release from the fuel is assumed.

7.5.1.2 Fuel Element Inventories

The fourth column of Table A-1 lists the nuclide inventory of an average fuel element which has operated in a core at 102% power for 2.82 years (94% of 3.0 years). Columns 5 through 7 give the nuclide inventories after 1, 10, and 100 days of decay, respectively. There is a total of 1020 fuel elements in the core.

7.5.1.3 Steady-State Circulating Inventories

The "Design" equilibrium core average release fractions (release rate into coolant/birth rate in fuel) are 3.7×10^{-6} for Kr-85m and 2.7×10^{-7} for Xe-138. These values define the release

fractions for other isotopes of krypton and xenon (by assuming that release fractions vary as the square root of the isotope half-life). Isotopes of bromine and selenium are assumed to have the same release characteristics as krypton; isotopes of iodine and tellurium, the same as xenon.

The "Design" circuit activities are given in Table A-3 (see Appendix A). Column 3 lists the steady-state values of the fission product and activation product nuclides in the primary coolant at full power with normal operation of the purification system. These are based on the assumption of 1% plateout of condensable isotopes per pass around the circuit. This value is chosen to account for the possibility of iodine "saturation" and circulating dustborne activity. These circulating activities represent equilibrium values during the fuel lifetime (3.0 years).

Column 4 of Table A-3 lists the cumulative activities in the helium purification system, during the plant lifetime (60 years).

7.5.1.4 Primary Circuit Plateout

The total primary circuit "Design" plateout inventories following shutdown after operation at 102% power for 94% of 60 yr are given in Column 5 of Table A-3. Columns 6 and 7 give corresponding values after 1 and 10 days of decay, respectively.

The calculation of the circulating and plateout inventories in the primary circuit is decoupled. The circulating activity is calculated using an appropriate plateout per pass. The total plateout inventory is calculated independently by conservatively assuming that all the condensable radionuclides that are released from the fuel elements plate out in the primary circuit. Consequently, an exact mass balance is not preserved; i.e., the sum of the plateout inventory, the circulating inventory, and the purification system inventory slightly exceeds the total core release. However, even with a plateout per pass as small as 1%, >99% of the condensable activity is plated out so the degree of conservatism is small.

The plateout inventories of the condensable fission gases, e.g., iodine and tellurium, were calculated with the same core release fractions as used to calculate their circulating activities. The "Design" fractional releases for silver, cesium, and strontium isotopes are 5.0×10^{-3}, 1.0×10^{-4}, and 3.0×10^{-7}, respectively. Based upon their relative volatilities (as inferred from their elemental boiling points), As, Rb, and Cd isotopes are assumed to have the same release fractions as Cs; and Eu, Sb, Ba, and Sm isotopes, to have the same release fractions as Sr [Alberstein 1976].

The 60-year total plateout values are given in the tables, and any plateout values for a shorter period of time (T = years) is obtained by multiplying the 60-year value by [1 - exp (-λ x T)]/[1 - exp (-λ x 60)] (λ = decay constant of the radionuclide of interest).

7.5.2 "Maximum Expected" Nuclide Inventories

The "Maximum Expected" fuel activities are given in Table A-2. These fuel activities are based upon nominal cumulative yields from U-233, U-235, Pu-239, and Pu-241.

The "Maximum Expected" steady-state coolant and 60-year plateout values of the fission product nuclides and the activation product nuclides are given in Table A-4 (see Appendix A). The coolant activities are based on 40% plateout per circuit loop for all condensable nuclides except iodine, for which 1% plateout/pass was assumed. The "Maximum Expected" core-average release fractions for gases are a factor of four lower than the "Design" release fractions: and the "Maximum Expected" release fractions for metals, a factor of 10 lower. The minimum release fraction for the "Maximum Expected" conditions is set equal to 4.8×10^{-9}.

All other conditions for the "Maximum Expected" values are identical to the "Design" conditions and, hence, are not repeated here.

7.6 Sensitivity Study

With the base case results described above, a sensitivity study was performed to identify dominant variables for radionuclide mass balances to provide guidance to plant optimization studies. This study investigated the effects of various design parameters on the radioactivity of circulating coolant and plateout in the primary circuit at the end of plant life. Variables studied included core and system design parameters such as HM contamination fraction, fuel failure fraction, helium purification constant, overall plateout removal constant, iodine plateout removal constant and silver diffusive release fraction from the core.

The range of one order of magnitude above and below the “maximum expected” value in the base case was considered in each variable in the sensitivity study (a factor of 10 is perhaps too large for some variables such the HM contamination fraction). A description of the input data used for the 12 sensitivity study cases is given in Table 7-2.

The key radionuclides of interest in the sensitivity study for the circulating coolant activities are I-131 and Xe-133, and for the plateout activities are I-131, Cs-137, Ag-110m, and Sr-90.

Absolute circulating- and plateout activities and normalized change factors for the 12 sensitivity study cases are presented in Table 7-3 and Table 7-4, respectively. The changes in coolant

activity and in plateout activity are shown graphically in Figures 7-1 and 7-2, respectively. The main conclusions of the sensitivity study are summarized below.

Circulating Inventory

- The coolant activity is most affected with the change of the HM contamination fraction and fuel failure fraction. The activity levels of I-131, Xe-133 and total circulating activity change by ~5 times or by ~0.5 times when the HM contamination and fuel failure fraction parameters are changed by an order of magnitude above or below the base case, respectively.
- The He purification constant parameter has a large effect on the activity of Xe-133 but a smaller effect on the activity of I-131 and the total circulating activity.
- The activity level of I-131 is affected by the same order of magnitude with the change of the iodine plateout removal constant. However, the total circulating activity is virtually unchanged because the contribution of I-131 to the overall circulating activity is small.

Plateout Inventory:

- The plateout activity is not affected in the study range of the purification removal constant, overall and iodine plateout removal constants.
- The plateout activity is most affected with the change of fuel failure fraction and Ag diffusive release fraction. The plateout activity increases ~ 4 times when the fuel failure and Ag diffusive release fraction parameters are increased by 10 times. It decreases 0.7 times when these parameters are decreased by 10 times.
- The plateout activity is also affected by the change of the HM contamination fraction but to a lesser degree.

Table 7-2. Input Data Summary for Sensitivity Cases

Parameter	Intact diffusion coef. (Xe) (1/sec)	Intact diffusion coef. (Kr) (1/sec)	Ag fraction release	Cs fraction release	Fuel failure fraction	He purification constant, (1/sec)	Plateout removal constant (1/sec)	I plateout removal constant (1/sec)
Base Case	**1.10E-19**	**1.70E-18**	**5.00E-04**	**1.00E-05**	**5.00E-05**	**2.40E-05**	**3.60E-02**	**7.10E-04**
10 x HM contamination	1.10E-17	1.70E-16	5.90E-04	1.82E-05	unchanged	unchanged	unchanged	unchanged
1/10 x HM contamination	1.10E-21	1.70E-20	4.91E-04	9.18E-06	unchanged	unchanged	unchanged	unchanged
10 x fuel failure fraction	unchanged	unchanged	9.50E-04	5.09E-05	5.00E-04	unchanged	unchanged	unchanged
1/10 x fuel failure fraction	unchanged	unchanged	4.55E-04	5.91E-06	5.00E-06	unchanged	unchanged	unchanged
10 x He purification constant	unchanged	unchanged	unchanged	unchanged	unchanged	2.40E-04	unchanged	unchanged
1/10 x He purification constant	unchanged	unchanged	unchanged	unchanged	unchanged	2.40E-06	unchanged	unchanged
10 x plateout removal constant	unchanged	unchanged	unchanged	unchanged	unchanged	unchanged	3.60E-01	unchanged
1/10 x plateout removal constant	unchanged	unchanged	unchanged	unchanged	unchanged	unchanged	3.60E-03	unchanged
10 x I plateout removal constant	unchanged	unchanged	unchanged	unchanged	unchanged	unchanged	unchanged	7.10E-03
1/10 x I plateout removal constant	unchanged	unchanged	unchanged	unchanged	unchanged	unchanged	unchanged	7.10E-05
10 x Ag diffusive release fraction	unchanged	unchanged	4.01E-03	unchanged	unchanged	unchanged	unchanged	unchanged
1/10 x Ag diffusive release fraction	unchanged	unchanged	1.49E-04	unchanged	unchanged	unchanged	unchanged	unchanged

Table 7-3. Change in Activities for Sensitivity Cases

Parameter	Circulating Activity (Ci)			Plateout Activity (Ci)				
	I-131	Xe-133	Total	I-131	Cs-137	Ag-110m	Sr-90	Total
Base Case – Max. Expected	**0.0445**	**5.02**	**45.8**	**36.4**	**244**	**16.6**	**1.25**	**1150**
10 x HM contamination	0.246	27.6	264	200	446	19.5	4.6	2560
1/10 x HM contamination	0.0244	2.76	24.5	20	224	16.3	0.949	1010
10 x fuel failure fraction	0.244	27.5	234	199	1240	31.5	3.79	4530
1/10 x fuel failure fraction	0.0246	2.77	27	20.1	144	15.1	1	814
10 x He purification constant	0.0345	0.529	20.4	36.4	244	16.6	1.25	1140
1/10 x He purification constant	0.0459	32.8	85	36.4	244	16.6	1.25	1150
10 x plateout removal constant	0.0445	5.02	44.7	36.4	244	16.6	1.25	1150
1/10 x plateout removal constant	0.0447	5.02	51.7	36.4	244	16.6	1.25	1150
10 x I plateout removal constant	0.00459	5.02	43.3	36.4	244	16.6	1.25	1150
1/10 x I plateout removal constant	0.342	5.02	54.8	36.4	244	16.6	1.25	1150
10 x Ag diffusive release fraction	0.0445	5.02	45.9	36.4	244	133	1.25	4080
1/10 x Ag diffusive release fraction	0.0445	5.02	45.8	36.4	244	4.94	1.25	858

Table 7-4. Change Factors for Sensitivity Study

Parameter	Change in Circulating Activity			Change in Plateout Activity[1]				
	I-131	Xe-133	Total	I-131	Cs-137	Ag-110m	Sr-90	Total
Base Case – Max. Expected	**1x**	**1x**	**1x**	**1x**	**1x**	**1x**	**1x**	**1x**
10 x HM contamination fraction	5.5x	5.5x	5.8x	5.5x	1.8x	1.2x	3.7x	2.2x
1/10 x HM contamination fraction	0.5x	0.5x	0.5x	0.5x	0.9x	1.0x	0.8x	0.9x
10 x HM fuel failure fraction	5.5x	5.5x	5.1x	5.5x	5.1x	1.9x	3.0x	3.9x
1/10 x HM fuel failure fraction	0.6x	0.6x	0.6x	0.6x	0.6x	0.9x	0.8x	0.7x
10 x He purification constant	0.8	0.1x	0.4x	1.0x	1.0x	1.0x	1.0x	1.0x
1/10 x He purification constant	1.0x	6.5x	1.9x	1.0x	1.0x	1.0x	1.0x	1.0x
10 x plateout removal constant	1.0x	1.0x	1.0x	1.0x	1.0x	1.0x	1.0x	1.0x
1/10 x plateout removal constant	1.0x	1.0x	1.1x	1.0x	1.0x	1.0x	1.0x	1.0x
10 x I plateout removal constant	0.1x	1.0x	0.9x	1.0x	1.0x	1.0x	1.0x	1.0x
1/10 x I plateout removal constant	7.7x	1.0x	1.2x	1.0x	1.0x	1.0x	1.0x	1.0x
10 x Ag diffusive release fraction	1.0x	1.0x	1.0x	1.0x	1.0x	8.0x	1.0x	3.5x
1/10 x Ag diffusive release fraction	1.0x	1.0x	1.0x	1.0x	1.0x	0.3x	1.0x	0.7x

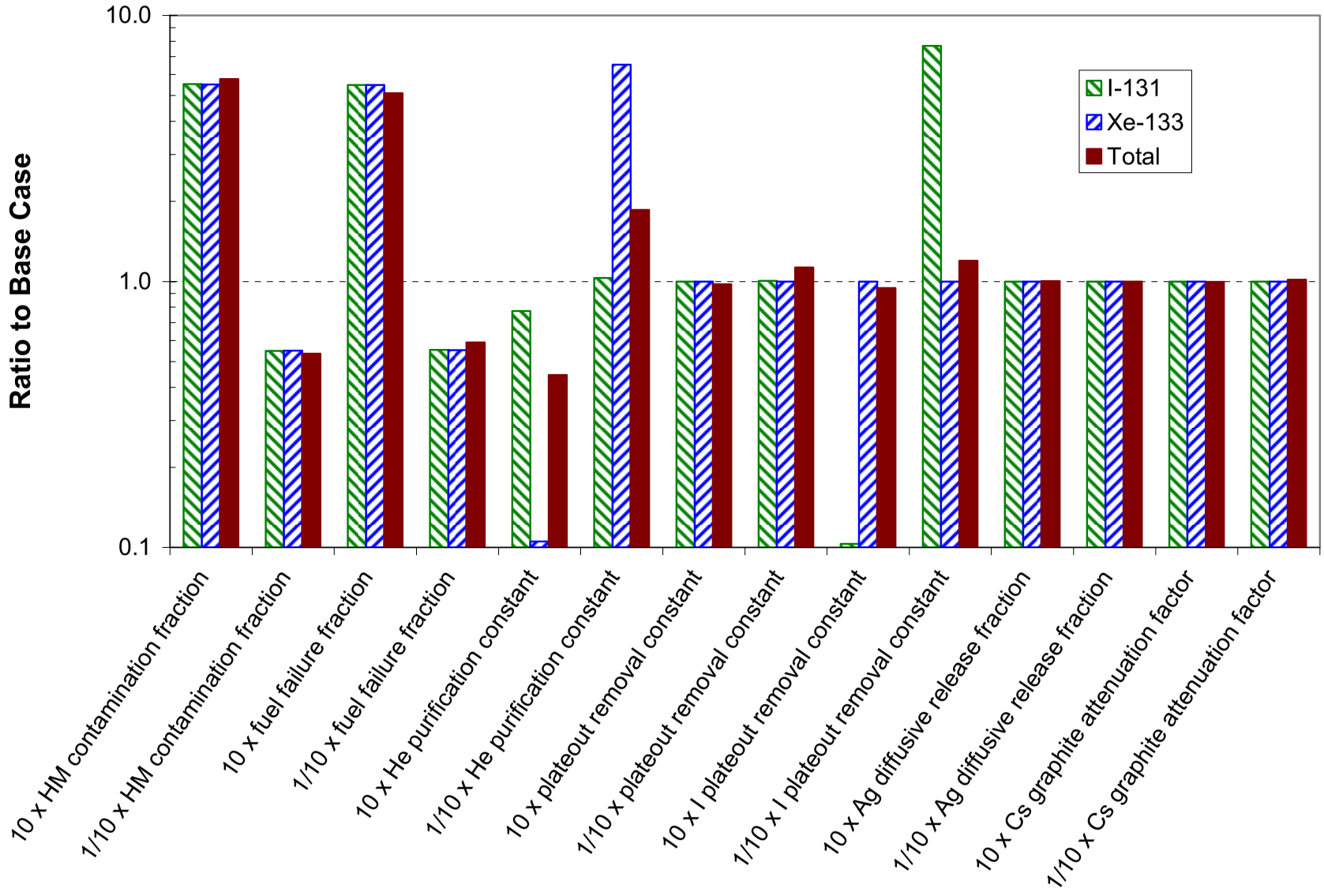

Figure 7-1. Change in Circulating Coolant Activity

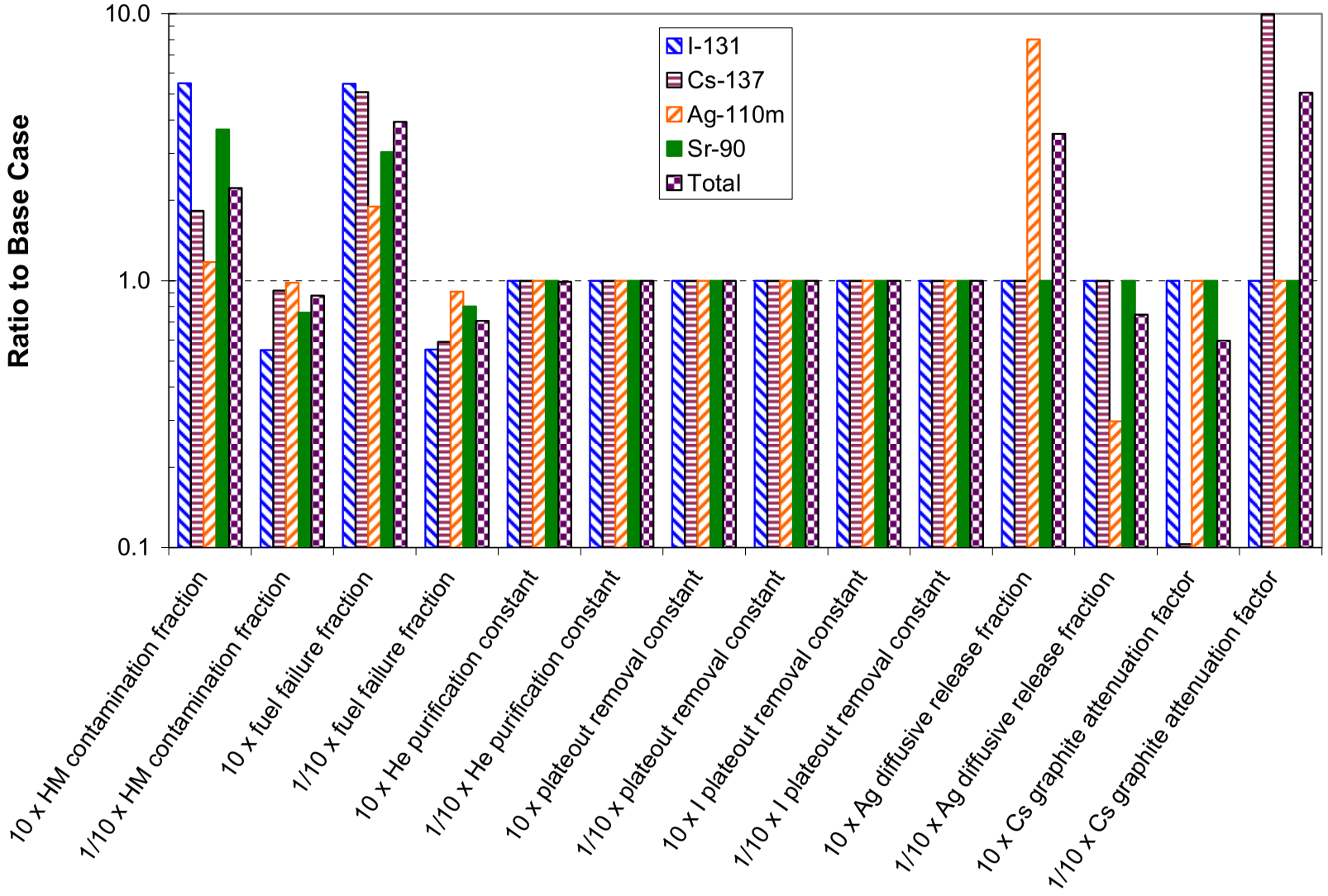

Figure 7-2. Change in Plateout Activity

8. PLANT MASS BALANCE FOR TRITIUM

A plant mass balance for H-3 for three different notional plant configurations was predicted by KAERI using the TRITGO code [Hanson 2006a].

8.1 Design Methods

The design methods used at GA to predict H-3 transport in HTGRs are summarized in this section.

8.1.1 Computer Codes

The TRITGO code was originally developed at ORNL to assess tritium production and distribution in HTGRs [Compere 1974]. TRITGO was slightly modified and used in the 1980s at GA to predict the tritium production and distribution within a steam-cycle MHTGR. It was further modified in the early 1990s for use in predicting H-3 source terms for the NPR program. The most significant modification for the NPR application was the addition of H-3 producing Li targets to the code; that version of the code is Unclassified Controlled Nuclear Information and is not generally available. More recently, the target-related information has been removed, and a non-UCNI version of the TRITGO user's manual has been prepared [Hanson 2006a].

The basic computational model in TRITGO was also adopted for analysis of pebble-bed HTRs by Cordewiner [1979] at KFA Juelich. TRITGO was originally developed for the analysis of HTGRs with prismatic (block) cores; consequently the core model in the code had to be modified extensively to account for the spherical fuel elements and, in particular, for the recirculation of the fuel spheres.

For a typical application of TRITGO, the reactor is divided into a number of tritium source regions such as the active core, the inner reflector, the outer reflector, the top reflector, the bottom reflector, and the control rods. The user inputs characteristic parameters for each region, including the average neutron flux, average temperature, impurity concentrations, and total mass. As illustrated in Figure 8-1, TRITGO determines the amount of tritium present in each region due to ternary fission, neutron reactions with graphite impurities, neutron capture in boron control materials, and He-3 activation in the coolant. The TRITGO output includes the amount of tritium bound in solids, adsorbed on graphite surfaces, in the primary coolant, in the HPS, in the steam generator (SG), and lost to the environment through blowdown or steam generator leakage.

TRITGO would need further modification for rigorous application to an H2-MHR with a secondary heat transport loop since the code as written models H-3 transport from a primary- to

a secondary coolant loop, and H2-MHR has three loops (primary, secondary, and H_2 process). Rather than adding a third loop to the code, it may be sufficient to slightly modify the code such that the H2-MHR is modeled in two sequential runs: (1) the H-3 transport from the primary to secondary loop is first calculated; and (2) the H-3 transport from the secondary loop to the process loop is calculated using the H-3 concentration in the secondary coolant from the first run as the source term.

Alternatively, it may prove more efficient to write a new three-loop code for H2-MHR applications using essentially the same component models that are used in TRITGO. The TRITGO code makes a number of simplifying assumptions such that a system of coupled, linear, first-order ordinary differential equations can be solved analytically. Undoubtedly, in any new code, would be solved numerically and would include modern user friendly features, such as a graphical user interface.

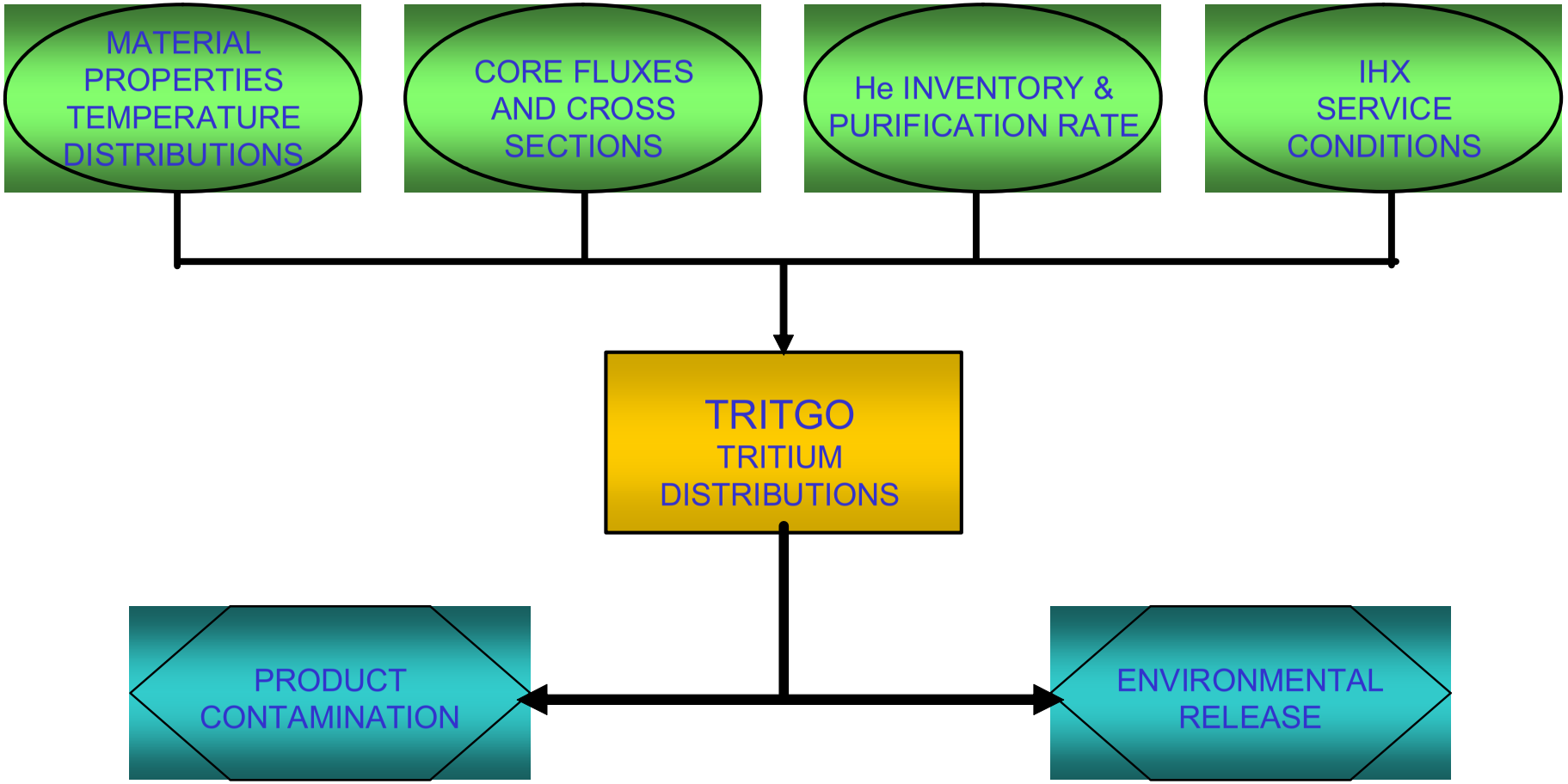

Figure 8-1. TRITGO Code Data Management

8.1.2 H-3 Transport Models

The H-3 transport models currently in use at GA are described in this section. Some of these component models have not yet been incorporated into the TRITGO code described above. It is anticipated that they would be incorporated into a modified version of TRITGO or into a new code written for H2-MHR applications.

8.1.2.1 H-3 from Fuel Particles

Using the available information on H-3 release rates from TRISO-coated particles, especially target particles (Section 5.5.1.1), models were developed at GA for predicting H-3 release from failed and intact TRISO fuel particles [Martin 1993]. The transport of tritium in the kernel and coating layers of intact, TRISO-coated fuel particles is calculated with an effective permeation coefficient given by

$$K = K_o \exp(-Q / RT) \tag{8-1}$$

where K = effective permeation coefficient (m^2/sec),

K_o = preexponential constant (m^2/sec),
Q = activation energy (J/mol)
T = absolute temperature (K)
R = gas constant = 8.314 J/mol-K.

The effective permeation coefficient K may be used in place of the diffusion coefficient in codes such as TRAFIC [Tzung 1992a] which use solutions of the classical diffusion equation to calculate radionuclide transport in HTGR prismatic cores. The constants for Eqn (8-1) are given in Table 8-1, and the predicted fractional release of tritium from intact TRISO-coated particles as a function of temperature for selected times is shown in Figure 8-2.

Table 8-1. H-3 Permeation Constants for TRISO Particles

Particle Component	K_o (m^2/sec)	Q (J/mol)
Kernel	1.0×10^{-6}	0.0
Buffer	1.0×10^{-6}	0.0
IPyC	1.0×10^{-6}	0.0
SiC	4.7×10^{-15}	76,500
OPyC	1.0×10^{-6}	0.0

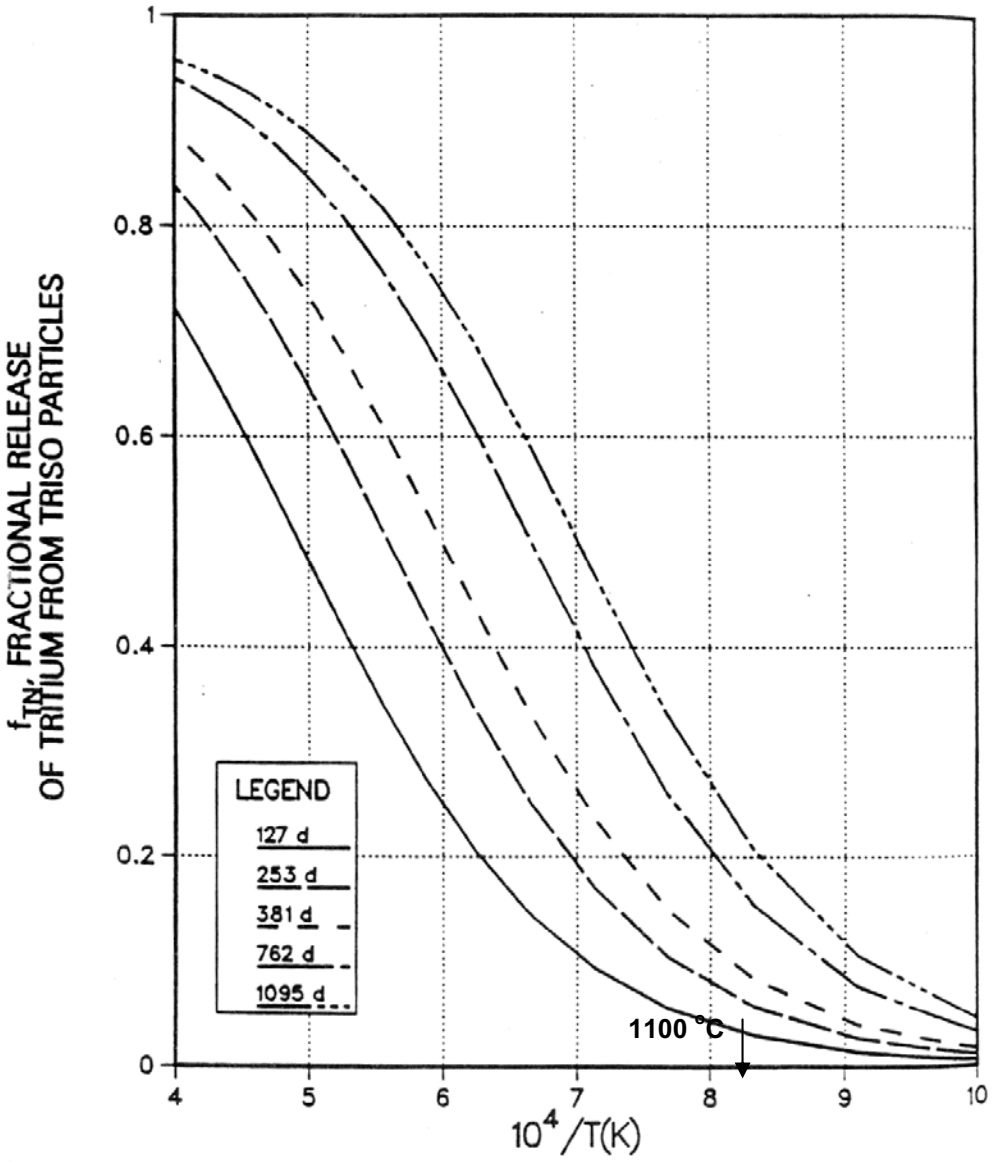

Figure 8-2. H-3 Release from Intact TRISO Particles

The release of tritium from failed particles, defined in this case as particles with failed SiC layers, is assumed to be complete and time independent [Martin 1993]. This assumption may be conservative by a factor of two or three, based upon the data for release from failed UO_2 and UC_2 fuel particles [Gainey 1976]. However, for modern MHR core designs with high-quality TRISO fuel particles, the typical core-average failure fraction is $<10^{-4}$; consequently, this degree of conservatism is of little consequence compared to the predicted H-3 release from intact TRISO particles (Figure 8-2). Note also from Table 8-1 that no hold up by the pyrocarbon layers is assumed; this assumption is clearly conservative based upon measured H-3 retention by

BISO particles. However, for the reason noted above, this conservatism is of little consequence.

This H-3 release model for intact TRISO particles has not been incorporated into the TRITGO code as of this writing.

8.1.2.2 H-3 Release from B_4C Pellets

Using the limited data available (Section 5.5.1.3), a model was developed for H-3 release from B_4C pellets [Martin 1993].

$$f = 1 - \frac{1}{g_1 g_2} \tag{8-2}$$

$$g_i = 1 + \exp\left[a_i \left(\frac{10^4}{T} - \frac{10^4}{T_{oi}} \right) \right], \quad i = 1,2 \tag{8-3}$$

where: f = fractional release of tritium from B_4C,

g_i = curve-fitting parameters, i = 1, 2 (dimensionless)

a_i = constant (K^{-1}),

T = absolute temperature (K),

T_{oi} = reference temperature, i = 1, 2 (K).

The values for the constants are given in Table 8-2, and the resulting correlation is shown in Figure 8-3. This H-3 release model for B_4C pellets has not been incorporated into the TRITGO as of this writing.

Table 8-2. H-3 Release Constants for B_4C Pellets

Parameter	Units	Value
a_1	1/K	0.65
$10^4/T_{o1}$	K	11.6
a_2	1/K	-6.26
$10^4/T_{o2}$	K	8.87

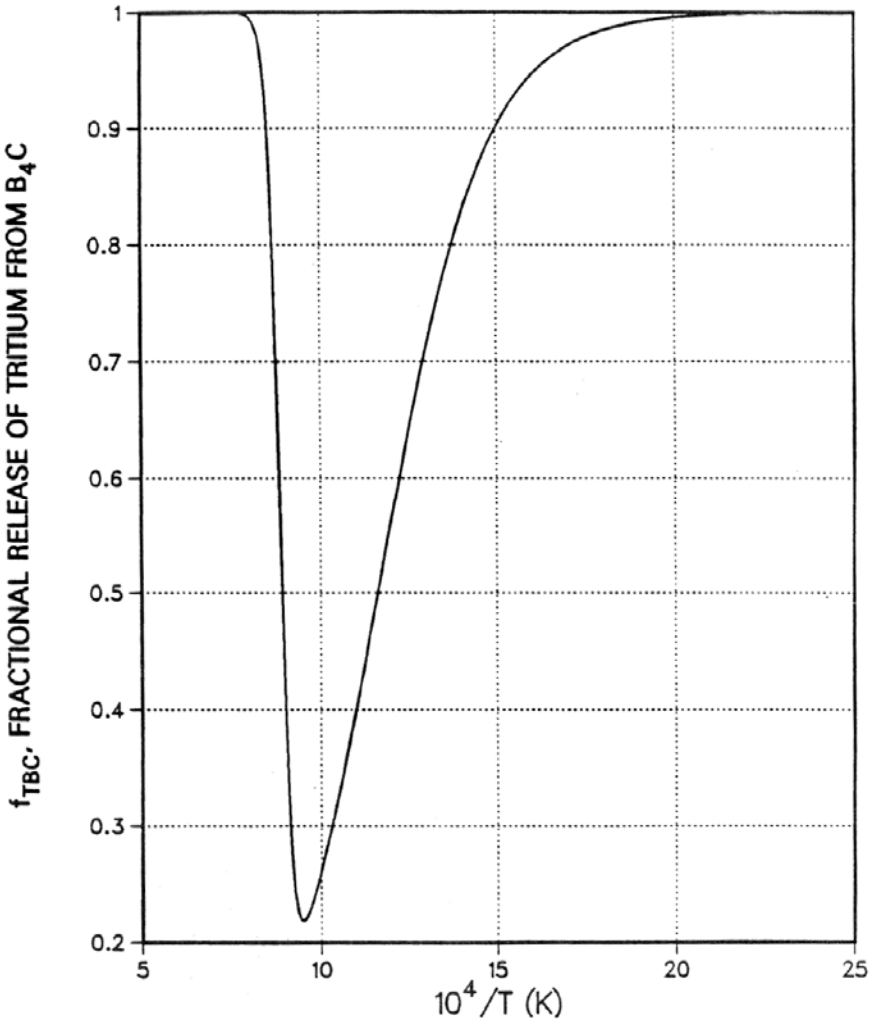

Figure 8-3. H-3 Release from B_4C Granules

8.1.2.3 H-3 Sorption on Graphite

When the TRITGO code was first developed at ORNL [Compere 1974], an isotherm for H-3 sorption on graphite was derived by fitting the sparse experimental data then available to a Temkin isotherm. They concluded that their isotherm fit the literature data well with respect to the pressure dependence, but it did not include a temperature dependence which was clearly incorrect, at least over a broad temperature range considering the data now available [e.g., Strehlow 1985]. The ORNL isotherm was written in a form that had to be solved iteratively:

$$A = A_m / B_1 \ln[B_2 P_{H_2} (A_m - A) / A] \quad (8\text{-}4)$$

where: A = tritium sorbed on graphite per BET surface area [cm^2(STP)/m^2],
A_m = monolayer saturation value [0.2 cm^2(STP)/m^2] [21],
B_1 = constant (17.97),
B_2 = constant (16.54 mm Hg^{-1}),
P_{H2} = hydrogen partial pressure (mm Hg^{-1}).

Later, Myers [1986] derived a new isotherm which includes crude temperature dependence, and this new isotherm has also been added as an option in the TRITGO code [Hanson 2006a]. The new isotherm is also based upon very limited experimental data. It assumes no H-3 sorption at temperatures below 650 °C. For temperatures between 650 °C and 1250 °C, the sorptivity of H-3 is assumed to be a function of the hydrogen partial pressure and fast fluence but independent of temperature. Above 1250 °C, tritium begins to have a significant desorption pressure, and effective sorptivity decreases with increasing temperature. The Myers isotherm has the following form:

$$A = 0 \text{ , T < 650 °C} \tag{8-5}$$

$$A = C_1(1 + fC_2C_H)P_{H_2} / \{1 + \exp[C_3(T - T_o)]\} \text{ , T > 650 °C} \tag{8-6}$$

and:
$$C_H = \{1 + \exp[C_3(T - 1423)]\}^{-1} \tag{8-7}$$

where: C_1 = constant [[1.38 x 10^3 cm^3(STP)/m^2-mmHg],
C_2 = constant (2.6 x 10^{-25} m^2/n),
C_3 = constant (0.0439 K^{-1}),
P_{H2} = partial pressure of hydrogen (Pa),
f = fast fluence (n/m^2),[22]
C_H = annealing factor,
T = graphite temperature (K),
T_o = reference temperature (1523 K).

The resulting isotherm is displayed in Figure 8-4, which shows the H-3 loading as a function of partial pressure and temperature at a constant fast fluence and the H-3 loading as a function of temperature and fast fluence at a constant partial pressure. Presumably, the Myers isotherm is an improvement over the original isotherm in that it includes crude temperature dependence

---

[21] Typical value for H-327 graphite which was used for the fuel elements in the FSV initial core and the first reload; fuel blocks for subsequent reloads were made from more dimensionally stable H-451 graphite.

[22] At present, a fast fluence of 6 x 10^{25} n/m^2 is hard wired into the TRITGO code (Hanson 2006a); at minimum, the fast fluence should be made an input variable.

and a fast fluence dependence that the now available experimental data indicate; however, the uncertainties in the Myers isotherm are clearly quite large and unquantified.

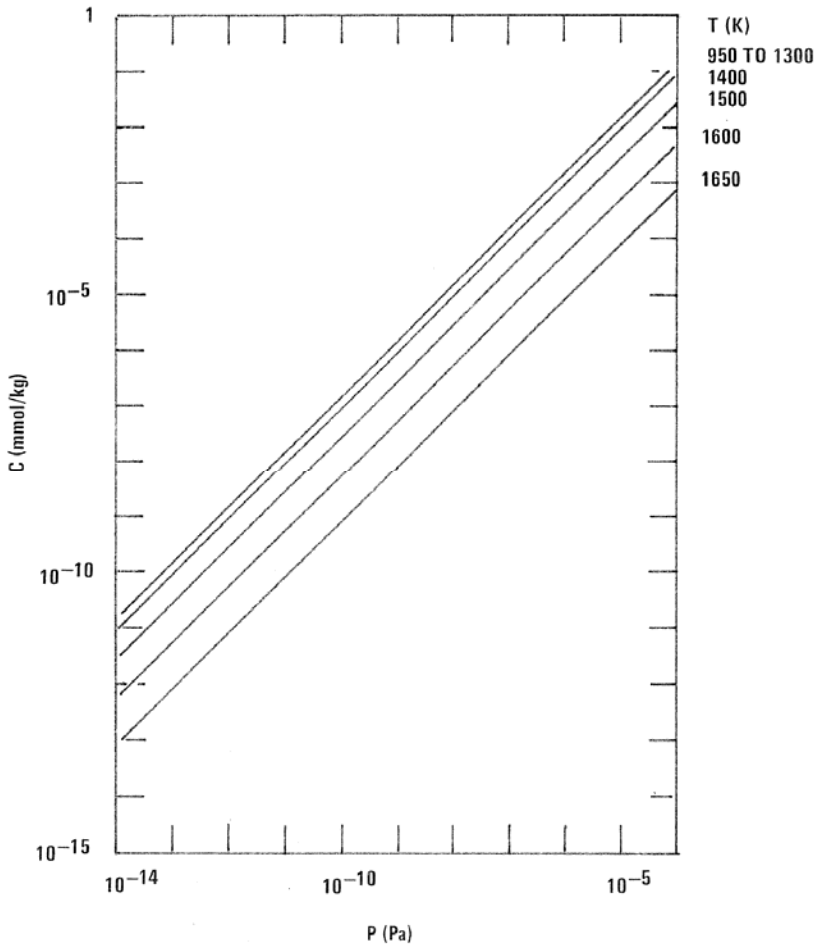

H-3 Loading as Function of Pressure and Temperature

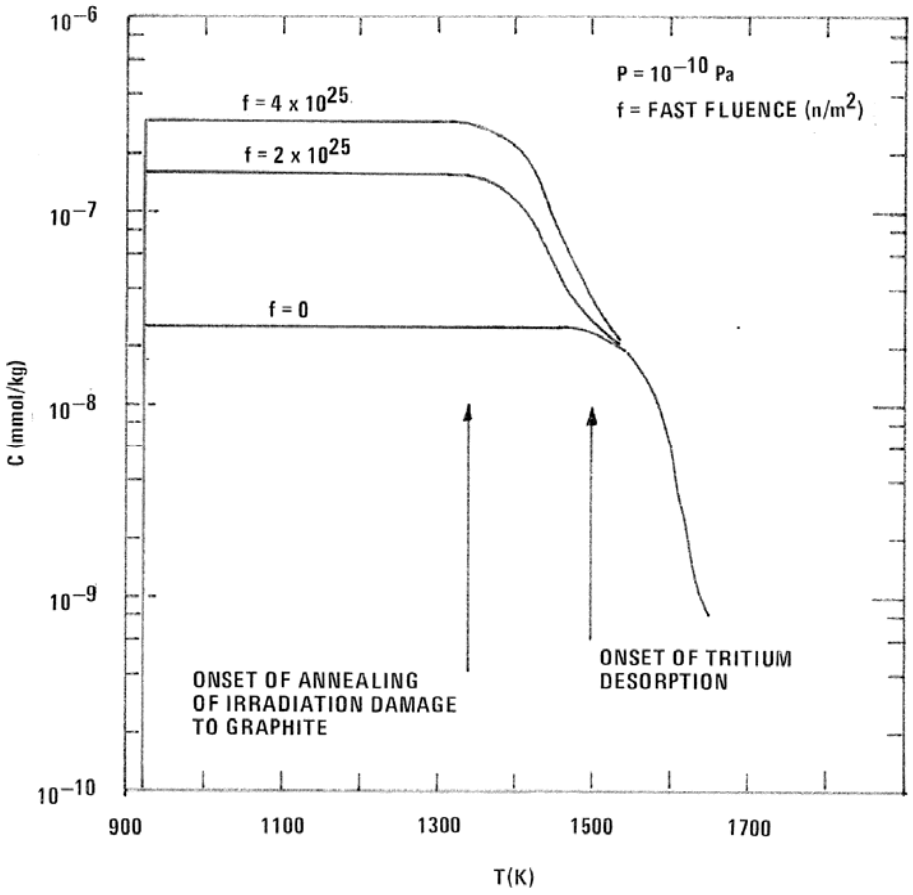

H-3 Loading as Function of Temperature and Fast Fluence

Figure 8-4. Myers Isotherm for H-3 Sorption on Graphite

8.1.2.4 H-3 Permeation through Metals

The permeation models considered for use in the TRITGO analysis of the NGNP are described below.

8.1.2.4.1 FDDM/F Model

Models for H-3 permeation through heat exchanger tubes were developed by Myers at GA in the late 1980s [Martin 1993]. At that time, the primary interest was in steam-cycle HTGRs, and the preferred materials of construction for steam generator tubes were typically Alloy 800H for the superheater section and T22 (2¼% Cr-1% Mo steel, SA-387) for evaporator/economizer sections. The following correlation was derived for H-3 permeation through Alloy 800H and T22:

$$P_r = P_o \left(\frac{C_T}{C_{T_o}} \right)^n \left(\frac{\Delta C_T}{\Delta \tau_w} \right) \exp(-Q / RT) \tag{8-8}$$

with

$$n = n_o \exp(Q_o / RT) \tag{8-9}$$

where: P = permeation rate (μCi/m^2-hr)

P_o = constant (m-mm/hr),

C_T = tritium concentration on coolant side of tube [μCi/m^3(STP)],

C_{T_o} = reference tritium concentration on coolant side of tube [μCi/m^3(STP)],

τ_w = wall thickness of the SG tube (mm),

$\frac{\Delta C_T}{\Delta \tau_w}$ = tritium concentration gradient across the tube wall (μCi/m^3-mm),

Q/R, Q_o/R = temperature coefficients (K),

T = temperature (K),

n_o = constant (dimensionless).

The values of the parameters of Eqns. 8-8 and 8-9 are presented Table 8-3. In computing the concentration gradient, the concentration on the steam side of the steam generator tube is assumed to be zero. The tritium permeation rates are shown in Figure 8-5 as a function of temperature for selected H-3 concentrations and a SG wall thickness of 3.2 mm for Alloy 800H and T22.

In fact, this FDDM/F correlation cannot be used in the TRITGO code as formulated because the dependence of the permeation rate P on the tritium concentration in the coolant C_T is not linear (in fact, it varies with temperature). The TRITGO code is an analytical solution to a coupled set of ordinary differential equations which are solved to give the H-3 concentration in a number of compartments including the primary coolant.

Table 8-3. Coefficients for H-3 Permeation Correlations

Parameter	Alloy	
	Alloy 800H	T22 (SA-387)
P_o (m-mm/h)	9.10E+00	1.42E+00
C_{T_o} (μCi/cm^3)	6.00E+02	6.00E+02
Q (J/mol)	5.35E+04	4.20E+4
n_o	9.35E-01	9.35E-01
Q_o (J/mol)	2.29E+03	2.29E+03

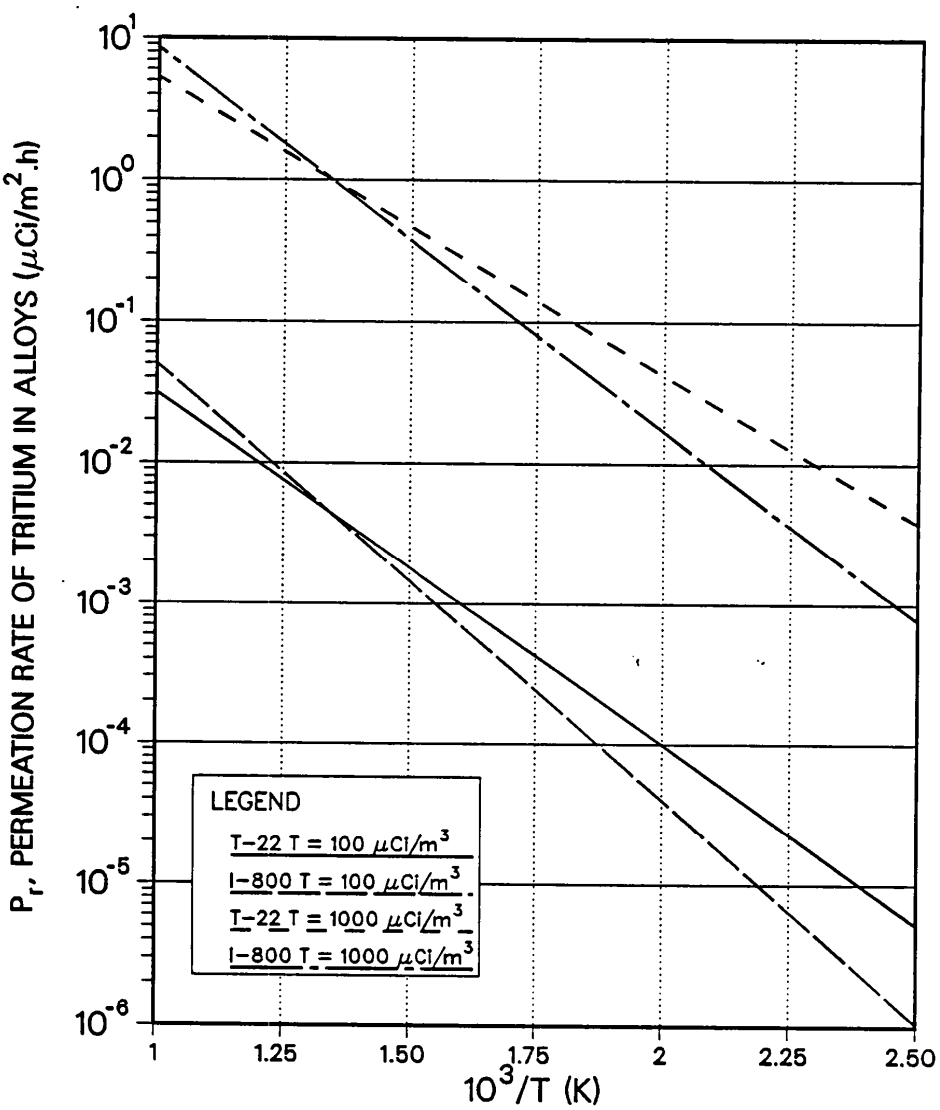

Figure 8-5. H-3 Permeation in Alloy 800H and T22

8.1.2.4.2 CEGA Correlation

In 1991, the available data for H-3 permeation through Alloy 800 was reevaluated. The Myers correlation given above is based primarily upon the H-3 permeation rates measured for Incoloy 800 tube specimens removed from the Peach Bottom steam generator at end-of-life [Yang 1977]. These data were refit, and the following correlation was derived [Czechowicz 1991]:

$$R_{perm} = (R_o / \tau_w) C_T (P_{pri})^{1/2} (ppmv_{H_2})^{-1/2} \exp(B/T) \quad (8\text{-}10)$$

where: R_{perm} = permeation rate (μCi/m^2-hr),
R_o = constant [61.02 ppmv$^{1/2}$-m^3(STP)-mm/atm$^{1/2}$-m^2-hr],
τ_w = wall thickness of the SG tube (mm),
C_T = tritium concentration on coolant side of tube [μCi/m^3(STP)],
P_{pri} = primary coolant pressure (atm),
$ppmv_{H2}$ = hydrogen concentration (ppmv),
B = constant (-6249 K)
T = absolute temperature (K).

This new correlation for H-3 permeation through Alloy 800 tubes is used in the TRITGO code (Hanson 2006a).

The leading candidate material for the IHX and for the superheater section of the steam generator is IN 617. While the tritium permeability of IN 617 has not been as well characterized as that of some other metals, including Alloy 800H, there are several German comparative studies that indicate the tritium permeabilities of IN 617 and Alloy 800H are quite comparable at the service temperatures anticipated for the NGNP IHX and steam generator (see Figure 5-12). Consequently, the CEGA correlation was used for IN 617 as well as for Alloy 800H.

8.1.3 Material Property Data

Fundamental nuclear data, including microscopic cross sections, are obtained from standard nuclear industry sources, such as Evaluated Nuclear Data File B, Version 6 (ENDF/B-6) that are then modified as appropriate for application to graphite-moderated, gas-cooled reactor core design.

For reactor design and safety analysis, the H-3 producing impurities in the core components are assumed to be at the limits permitted by the fuel product specifications and graphite material specifications. These specifications for various HTGR applications limit the chemical impurities in core materials in several ways: (1) explicit limits on certain neutron poisons, especially boron, expressed in terms of total allowed boron equivalents; (2) explicit limits on certain chemical impurities, such as lithium, iron, and classes of chemical impurities, such as transition metals; and (3) nonspecific limits on “total ash.”

8.2 Plant Configurations

Three plant configurations were considered by KAERI in this evaluation, consistent with the configurations defined in the Workplan [2007]. In all cases, the total core power was assumed to be 600 MW(t), and the core inlet and outlet temperatures were assumed to be 490 and 950 °C, respectively, to maximize the predicted tritium permeation through the heat exchangers.

As shown in Figure 8-6, Configuration 1 has a two-stage IHX in the primary circuit (two modules) and a steam generator in the secondary circuit. All of the primary He coolant passes through the two-stage IHX. The helium inlet temperature for the first stage of IHX is 950°C, and the outlet temperature from the first stage of two heat exchangers is 782 °C. The helium inlet temperature for the second stage of the IHX is 782 °C, and the outlet temperature from the second stage is 486 °C. The secondary helium inlet temperature for the first stage of IHX is 705 °C, and the secondary outlet temperature is 925°C. The secondary helium inlet temperature for the second stage of IHX is 310 °C, and the secondary outlet temperature is 704 °C.

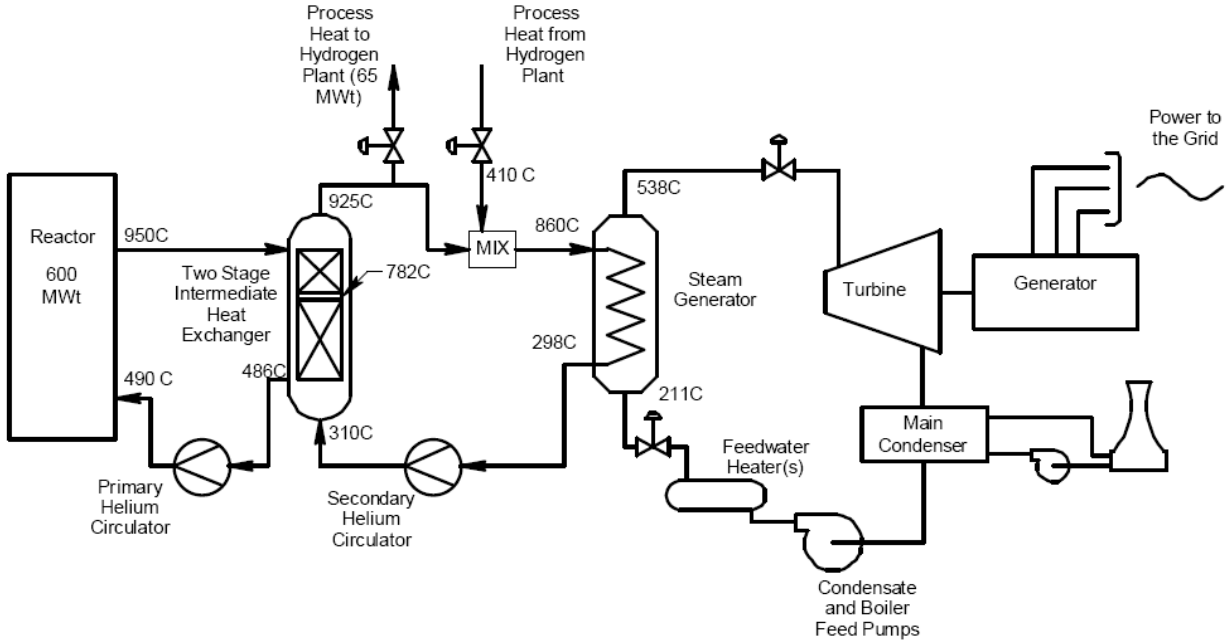

Figure 8-6. Plant Configuration 1 with Two-Stage IHX in Primary Circuit

In the secondary loop, only ~10% of the He flow is routed to the hydrogen plants (60 MW of 600 MW are transferred to the SI plant and 4 MW to the HTE plant). This helium is returned from the hydrogen plants at 410 °C, mixes with the remaining 90% of the primary flow and enters the steam generator at a mixed mean temperature of 860 °C. The tritium is produced in a tertiary loop; however, the TRITGO code can only model two loops in the single run.

Consequently, it is conservatively assumed 10% of the tritium entering into the secondary circuit will eventually be introduced into the product hydrogen unless it is removed by a secondary HPS.

As shown in Figure 8-7, Configuration 2 has two primary loops with IHXs and a steam generator installed a secondary loop. One primary loop has a small 65 MW(t) IHX which supplies the hydrogen plants, and the other loop has a large 547 MW(t) IHX supplying the steam generator.
\
The heat from the small 65 MW(t) intermediate heat exchanger in the primary loop is transferred to the hydrogen plants via process heat exchangers.

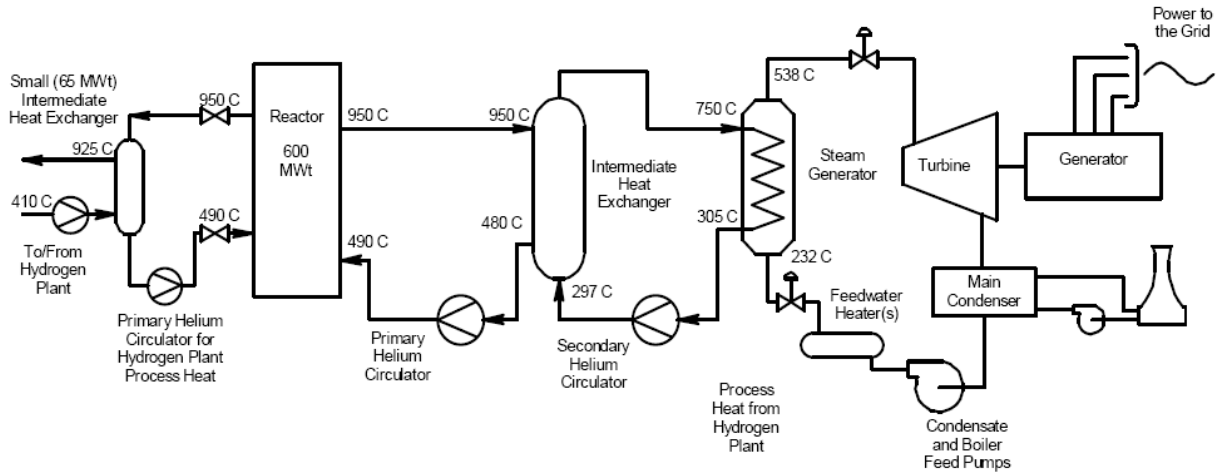

Figure 8-7. Configuration 2 with Steam Generator in Secondary Loop

The helium inlet temperature for both IHXs is 950 °C, and the outlet temperature is 480 °C. The secondary helium inlet temperature for the small 65 MW(t) IHX is 410 °C, and the secondary outlet temperature is 925 °C. The secondary helium inlet temperature for the 547 MW(t) IHX is 297 °C, and the secondary outlet temperature is 750 °C.

Given the aforementioned limitations of the TRITGO code, the two loops of Configuration 2 are analyzed in separate runs. As elaborated below, the degree of conservatism introduced by this approach is minimal because the H-3 concentration in the primary He is effectively determined by a balance of the various sources and the graphite sink and, to a lesser extent, the HPS. The permeation sink is negligible by comparison. Again, the conservative assumption is made that all of the tritium that permeates into the secondary loop will eventually permeate into the hydrogen plant or the steam generator unless it is removed by an HPS in the secondary circuit because there is no other major sink for tritium in the secondary loop.

As shown in Figure 8-8, Configuration 3 also has two primary loops: one with a 65 MW(t) IHX supplying the hydrogen plants (which is identical to the small IHX in Configuration 2) and a second loop with a 545 MW(t) steam generator in the primary circuit (like a conventional steam-cycle HTGR). The inlet helium temperature for the steam generator is 950 °C, and the helium outlet temperature is 481 °C. The water inlet temperature for the secondary side of the steam generator is 230 °C, and the steam outlet temperature is 538 °C.

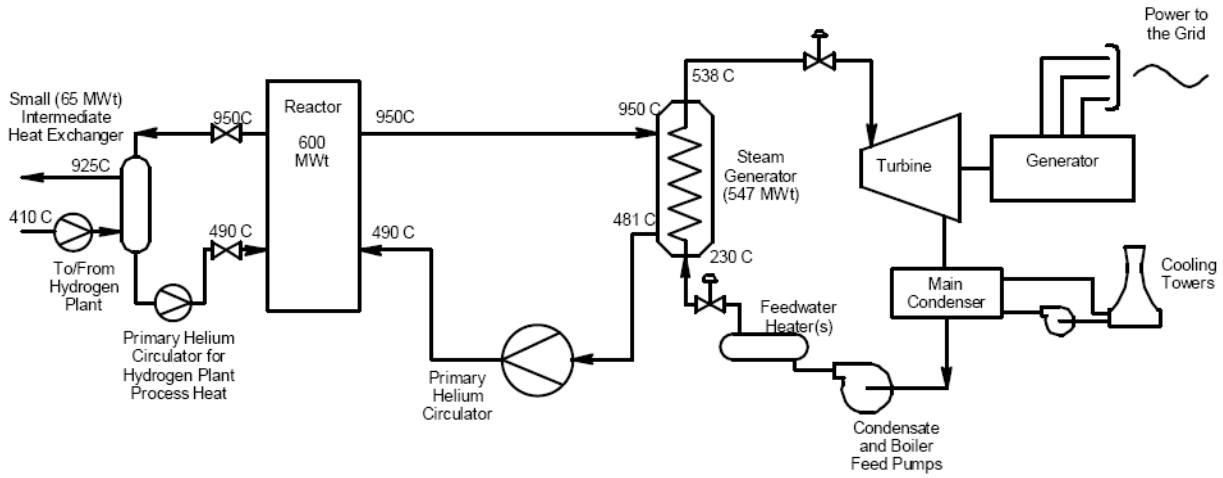

Figure 8-8. Configuration 3 with Steam Generator in Primary Loop

Once again, the two loops of Configuration 2 are analyzed in separate TRITGO runs. In fact, the analysis of the 65 MW(t) IHX loop is common to both Configurations 2 and 3.

8.3 Tritium Source Terms

As previously discussed in Section 5, tritium will be produced in a VHTR by ternary fission and by activation reactions with trace impurities in the graphite reflector and with boron containing control materials. In addition, tritium is generated from the helium coolant itself by the neutron activation of He-3 in the He coolant (natural abundance = 2×10^{-7}). Ternary fission is the dominant tritium source; therefore, it is important to estimate the tritium release fraction from TRISO fuel particles as accurately as possible.

The most accurate estimate of the tritium release fraction from the TRISO fuel particles would result from a full-core analysis accounting for the time-at-temperature histories throughout the core with a code such as TRAFIC [Tzung 1992a] and using best-estimate effective diffusion coefficients for tritium transport through the SiC coatings. A conceptual prismatic core design is not yet available so an approximate approach was used to estimate the tritium release fraction from intact TRISO fuel particles; H-3 release from failed particles is negligible by comparison (with an assumed fuel fraction of 5×10^{-5}). As described in Section 8.1.2.1 and shown in

Figure 8-2, GA had previously developed a model for predicting the tritium release fraction from TRISO particles as a function of time at constant temperature [Martin 1993].

Assuming the volumetric fuel temperature distribution shown Figure 8-9 for a 950 °C prismatic core design [Richards 2007], one can estimate a core-average H-3 release fraction from intact TRISO particles using the GA correlation. The approach taken was to calculate the fractional H-3 release for 10 subvolumes, assuming that the fuel in each subvolume operated isothermally for its entire lifetime of three years and then to estimate the core-average H-3 release fraction. The result was an estimated, core-average, H-3 fractional release of 30%; this value is clearly conservative, probably excessively so. Since the diffusive release of H-3 from intact TRISO particles is predicted to the dominant source of H-3 in the primary He coolant, it will be important to refine this estimate once a conceptual core design becomes available.

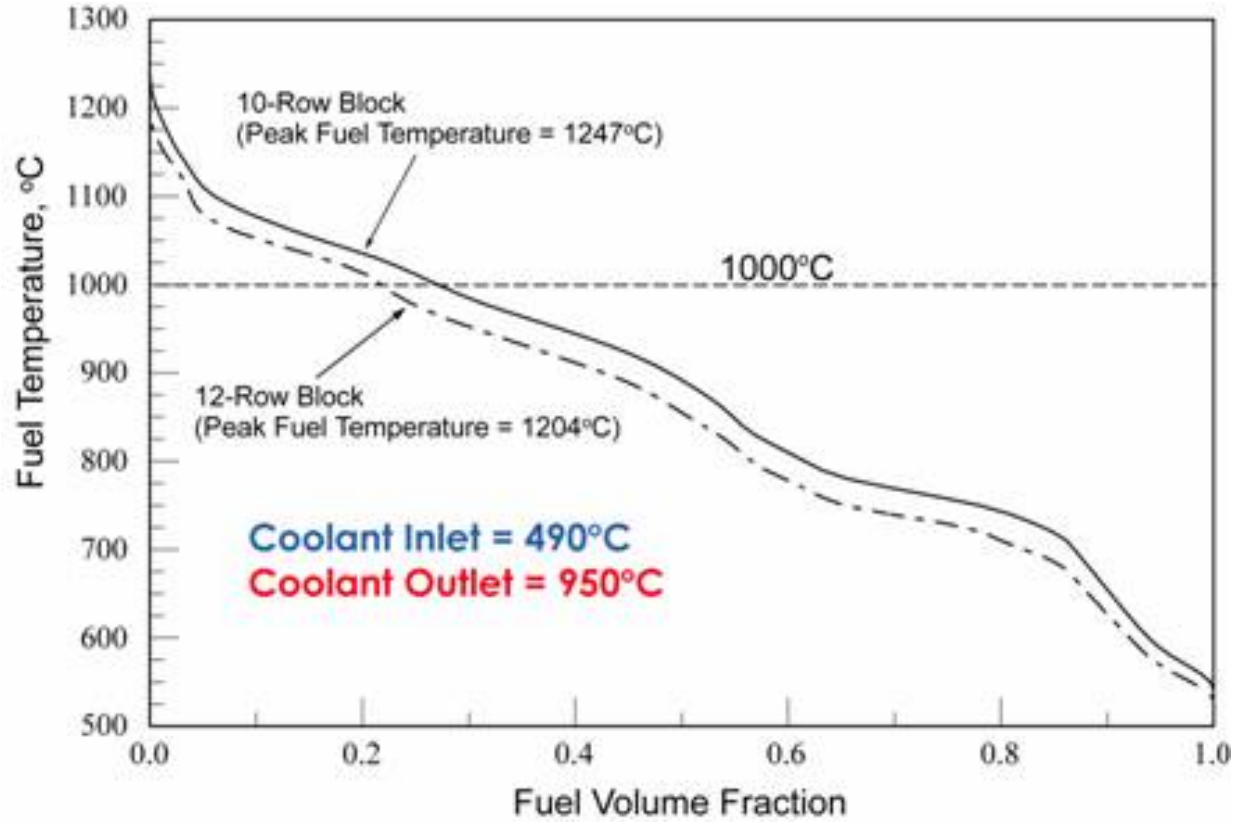

Figure 8-9. Fuel Volume Temperature Distribution for a 950 °C Core

8.4 TRITGO Model of NGNP

An 11-region core model of a notional 600 MW(t) NGNP was constructed as shown in Figure 8-10 within the severe modeling constraints of the TRITGO code (e.g., constant average temperature within a region, etc.).[23] The choice of average temperature was rather arbitrary for certain large core components, such as the inner reflector, which experience a broad range of temperatures. The core temperature distributions were taken from KAERI results obtained with the GAMMA code. The neutron flux distributions were obtained from [OSU 2003]. The masses of graphite in each region were calculated from the information for the 600 MW(t) commercial GT-MHR given in [Phelps 2008]. The boron loading in each of the 36 operating control rods in the permanent side reflector was assumed to be the same as that for an average operating control rod in the 350 MW(t) NP-MHTGR design [RSSDD 1994, Gillespie 1993]. The 12 startup control rods in the inner fuel ring were ignored since they are always fully withdrawn before the core goes critical so they are exposed to a relatively low neutron flux [RSSDD 1994].

[23] The number of blocks listed in Figure 8-10 is the equivalent number of full length fuel elements (e.g., the replaceable bottom reflector which is listed as “1 block” is actually two ½ length blocks).

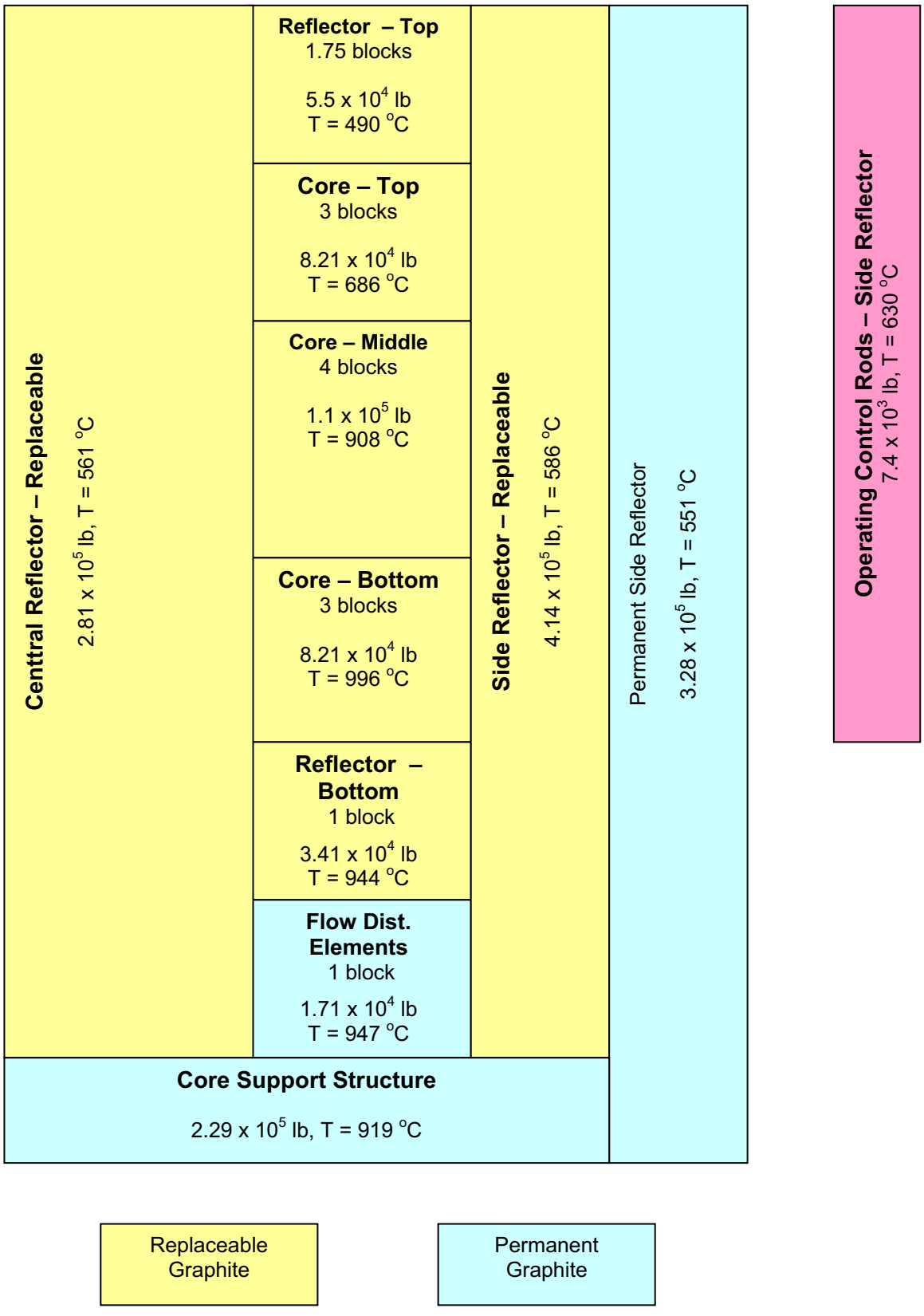

Figure 8-10. TRITGO Core Model

The simple TRITGO heat exchanger models for the three plant configurations considered (Section 8.2) are summarized in Table 8-4.

Table 8-4. TRITGO Heat Exchanger Models

Component	Total Surface Area (m^2)	Wall Thickness (mm)	Temperature (°C)
600 MW(t) Two-Stage IHX (Configuration 1)			
IHX Sect-1 Stage 1	1104.8	2.4	938.5
IHX Sect-2 Stage 1	1104.8	2.4	870.0
IHX Sect-3 Stage 1	1104.8	2.4	746.3
IHX Sect-1 Stage 2	791.8	2.4	746.7
IHX Sect-2 Stage 2	791.8	2.4	609.6
IHX Sect-3 Stage 2	791.8	2.4	407.1
547 MW(t) IHX (Configuration 2)			
IHX-Sect-1	621.2	2.4	856.1
IHX-Sect-2	621.2	2.4	620.1
IHX-Sect-3	621.2	2.4	393.9
65 MW(t) IHX (Configurations 2 & 3)			
IHX sect-1	351.8	2.4	938.1
IHX sect-2	351.8	2.4	861.1
IHX sect-3	351.8	2.4	753.5
IHX sect-4	351.8	2.4	615.4
IHX sect-5	351.8	2.4	446.7
545 MW(t) Steam Generator (Configuration 3)			
IHX sect-1	351.8	3.8	938.1
IHX sect-2	351.8	3.8	861.1
IHX sect-3	351.8	3.8	753.5
IHX sect-4	351.8	3.8	615.4
IHX sect-5	351.8	3.8	446.7

8.5 Description of Analysis

The key input parameters in the TRITGO model of the 600 MW NGNP are summarized in Table 8-5. A complete listing of the input parameters is given in the TRITGO sample output file reproduced in Appendix B.

The assumed concentrations of impurities that yield tritium as a result of various neutron reactions are summarized in Table 8-6; the Li concentration in the replaceable graphite components was assumed to be the same as that for H-451 graphite, and the Li concentration in the permanent graphite components was assumed to be the same as that for Stackpole 2020 graphite [GDDM 1984].

Table 8-5. Key Input Parameters in TRITGO NGNP Model

PARAMETER	600 MW NGNP
Plant Parameters	
Thermal power (MW)	600
Plant lifetime (yr)	60
Plant capacity factor	0.94
Primary Coolant Mass flow rate (lb/hr)	2.54×10^{6}
Circulating He inventory (lb)	10,000
He-3 mol fraction in He coolant (atom/atom)	2×10^{-7}
He purification constant (sec^{-1})	2.4×10^{-5}
Hydrogen (protium) concentration in primary He (ppm)	10
Core Parameters	
Fuel cycle	LEU/NatU
Core power density (w/cm^3)	6.6
Fuel residence time (yr)	3
Number of fuel elements	1020
Tritium Transport Parameters	
Release fraction from intact TRISO particles	0.3
Release fraction from Li activation in graphite	0.01
Release fraction from boron control materials	0.01

Table 8-6. Assumed Impurities in Core Components

Impurity (ppm)	Core Component			
	Fuel Elements	Replaceable Reflectors	Permanent Core Components	Control Rods
Li	0.036	0.036	2	0
B	41 (LBP)	2	8 (B-steel pins)	4×10^5
Be	0	0	0	0

8.5.1 Predicted H-3 Distribution in NGNP

The primary purpose of this study was to estimate the amount of tritium permeation from the primary coolant into the hydrogen product in the hydrogen process plants and into the process steam in the steam generator. The hydrogen is actually produced in a third loop, but TRITGO can only model the permeation from the primary loop to a secondary loop. However, all of the tritium which permeates into the secondary loop will eventually permeate into the hydrogen plant or into the process steam unless it is removed by an HPS in the secondary circuit because there is no other significant sink for tritium in the secondary circuit (i.e., there is nothing equivalent to the core graphite in the secondary circuit). Consequently, it was simply assumed that all of the tritium in the secondary loops will eventually permeate through the process heat exchanger into the hydrogen plants or through the steam generator (the degree of conservatism is expected to be small).

Figure 8-11 shows the total amount of tritium generation, the amount of tritium bound in solids, the amount of tritium produced by ternary fission, and the amount of tritium produced by the various neutron reactions. The results are the same for all three configurations because the reactor system design and operating conditions are assumed to be same for each configuration.

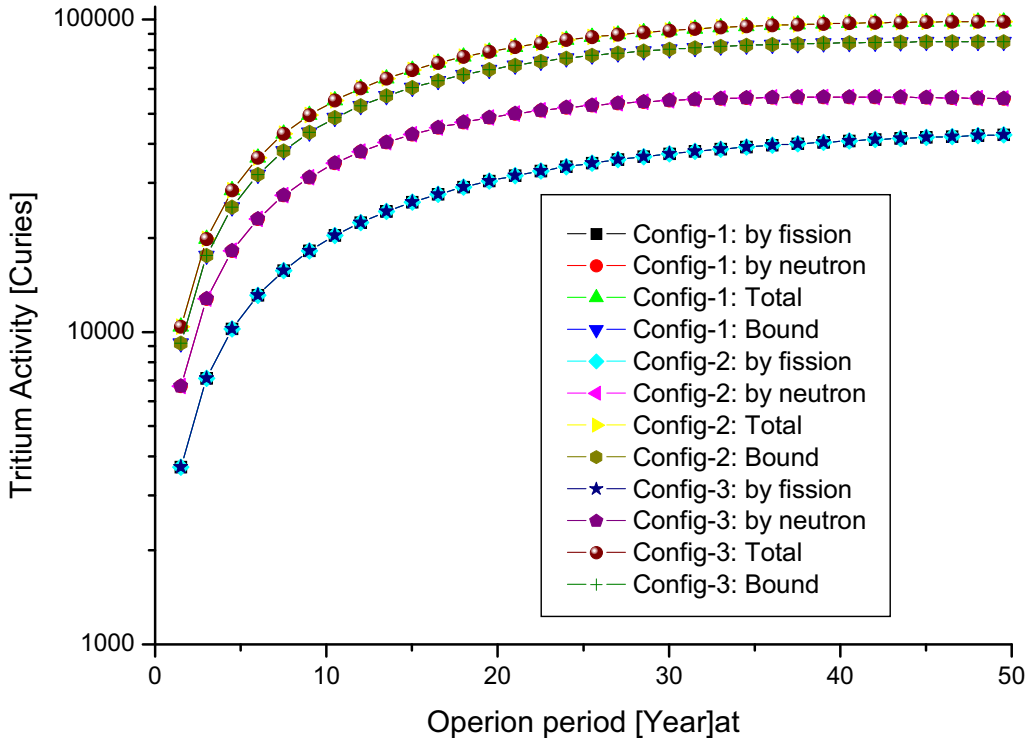

Figure 8-11. Total H-3 Production and Bound in Solids

Figure 8-12 shows that the amount of tritium generation from B-10 by fast neutrons, from the activation reaction of Li-7 impurity in the graphite and from the neutron activation of He-3 in the He coolant; the results are the same for all three configurations.

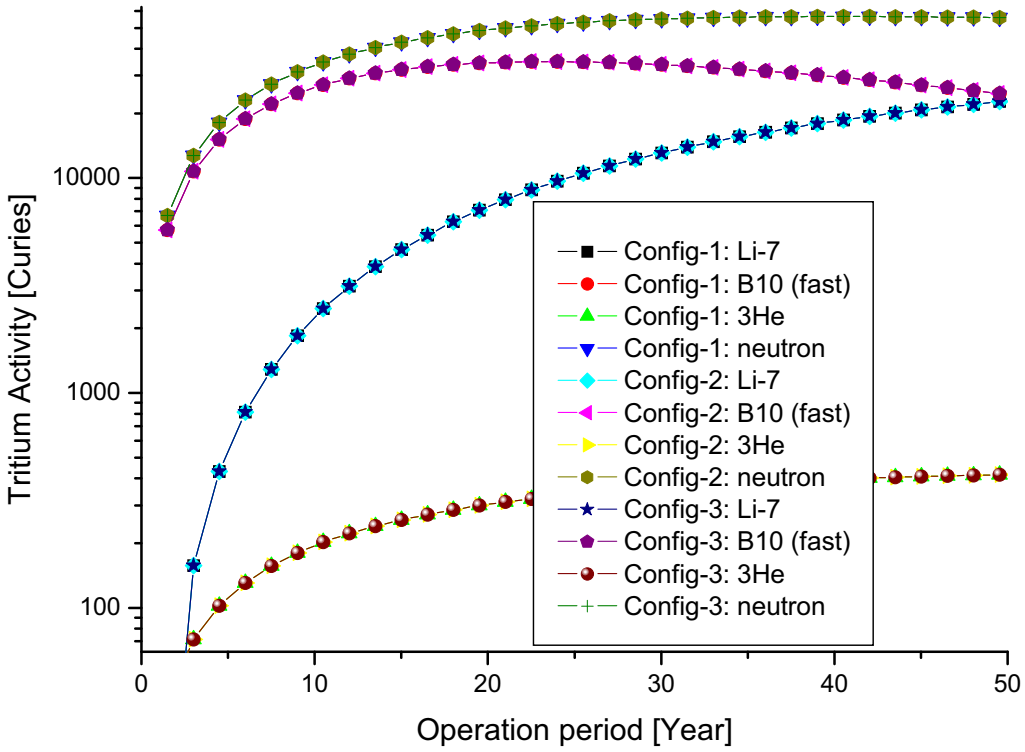

Figure 8-12. H-3 generation from Li-3, B-10 and He-3

The predicted tritium inventories in the primary He coolant for the three plant configurations are shown in Figure 8-13. Configuration 3 showed the highest tritium activity in the primary coolant, presumably because the amount of H-3 lost by permeation was lowest in this case because the steam generator wall temperatures are lower than the IHX wall temperatures in the other two configurations.

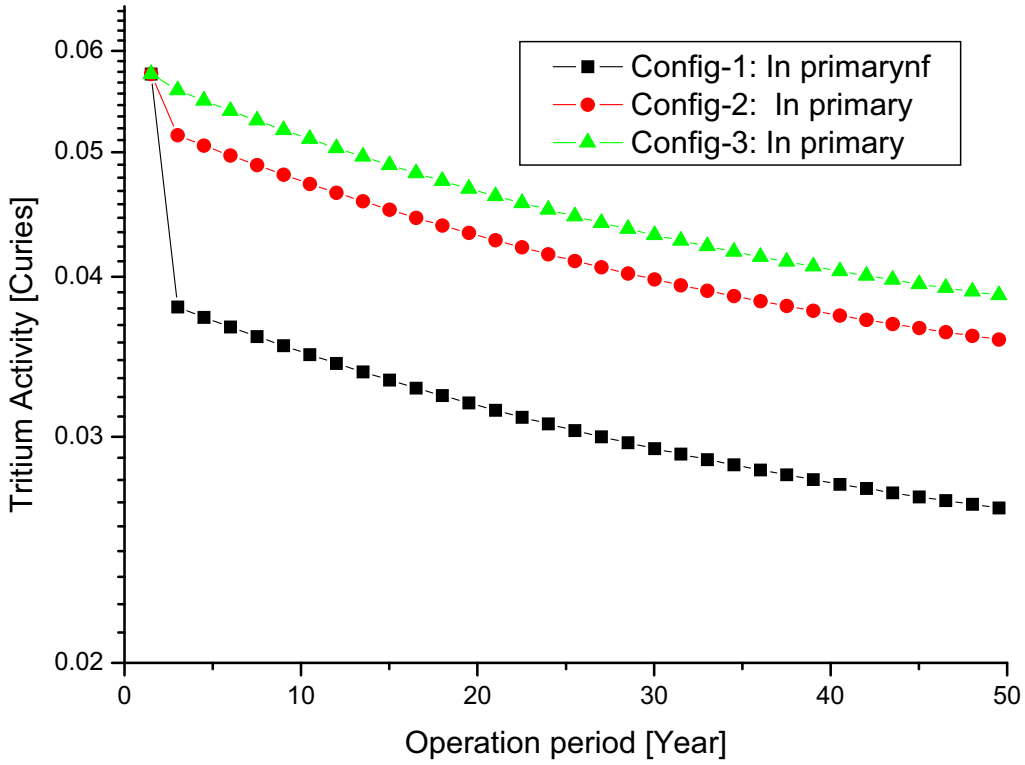

Figure 8-13. H-3 Inventories in the Primary He Coolant

The predicted tritium inventories in the He purification systems for the three plant configurations are shown in Figure 8-14. Configuration 3 again showed the highest tritium activity in the HPS because the amount of H-3 entering HPS is proportional to the amount of H-3 in the primary coolant which was highest for that configuration as described above.

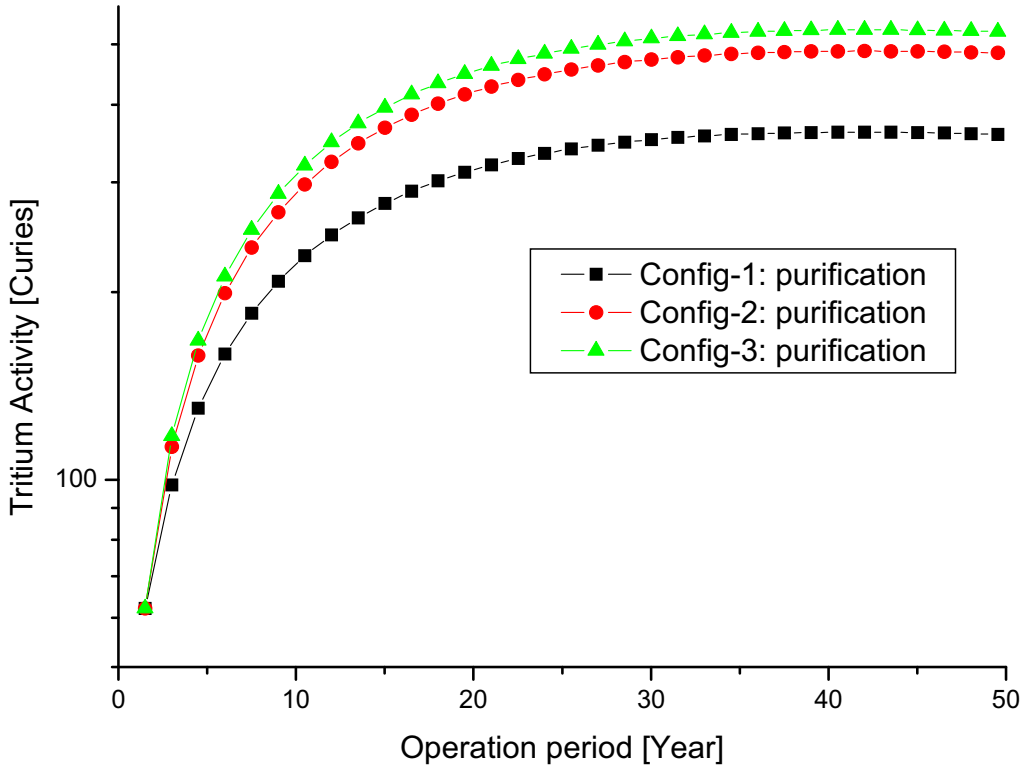

Figure 8-14. H-3 Inventories in the He Purification System

The predicted tritium inventories sorbed on the core graphite for the three plant configurations are shown in Figure 8-15. The results are virtually the same for all three plant configurations.

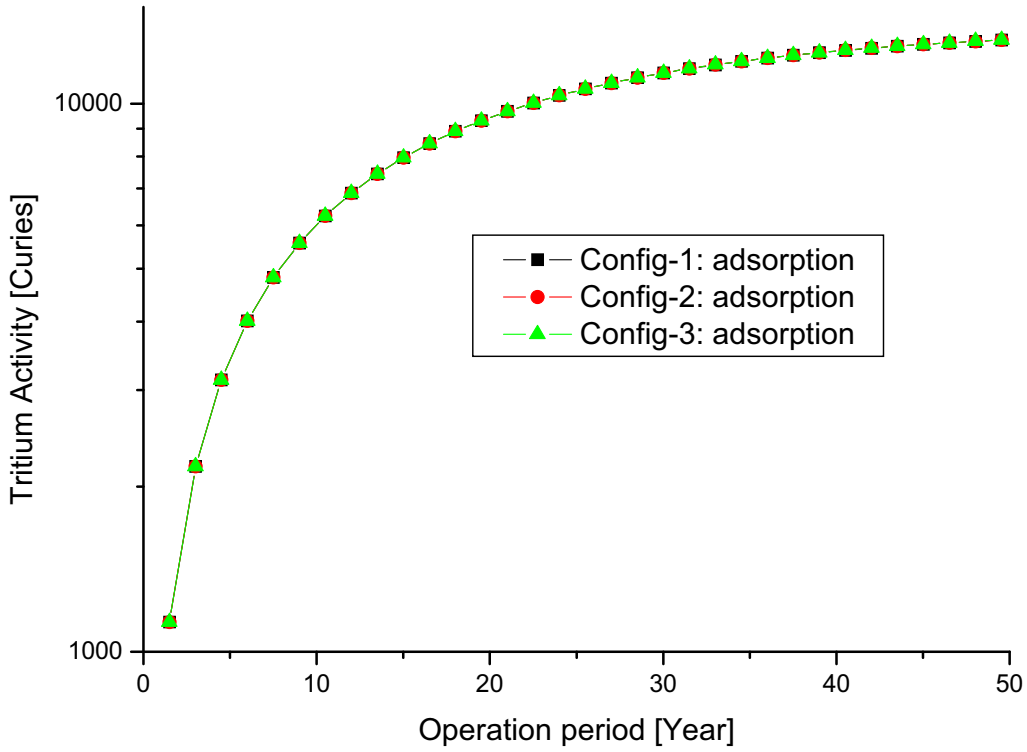

Figure 8-15. H-3 Inventories Sorbed on Core Graphite

The predicted inventories of tritium permeation through the heat exchangers for the three plant configurations are shown in Figure 8-16. The amount of permeation for was predicted to be the highest for Configuration 1 and the lowest for Configuration 3. The relative amounts of permeation were determined by the temperature distributions of the heat exchangers in the primary circuit.

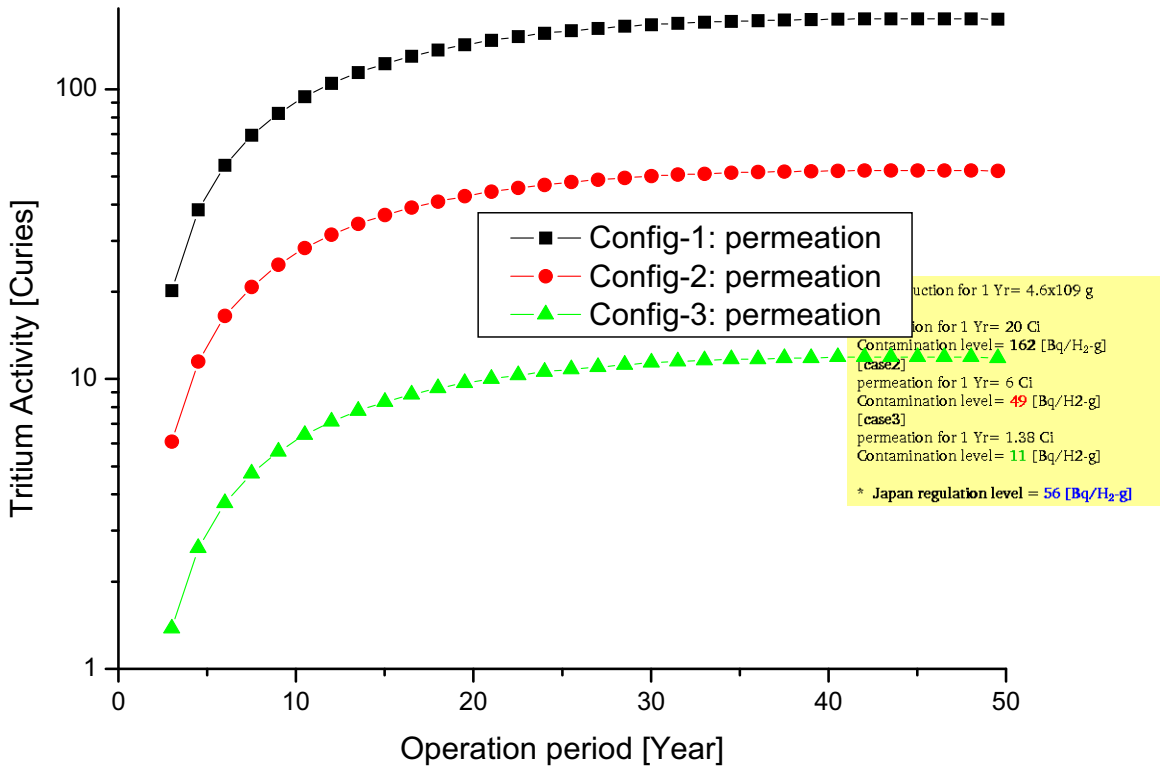

Figure 8-16. H-3 Inventories Permeating into Secondary Circuit

Based on the predicted amount of permeation shown in Figure 8-16, the level of the contamination for the hydrogen product was estimated. To make this estimation, it was necessary to determine the amount of annual hydrogen production. It was assumed that the annual H-2 production mass is 4.6×10^9 g/yr (approximately 10% of the hydrogen production rate in a 600 MW(t) commercial H2-MHR module). At the end of one year, the predicted contamination level of the produced hydrogen by tritium for the Configuration 1 was 162 Bq/H_2-g. The lowest contamination level was for Configuration 3 at 11 Bq/H_2-g. The intermediate contamination level for Configuration 2 was 49 Bq/H_2-g. The US drinking water standard (0.74 Bq/g) is exceeded by an order of magnitude for Configuration 2 and by two orders of magnitude for Configurations 2 and 3.

8.5.2 Sensitivity Study

A sensitivity study was performed to assist in the development of a strategy for reducing the amount of tritium permeation through the heat exchangers. Configuration 1 was chosen for this sensitivity calculation because it had the highest predicted H-3 permeation. Table 8-7 lists the

selected parameters and their base case values for these sensitivity studies. All of the parameters can be modified through the input except that the amount of graphite sorption and permeation needed to be changed by simple modifications to the TRITGO2 program.

Table 8-7. Sensitivity Calculation Matrix

Case	Sensitivity Parameters	Default Values
Case-1	Reduction of Li impurity (x1/10)	0.036 [ppm] (other region) 2.0 [ppm] (permanent reflector)
Case-2	Reduction of fuel release fraction (x1/10) : 3%	30%
Case-3	Reduction of B-10 release fraction (x1/10) : 0.1%	1% release
Case-4	Increase of B-10 release fraction (x10) : 10%	
Case-5	Increase of H-3 bound in a solid : 99.9%	99%
Case-6	Reduction of H-3 bound in a solid : 90%	
Case-7	Increase of Purification rate (x10): 2.36×10^{-4} (card 6)	2.36×10^{-5}
Case-8	Reduction of adsorption on graphite (x1/10)	
Case-9	Increase of adsorption on graphite (x10)	
Case-10	Reduction of permeation rate (x1/10)	
Case-11	Increase of permeation rate (x10)	
Case-12	Decrease circuit temperature (-100 C): (card 16)	
Case-13	Increase circuit temperature (+100 C): (card 16)	

The predicted tritium inventories in the primary He coolant for all of the sensitivity cases are shown in Figure 8-17. Reducing the core graphite sorptivity (Case 8), reducing the permeation rate (Case 10), and increasing the release fraction from the boron (Case 4) served to increase the predicted H-3 inventories in the primary He coolant; increasing the the release fraction from the boron (Case 4) had the largest effect. Increasing the purification rate (Case 7), increasing permeation rate (Case 11) and decreasing the release fraction from boron (Case 3) served to decrease the H-3 inventory in the primary He.

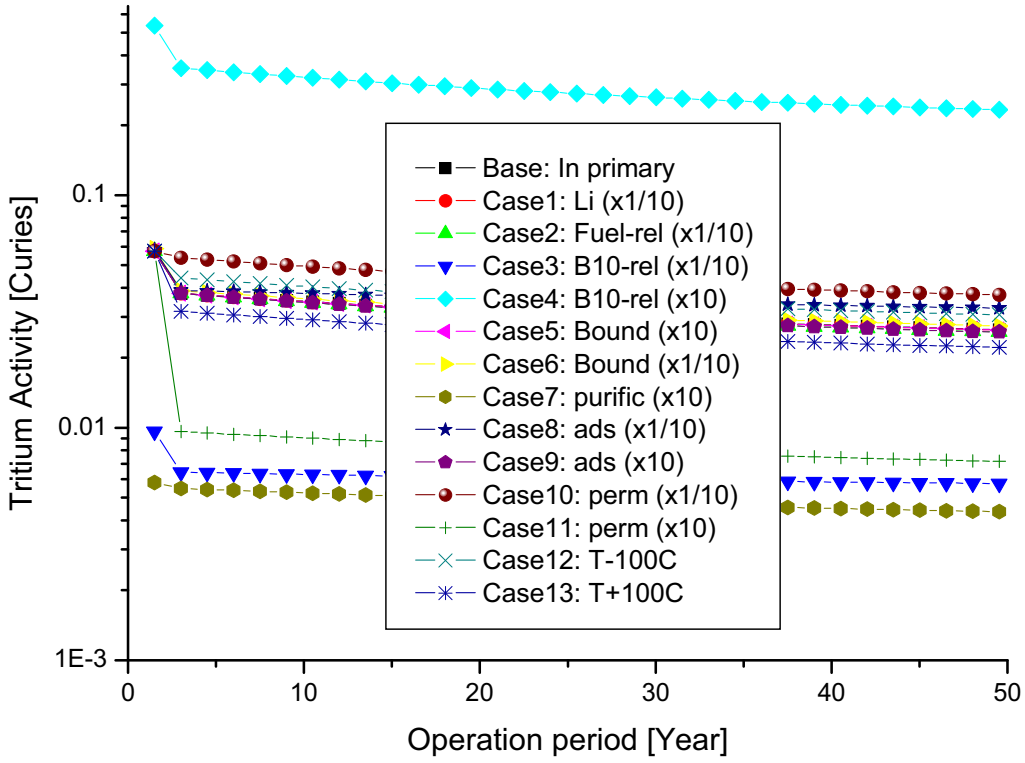

Figure 8-17. Sensitivity Study: H-3 Inventories in the Primary He Coolant

The predicted tritium inventories in the primary HPS for all of the sensitivity cases are shown in Figure 8-18. As expected, the trends are similar as for the primary He coolant inventories.

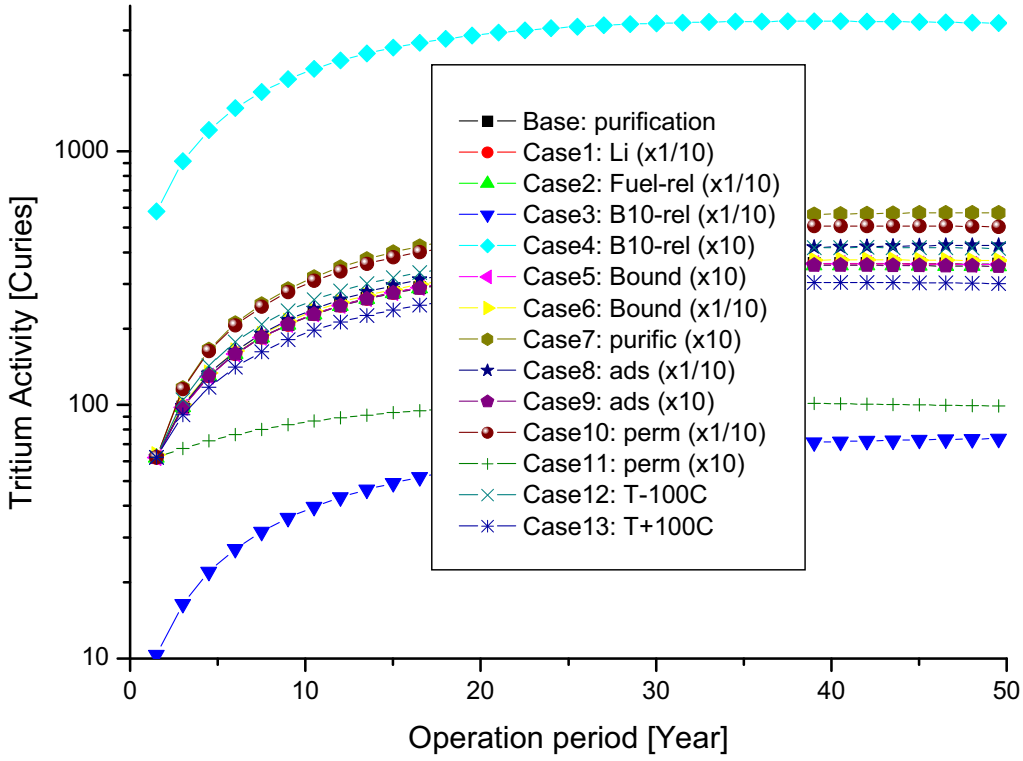

Figure 8-18. Sensitivity Study: H-3 Inventories in the Primary HPS

The predicted tritium inventories sorbed on the core graphite for all of the sensitivity cases are shown in Figure 8-19. Reducing the tritium release fraction from the fuel (Case 2) produced the greatest reduction because the amount of graphite sorption is proportional to the amount of tritium released into the coolant, and the fractional release from the fuel dominates the total amount of H-3 introduced into the He coolant. Beyond that, the total amount of H-3 sorbed on the graphite is predicted to be insensitive to the other variables, a surprising and non-intuitive result, especially for changes in the graphite sorptivity (Cases 8 and 9). In effect, with the Myers sorption isotherm as programmed in TRITGO, the core graphite is effectively an infinite sink for tritium at the predicted partial pressure of H-3 in the primary coolant. Even when the sorptivity is reduced by a factor of 10, the core graphite is still predicted to be an infinite sink.

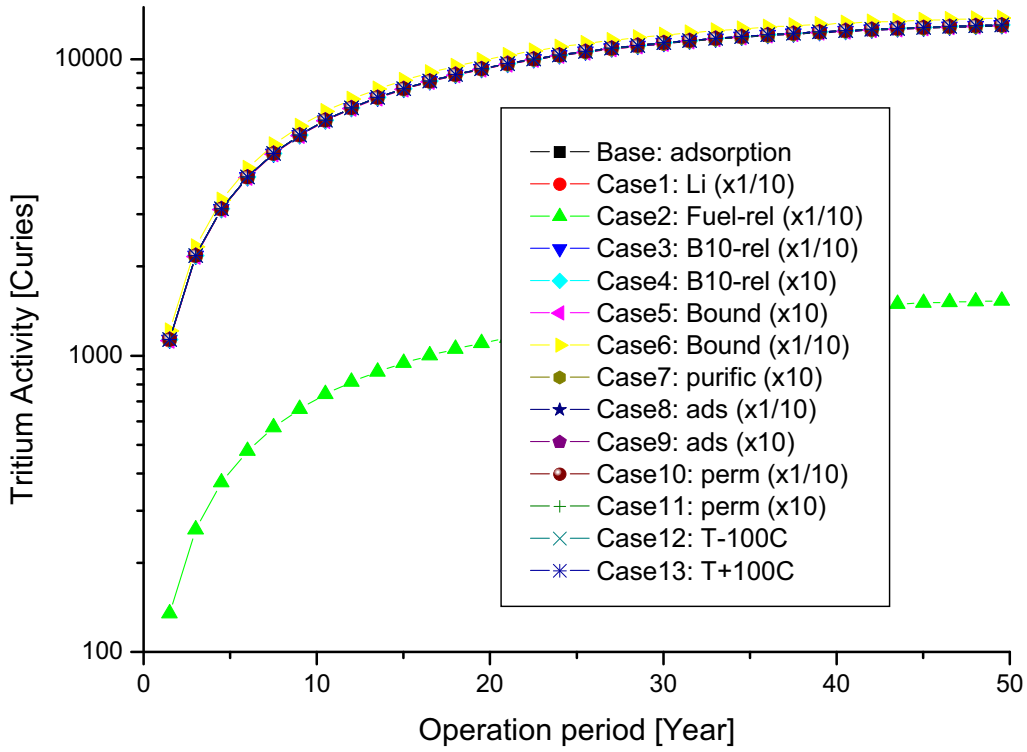

Figure 8-19. Sensitivity Study: H-3 Inventories Sorbed on Core Graphite

To investigate this behavior further, the graphite sorptivity was reduced by additional factors of 100, 1000, and 10,000. Reduction factors between 100 and 1000 were necessary before the amount of H-3 predicted to be sorbed on the graphite was significantly reduced, as indicated in Figure 8-20. This prediction should be viewed with a degree of skepticism. At this writing, the specialists at KAERI responsible for the TRITGO analysis are confident that the code is functioning properly within the considerable constrants of the program (see Section 11.1). This prediction dramatically illustrates the need for an improved graphite sorption isotherm and suggests that the way that the isotherm is used within TRITGO should be systematically investigated.

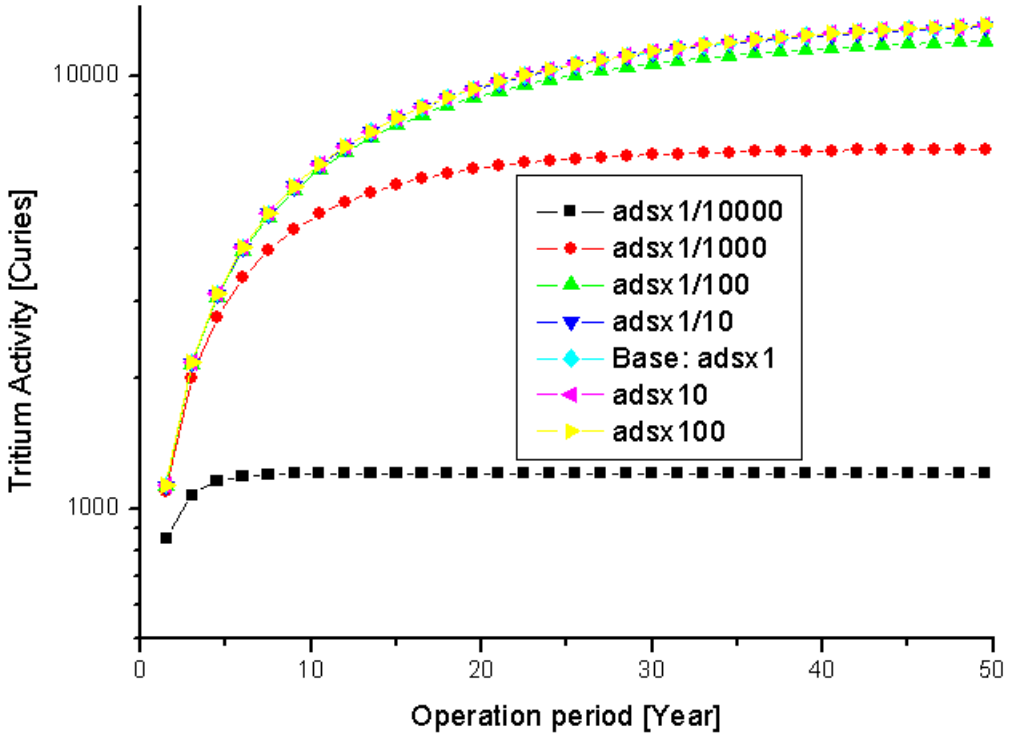

Figure 8-20. Effect of Large Reduction in Graphite Sorptivity

The predicted tritium inventories permeating the heat exchangers for all of the sensitivity cases are shown in Figure 8-21. From the figure, the predicted amount of H-3 permeation clustered in three groups. Increasing the permeability (Case 11) and increasing the fractional release from boron (Case 4) significantly increased the amount of H-3 permeation. Decreasing the permeability (Case 10), decreasing the fuel release fraction (Case 2) and decreasing the boron release (Case 3) reduced the amount of H-3 permeation. Once again, changes in the graphite sorptivity (Cases 8 and 9) had little effect on the predicted amount of H-3 permeation for the reasons discussed above; once again, this prediction should be viewed with a degree of skepticism. The remaining variables, including reducing the service temperatures in the primary circuit by 100 ^{o}C (Case 12), had only a small effect on the predicted amount of H-3 permeation.

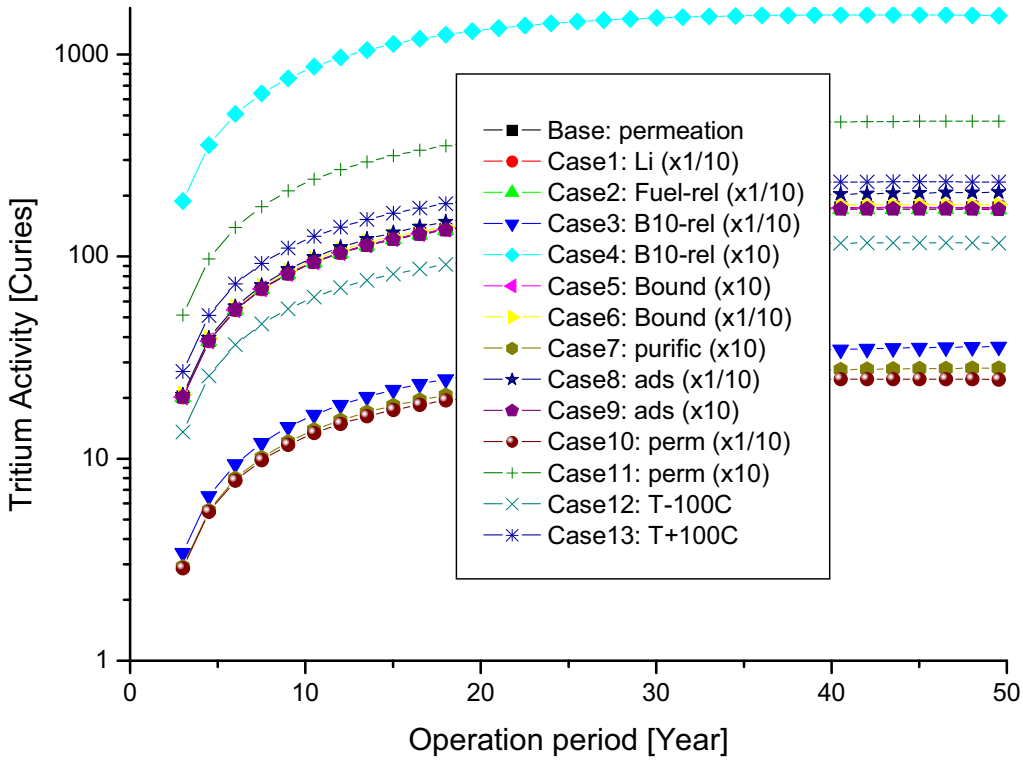

Figure 8-21. Sensitivity Study: H-3 Permeation Inventories

The results of this sensitivity study reinforce the urgent need for better material property data to describe tritium transport as defined in the transport H-3 DDNs (Section 10.2). It is particularly important to better characterize the tritium release from intact TRISO particles and from boron control materials and, in particular, to determine the H-3 sorptivities of irradiated core graphites.

8.6 Implications of FSV H-3 Surveillance Data

Tritium has been monitored in all operating HTGRs to characterize its transport behavior and to demonstrate compliance with regulatory requirements for occupational exposures and environmental discharges [e.g., Hanson 2006b]. As with the dust data (Section 6), the most prototypical H-3 data for a prismatic-core NGNP are expected to be those from the Japanese HTTR which has a prismatic core, an IHX, and has operated with reactor outlet temperatures of up to 950 °C. While it is known that H-3 transport has been investigated in HTTR, the results have not been published at this writing. The second most relevant H-3 surveillance data should be that from the Fort St. Vrain HTGR. These FSV H-3 data are reviewed in this subsection to

provide a basis for judging the reliability of the H-3 mass balance predictions for the NGNP presented above.

8.6.1 Observed H-3 Transport Behavior

As introduced in Section 6.3.2, the FSV HTGR was designed to produce 842 MW(t) and 330 MW(e) and had many design features common to prismatic-core MHRs (e.g., graphite moderator, helium coolant, and similar designs for fuel particles, fuel elements, and control rods) [e.g., Baxter 1994].

The H-3 concentrations in the FSV primary and secondary coolants and in the discharges from the plant were routinely monitored as part of the reactor surveillance program, and considerable data were generated during the plant's operating lifetime. However, the FSV surveillance measurements were not as extensive as those made for Peach Bottom or AVR. In particular, there were few measurements made of the H-3 concentrations in the FSV graphite core components which presumably contained significant H-3 inventories. Hence, the overall H-3 plant mass balance for FSV is not nearly as complete as those developed for Peach Bottom [Wichner 1979] and for AVR [Cordewiner 1979, Steinwarz 1981].

As part of FSV decommissioning, all of the core graphite was disposed of as Low Level Waste at the DOE Hanford Site without any reported complications [Fisher 1996]; more than 90% of the FSV graphite qualified as Class A waste (the lowest-level classification). There was an opportunity to conduct an EOL R&D program in conjunction with the plant decommissioning which could have included the determination of an overall H-3 balance for the plant, especially the H-3 inventories in the graphite components; unfortunately, no such R&D program was conducted.

8.6.1.1 H-3 Sources

The GA and Public Service Company (PSCo, the plant owner/operator) teams investigating H-3 behavior in FSV considered the standard H-3 sources: (1) ternary fission, (2) neutron activation of He-3 in the primary coolant and of Li-6 in the core graphitic materials, and (3) neutron capture in the B-10 in the control materials. No unusual sources of H-3 production were identified in FSV. PSCo estimated an annual H-3 production of ~4600 Ci at 100% power [Brey 1981] with 76% of the total from ternary fission and 17% from neutron activation of He-3 in the primary coolant. Tritium production from Li-6 activation was only 3% of the total because the Li content of the graphite components was generally below detection limits (and usually assumed to be 50 ppb for calculation purposes).

8.6.1.2 H-3 Transport

Without any direct confirmatory evidence, GA and PSCo investigators assumed that tritium was completely released from failed fuel particles and HM contamination in the fuel-compact matrix and completely retained by intact fuel particles. They further assumed that the H-3 produced by Li-6 activation in the core graphite and by B-10 capture reactions in the control materials was also essentially completely retained. Consequently, the dominant source of H-3 in the primary coolant was presumed activation of He-3. The primary justification for that conclusion was the steady-state H-3 concentration in the primary helium was much lower than would result a balance of H-3 production from He-3 activation and removal by action of the HPS.

The H-3 behavior in FSV was similar to that reported for Peach Bottom and AVR although the steady-state concentrations in the primary coolant were lower. As observed earlier, the core graphite was a major sink for tritium with an effective removal rate at least an order-of-magnitude greater than the HPS [Acharya 1983, Montgomery 1986]. However, as alluded to above, FSV operation was plagued with frequent water ingresses due to malfunctioning of the water bearings used in the main He circulators. As illustrated in Figure 8-11, whenever water was introduced into the primary circuit, the H-3 concentration in the primary coolant increased by an order-of-magnitude, indicating a rapid exchange between the H-3 sorbed on the graphite and the water in the primary He to produce HTO. As a result, most of the H-3 removed from the primary coolant was in the form of tritiated water trapped by the dryers in the HPS (in fact, the dryers were frequently saturated by excessive water which then froze out in the downstream liquid nitrogen-cooled charcoal beds that were intended primarily to remove noble gases).

The FSV data clearly indicate that sorption on the core graphite is the dominant sink for tritium in the primary coolant circuit and much more important than removal by the HPS or permeation. This observation is qualitatively consistent with the H-3 predictions for the NGNP. However, it is suspected that the Myers isotherm employed in TRITGO overpredicts the graphite sorptivity for reasons discussed. It is unfortunate that direct measurements of the H-3 contents of the FSV core components were evidently not made.

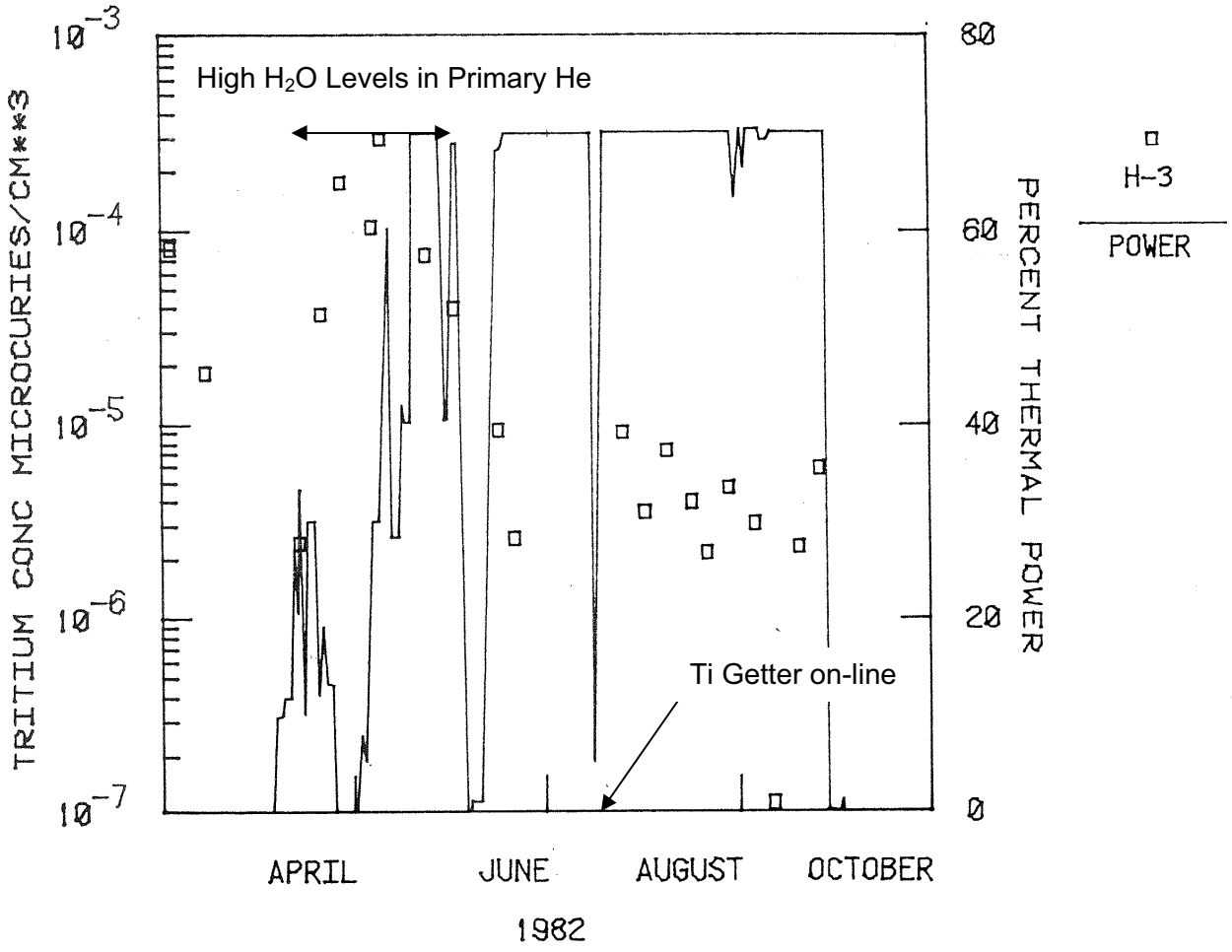

Figure 8-22. H-3 Concentration in Fort St. Vrain

Tritium also permeated through the steam generator tubes into the secondary coolant water. As shown in Figure 8-12 [Burnette 1984], the H-3 concentration in the secondary coolant water remained rather constant even though the H-3 concentration in the primary coolant varied considerably. At most, H-3 permeation through the SG tubes accounted for only a few percent of the total H-3 removal from the primary coolant.

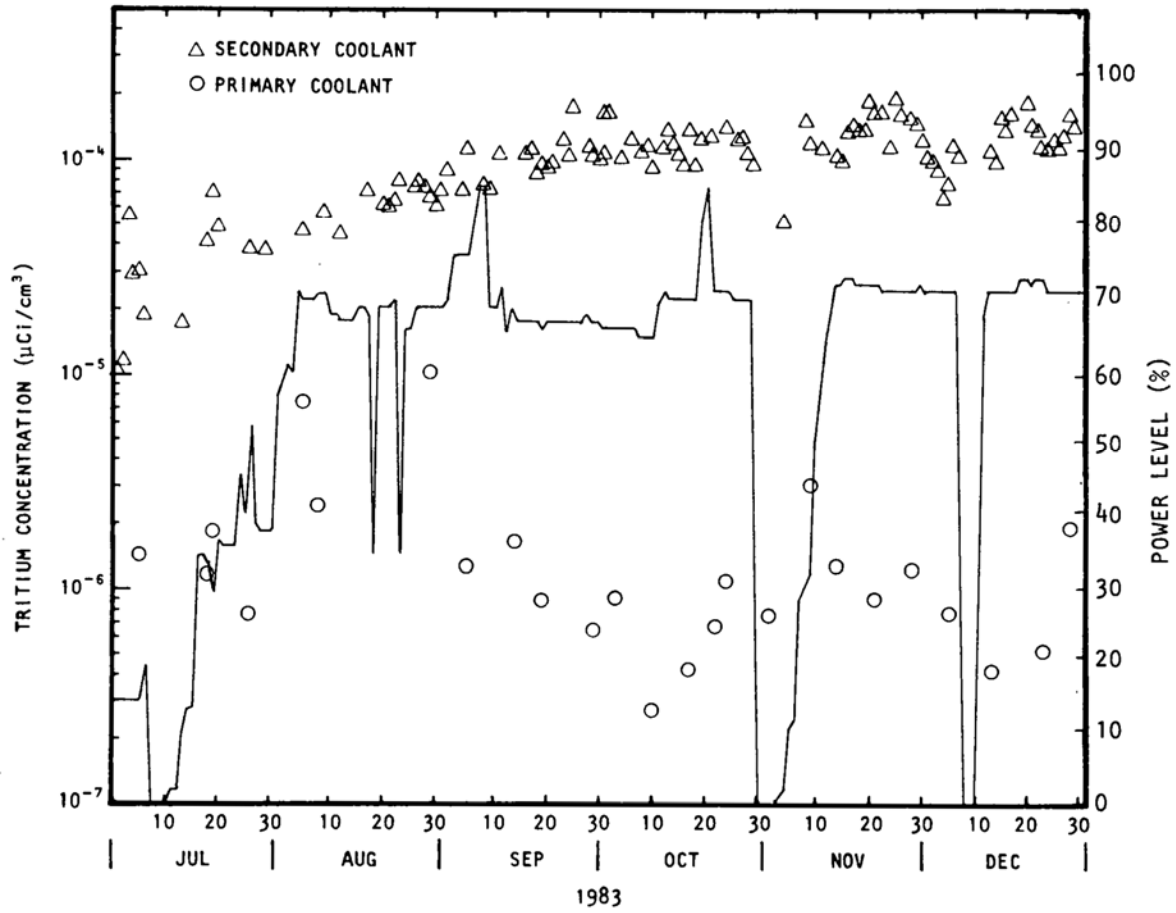

Figure 8-23. H-3 Concentration in FSV Primary and Secondary Coolants

Given all the uncertainties in the TRITGO predictions for the NGNP, it is perhaps somewhat surprising to note that the predicted H-3 concentrations in the primary He and in the secondary water for the steam generator loop in plant Configuration 3 are in excellent apparent agreement with the FSV surveillance data in Figure 8-22. The predicted H-3 concentration in the He coolant is 1.5×10^{-6} μCi/cm^3 (STP), and the predicted H-3 concentration in the secondary water is 1.1×10^{-4} μCi/cm^3. This apparent agreement could well be fortuitous and the result of compensating errors. In fact, the steam-generator metal temperatures in FSV were significantly lower than those assumed for the NGNP steam generator; consequently, the apparent agreement really implies an underprediction of the H-3 permeation rates in the NGNP. Nevertheless, the predictions for the NGNP for the steam generator loop in Configuration 3 appear to be in the right decade.

It would be instructive to benchmark TRITGO against the FSV H-3 surveillance data using actual FSV design parameters and service conditions. In fact, a TRITGO analysis of FSV was performed was performed previously [Acharya 1983]. However, that analysis was performed before the Myers sorption isotherm [Myers 1986] and the CEGA permeation correlation

[Czechowicz 1991] were derived so it is not particularly relevant to judging the current version of TRITGO. The main conclusion of the 1983 analysis was that the core graphite was evidently a much more important H-3 sink than the He purification system.

8.6.2 HPS Performance

Water ingress occurred frequently into FSV primary circuit as a result of malfunctioning of the bearing water supply system for He circulators; occasionally, the quantity of water ingresses into the primary circuit was significant (100s of gallons). Since there was no mechanism for removing water from the PCRV other than by the HPS, the quantity of water processed by the HPS far exceeded design expectations. As indicated above, the H-3 sorbed on the graphite exchanged with the ordinary hydrogen in the water producing HTO which was subsequently removed by the dryers in the HPS.

In addition, malfunctioning of the bearing water supply system introduced nitrogen into the primary circuit since high-pressure nitrogen was used to supply emergency water to circulator bearings when the main water supply malfunctioned. This ingressed nitrogen and the small quantities of carbon monoxide produced by reaction of the water with the core graphite served to deactivate the Ti getter beds so that they were ineffective for the removal of hydrogen and tritium [e.g., Copinger 2004]. Fortunately, the Ti getter beds proved unnecessary for plant operation because hydrogen and tritium were far more effectively removed by sorption on graphite than by the HPS. As indicated in Figure 8-11, bringing the TI getter beds back on-line after a long period of operation without them in service had no effect on the circulating H-3 concentration in the primary coolant.

Based upon the poor performance of these Ti getter beds in FSV, all subsequent GA HPS designs have utilized copper oxide oxidizer beds and molecular sieve dryers for the removal of hydrogen and tritium as H_2O and HTO, respectively.

8.6.3 Environmental H-3 Releases

Fort St. Vrain operation was characterized by extremely low occupational exposures, waste streams, and environmental releases compared to contemporary LWRs [Brey 1981]. For example, in 1978, the occupational exposure for FSV was 11.5 person-rem/GW(e)-yr compared to an average of 1000 person-rem/GW(e)-yr for US LWRs at the time. As shown in Table 8-7, the environmental radioactive discharges from FSV were also much less than the average US LWR with the exception of H-3 releases which were comparable to PWR releases on a Curie basis and actually higher on a Ci/GW(e)-yr basis. While the FSV H-3 releases to the environment were well below regulatory limits and presented no operational difficulties, tritium was nevertheless the dominant off-site dose contributor during plant operation.

Table 8-8. Comparison of FSV and US LWR Environmental Releases

Noble Gas Airborne Effluent Releases (Ci)	
FSV total, 1978	332
BWR average total per unit, 1977	120,000
PWR average total per unit, 1977	6600
Liquid Effluent Releases (Ci)	
(a) Mixed fission and activation products	
FSV total, 1978	0
BWR average total per unit, 1977	2.63
PWR average total per unit, 1977	4.43
(b) Tritium	
FSV total, 1978	223
BWR average total per unit, 1977	11
PWR average total per unit, 1977	554
Power Generated per Unit, MWH(t)	
FSV, 1978	2.0×10^6
BWR average, 1977	10.8×10^6
PWR average, 1977	13.4×10^6

8.7 Comparison with the Ohashi and Sherman Evaluation

In 2007, Ohashi (JAEA) and Sherman (INL) published the results of their extensive evaluation of H-3 transport in a notional NGNP with emphasis on H-3 transport in conceptual HTE and SI hydrogen production plants [Ohashi 2007]. The tritium generation and transport mechanisms in the NGNP were described, and basic mass balance equations were developed and then codified and analyzed using the JAEA tritium mass balance code THYTAN (Tritium and Hydrogen Transportation Analysis code). As a preliminary step, the THYTAN code was benchmarked against H-3 surveillance data available from the Peach Bottom HTGR. After benchmarking (perhaps better described as calibrating), various configurations of the NGNP employing an HTE hydrogen plant and an NGNP employing an SI hydrogen plant were analyzed, and the concentrations of tritium in the process and product streams were compared to current regulatory effluent limits in groundwater and in air.

An HTE hydrogen plant was extensively analyzed for tritium behavior. A reference case was constructed, and tritium concentrations in the primary, secondary, and tertiary coolants were

determined, as were the concentrations of tritium in HTE process chemicals and in the hydrogen and oxygen products. For the reference case, tritium in the hydrogen product was predicted to be 2.67 x 10^{-3} Bq/cm^3 [STP], which is below the NRC gaseous effluent limit of 3.7 x 10^{-3} Bq/cm^3 (STP). Tritium concentrations in process chemicals and in the primary, secondary, and tertiary coolants exceeded the NRC gaseous effluent limit, and, in the case of liquid-phase chemicals, exceeded the EPA drinking water effluent limit of 37 Bq/cm^3. The report concluded that the amount of tritium in the hydrogen product and process fluid streams could be lowered by reducing the heat exchanger material permeabilities, increasing the hydrogen purification system flow rates, and by injecting additional hydrogen into the primary, secondary, or tertiary helium loops to affect tritium permeation chemistry at the heat exchanger surfaces, and the degree of tritium reduction in each process stream is dependent upon the extent of the measures taken.

An SI hydrogen production process was also extensively analyzed for tritium. A reference case was again constructed, and tritium concentrations in the coolant loops and SI process chemicals were estimated. For the reference case, the tritium concentration in the hydrogen product was predicted to be 1.23 Bq/cm^3 (STP), which exceeds the NRC gaseous effluent limit by a factor of 305. Tritium in the liquid process chemicals also exceeded the liquid effluent limit by a large margin. The report concluded that the H-3 contamination levels in the SI could be reduced by reducing heat exchanger permeabilities, increasing the helium purification system flow rates, and injecting hydrogen into the primary, secondary, or tertiary helium coolants, but that more drastic measures would needed to achieve the desired effluent limits with the SI process than are required by an NGNP using an HTE hydrogen production process.

The report does a commendable job summarizing all of regulations that may constrain the amount of tritium contamination allowed in the product hydrogen. The report also identified a number of Design Data Needs (although that exact terminology was not used) relating to H-3 transport in the HTE and SI plants and confirmed the DDNs described herein regarding H-3 transport behavior in the primary coolant circuit (e.g., H-3 sorption on core graphites).

The subject evaluation would appear to invite a comparison with the NGNP tritium mass balance performed here with TRITGO. In fact, such a comparison is not particularly instructive. In principle, the THYTAN code models all of the H-3 transport phenomena that are modeled in TRITGO and more (e.g., H-3 transport in the hydrogen plants, etc.). THYTAN is a far more versatile code than TRITGO and evidently free of many its limitations (Section 10.1). However, THYTAN's capabilities to predict H-3 generation and transport in the primary coolant circuit were not exercised in this evaluation even though a considerable effort was made to calibrate those features with Peach Bottom H-3 surveillance data. Instead, "…for this study, the tritium release rate of NGNP is assumed to be the tritium birth rate for the Fort St. Vrain (i.e., 3.10 x 10^{11} Bq/y/MW$_t$) by conservatively neglecting tritium retained by the graphite core and the

TRISO coating system. The tritium release rate to the primary coolant in NGNP (600 MW_t) is given by 1.86×10^{14} Bq/y ($3.10 \times 10^{11} \times 600$)." [Ohashi 2007, page 51]. In fact, the FSV core graphite proved to be the dominant sink for H-3 in the primary circuit; only a few percent of the H-3 released into the He coolant permeated through the steam generators (Section 8.6). Assuming complete H-3 release from the TRISO fuel and zero retention by the core graphite is considered to be excessively conservative and precludes any meaningful comparison with the predictions made here.

The report concludes that "…drastic measures…" may be needed with SI process to meet regulatory limits for H-3 contamination in the product hydrogen and that tritium control challenge will be much greater with the SI process than with the HTE process. The primary basis for the latter assertion is that the required heat exchangers, the primary pathway for H-3 contamination of the product hydrogen, are significantly larger with the SI which is clearly correct; however, the assertion that drastic measures may be needed with SI process is at best premature. First, as already noted, the assumed H-3 source term in the primary coolant is grossly conservative. Secondly, as the report notes, "…in practice the PHX [process] heat transfer tube will be made of ceramics (e.g., SiC, Si_3N_4, others) due to the highly corrosive environment associated with the H_2SO_4 decomposer and perhaps the HI decomposition section. The tritium permeability of the material that will be applied to the PHX is not available. Therefore, the permeability of the superheater of the Peach Bottom HTGR, Incoloy 800, is also employed to that of PHX for the base case; this is the same as for the NGNP using the HTE process." [Ohashi 2007, page 107].

In fact, it is well established that the H-3 permeability of SiC is orders of magnitude lower than the H-3 permeability of Alloy 800 (e.g., see Figure 2-4). The availability of a ceramic heat exchanger with the current NGNP deployment schedule may be debated (Section 9.2), but the superiority of SiC as a H-3 permeation barrier compared to Alloy 800 is clear. The present report has repeatedly affirmed that tritium contamination of the hydrogen product in the NGNP will be a design issue that needs to be addressed and that design methods for predicting H-3 transport urgently need to be upgraded to support NGNP design and licensing. However, it is judged to be a manageable problem that is unlikely to require drastic measures to resolve.

8.8 Implications of the TRITGO Analysis for NGNP Design

While the uncertainties in the predictions presented herein are large and the limitations of the TRITGO code have been demonstrated to be substantial, the results do convincingly indicate that significant tritium permeation through the heat exchangers should be expected for all three configurations. This prediction that tritium contamination will be a design issue for the NGNP is supported by the observed tritium behavior in operating HTGRs. It is of particular interest to consider the implications of this prediction for judging the relative merits of locating a steam

generator in a primary- or secondary coolant loop (i.e., the relative merits of Configuration 2 versus Configuration 3).

Based upon the surveillance data from FSV and other steam-cycle HTGRs (Dragon, Peach Bottom, AVR and THTR) [e.g., Hanson 2006b], tritium will contaminate the process steam to some degree regardless of the location of the steam generator in the NGNP. However, it is noteworthy that for these earlier steam-cycle plants, all of which had their steam generators located in the primary circuit, tritium contamination control was not a significant operational or compliance issue.

Without engineered mitigating design features, the relative amount of tritium permeation through the heat exchangers of the NGNP will likely be higher than through the steam generators of previous operating HTGRs. First, more tritium will be released into the primary coolant of the NGNP because of the higher core temperatures in the NGNP compared to the earlier steam-cycle plants (the exception may be the AVR which operated with a core outlet temperature of 950 ^{o}C for a significant period of time). Secondly, the metal temperatures in the heat exchangers of the NGNP will be significantly higher than the metal temperatures in the steam generators of the previous steam-cycle plants (including AVR which had a co-current superheater), and the permeation rate is exponentially temperature dependent.

Once programmatic limits on the allowable tritium contamination levels in the product hydrogen are adopted and a comparison has been made with the expected H-3 contamination levels for a specific NGNP plant design, trade studies can be conducted to determine which design option for H-3 control, or combinations thereof, is optimal for that plant design. At this point, the addition of a large helium purification system to the secondary coolant loop for tritium removal appears to be essential for the hydrogen plant loop. Also, as indicated above, the allowable Li impurity in core graphite should be reduced to the extent practical, and the B_4C granules in the lumped burnable poison and in the control rods should be coated to improve tritium retention (and resistance to hydrolysis). These H-3 control options are discussed further in Section 10.

For the steam production circuit, tritium control will be manageable regardless of whether the steam generator is located within the primary- or secondary coolant circuit of the NGNP, but it will be relatively easier if the steam generator is located in the secondary circuit because that configuration allows for the inclusion of a second purification system in the secondary coolant circuit.

With the steam generator in the primary circuit, the size of the He purification system can be increased, but the dominant tritium sink in the primary circuit is expected to be the core graphite. Consequently, rather large increases in the He purification system would be required to significantly reduce the amount of permeation into the secondary steam.

While locating the steam generator in the secondary circuit would facilitate tritium control, the cost penalty for the inclusion of an extra loop with a large IHX and another large circulator is judged to be excessive. Consequently, it is expected that any steam generator will be located in the primary circuit of the NGNP and that tritium control will prove manageable for that configuration as it did for all previous operating steam-cycle HTGRs.

8.9 Effectiveness of Secondary He Purification System

It is apparent that a second helium purification system in the secondary coolant circuit will be necessary to help control the extent of H-3 contamination of the product hydrogen. In order to provide an estimate of the approximate size of such a secondary HPS, an EXCEL spread sheet was prepared that solves a simple, steady-state mass balance for the secondary loop: the H-3 permeation rate from primary circuit (the source) equals the sum of the removal rates by the secondary HPS and by permeation into the process heat exchangers (the two sinks). A number of assumptions had to be made since the design of the secondary coolant circuit is not complete. It was assumed that the circulating helium mass in the secondary circuit was the same as that for the primary circuit (10,000 lb). It was further assumed that the permeation rate constant for the process heat exchanger was the same as for the IHX (i.e., that at steady-state and in the absence of a secondary HPS, the permeation rate into and out of the secondary circuit were equal). The results are shown in Figure 8-23 for plant Configuration 1.

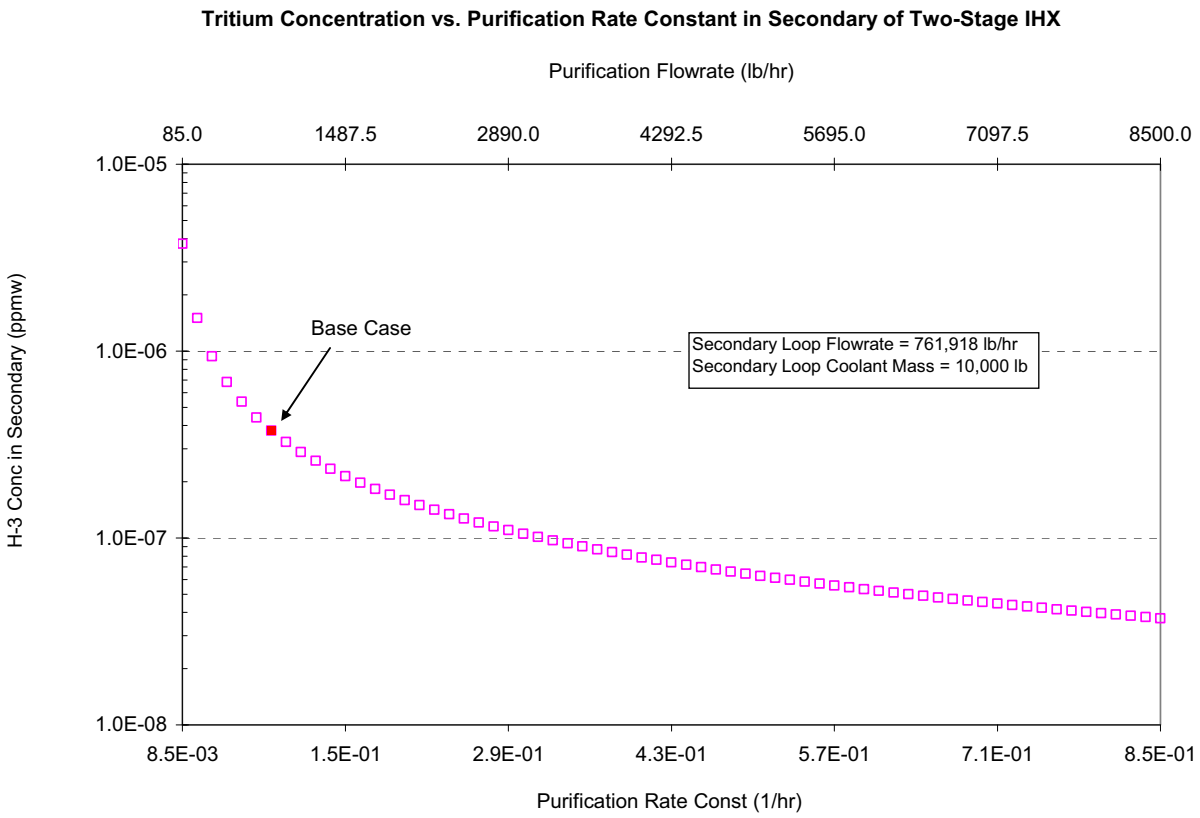

Figure 8-24. Effect of an HPS in the Secondary Coolant Circuit

For the assumptions made, a very large secondary HPS would be required to significantly reduce the H-3 concentration in the secondary coolant. For example, to reduce the H-3 concentration by 10x, would require a secondary HPS flow rate of 8500 lb/hr. For perspective, the design flow for primary HPS in the 350 MW(t) NP-MHTGR was 4000 lb/hr [Weaver 1990].

9. DESIGN OPTIONS FOR RADIONUCLIDE CONTROL IN HTGRS

The design options for controlling radionuclides in general and tritium in particular are summarized in the following subsections.

9.1 Radionuclide Controls in HTGRs

The NGNP and commercial H2-MHR plants will generate radioactive and chemical waste streams; this topic was addressed in some detail in a Phase 1 study on NGNP end products [Hanson 2007a]. Every effort should be made to minimize these waste streams; in general, the most effective means of controlling radioactive contamination is source reduction, especially during the plant design phase.

9.1.1 Source Reduction

Past operating experience with HTGRs and past design experience with advanced MHRs indicates radioactive waste streams can be reduced to well below current LWR practice. The key to minimizing radioactive waste is the use of high quality, high performance TRISO-coated fuel to retain the fission products in the core to the fullest extent practical during normal operation and postulated accidents. It is also important minimize the production of neutron activation products by limiting the use of high Co-content metals, including IN 617, to locations with negligible neutron flux and to control the primary coolant chemistry sufficiently to preclude the spallation of high Co-content metals.

9.1.2 Radioactive Waste Management

The NGNP and commercial H2-MHRs will generate certain waste streams. As with all nuclear power plants, the most significant waste stream will be the spent fuel from the nuclear heat source. The fuel burnup should be maximized to the fullest extent practical to minimize the amount of spent fuel per unit electrical production and unit mass of hydrogen. The spent fuel elements will be stored on site to cool for at least one year. Depending upon the availability of a federal repository, the NGNP spent fuel may be stored on-site for several decades. The spent fuel elements from commercial H2-MHRs will be stored on-site for up to 10 years. This study assumed that unprocessed spent fuel elements will ultimately be disposed of permanently in a federal geological repository (presumably at Yucca Mountain). Unprocessed, spent MHR fuel elements have been shown previously to be a nearly ideal waste form for geological disposal, far superior to zircaloy-clad LWR fuel bundles [Richards 1994, Richards 2002].

9.1.3 Decontamination and Decommissioning

The NGNP will be designed to have a 60-year lifetime (SRM, PLT 3.0.9), and a commercial H2-MHR is expected to have a comparable design lifetime [Richards 2006a and Richards 2006b]. At the end of its operational lifetime, the physical plant will represent the ultimate "by-product" of electricity and hydrogen production, and both the reactor plant and the hydrogen plant will have to decontaminated and decommissioned (SRM, PLT 3.1.11.14). The specific decontamination and decommissioning (D&D) requirements will be determined during the licensing process and by the prevailing regulatory climate at the plant end-of-life. Nevertheless, D&D requirements need to be considered during design, and D&D costs need to be included in the economic assessment of a commercial H2-MHR.

A comprehensive discussion of the D&D of the NGNP and future H2-MHR reactor plants is beyond the scope of the present study. Nevertheless, it is noteworthy that the D&D of future MHRs was addressed in some detail in 2005, and the results of that evaluation, including a cost estimate for the D&D of a GT-MHR, are summarized below [Hanson 2005].

The primary motivation for performing the subject evaluation was a 2003 NEA report on the decommissioning costs for various types of nuclear power reactors, based upon a survey of its member countries. The report (NEA 2003) concluded: "…decommissioning cost estimates reported remain below 500 USD/kW_e for nearly all water reactors but are significantly higher for gas-cooled reactors (around 2500 USD/kW_e)." The report raised concern that this conclusion might be taken to reflect negatively upon future development and deployment of advanced MHRs. In response, the past experience with D&D of gas-cooled reactor was reviewed, and the "lessons learned" to guide future MHR D&D, including projected costs, were determined.

Three types of gas-cooled, graphite-moderated nuclear reactors have been used for electrical power generation: CO_2-cooled MAGNOX reactors, CO_2-cooled AGRs, and He-cooled HTGRs (the latter category includes both prismatic core and pebble-bed core HTGRs). Reactors of each type are now in various stages of decontamination and decommissioning. Since these gas-cooled reactors share certain common features, notably graphite moderation, the D&D experience with each type is of some relevance to the eventual D&D of future MHRs.

While regulations and terminology differ somewhat internationally, there are three basic decommissioning options (along with combinations and variants thereof); using US terminology and criteria, they can be summarized as follows:

"DECON" (Decontamination): In DECON, all radioactive components and structures are decontaminated or dismantled, packaged and shipped to a low-level waste (LLW) disposal site

(they may be first stored temporarily on site). Once this task is completed and the NRC terminates the plant's license, that portion of the site can be reused for other purposes.

"SAFSTOR" (Safe Storage): In SAFSTOR, the nuclear plant is kept intact and placed in protective storage for up to 60 years. This method, which involves securing and safeguarding that part of the plant, which contains radioactive materials, allows time for radioactive decay to reduce the in-plant radiation fields and the inventories of radionuclides that must be transported and dispositioned off-site. Once the radionuclides have decayed to lower levels, the unit is dismantled similar to the DECON option.

"ENTOMB" (Entombment): This option involves encasing the radioactive structures, systems and components in a stabilizing medium, such as concrete, to provide shielding and isolation. The encased plant would be appropriately maintained, and surveillance would continue until the radioactivity decays to a level that permits termination of the plant's license.

The data in the NEA report provide little or no insight into the projected D&D costs for advanced HTGRs, including the GT-MHR, because no He-cooled reactor was included in their data base. In fact, data from the successful D&D of the Fort St. Vrain HTGR, which cost <$573/$kW_e$, suggest that the D&D costs for future MHRs should be comparable to that for water reactors. This extrapolation is supported by a 1993 Bechtel study, which estimated that the D&D costs for a four-module 600 MW_t GT-MHR at $243/$kW_e$ in 1992 dollars, which escalates to about $350/$kW_e$ in 2003 dollars. The cost data presented in the NEA report for MAGNOX reactor D&D are summarized in Table 9-1 along with the Bechtel cost estimates for future MHRs.

The D&D cost data presented in Table 9-1 need to be used with some caution. In particular, they are difficult to compare on a common basis because the work scopes can be quite different (e.g., some D&D cost estimates include the substantial cost of spent fuel storage and disposal, and other estimates do not). An important consideration is that for most of the gas-cooled reactors that have been decommissioned, or that are currently being decommissioned, the plant owners have chosen a variant of the SAFSTOR option; consequently, the final D&D of some of these units has been postponed by as long as ~135 years. In such cases, the ultimate total project costs are highly speculative. In this context, the completed D&D of the FSV HTGR - which led to a free release of the site and its subsequent reuse as a gas-fired power plant - is particularly significant and encouraging. A further complication is that permanent repositories for the final disposition of spent nuclear fuel (or reprocessed HLW) are not yet available in any industrialized country; obviously, projecting the eventual costs of spent fuel disposal under these circumstances is also speculative.

Given the complexity of a D&D project for a nuclear power plant, it should be anticipated that numerous licensing issues could arise for any such project. Many of these licensing issues will be largely specific to the particular project and to the particular site and country of residence. However, the potential licensing issues of interest in the present context are those that are more generic in nature and, hence, that might arise during the D&D of future MHRs. The following licensing issues related to D&D were judged to have the potential to negatively impact the prospects for the construction of a future commercial MHR (i.e., they are potential feasibility issues):

The assured availability of off-site, long-term interim storage facilities and/or a permanent repository for the spent fuel generated throughout the plant operating lifetime is essential for viability of any new nuclear power plant construction.

Unprocessed, coated-particle spent fuel – whether in the form of prismatic blocks or spherical fuel elements – must be determined to be an acceptable waste form for disposal in a permanent repository. In particular, the fuel-element graphite and fuel-compact matrix (or pebble matrix) must be classified as a “non-combustible” material [Hanson 2002a].

The core graphite – or at least the vast bulk of it – should qualify as low-level waste. The graphite components would likely have to be surveyed to determine their radionuclide inventories, and it is conceivable that the most contaminated components (e.g., the replaceable reflector blocks at the core exit of a prismatic MHR) might need to be partially decontaminated or classified as intermediate level waste. In fact, all of the FSV core graphite was disposed of as Class A LLW, the lowest classification [Fisher 1998].

The assured availability of future LLW repositories that will accept the full spectrum of wastes generated by the D&D of an MHR.

Table 9-1. Nuclear Power Plant D&D Experience

Reactor	Net Plant Efficiency (%)	Current D&D Status	Final D&D Option[24]	Average D&D Cost[25] ($/kWe)	Comments
NEA Survey					
PWRs	~32	Various	DECON	320	Range of 200 – 500 $/kW$_e$; "extreme" data sets excluded (e.g. a PWR @ 909 $/kW$_e$)
BWRs	~32	Various	DECON	420	Range of 300 – 550 $/kWe; "extreme" data sets excluded. (e.g. a BWR @ 2300 $/kW$_e$)
GCRs	~25[26]	Various	DECON	2500	MAGNOX data only (11 units); no data sets excluded ("insufficient" statistical basis)
HTGR D&D Data					
Dragon	N/A	SAFSTOR	?	?	No turbine-generator
Peach Bottom	35	SAFSTOR	DECON	?	Prototype; plant efficiency not optimized. DECON with Peach Bottom 2&3 in ~2030.
AVR	33	SAFSTOR	DECON	?	Prototype; plant efficiency not optimized
THTR	40	SAFSTOR	DECON	?	Demonstration plant
FSV	39	Complete	DECON	573	Demonstration plant
Bechtel 1992 D&D Cost Study[27]					
4 x 450 MW$_t$ MHTGR	38.5	Planned	DECON	456	Steam-cycle MHR
4 x 600 MW$_t$ GT-MHR	48	Planned	DECON	311	Direct-cycle MHR

[24] Other D&D options, particularly ENTOMB or ENTOMB in combination with partial DECON, could be considered if regulatory & political climates change.
[25] All costs in 2003 dollars (the escalation factor from 2003 to 2007 is 1.10)
[26] The plant efficiencies for MAGNOX reactors vary from 22% for the oldest units to 28% for the newest units.
[27] Bechtel cost estimate of July, 1993, escalated by 28% to September, 2003, dollars for consistency with the NEA cost data.

9.2 H-3 Control in HTGRs

While there are uncertainties in the H-3 production rates and distribution throughout an H2-MHR, especially with regard to the expected levels of H-3 contamination in the product hydrogen, there are a number of design options for H-3 control in HTGRs. Once limits on the allowable H-3 levels in the product hydrogen are established and a comparison with the expected H-3 contamination levels has been made, a study can be conducted to determine which design option for H-3 control, or combinations thereof, is optimal for the reference H2-MHR plant design. These design options are summarized below; they will be given further definition and quantified as the plant design evolves.

Realistic Limits on H-3 Contamination of Product Hydrogen. While perhaps more of a prerequisite than a design option, realistic limits on allowable H-3 contamination in the product hydrogen are nevertheless critically important. H-3 contamination limits proposed by the design organizations early in the design and licensing process may set precedents that could prove difficult to change in the future. Therefore, it is prudent to propose realistic limits initially and to demonstrate compliance with large safety margins to accommodate uncertainties in the predicted contamination levels rather than to adopt ultraconservative limits initially simply because they appear achievable based upon early scoping assessments.

As an example of an ultraconservative limit on H-3 contamination of nuclear-derived commercial products, the German PNP project in the early 1980s adopted a provisional limit of 10 pCi H-3/g of synthetic natural gas derived from coal gasification; this contamination level corresponds to a radiation dose of only 20 µrem/year to the critical population group [Steinwarz 1984]. Obviously, this radiation dose is of no consequence compared to natural background radiation which is about four orders-of-magnitude higher.

There are established H-3 contamination limits for both occupational and public exposures that have been set by national and international regulatory agencies, including the US NRC and the US EPA. They include allowable limits on H-3 concentrations in air (e.g., 100 pCi/l, NRC) and in drinking water (e.g., 20,000 pCi/l, EPA). The dose limits corresponding to these concentration limits should be carefully considered when proposing a H-3 contamination limit for nuclear-derived hydrogen. The allowable contamination limits, and the corresponding dose limits, for other radionuclides in commercial products and/or public use commodities may also provide guidance (e.g., the dose equivalent to allowable radon in natural gas or drinking water).

The allowable H-3 contamination limits may be dependent upon the assumed commercial scenario. For example, the limit derived upon assumption that nuclear-derived hydrogen will be become the dominant transportation fuel in the future may be more stringent than the limit derived upon assumption that nuclear hydrogen will used for manufacture of liquid-ammonia

fertilizer or to sweeten sour crude oil. Establishment of accepted H-3 contamination limits may well involve a protracted negotiation with regulatory authorities.

Stringent Limits on Li Impurities in Core Materials. The most fundamental way to control H-3 in HTGRs is to limit its production to the fullest extent practical. Obviously, it is impractical to reduce the production of H-3 by ternary fission or by neutron activation of He-3 in the primary helium coolant.[28] However, H-3 production from activation of Li impurities in core materials can be, and should be, controlled. Since Li is an effective neutron poison, stringent limits (e.g., <~50 ppb) are typically set for the allowable Li impurity levels in the components that constitute the active core, including the fuel-compact matrix and fuel-element graphite in a prismatic core. However, it is important to also limit the Li impurity levels in the permanent graphite structures in the reactor system. In the case of the German AVR, the "carbon brick" (Koehlestein) used for the permanent side reflector had an unusually high Li impurity level estimated to be ~4 ppm [Cordewiner 1979]; consequently, Li activation was the dominant source of H-3 production in that pebble-bed HTR.

Coated B_4C Granules in Control Materials. The B-10 used in HTGR cores as a neutron absorber is typically present as B_4C granules, which have been pressed into pellets with a carbonaceous binder. The production of H-3 in these control materials is typically predicted to be a minor contributor to the total H-3 production in the plant. Nevertheless, should release of H-3 from control materials become a significant contributor to the total H-3 present in the primary coolant, the B_4C granules can be encapsulated with dense pyrocarbon and/or SiC coatings that will dramatically decrease the H-3 release rates from them.

Increased He Purification Rate in Primary Loop. The typical He purification system design that utilizes oxidizer beds/dryers for control of H-3 and hydrogen efficiently removes H-3 from the processed primary coolant. Thus, the H-3 concentration in the primary coolant can, in principle, be reduced by increasing the mass flow rate through the HPS. However, as the mass flow rate is increased, the HPS becomes increasingly more expensive. In addition, based upon HTGR operating experience, the H-3 removal rate from the primary coolant by sorption on the core graphite is expected to be much larger than the removal rate by purification. Consequently, the mass flow rate through the HPS would have to be increased substantially before it would effect a dramatic reduction in the circulating H-3 level. Therefore, this option is probably less attractive than adding a purification system to the heat transport loop (see below).

---

[28] The concentration of He-3 in helium extracted from natural gas wells is generally much lower than the concentration of He-3 in atmospheric helium; however, gas wells are the commercial source of helium in any case so the point is moot.

The cost of a large primary circuit HPS can be mitigated by taking the design approach used for the NP-MHTGR [Weaver 1990]. Because of its tritium production mission, the predicted tritium release rates into primary He were quite significant; consequently, the NP-MHTGR had a large primary circuit HPS. However, only the front-end unit operations required for tritium (and hydrogen) removal, including copper-oxide oxidizer beds and molecular sieve driers, were scaled up compared to earlier commercial steam-cycle plant designs. After being processed through the front end of the HPS, half of the flow was returned to the primary circuit, and the remaining half was further processed through the LN_2-cooled charcoal beds for removal of the noble gases and residual chemical impurities.

Purification System for Secondary Loop. A simplified purification system can be added to the secondary loop (assuming that the secondary heat transport fluid is also helium rather than molten salt). The secondary-loop HPS might be dedicated to H-3 removal although some control of chemical impurities might be desirable as well. It is likely that the liquid nitrogen-cooled charcoal beds could be eliminated from the design. It is expected that adding a simplified HPS to the secondary loop would be much more cost effective than large increases in the primary loop purification rate.

Customized Coolant Chemistry in the Secondary Loop. It may well be possible to control the helium chemistry in the secondary loop such that coherent oxide films are produced on the heat exchanger surfaces in the IHX, thereby reducing the H-3 permeation rates through the walls separating the primary and secondary loops. The presence of coherent oxide films can reduce the H-3 permeation rates by several orders of magnitude. However, the in-reactor effectiveness is not well known. There is evidence that thermal cycling as a result of transient reactor operations (e.g., startup/shutdown, loading following, etc.) can cause cracking of oxide films resulting in increased H-3 permeation rates. Custom tailoring of the coolant chemistry to limit core corrosion in the British CO_2-cooled Advanced Gas Reactors (AGRs) has proven practical (e.g., Faircloth 1981), and, of course, it is extensively practiced in water-cooled reactors to control “crud” formation and to protect the fuel rod cladding. Buchkremer [1984] described how the coolant chemistry in an HTR could be adjusted to produce coherent oxide films on high-temperature alloys that would serve as tritium permeation barriers.

Permeation Resistant Coatings on Heat Exchanger Surfaces. The observation that coherent oxide layers on certain metals can reduce the hydrogen permeation rates by orders of magnitude has long suggested that other ceramic coatings might also reduce permeation rates by large factors and over broader ranges of coolant chemistries than those that produce stable oxide films. Consequently, candidate hydrogen permeation barriers have been under

investigation internationally for decades, especially within the fusion community which must address containment of large quantities of tritium generated in breeding blankets.[29] An example of this fusion community work is described below.

Konys [2005] recently gave a status report on the development of tritium permeation barrier coatings within the European fusion community. The goal of the work funded by the European Commission (EC) during the last 10 years was to develop a coating that would produce a permeation reduction factor (PRF) of >1000. The coating would be used on the structural components of a lithium-lead cooled blanket and would have to be effective for tritium-hydrogen gaseous environments as well as for tritium in association with a Pb-17Li melt.
Early screening studies led the EC R&D programs to focus on alumina, which is known to be an effective hydrogen permeation barrier. Alumina coatings were deposited on ferritic martensitic steels by different techniques like hot-dip aluminizing (HDA) by Forschungszentrum Karlsruhe, Germany and chemical vapor deposition (CVD) by Commissariat a l'Energie Atomique, France. The results for CVD and HDA coatings showed that PRFs of >1000 were exceeded in H2 gas, but that much lower values were obtained with the Pb-17Li melt. The post-test analysis revealed that surface imperfections and spallation of parts of the coatings were responsible for the low PRFs for the melt.

Hydrogen permeation barrier coatings are being investigated for other applications as well. The relevant question here is whether such coatings might have practical application for reducing product contamination in an H2-MHR. The immediate answer appears to be a qualified “maybe” pending further evaluation. Any such coating would probably best be applied on the heat exchanger surfaces exposed to the secondary coolant (assumed here to be helium). Applying such coatings on surfaces exposed to primary coolant could lead to the possibility of coating spallation and circulation of spalled material in the primary helium; depending upon the composition of spalled material, it could be activated when passing through the core and pose an additional radiation hazard. Applying such coatings on surfaces exposed to the SI process streams would raise an issue of coating longevity because certain of the process chemicals (e.g., high-temperature sulfuric acid) are highly corrosive. Perhaps, an even more fundamental question is whether or not it would be technically feasible to apply such coatings with a printed-circuit type (Heatrix) IHX which is the leading candidate design [Richards 2006a].

In addition, the long-term, in-reactor effectiveness of such coatings would have to be assessed, including the effects of thermal cycling, etc. It is well established that the effectiveness of

[29] For example, a Google search in April, 2006, for “hydrogen permeation barrier coatings metals” resulted in ~68,000 hits, and a search for “tritium permeation barrier coatings metals” resulted in ~10,000 hits.

intrinsic oxide films as tritium barriers in operating reactors is compromised by thermal cycling, startup/shutdown, etc. In the other hand, anti-corrosion coatings on the blades of combustion turbines perform well under severe thermal cycling.

Ceramic Process Heat Exchangers. Ceramic heat exchangers, especially those fabricated of silicon carbide, should have far lower tritium permeabilities than metallic heat exchangers (e.g., see Figure 2-4). The programmatic issue has been whether or not industrial-scale ceramic heat exchangers could reasonably be expected to be available in the 2018 to 2021 timeframe required for the NGNP.

The conventional wisdom has been that such ceramic heat exchangers will not be available until well beyond the NGNP need date. However, certain materials specialists, principally at Sandia National Laboratories, have argued that bayonet-type heat exchangers constructed of SiC are currently available in industrial-scale sizes [e.g., Pickard 2006]. As evidence, they cite the Hexoloy© SiC tubes available from Saint-Gobain Ceramics that are used in shell-and-tube heat exchangers in the chemical process industry. Hexoloy© tubes are available in a variety of diameters and in lengths of up to 14 feet according to the company's website.[30] Sandia estimates that a 100 MW sulfuric acid decomposer could be constructed of 3300 Hexoloy© SiC tubes with an overall tube bundle diameter of ~5.5 m. The extent to which such a conceptual SiC heat exchanger has been evaluated (e.g., structural performance, corrosion resistance, etc.) has not been reported. It is perhaps noteworthy that the Saint-Gobain Ceramics website reports a corrosion rate for their Hexoloy© SiC tubes of 1.8 mg/cm^2-yr in 98% sulfuric acid at 100 ^{o}C (normal boiling point = ~340 ^{o}C). It is not known at this writing whether the corrosion rates of this material in decomposing sulfuric acid at temperatures >850 ^{o}C and elevated pressures have been determined.

[30] http://www.hexoloy.com/product-applications/heat-exchanger-tubing

10. ADEQUACY OF CURRENT NGNP TECHNOLOGY PROGRAMS

The adequacy of the current NGNP technology programs to support the preconceptual design recommended by the GA NGNP team which included a direct-cycle, gas-turbine, power conversion system [GA PCDSR 2007] was assessed in [NGNP TDP 2007], including those aspects of contamination control in a VHTR where the current technology was judged to be inadequate to support NGNP design and licensing. As described previously, the NGNP Project rejected the inclusion of a direct-cycle PCS in the NGNP conceptual design and mandated the inclusion of a steam generator in either the primary- or secondary heat transport system [NGNP PCD 2007].

Now that the current contamination control study has been completed for the plant configurations described in Section 8, the NGNP DDNs have been reassessed. The DDNs will need to be revisited again when the NGNP conceptual design is completed and likely again at the end of the Preliminary design phase. At this writing, the DDNs related to fuel performance and radionuclide transport, including tritium transport, are judged to be largely unaffected since they are mostly generic.

10.1 Radionuclide Control

The following assessment of the current NGNP technology programs related to fuel performance and radionuclide control is largely unchanged from the assessment in [NGNP TDP 2007] because the radionuclide control requirements are largely unchanged as are the anticipated fuel service conditions assuming that the plant will operated for long periods of time with a core outlet temperature of ~900 ^{o}C.

The DOE AGR Fuel Development and Qualification Program (AGR Plan/1) has the mission to develop and qualify fuel for the NGNP. The AGR fuel program is developing and qualifying conventional, SiC-based TRISO fuel particles with the assumption that conventional TRISO particles will be adequate for use in the initial core of the NGNP. However, there was no NGNP reference design when the AGR Fuel Program was first planned in 2003. Consequently, the program initially selected the GT-MHR fissile particle as the reference particle design for fuel fabrication process development and irradiation testing. Validation of radionuclide source terms is also within the scope of the AGR Fuel Program.

The AGR program plan is a comprehensive plan which the GA team continues to endorse with the caveats summarized below (GA was a member of the team who prepared the AGR plan and continues to participate in the program). The NGNP Preliminary Project Management Plan (PPMP) and the Independent Technology Review Group (ITRG) identified a number of risks associated with the overall NGNP fuel qualification effort. The GA team agrees with these concerns and has identified additional deficiencies. The scope of the AGR program is largely

responsive to the NGNP DDNs; the fundamental problem is that the AGR program schedule does not support the NGNP design and licensing schedule. Moreover, given the limited existing test facilities in the USA, it would be difficult to significantly accelerate the AGR program even with unconstrained funding.

10.1.1 Fuel Process Development

The AGR fuel development schedule does not support a 2018 startup of the NGNP. As an expedient, GA proposes the use of 10%-enriched UO_2 TRISO fuel fabricated by Nuclear Fuel Industries (NFI) in Japan for the NGNP first core fuel load (and possibly for one or more reload segments). However, GA views this as a necessity only to allow the 2018 startup because the NGNP Project must develop a domestic supply of UCO TRISO fuel (assuming that the NGNP is a prismatic block MHR) in order to meet the NGNP project objectives as identified in the NGNP PPMP. Consequently, GA believes that it is essential that the NGNP Project build, license, and operate a fuel manufacturing pilot plant for the NGNP to demonstrate the viability of economical mass production of UCO TRISO fuel, thereby satisfying the fuel fabrication process DDNs

The 510 fuel element/year process line that would be built and demonstrated in the NGNP Fuel Fabrication Facility (FFF) during production of the second NGNP core would be the basic production module that would be replicated in a commercial fuel fabrication facility (comparable to the Initial Modular Fuel Process Line planned for the NP-MHTGR project). Thus, the NGNP FFF would demonstrate the fuel fabrication technology needed for a commercial fuel supply business, thereby greatly reducing the costs and risk that would be associated with a first-of-a-kind fuel manufacturing facility. This conclusion is, of course, based on the premise that the US government would make the NGNP pilot line technology available to any US company that wishes to replicate the technology to develop a commercial MHR fuel manufacturing business.

Another issue with respect to fuel process development is coater scale-up. The fuel currently being irradiated in AGR-1 was made in a laboratory scale coater at ORNL. Coating process development is currently proceeding at BWXT to scale up the coating process to a 15-cm diameter coater. Commercial scale coaters operated at GA and at HOBEG GmbH in Germany had a diameter of 24 cm. The AGR program recognizes the need to scale up the coating process to commercial coater, but the second scale-up step is not currently in the AGR program plan.

10.1.2 Fuel Materials Qualification

Both the ITRG and the PPMP have recognized the risks associated with the AGR Fuel Program's single-path approach to fuel qualification. Indeed, the PPMP calls for expansion of the program to include a dual path involving irradiation testing of UCO fuel fabricated in the USA by BWXT and UO_2 fuel fabricated by NFI. The UCO fuel would be irradiated in test AGR-2 as

originally planned, and a new irradiation test ("AGR-2a") would be added to the program for irradiation testing of UO_2 fuel fabricated by NFI. Irradiated fuel from both irradiation tests would be subjected to heating tests to simulate accident conditions (i.e., "safety tests"). The irradiation and safety testing of NFI UO_2 fuel is not currently included in the AGR Plan.

GA endorses the approach described in the PPMP to irradiate both UCO fuel and NFI UO_2 fuel. However, consistent with GA's view that demonstration of UCO fuel in the NGNP is essential for deployment of commercial MHRs in the USA, GA does not agree that a down selection for qualification testing should be made between UCO fuel and NFI UO_2 fuel. Rather, UCO fuel should be qualified as rapidly as possible, and NFI UO_2 fuel should be qualified for use in the initial core and early reload(s), based on Japanese and confirmatory US irradiation and safety test data. It is also assumed that a fuel performance monitoring program in the NGNP would be necessary to supplement the irradiation and safety testing data for NFI UO_2 fuel.

10.1.3 Radionuclide Transport

As indicated in the PPMP, there is a substantial risk that the RN transport workscope included in the AGR Plan will be inadequate to support NGNP design and licensing. This problem has been exacerbated by chronic funding shortfalls for the AGR program; consequently, no experimental work in the RN transport area has been initiated to date with the exception that the driver fuel has been fabricated for irradiation tests AGR-3 and AGR-4. In fact, no experimental work on RN transport outside of the core is planned until FY12. The significant RN transport issues identified with the AGR Plan are summarized below.

A series of fission product transport tests in an in-pile loop are needed in order to generate the integral test data necessary to validate the predicted source terms for the NGNP. The AGR Plan contains tasks to construct an in-pile loop and to perform an in-pile test program. However, the design and construction of the loop are not initiated until FY13. The technical feasibility of constructing such a facility (presumably in the ATR at INL) and the attendant costs and schedule must be established far earlier if the design methods for predicting RN transport in the primary circuit are to be validated before the end of Final Design. In addition, the cost and schedule estimates for loop design and construction appear to be extremely optimistic.

The AGR Plan does not address RN transport in the vented low-pressure containment (VLPC). It only includes an evaluation of the extent to which the experimental water-reactor database for RN transport in high-pressure containment buildings might be applicable to the VLPC. A recent evaluation concluded that these data are of limited value for refining and independently validating the design methods used to predict RN transport in VLPCs because the radionuclide concentrations and the physical and chemical forms in the two systems are too different. As a result, new DDNs have been identified that the AGR program needs to address.

10.2 Tritium Control

The current AGR Plan does not address tritium transport (perhaps, in part, because it is a generic development plan which does not focus on a specific reactor design). However, a test plan to characterize tritium transport behavior in VHTRs was recently prepared [Hanson 2007b]. It is anticipated that this tritium characterization plan will be incorporated into the on-going, AGR program.

The tritium transport issues addressed in this test plan are generic to all HTGRs, but the test program priorities and test articles are design specific. The NGNP is still in the preconceptual design phase at this writing; consequently, this test plan will need to be reviewed and revised as appropriate when the conceptual design of the NGNP is finalized. In particular, the inclusion of a steam generator in the primary coolant circuit of the NGNP would increase the priority of the tests to determine the effects of water on tritium transport behavior,

The design methods that available to estimate H-3 production, distribution, and release, are rather rudimentary and characterized by large uncertainties (see Section 8). They will need to be upgraded for preliminary design and independently validated prior to completion of final design. Some technology development will be necessary to provide the bases for these design methods improvements and validation. Four Design Data Needs (DDNs) related to tritium behavior have been identified at this writing (more may be identified as the NGNP design matures): (1) measurement of H-3 release from irradiated, failed and intact TRISO particles, (2) measurement of the H-3 sorptivities of irradiated core graphites, (3) measurement of H-3 release from irradiated, bare and coated B_4C granules, and (4) measurement of H-3 permeation rates through candidate IHX and steam generator metals.

The workscopes for the resulting H-3 transport DDNs are summarized in Table 10-1 [Hanson 2007b]. These DDNs apply to both prismatic- and pebble bed core designs although some of the test articles would be core design specific (e.g., different core graphites are used in prismatic and pebble-bed cores). Of these DDNs, H-3 metal permeabilities and H-3 release from TRISO particles are the highest priorities, and H-3 release from B_4C is the lowest. The priority of the latter DDN would increase if the plant design includes a steam generator in the primary circuit because water ingress can lead to hydrolysis and subsequent boron migration as well as to enhanced H-3 release.

Table 10-1. Workscope for Tritium Transport DDNs

DDN No.	DDN Title	Workscope	Priority
C.07.03.05	Tritium Permeation in Heat Exchanger Tubes	Data are needed describing the permeation of tritium through heat exchanger material(s) used the intermediate heat exchanger and steam generator as function of temperature, H-3 partial pressure, system pressure, coolant impurity concentrations and tube surface oxidation state. The effects of thermal cycling, which would occur as a result of reactor startup, shutdown, and load changes, needs to be determined. Sufficient data are needed to develop and refine H-3 permeation models with uncertainties [<10x][31] at 95% confidence.	High
C.07.03.06	Tritium Transport in Core Materials	Data are needed to determine sorptivities of tritium on core structural graphites as a function of temperature, tritium partial pressure, fluence, and coolant impurity concentrations, especially H_2O and H_2, during normal and accident conditions. Sufficient data are needed to develop and refine H-3 transport models with uncertainties [<10x] at 95% confidence.	High/Medium[32]
N.07.03.23	Tritium Release from TRISO Particles	Data are needed to determine H-3 release rates from failed and intact, reference TRISO particles as a function of temperature and burnup (H-3 release from intact particles is more important since the H-3 fractional release from failed particles is expected to approach 100%). Sufficient data are needed to develop and refine H-3 release models with uncertainties [<10x] at 95% confidence.	High
N.07.03.24	Tritium Release from Control Materials	Data are needed to determine H-3 retention by boron-based control materials. H-3 release rates need to be measured as a function of temperature, fast fluence, and water partial pressure. The need for applying pyrocarbon and/or SiC coatings to the B_4C granules (expected to be used in the control materials) should be determined. Sufficient data are needed to develop and refine H-3 transport models with uncertainties [<10x] at 95% confidence.	Medium/Low[8]

[31] Numerical values given in [square brackets] are tentative values subject to change when test specifications are written.
[32] Priority increases if a steam generator is included in the primary coolant circuit.

To satisfy these tritium DDNs, a series of single-effects tests to provide the experimental bases for deriving improved component models and material property correlations are proposed. The experimental techniques are reasonably well established based upon previous work performed to characterize tritium behavior in steam-cycle HTGRs and in fusion systems, especially in lithium blankets designed to breed tritium. The greatest experimental challenge will be to obtain on a timely basis the required irradiated test articles: TRISO particles, core graphite specimens, and bare and coated B_4C. In contrast, metal specimens for permeation testing are readily available, and these tests could begin as soon as funds are available. Measuring the tritium permeability of IN 617, the leading candidate IHX material, is judged the highest priority task. These measurements could be performed in the tritium laboratory at the Idaho National Laboratory where the tritium permeabilities of other metals have been measured.

10.3 Dust Production and Effects

The only Design Data Need identified to date related to the effects of dust in the primary circuit is GT-MHR DDN C.07.03.11, “Characterization of the Effects of Dust on Radionuclide Transport” [GT-MHR DDNs 1996]. This DDN calls for measurements under representative GT-MHR conditions which elucidate the effects of particulate matter ("dust") on the transport of condensable radionuclides in the PCU during normal operation and during transients, especially the effects upon the reentrainment/redeposition characteristics during dry and wet depressurization transients. A prerequisite to these measurements is the determination of the representative dust (chemical composition, concentration, particle size distribution) in an HTGR with a prismatic core. As discussed in Section 6, it is anticipated that the HTTR dust data provide the best indication of the nature and consequences of the dust to be expected in a prismatic-core NGNP.

The conclusion presented in Section 6 was that the dust concentrations in the circulating He coolant and deposited on primary circuit surfaces of a prismatic-core MHR should be sufficiently low to not cause any deleterious effects, such as heat exchanger fouling. Consequently, no new DDNs related to dust effects beyond its potential impact on plateout and liftoff have been identified at this writing. It is expected that dust effects would become a greater concern if the NGNP should select a pebble-bed core.

11. Adequacy of Current Design Methods

Both the TRITGO and RADC codes used in this study are GA legacy codes that need to be upgraded for conceptual design and replaced by modern codes for preliminary and final design.

11.1 TRITGO, Plant Tritium Mass Balance Code

The current limitations with TRITGO [Hanson 2006a] have proven to be particularly problematic in the current analysis. As indicated above, TRITGO was written at ORNL in the mid-1970s for predicting the tritium mass balance in a steam-cycle HTGR which is represented by a collection of coupled compartments (e.g., active core, primary He coolant, He purification system, secondary water coolant, etc.). A differential mass balance is formulated for each compartment including the various H-3 sources and sinks described in Section 5 are modeled in each compartment as appropriate. The H-3 concentration in each compartment is determined by solving analytically a coupled set of linear first-order differential equations. The fundamental limitation with TRITGO is this analytical solution technique which necessitates that the H-3 concentrations be linear functions of the various material properties, such as the H-3 permeability of metals, and independent of time. Beyond this fundamental limitation, there are additional major limitations with the current version of TRITGO:

1. Only a plant configuration with a single primary and second coolant circuit (steam cycle) can be rigorously modeled. The code cannot simultaneously analyze a plant configuration that contains dissimilar parallel loops (e.g., an IHX in one primary loop and a steam generator in a second primary loop) or a plant configuration with tertiary serial loops (i.e., the hydrogen plant).

2. The secondary heat transport fluid is assumed to be water. For a gas-to-gas IHX, the mass concentrations calculated for the secondary loop are non-physical.

3. The code cannot model a second helium purification system in the secondary loop.

4. Only a very coarse core model can be accommodated wherein each core region has constant average properties (e.g., a constant average temperature).

5. The code requires a constant, core-average release fraction of tritium from the fuel.

6. The fractional releases of H-3 produced by Li activation and by B capture reactions are constant for each core region.

7. The code does not calculate fast fluence in the various core material regions as a function of space and time. This limitation is problematic when certain material properties are functions of fast fluence. For example, with the Myers isotherm the H-3 sorptivity of graphite is

assumed to increase as a linear function of the fast fluence. As currently programmed, a constant fast fluence must be assumed.

8. The code cannot accommodate different functional forms for permeation correlations. The permeation rate must be a linear function of tritium concentration in the primary coolant.

9. The code cannot model H-3 transport in the hydrogen production plants.

The above are structural limitations of the TRITGO code which are largely acknowledged in the TRITGO manual [Hanson 2006a] and which have been encountered during previous applications of the code [e.g., Gillespie 1993]. However, the sensitivity study (Section 8.5.2) performed as part of this evaluation raised issues about how H-3 sorption on graphite is modeled within TRITGO as well as about the reliability of the sorption isotherm used in the code. This issue has not been raised previously.

In principle, the TRITGO code could be extensively modified to include an arbitrary number of parallel and coupled serial loops, to calculate fast fluence as a function of time and space, etc (i.e., to correct the structural limitations). However, the fundamental limitation, the analytical solution technique, is so restrictive that it would be far more practical to write a new code that was solved numerically and that allowed non-linear and time-dependent functionalities. In summary, TRITGO is at best marginally adequate for conceptual design, and it should be replaced as soon as practical with a new tritium mass balance code which employs a numerical solution technique. The H-3 transport DDNs should be assigned a high priority.

11.2 RADC, Plant Radionuclide Mass Balance Code

The RADC code [Eichenberg 1993] is a zero-dimensional, radionuclide inventory code that is a modification of the RAD2 code [Vanslager 1965] that was written in the mid-1960s to predict a radionuclide mass balance for the Peach Bottom HTGR. RADC has a number of significant limitations [e.g., Hudritsch 1977]. In particular, it does not calculate neutron activation products from neutron reactions with fission products [e.g., Ag^{109} $(n,\gamma)Ag^{110m}$, $Cs^{133}(n,\gamma)Cs^{134}$, etc.], neutron reactions with core impurities [$N^{14}(n,p)C^{14}$, $Li^{6}(n,\alpha)H^{3}$, etc.], or neutron reactions with control materials [e.g., $B^{10}(n,2\alpha)H^{3}$, etc.]. It also does not calculate heavy-metal buildup and decay chains; instead, the core inventories of important activation product have to be calculated externally and an effective fission yield supplied to RADC.

These limitations and other limitations in RADC have long been recognized, and a replacement code called RANDI was written to eliminate them [Hudritsch 1977]. Specifically, RANDI incorporates the following improvements:

1. Separate fissile and fertile particles

2. Better spatial definition in the core (segments, regions),
3. Depletion of fuel and fission products,
4. Correct mass balance for all regions,
5. Correct modeling of long depletion chains,
6. Modeling of neutron activation processes,
7. Transient release of stored fission gases (the “burst effect“) upon particle failure,
8. Refined modeling realistic reactor operating and shutdown conditions.

However, RANDI requires extensive automated input from other codes. As written, RANDI cannot be conveniently used in a stand-alone mode to generate radionuclide design criteria independent of a core nuclear design and a full-core fuel performance and fission product release analyses (which provide fuel failure fractions, fission product release fractions, etc.).

RADC is adequate for conceptual design, but it should be replaced for preliminary and final design. The possibility of modifying and simplifying the RANDI code so that it can be used in a stand-alone mode should be investigated before committing to writing an entirely new code. In particular, the utility of modifying RANDI so that the core inventories could be automatically input from a general purpose, radionuclide generation and depletion code, such as the industry standard ORIGIN-2 code [Croff 1980] or the GA GARGOYLE code [Shirley 1993] should be determined.

12. CONCLUSIONS AND RECOMMENDATIONS

The conclusions and recommendations resulting from this evaluation are summarized below. Some of the conclusions and many of the recommendations are tentative because the NGNP is still in the pre-conceptual design phase.

12.1 Conclusions

The following conclusions apply to both the NGNP and to commercial H2-MHRs unless otherwise noted.

Radionuclide Control

1. The most effective means of limiting radioactive contamination the NGNP plant will be source reduction.
2. Radionuclide contamination in the NGNP plant will be dominated by relatively small quantities of fission and neutron activation products released from the core. *In situ* activation of structural materials will be limited and the activation products will be fixed.
3. There will be no analog in the NGNP to radioactive “crud” in water-cooled reactors since the helium coolant is chemically inert; this conclusion assumes that the surface films on the high Co-content alloy IN 617 will not spall and generate a radioactive aerosol.
4. The dominant sources of radionuclide release from the core will be as-manufactured heavy-metal contamination and fuel particles whose coatings fail in service. Both sources can be limited by proper particle design and optimized fuel fabrication processes.
5. In addition to radionuclide release from HM contamination and failed particles, Ag-110m and H-3 will be diffusively released from intact TRISO particles at sufficiently high temperatures for sufficiently long times.
6. The NGNP will be designed to have a 60-year lifetime, and a commercial H2 MHR is expected to have a comparable design lifetime. At the end of its operational lifetime, the physical plant will represent the ultimate “by-product” of electricity and hydrogen production, and both the reactor plant and the hydrogen plant will have to be decontaminated and decommissioned.
7. Based upon the past D&D experience with gas-cooled reactors, especially the successful D&D of the Fort St. Vrain HTGR, the D&D costs for both the NGNP and commercial H2-MHR reactor plants should be comparable to that for a LWR on a per MW(e) basis.
8. An important component of the above conclusion is that the core graphite – or at least the vast bulk of it – should qualify as low-level waste. In fact, >90% of the FSV core graphite qualified as Class A low-level waste (the lowest level classification).

Dust Effects

1. The amount of dust in the primary circuit of a prismatic-core NGNP should be minimal and should far less than in a pebble-bed NGNP.

2. Based upon operational experience with FSV and HTTR, the prismatic core should not be a significant source of dust.

3. The expected quantities of dust in the primary should not present any operational problems, such as a heat-exchanger fouling.

4. The effect of low concentrations of dust on the plateout and liftoff of condensable radionuclides, especially I-131, needs to be better characterized.

Tritium Control

1. Tritium will be produced in the NGNP and commercial H2-MHR by various nuclear reactions. Ternary fission will produce the largest inventory of tritium, but that tritium will be largely retained in the TRISO fuel particles. A major source of tritium in the primary coolant will likely be the neutron activation of the He-3 in the primary helium.
2. Given its high mobility, especially at high temperatures, some tritium will permeate through the intermediate heat exchanger and the hydrogen plant process vessels, contaminating the product hydrogen.
3. This tritium contamination of the hydrogen will contribute to public and occupational radiation exposures; consequently, stringent limits on tritium contamination in the product hydrogen are anticipated to be imposed by regulatory authorities.
4. Realistic limits on allowable tritium contamination of the product hydrogen need to adopted early in the design process.
5. Design options are available to control tritium in an H2-MHR, but they can be expensive so an optimal combination of mitigating features must be implemented in the design.
6. The most cost-effective means of controlling tritium contamination appears to be the addition of a He purification system to the secondary loop which transfers heat from the primary coolant loop containing the reactor to the hydrogen production plant.

12.2 Recommendations

The following recommendations apply to both the NGNP and to commercial H2-MHRs unless otherwise noted.

Radionuclide Control

1. Radioactive source reduction should be assigned the highest priority during all phases of NGNP design.
2. The use of high Co-content alloys, including IN 617, should be limited to locations where the neutron flux is negligible.
3. The primary coolant chemistry should be controlled and perhaps custom tailored by impurity injection to assure that the surface films on high Co-content alloys, including IN 617, will not spall and generate a radioactive aerosol.
4. Credit should be taken for all of the RN release barriers in the MHR radionuclide containment system.

5. The AGR program should develop and qualify a two-particle (fissile/fertile) UCO TRISO fuel system to facilitate core power shaping to minimize fuel temperatures and, hence, RN release.
6. The AGR program should conduct the requisite technology programs to provide a defensible basis for validation the radionuclide source terms used for NGNP design and licensing.
7. An improved RN plant mass balance code should be developed to replace the RADC code for NGNP preliminary and final design.

Tritium Control

1. Realistic design goals for allowable H-3 contamination in the product hydrogen should be adopted early in the conceptual design of the NGNP and a legal limit negotiated with regulatory authorities during preliminary design.

2. The extensive literature on H-3 permeation through heat exchanger materials should be acquired, reviewed, and evaluated as a basis for selecting the best available correlations for predicting H-3 permeation from the primary to secondary loops and from the secondary loop to the hydrogen plant process streams.

3. The extensive literature on H-3 permeation barrier coatings should be acquired, reviewed, and evaluated for possible application in an H2-MHR. A feasibility study should be made to determine if there is a practical means of applying such coatings to a printed circuit-type IHX.

4. The practicality of using a SiC heat exchanger for the sulfuric acid decomposer should be determined early in the conceptual design phase since it could substantially mitigate the tritium contamination concern. This investigation should include a structural analysis which considers thermal transients and depressurization accidents and the measurement of the corrosion rates in decomposing sulfuric acid at temperatures >850 ^{o}C and elevated pressures.

5. Trade studies should be performed to identify the optimal combination of design options for assuring tritium contamination levels will be well below anticipated regulatory limits.

6. The validity of the TRITGO code should be assessed by analysis of the H-3 transport data available from FSV operations.

7. The AGR program should conduct the requisite technology programs to provide a defensible basis for validation the tritium source terms used for NGNP design and licensing.

8. An improved H-3 plant mass balance should be developed to replace the TRITGO code for NGNP conceptual design.

13. REFERENCES

Acharya, R., “Analysis of Tritium Behavior in FSV,” 906974, Rev. 1, GA Technologies, July 1983.

Acharya, R., “Cesium and Silver Transport in R2-K13 Experiment,” DOE HTGR-88148, General Atomics, 1987.

Acharya, R., et al., “Fuel Capsule HRB-21 Postirradiation Examination Data Report,” DOE-HTGR-100229 (ORNL-6836), Oak Ridge National Laboratory, April 1995.

[AGR Plan/1] “Technical Program Plan for the Advanced Gas Reactor Fuel Development and Qualification Program”INL/EXT-05-00465, Rev. 1, Idaho National Laboratory, August 2005.

Akers, D.W., “Examination and Analysis of the Second Plateout Probe from the Fort St. Vrain High-Temperature Gas-Cooled Reactor,” Report EGG-NPR-9441, EG&G Idaho, 1991.

Alberstein, D., P. D. Smith, and M. J. Haire, “Metallic Fission Product Release from the HTGR Core,” GA-A13258 (GA-LTR-20), General Atomic, May 1975.

ANL/EXT-06-46, “Preliminary Issues Associated with the Next Generation Nuclear Plant Intermediate Heat Exchanger Design”, Argonne National Laboratory, September 2006.

Asmussen, K., “Effects on FSV Core of Operating with Reserve Shutdown Material in Region 27,” 906618, Rev. A, GA Technologies, June 1983.

Baeumer, R., and I. Kalinowski, “THTR Commissioning and Operating Experience,” Energy, **16**, 1991, pp. 59-70.

Baxter, A. M., et al., “FSV Experience in Support of the GT-MHR Reactor Physics, Fuel Performance, and Graphite,” GA-A21925, General Atomics, November 1994.

Bansal, R. C., F. J. Vastola, and P. L. Walker, Jr., Carbon, **9**, 1971, p. 185.

Bell, J. T., et al., paper presented at the American Nuclear Society Conference on Remote Systems Technology, San Francisco, CA, October 1975.

Brey, H. L., et al. “Comparison of the Radioactive Materials Released from the Fort St. Vrain HTGR and LWRs,” Health Physics, **40**, January 1981, pp. 81-84.

Buchkremer, H. P., et al., “Oxide Films on Austenitic HTR Heat Exchanger Materials as a Tritium Permeation Barrier,” Specialists Meeting on Heat Exchanging Components of Gas-Cooled Reactors Düsseldorf (Germany), 16-19 April 1984, IWGGCR-9, International Atomic Energy Agency, Vienna, pp. 363-376.

Burnette, R., “Radiochemical Analysis of the First Plateout Probe from the Fort St. Vrain High-Temperature Gas-Cooled Reactor,” Report GA-A16764, GA Technologies Inc., 1982.

Burnette, R. D., et al., “Test Status Report on Fort St. Vrain HTGR Coolant and Radiochemistry: July 1983 through June 1984,” 907650, Rev. 1, GA Technologies, September 1984.

Buzzelli, G., S. Langer, C. Jones, and B. Gainey, "Tritium: Fast Fission Yields of U-238 and Th-232,” unpublished results, General Atomic, September 1976.

Causey, R. A., “The Interaction of Tritium with Graphite and its Impact on Tokamak Operations,” J. Nucl. Mat., **162-164**, 1989, pp. 151-161.

[CNSC], “Standards and Guidelines for Tritium in Drinking Water,” INFO-0766, Canadian Nuclear Safety Commission, January 2008.

Compere, E. L., et al., "Distribution and Release of H-3 in High-Temperature Gas-Cooled Reactors as a Function of Design, Operational and Material Parameters," ORNL-TM-4303, Oak Ridge National Laboratory, June 1974.

Copinger, D. A. and D. L. Moses, “Fort Saint Vrain Gas Cooled Reactor Operational Experience,” NUREG/CR-6839 (ORNL/TM-2003/223), Oak Ridge National Laboratory, January 2004.

Cordewiner, H. J., “Numerische Berechnung des Tritium-Verhaltens von Kugelhaufenreaktoren am Beispiel des AVR-Reaktors,“ Juel-1607, Kernforschungsanlage, Juelich, July 1979 *(in German)*.

Croff, A. G., “The ORIGEN-2 Computer Code,” ORNL-TM-7175, Oak Ridge National Laboratory, Oak Ridge, TN, 1980.

Czechowicz, D., and L. Brown, “New Correlation for Tritium Permeation through NP□MHTGR Steam Generator Tubes,” CEGA Internal Memorandum, CEGA-M-91-3066, November 18, 1991.

Dietrich, G., W. Neumann, and N. Roehl, “Decommissioning of the thorium high temperature reactor (THTR 300),” IAEA Technical Committee Meeting on Technologies for Gas-Cooled Reactor Decommissioning, Fuel Storage And Waste, Juelich, FRG, September 1997, IAEA-TECDOC-1043, September 1998.

Dyer, F. F., et al., “Distribution of Radionuclides in the Peach Bottom Primary Circuit during Core 2 Operation,” USERDA Report ORNL-5188, Oak Ridge National Laboratory, March 1977.

Eichenberg, T. W., “RADC Users Manual,” CEGA-002814, Rev. N/C, CEGA Corporation, September 1993.

Englelhard, J., K. Krueger, and H. Gottaut, “Investigation of the Impurities and Fission Products in the AVR Coolant Gas at an Average Hot-Gas Temperature of 950 ^{o}C,” Nucl. Eng. Des., **34**, 1975, pp. 85-92.

EPRI-CS-5071, “Fireside corrosion and fly ash erosion in boilers: Final report” - Battelle Columbus Div., OH (USA), Electric Power Research Institute, February 1987.

EPRI-CS-5195, Technical Report, “Fireside corrosion of superheater alloys for advanced-cycle steam plants: Final report” - Foster Wheeler Development Corp., Livingston, NJ (USA); Electric Power Research Institute, May 1987.

EPRI Sootblower Conference 2006 – “Advanced Erosion Protection Technology for Steam Boiler Superheat, Reheat and Evaporator Tubes,” May 2006.

Faircloth, R. L., et al., “Coolant Chemistry of the Advanced Carbon Dioxide Cooled Reactor,” Proceedings of IAEA Specialists Meeting, Coolant Chemistry, Plateout and Decontamination in Gas-Cooled Reactors, Juelich, 2-4 December 1980, IWGGCR/2, International Atomic Energy Agency, 1981, pp. 125-131.

Fischer, et al., "Contributions to the Transport Characteristics of Fission Products and Tritium in HTRs," in Reaktortagung, Proceedings of the Reactor Conference, Berlin, 1974, p. 420.

Fisher, M., “Fort St. Vrain Decommissioning Project,” in Technologies for gas cooled reactor decommissioning, fuel storage and waste disposal, Proceedings of a Technical Committee meeting, Juelich, Germany, 8-10 September 1997, IAEA TECDOC 1043, International Atomic Energy Agency, Vienna, September 1998.

Fluss, M. J., N. D. Dudey, and R. L. Malewicki, Phys. Rev. **C6**, 1972, p. 2252.

Forsyth, R., “Tritium Production and Distribution in High Temperature Gas-Cooled Reactors: Tritium Generation, Retention, Distribution, and Environmental Release in a Notional 1,500 MW (th) HTR, DP-905, Dragon Project, October 1974.

Fujikawa, S., et al., "Achievement of Reactor-Outlet Coolant Temperature of 950°C in HTTR," J. Nucl. Sci. & Tech., **41**(12), 2004, pp. 1245-1254.

Furusawa, T., et al., “Investigation of Dust Captured by Quintuple Filter Installed at Upstream of Primary Helium Circulator of Japan’s HTTR,” Japan Atomic Energy Agency, March 2008 *(JAEA proprietary information)*.

[GA PCDSR] “NGNP and Hydrogen Production Preconceptual Design Studies Report,” 911107, Rev. 0, General Atomics, July 2007.

[GA] "HTGR Base Program Quarterly Progress Report for the Period Ending August 31, 1972," GA-A12222, Gulf General Atomic, September 30, 1972.

Gainey, G. W., "A Review of Tritium Behavior in HTGR Systems," GA-A13461, General Atomic, April 1976.

[GDDM] Price, R. J., “Graphite Design Data Manual,” 906374, Rev. A, GA Technologies, September 1984.

Gillespie, A. G., “Tritium Analysis for the NP-MHTGR,” CEGA-002513, Rev. 0, CEGA Corporation, January 1993 *(UCNI)*.

Gillespie, A. G., “NP-MHTGR Tritium Analysis Calculation Report,” CEGA-002684, Rev. 0, CEGA Corporation, January 1993 *(UCNI)*.

Gottaut, H., and K. Krueger, “Results of Experiments at the AVR Reactor,” Nucl. Eng. Des., 121, 1990, p. 143-153.

[GT-MHR DDNs] DOE-GT-MHR-100217, “600 MW(t) Gas Turbine Modular Helium Reactor Design Data Needs,” (Draft), General Atomics, July 1996.

Haire, M.J., and D.W. McEachern, "Gaseous Radioactivity Levels in the Primary Coolant of an HTGR," GA-A12946 (GA-LTR-14), General Atomic, October 1974.

Halpen, I., Ann. Rev. Nucl. Sci., **21**, 1971, p. 245.

Hanson, D. L., “Logic for Deriving Fuel Quality Specifications,” PC-000498, Rev. 0, General Atomics, March 2001.

Hanson, D. L., and M. B. Richards, “[Commercial GT-MHR] Spent Fuel Disposal Confirmatory Test and Analysis Plan,” PC-000503, Rev. 0, General Atomics, June 2002a.

Hanson, D. L., “Plate-Out Phenomena in Direct-Cycle High Temperature Gas Reactors,” 1003387, Electric Power Research Institute, June 2002b.

Hanson, D. L., and J. J. Saurwein, “Development Plan for Advanced High Temperature Coated-Particle Fuels,” PC 000513, Rev. 0, General Atomics, December 2003.

Hanson, D. L., and M. P. LaBar, “Decontamination And Decommissioning of HTGRs, A Status Report,” PC-000524, Rev. 0, General Atomics, April 2005.

Hanson, D. L., “TRITGO Code Description and User’s Manual,“ GA Document 911081, Rev. 0, General Atomics, February 2006a.

Hanson, D. L., “Review of Tritium Behavior in HTGRs,” PC-000535, Rev. 0, General Atomics, May 2006b.

Hanson, D. L., “NGNP End-Products Study,” 911106, Rev. 0, General Atomics, April 2007a.

Hanson, D. L., “Test Plan for Characterizing Tritium Transport in a VHTR,” PC-000550, Rev. 0, General Atomics, December 2007b.

Heffernan, T. F., “Capsule HRB-21 Preirradiation Report,” DOE-HTGR-88357, Rev. C, General Atomics, April 1991.

Horrocks, D. L., "Yields of Tritium During the Fissioning of Nuclides of Interest in the Operation of Nuclear Power Reactors," in *Tritium*, A. A. Moghissi and M. W. Carter (eds.), Messenger Graphics, Phoenix, Arizona, 1973, p. 30.

Hudritsch, W. W., “RANDI, A Zero-Dimensional Computer Program for Calculating HTGR Activities,” GA-A14091, General Atomic, March 1977.

Jovanovic, V., “Radionuclide Design Criteria for the MHTGR Primary Coolant Circuit,” 908095, Rev. 4, GA Technologies, June 1989.

“Long Time Investigation of the Effect of Fouling on the Super-Heaters in a Circulating Fluidizer Biomass Boiler,” International Journal of Energy Research, **30**(13), October 25, 2006

Kirch, N., and G. Scheidler, “ Control of the Tritium Path in Process Heat HTR’s,” Fission Product Release and Transport in Gas-cooled Reactors, Proceedings of IAEA Specialists Meeting, Berkeley, 1985, IWGGCR13, International Atomic Energy Agency, Vienna, 1986, pp. 236-249.

Konys, J., et al., “Status of Tritium Permeation Barrier Development in the EU,” Fusion Science and Technology, **47**(4), May 2005, pp. 844-850.

Labar, M., “Steam Generator Alternatives Study,” 911120, Rev. 0, General Atomics, April 2008.

Maki. J., “AGR-1 Irradiation Experiment Test Plan,” INL/EXT-05-00593, Idaho National Laboratory, August 2005.

Marnet, C., et al., “AVR Experience for Future HTGR Development,” Proceedings of IAEA TCM, Petten, The Netherlands, Nov. 1994, ECN-K-95-026, p. 86.

Marshall, M., and J. Scobie, Phys. Letters, **23**, 1966, p. 583.

Martin, R. C., “Compilation of Fuel Performance and Fission Product Transport Models and Database for MHTGR Design,” ORNL/NPR-91/6, Oak Ridge National Laboratory, October 1993.

Montgomery, F. C., “Test Report on Sulfate from MoS_2 Oxidation,” 907877, Rev. N/C, GA Technologies, May 1985.

Montgomery, F. C., “FSV Cycle 4 Coolant Chemistry and Tritium Sorption on Moderator Graphite,” 908947, Rev. 0, GA Technologies, September 1986.

Munoz, S. P., “Fuel Product Specification [for the GT MHR],” DOE-GT-MHR-100209, Rev. 0, General Atomics, May 1994.

Myers, B. F., "Update of Fuel Performance Data and Models,” 908721, Rev. 0, GA Technologies, February 1986 (GA Proprietary Information).

Myers, B. F., "Fuel Design Data Manual," 901866, Issue F, General Atomics, August 1987 (GA Proprietary Information).

Myers, B. F., “The Effect of Water Vapor on the Release of Fission Gas from the Fuel Elements of High-Temperature, Gas-Cooled Reactors: A Preliminary Assessment of Experiments HRB-

17, HFR-B1, HFR-K6 and KORA," Report ORNL/TM-4294, Oak Ridge National Laboratory, 1995.

Nabielek, H., et al., "Performance Limits of Coated Particle Fuel; Part III: Fission Product Migration in HTR Fuel," DP-828 (Pt. 3), Dragon Project, June 1974.

[NEA] "Decommissioning Nuclear Power Plants: Policies, Strategies and Costs," NEA, OECD, 2003 (http://oecdpublications.gfi-nb.com/cgi-bin/OECDBookShop.storefront/EN/product/662003221P1).

[NGNP PCD] "Next Generation Nuclear Plant Pre-Conceptual Design Report," INL/EXT-07-12967, Idaho National Laboratory, September 2007.

[NGNP TDP] Hanson, D. L., "NGNP Umbrella Technology Development Plan," PC-000543, Rev. 0, General Atomics, July 2007.

NUREG/CR-6824, ANL-02/37 "Materials Behavior in HTGR Environments", Argonne National Laboratory, U.S. Nuclear Regulatory Commission Office of Nuclear Regulatory Research, February, 2003.

Ohashi, H., and S. R. Sherman, "Tritium Movement and Accumulation in the NGNP System Interface and Hydrogen Plant," INL/EXT-07-12746, Idaho National Laboratory, June 2007.

[OSU] "Nuclear Reactor Power Monitoring Using Silicon Carbide Semiconductor Radiation," NERI Quarterly Progress Report for Quarter 4, 2003, Ohio State University, October 2003.

[PC-MHR] "MHTGR Plutonium Consumption Study Phase II Extension FY-94 Final Report," GA/DOE-186-94, September 1994.

Phelps, R. D., "Graphite Block Requirements for the GT-MHR Reactor Core," PC-000560, General Atomics, March 2008 *(GA Proprietary Information).*

Pickard, P., et al., "Sulfur-Iodine Thermochemical Cycle," in DOE Hydrogen Program, 2006 Annual Progress Report (http://www.hydrogen.energy.gov/annual_progress06.html).

Pitner, A. L., and J. A. Basmajian, "Tritium Production and Retention," W/FFTF-7311159, Westinghouse Hanford, December 1973.

[PSID] "Preliminary Safety Information Document for the Standard MHTGR," Volumes 1-6, HTGR-84-024, Amendment B, August 1992.

Richards, M., and A. Shenoy, "Hydrogen Generation using the Modular Helium Reactor," Proceedings of ICONE12: 12th International Conference on Nuclear Engineering, April 25-29, 2004, Arlington, Virginia USA, ICONE12-49228, ASME, 2004.

Richards, M. B. and D. W. Ketchen, "PC-MHR Spent Fuel Disposal: Preliminary Evaluation of Whole-Element Disposal Using Multipurpose Canisters," GA/DOE-164-94, General Atomics, September 30, 1994.

Richards, M., "Assessment of GT-MHR Spent Fuel Characteristics and Repository Performance," GA Document PC-000502, Rev. 0, General Atomics, March 2002.

Richards, M., et al., "H2-MHR Conceptual Design Report: SI-Based Plant," GA-A25401, General Atomics, April 2006a.

Richards, M., et al., "H2-MHR Conceptual Design Report: HTE-Based Plant," GA-A25402, General Atomics, April 2006b.

Richards, M. B., "Optimization of VHTR Block-Type Core Design," PC-000542, Rev. 0, General Atomics, July 2007.

Rider, B. F., and M. E. Meek, "Compilation of Fission Product Yields," General Electric Co. Report No. NEDO-12154-2(E), June 1978.

Roellig, K., "The THTR Coolant Gas Activity, an Indicator of Fuel Performance," Proc. of IAEA Specialists Meeting: Behaviour of GCR Fuel under Accident Conditions, Oak Ridge, 1990, IWGGCR/25, Vienna, 1991, p. 99-108.

[RSSDD] "Reactor System Design Report [for the Commercial GT-MHR]," DOE-GT-100011, Rev. 0, General Atomics, September, 1994 (Draft).

Saito, S., et al., "Design of High Temperature Engineering Test Reactor (HTTR)," JAERI-1332, Japanese Atomic Energy Research Institute, 1994.

Schaefer, J., D. Stoever, and R. Hecker, "Terms and results of hydrogen permeation testing of oxide-scaled high-temperature alloys," Nuclear Technology, **66**, 537-549 (1984).

Scheffel, W., and J. Saurwein, "Preliminary Fuel Product Specification for the Baseline Advanced Gas Reactor Fuel Design," GA Document 911034/0, General Atomic, September 2003.

Schmidt, A. S., F. Verfuss, and E. Wicke, 'Studies on the permeation of hydrogen and tritium through heat resistant alloys," Journal of Nuclear Materials, **131** (2-3), 247-260 (1985).

Shenoy, A. S., GT-MHR Conceptual Design Description Report, 910720, Rev. 1, General Atomics, July 1996.

Shirley, G., "User's Manual and Description for GARGOYLE: A Fuel Cycle Analysis Code with a Decay Heat Calculation Capability," CEGA-002922, CEGA Corporation, Rev. 0, October 1993.

Sparks, C. J., et at., "Characterization of Ft. St. Vrain Reactor Dust," ORNL/NPR-90/12, Oak Ridge National Laboratory, March 1991.

[SRM] Labar, M., D. Phelps, and J. Saurwein, "System Requirements Manual," 911102, Rev. 0, General Atomics, March 2007.

Steinwarz, W., H. D. Roehrig, and R. Nieder, "Tritium Behaviour in an HTR-System based on AVR-Experience," ," Proceedings of IAEA Specialists Meeting, Coolant Chemistry, Plateout and Decontamination in Gas-Cooled Reactors, Juelich, 2-4 December 1980, IWGGCR/2, International Atomic Energy Agency, Vienna,1981, pp. 152-160.

Steinwarz, W., H. et al., "Distribution of Tritium in a Nuclear Process Heat Plant with HTR," Nucl. Eng. Des., **78**, 1984, pp. 267-272.

Strehlow, R. A., and H. C. Savage, "The Permeation of Hydrogen Isotopes through Structural Metals at low Pressures and through Metals with Oxide Film Barriers," Nucl. Tech., **22**, April 1974, p. 127.

Steward, K. P., "Final Summary Report on the Peach Bottom End-of-Life Program," GA-Al4404, General Atomic, July 1978.

Takeda, T., et al., "Study on Tritium/Hydrogen Permeation in the HTTR Hydrogen Production System," 7th International Conference on Nuclear Engineering, Tokyo, Japan, April 19-23, 1999, ICONE-7102, American Society of Mechanical Engineers.

[TECDOC-978] "Fuel Performance and Fission Product Behavior in Gas Cooled Reactors," International Atomic Energy Agency, November 1997.

Tzung, F., "TRAFIC-FD, A Finite Difference Program to Compute Release of Metallic Fission Products from an HTGR Core: Code Theory and Users Manual," CEGA-001904, CEGA Corporation, September 1992a

Tzung, F., “COPAR-FD, A Finite Difference Program to Compute Release of Metallic Fission Products from Coated Particles: Code Theory and Users Manual,” CEGA-002098, Rev. N/C, CEGA Corporation, September 1992b.

Vanslager, F. E., "RAD2: A Computer Program for Calculating Fission Product Radioactivities", GAMD-6519, Gulf General Atomic, July 1965.

Vorobiev, A. A., et al., Sov. J. At. Energy, 27, 1969, p. 713.

Wahsweiler, H.G., “THTR-300, F+E Teilvorhaben: Graphitstaub, 2,” HJ 1988, Technical Note HRB-419O4 (BH 0029}, Hochtemperatur-Reaktorbau GmbH (1989).

Walter, K. H., G. Lange, and K. H. Kienberger, J. Nucl. Mater, **48**, 1973, p. 287.

Wawrzik, U., “Staub im AVR-Reaktor, eine Analyse der Kaltgasfilterversuche,” Proc. Jarhrestagung Kerntechnik '87, Karlsruhe, 1987, Inforum GmbH, Bonn, 1987, p. 315-318.

Weaver, L., “Helium Purification Conceptual System Design Description,“ CEGA-000025, CEGA Corporation, April 1990 *(UCNI)*.

Wichner, R. P., and F. F. Dyer, “Distribution and Transport of Tritium in the Peach Bottom HTGR,” ORNL-5497, Oak Ridge National Laboratory, August 1979.

Wichner, R. P., “Fission Product Plateout and Liftoff in the MHTGR Primary System: A Review,” NUREG/CR-5647 (ORNL/TM-11685), Oak Ridge National Laboratory, April 1991.

[Work Plan] “Work Plan for FY08-1 Conceptual Design Studies for the NGNP with Hydrogen Production,” Battelle Energy Alliance, LLC, Contract No. 00060845, General Atomics, December 5, 2007.

Yang, L., W. A. Baugh, and N. L. Baldwin, “Study of Tritium Permeation through Peach Bottom Steam Generator Tubes,” GA-A14376, General Atomic, June 1977.

Yang, L., W. Baugh, and R. Medico, “Study of Tritium Release Characteristics of Irradiated TRISO Coated $LiAlO_2$ Particles,” GA-A16906, GA Technologies, December 1982.

Ziermann, E., “The AVR Nuclear Power Facility - A Progress Report,” Nuclear Engineering and Design, **78**, 1984, pp. 98-108.

APPENDIX A. RADIONUCLIDE DESIGN CRITERIA

Table A-1. 600 MW(t) Core – "Design" Fuel Activity

Nuclide	Half-life	Core Equilibrium (Ci)	Average Power Element After 3 Years Operation			
			Initial (Ci)	1-Day Decay (Ci)	10-Day Decay (Ci)	100-Day Decay (Ci)
[H3]	[12.3-Y]	[3.32E+0]3	[4.12E+00]	[4.12E+00]	[4.11E+00]	[4.05E+00\
C14	5730-Y	1.18E+02	1.55E-01	1.55E-01	1.55E-01	1.55E-01
GE79	43.0-S	2.22E+05	2.17E+02	0.00E+00	0.00E+00	0.00E+00
AS79	9.0-M	2.44E+05	2.39E+02	0.00E+00	0.00E+00	0.00E+00
SE79M	3.89-M	2.44E+05	2.39E+02	0.00E+00	0.00E+00	0.00E+00
*SE79	STABLE	7.92E+01	1.04E-01	1.04E-01	1.04E-01	1.04E-01
SE80	STABLE	2.23E+02	2.92E-01	2.92E-01	2.92E-01	2.92E-01
SE81	18.5-M	1.02E+06	9.96E+02	0.00E+00	0.00E+00	0.00E+00
BR81	STABLE	3.37E+02	4.41E-01	4.41E-01	4.41E-01	4.41E-01
SE82	STABLE	5.73E+02	7.49E-01	7.49E-01	7.49E-01	7.49E-01
SE83M	70.-S	1.33E+06	1.30E+03	0.00E+00	0.00E+00	0.00E+00
SE83	22.5-M	1.36E+06	1.33E+03	0.00E+00	0.00E+00	0.00E+00
BR83	2.4-H	2.79E+06	2.73E+03	2.92E+00	0.00E+00	0.00E+00
KR83M	1.86-H	2.79E+06	2.73E+03	1.18E+01	0.00E+00	0.00E+00
KR83	STABLE	9.49E+02	1.24E+00	1.24E+00	1.24E+00	1.24E+00
SE84	3.3-M	4.92E+06	4.82E+03	0.00E+00	0.00E+00	0.00E+00
BR84	31.8-M	5.05E+06	4.95E+03	0.00E+00	0.00E+00	0.00E+00
KR84	STABLE	1.78E+03	2.33E+00	2.33E+00	2.33E+00	2.33E+00
BR85	2.87-M	6.78E+06	6.65E+03	0.00E+00	0.00E+00	0.00E+00
KR85M	4.48-H	6.79E+06	6.66E+03	1.64E+02	0.00E+00	0.00E+00
KR85	10.73Y	1.90E+05	2.44E+02	2.44E+02	2.44E+02	2.40E+02
RB85	STABLE	1.93E+03	2.54E+00	2.54E+00	2.54E+00	2.55E+00
KR86	STABLE	3.61E+03	4.72E+00	4.72E+00	4.72E+00	4.72E+00
KR87	76.-M	1.31E+07	1.28E+04	2.54E-02	0.00E+00	0.00E+00
RB87	STABLE	4.75E+03	6.20E+00	6.21E+00	6.21E+00	6.21E+00
KR88	2.8-H	1.85E+07	1.81E+04	4.77E+01	0.00E+00	0.00E+00
RB88	17.7-M	1.89E+07	1.85E+04	5.33E+01	0.00E+00	0.00E+00
SR88	STABLE	6.82E+03	8.92E+00	8.92E+00	8.92E+00	8.92E+00

Table A-1. 600 MW(t) Core – "Design" Fuel Activit (Cont.)

Nuclide	Half-life	Core Equilibrium (Ci)	Average Power Element After 3 Years Operation			
			Initial (Ci)	1-Day Decay (Ci)	10-Day Decay (Ci)	100-Day Decay (Ci)
KR89	3.16-M	2.40E+07	2.35E+04	0.00E+00	0.00E+00	0.00E+00
RB89	15.2-M	2.52E+07	2.47E+04	0.00E+00	0.00E+00	0.00E+00
SR89	50.5-D	2.54E+07	2.49E+04	2.45E+04	2.17E+04	6.30E+03
Y89	STABLE	9.26E+03	1.21E+01	1.21E+01	1.22E+01	1.27E+01
KR90	32.3-S	2.63E+07	2.58E+04	0.00E+00	0.00E+00	0.00E+00
RB90M	4.28-M	6.51E+06	6.38E+03	0.00E+00	0.00E+00	0.00E+00
RB90	2.7-M	2.44E+07	2.39E+04	0.00E+00	0.00E+00	0.00E+00
SR90	29.-Y	1.51E+06	1.97E+03	1.97E+03	1.97E+03	1.95E+03
Y90	64.-H	1.51E+06	1.97E+03	1.97E+03	1.97E+03	1.95E+03
ZR90	STABLE	6.19E+02	9.68E-01	9.68E-01	9.68E-01	9.68E-01
KR91	9.0-S	1.77E+07	1.74E+04	0.00E+00	0.00E+00	0.00E+00
RB91	58.5-S	2.95E+07	2.89E+04	0.00E+00	0.00E+00	0.00E+00
SR91	9.48-H	3.09E+07	3.03E+04	5.24E+03	7.26E-04	0.00E+00
Y91	58.6-D	3.08E+07	3.03E+04	3.01E+04	2.71E+04	9.34E+03
ZR91	STABLE	1.15E+04	1.51E+01	1.51E+01	1.52E+01	1.59E+01
SR92	2.71-H	3.08E+07	3.02E+04	6.51E+01	0.00E+00	0.00E+00
Y92	3.53-H	3.11E+07	3.04E+04	9.54E+02	0.00E+00	0.00E+00
ZR92	STABLE	1.17E+04	1.53E+01	1.53E+01	1.53E+01	1.53E+01
SR93	7.5-M	3.25E+07	3.19E+04	0.00E+00	0.00E+00	0.00E+00
Y93	10.2-H	3.32E+07	3.26E+04	6.45E+03	2.71E-03	0.00E+00
ZR93	STABLE	1.27E+04	1.66E+01	1.66E+01	1.66E+01	1.66E+01
SR94	1.29-M	3.13E+07	3.07E+04	0.00E+00	0.00E+00	0.00E+00
Y94	19.0-M	3.33E+07	3.27E+04	0.00E+00	0.00E+00	0.00E+00
ZR94	STABLE	1.29E+04	1.69E+01	1.69E+01	1.69E+01	1.69E+01
Y95	10.5-M	3.34E+07	3.27E+04	0.00E+00	0.00E+00	0.00E+00
ZR95	65.5-D	3.37E+07	3.31E+04	3.28E+04	2.98E+04	1.15E+04
NB95M	3.61-D	3.37E+05	3.31E+02	3.31E+02	3.13E+02	1.22E+02
NB95	35.1-D	3.37E+07	3.31E+04	3.31E+04	3.28E+04	1.93E+04
MO95	STABLE	1.31E+04	1.72E+01	1.72E+01	1.72E+01	1.76E+01
Y96	6.0-S	3.13E+07	3.07E+04	0.00E+00	0.00E+00	0.00E+00

Table A-1. 600 MW(t) Core – "Design" Fuel Activit (Cont.)

Nuclide	Half-life	Core Equilibrium (Ci)	Average Power Element After 3 Years Operation			
			Initial (Ci)	1-Day Decay (Ci)	10-Day Decay (Ci)	100-Day Decay (Ci)
ZR96	STABLE	1.29E+04	1.68E+01	1.68E+01	1.68E+01	1.68E+01
ZR97	16.8-H	3.08E+07	3.02E+04	1.12E+04	1.52E+00	0.00E+00
NB97	73.6-M	3.09E+07	3.03E+04	1.21E+04	1.63E+00	0.00E+00
MO97	STABLE	1.23E+04	1.61E+01	1.61E+01	1.61E+01	1.61E+01
NB98	51.0-M	4.32E+05	4.24E+02	1.34E-06	0.00E+00	0.00E+00
MO98	STABLE	1.22E+04	1.59E+01	1.59E+01	1.59E+01	1.59E+01
NB99M	2.5-M	1.21E+07	1.18E+04	0.00E+00	0.00E+00	0.00E+00
NB99	14.0-S	2.21E+07	2.17E+04	0.00E+00	0.00E+00	0.00E+00
MO99	66.2-H	3.26E+07	3.20E+04	2.49E+04	2.57E+03	0.00E+00
TC99M	6.02-H	2.87E+07	2.81E+04	2.39E+04	2.49E+03	0.00E+00
TC99	STABLE	1.32E+04	1.73E+01	1.73E+01	1.73E+01	1.73E+01
NB100M	7.0-S	1.74E+07	1.70E+04	0.00E+00	0.00E+00	0.00E+00
NB100	2.9-M	1.74E+07	1.70E+04	0.00E+00	0.00E+00	0.00E+00
MO100	STABLE	1.45E+04	1.90E+01	1.90E+01	1.90E+01	1.90E+01
MO101	14.6-M	3.12E+07	3.06E+04	0.00E+00	0.00E+00	0.00E+00
TC101	14.2-M	3.12E+07	3.06E+04	0.00E+00	0.00E+00	0.00E+00
RU101	STABLE	1.29E+04	1.69E+01	1.69E+01	1.69E+01	1.69E+01
MO102	11.1-M	3.32E+07	3.26E+04	0.00E+00	0.00E+00	0.00E+00
TC102M	4.3-M	3.32E+07	3.26E+04	0.00E+00	0.00E+00	0.00E+00
RU102	STABLE	1.39E+04	1.82E+01	1.82E+01	1.82E+01	1.82E+01
MO103	60.-S	3.54E+07	3.47E+04	0.00E+00	0.00E+00	0.00E+00
RU103	39.6-D	3.61E+07	3.54E+04	3.48E+04	2.97E+04	6.15E+03
RH103M	56.-M	3.58E+07	3.51E+04	3.45E+04	2.95E+04	6.10E+03
RH103	STABLE	1.53E+04	2.00E+01	2.00E+01	2.00E+01	2.00E+01
MO104	1.6-M	3.52E+07	3.45E+04	0.00E+00	0.00E+00	0.00E+00
TC104	18.-M	3.58E+07	3.51E+04	0.00E+00	0.00E+00	0.00E+00
RU104	STABLE	1.53E+04	1.99E+01	1.99E+01	1.99E+01	1.99E+01
TC105	8.0-M	3.19E+07	3.13E+04	0.00E+00	0.00E+00	0.00E+00
RU105	4.44-H	3.20E+07	3.13E+04	7.62E+02	0.00E+00	0.00E+00
RH105	35.5-H	2.59E+07	2.54E+04	1.86E+04	2.75E+02	0.00E+00
PD105	STABLE	1.38E+04	1.80E+01	1.80E+01	1.80E+01	1.80E+01

Table A-1. 600 MW(t) Core – "Design" Fuel Activit (Cont.)

Nuclide	Half-life	Core Equilibrium (Ci)	Average Power Element After 3 Years Operation			
			Initial (Ci)	1-Day Decay (Ci)	10-Day Decay (Ci)	100-Day Decay (Ci)
RU106	369.-D	2.39E+07	2.72E+04	2.71E+04	2.67E+04	2.25E+04
PD106	STABLE	1.09E+04	1.57E+01	1.58E+01	1.59E+01	1.71E+01
RU107	4.2-M	2.71E+07	2.66E+04	0.00E+00	0.00E+00	0.00E+00
RH107	21.7-M	2.71E+07	2.66E+04	0.00E+00	0.00E+00	0.00E+00
PD107	STABLE	1.19E+04	1.55E+01	1.55E+01	1.55E+01	1.55E+01
RU108	4.5-M	2.03E+07	1.99E+04	0.00E+00	0.00E+00	0.00E+00
PD108	STABLE	8.03E+03	1.02E+01	1.02E+01	1.02E+01	1.02E+01
RH109	1.5-M	1.17E+07	1.15E+04	0.00E+00	0.00E+00	0.00E+00
PD109M	4.69-M	5.86E+06	5.75E+03	0.00E+00	0.00E+00	0.00E+00
PD109	13.5-H	1.17E+07	1.15E+04	3.35E+03	4.97E-02	0.00E+00
AG109	STABLE	2.78E+03	3.19E+00	3.19E+00	3.20E+00	3.20E+00
PD110	STABLE	2.74E+03	3.58E+00	3.58E+00	3.58E+00	3.58E+00
AG110M	252.-D	2.81E+04	3.06E+01	3.05E+01	2.97E+01	2.32E+01
RH111	63.-S	2.92E+06	2.86E+03	0.00E+00	0.00E+00	0.00E+00
PD111	22.-M	2.96E+06	2.90E+03	0.00E+00	0.00E+00	0.00E+00
AG111M	74.-S	2.95E+06	2.89E+03	0.00E+00	0.00E+00	0.00E+00
AG111	7.47-D	2.96E+06	2.90E+03	2.64E+03	1.15E+03	2.71E-01
CD111	STABLE	1.30E+03	1.68E+00	1.68E+00	1.69E+00	1.70E+00
PD112	20.1-H	1.20E+06	1.18E+03	5.15E+02	3.00E-01	0.00E+00
AG112	3.13-H	1.20E+06	1.18E+03	6.09E+02	3.55E-01	0.00E+00
PD113	1.5-M	7.57E+05	7.43E+02	0.00E+00	0.00E+00	0.00E+00
AG113	5.3-H	6.81E+05	6.68E+02	2.91E+01	0.00E+00	0.00E+00
CD113	STABLE	1.53E+00	1.50E-03	1.62E-03	1.63E-03	1.63E-03
SN119M	245.-D	2.59E+03	2.81E+00	2.80E+00	2.73E+00	2.12E+00
SN119	STABLE	9.90E+01	1.29E-01	1.29E-01	1.30E-01	1.30E-01
SN123	129.-D	3.53E+04	3.57E+01	3.55E+01	3.38E+01	2.08E+01
SB123	STABLE	1.14E+02	1.50E-01	1.50E-01	1.50E-01	1.52E-01
SN125	9.65-D	1.90E+05	1.87E+02	1.74E+02	9.10E+01	1.42E-01
SB125	2.73-Y	2.35E+05	2.90E+02	2.90E+02	2.88E+02	2.72E+02
TE125M	58.-D	5.28E+04	6.52E+01	6.52E+01	6.54E+01	6.37E+01
TE125	STABLE	1.31E+02	1.98E-01	1.98E-01	1.99E-01	2.11E-01

Table A-1. 600 MW(t) Core – "Design" Fuel Activit (Cont.)

Nuclide	Half-life	Core Equilibrium (Ci)	Average Power Element After 3 Years Operation			
			Initial (Ci)	1-Day Decay (Ci)	10-Day Decay (Ci)	100-Day Decay (Ci)
SN126	STABLE	7.16E+02	9.36E-01	9.36E-01	9.36E-01	9.36E-01
SB126M	19.0-M	1.39E+06	1.37E+03	1.21E-02	1.21E-02	1.21E-02
SN127M	4.4-M	4.89E+05	4.79E+02	0.00E+00	0.00E+00	0.00E+00
SN127	2.12-H	1.89E+06	1.86E+03	7.26E-01	0.00E+00	0.00E+00
SB127	3.8-D	2.54E+06	2.49E+03	2.11E+03	4.10E+02	3.04E-05
TE127M	109.-D	4.00E+05	4.00E+02	3.99E+02	3.86E+02	2.19E+02
TE127	9.4-H	2.53E+06	2.48E+03	2.33E+03	7.62E+02	2.15E+02
I127	STABLE	1.32E+03	1.73E+00	1.73E+00	1.73E+00	1.73E+00
SN128	59.-M	3.23E+06	3.17E+03	1.42E-04	0.00E+00	0.00E+00
SB128M	10.4-M	3.53E+06	3.46E+03	1.72E-04	0.00E+00	0.00E+00
SB128	9.0-H	3.39E+05	3.33E+02	5.25E+01	3.14E-06	0.00E+00
TE128	STABLE	2.04E+03	2.67E+00	2.67E+00	2.67E+00	2.67E+00
SN129M	2.5-M	2.48E+06	2.43E+03	0.00E+00	0.00E+00	0.00E+00
SN129	7.5-M	2.48E+06	2.43E+03	0.00E+00	0.00E+00	0.00E+00
SB129	4.34-H	7.53E+06	7.38E+03	1.62E+02	0.00E+00	0.00E+00
TE129M	33.4-D	1.39E+06	1.36E+03	1.34E+03	1.11E+03	1.72E+02
TE129	70.-M	7.22E+06	7.08E+03	1.04E+03	7.08E+02	1.09E+02
I129	STABLE	4.09E+03	5.34E+00	5.35E+00	5.35E+00	5.36E+00
SN130	3.7-M	6.45E+06	6.32E+03	0.00E+00	0.00E+00	0.00E+00
SB130M	6.6-M	7.15E+06	7.01E+03	0.00E+00	0.00E+00	0.00E+00
SB130	37.-M	3.50E+06	3.43E+03	0.00E+00	0.00E+00	0.00E+00
TE130	STABLE	6.44E+03	8.42E+00	8.42E+00	8.42E+00	8.42E+00
SN131	63.-S	6.89E+06	6.76E+03	0.00E+00	0.00E+00	0.00E+00
SB131	23.-M	1.35E+07	1.33E+04	0.00E+00	0.00E+00	0.00E+00
TE131M	30.-H	5.61E+06	5.50E+03	3.17E+03	2.15E+01	0.00E+00
TE131	25.-M	1.52E+07	1.49E+04	5.78E+02	3.93E+00	0.00E+00
I131	8.04-D	2.00E+07	1.96E+04	1.83E+04	8.64E+03	3.69E+00
XE131M	12.0-D	2.80E+05	2.75E+02	2.65E+02	2.21E+02	2.47E+00
XE131	STABLE	1.07E+04	1.40E+01	1.41E+01	1.41E+01	1.42E+01
SN132	40.0-S	4.46E+06	4.37E+03	0.00E+00	0.00E+00	0.00E+00
SB132M	4.1-M	6.06E+06	5.94E+03	0.00E+00	0.00E+00	0.00E+00

Table A-1. 600 MW(t) Core – "Design" Fuel Activit (Cont.)

Nuclide	Half-life	Core Equilibrium (Ci)	Average Power Element After 3 Years Operation			
			Initial (Ci)	1-Day Decay (Ci)	10-Day Decay (Ci)	100-Day Decay (Ci)
SB132	2.1-M	1.11E+07	1.09E+04	0.00E+00	0.00E+00	0.00E+00
TE132	78.-H	2.71E+07	2.65E+04	2.14E+04	3.15E+03	0.00E+00
I132	2.29-H	2.80E+07	2.75E+04	2.21E+04	3.24E+03	0.00E+00
XE132	STABLE	1.52E+04	1.98E+01	1.98E+01	1.98E+01	1.98E+01
SB133	2.4-M	1.48E+07	1.45E+04	0.00E+00	0.00E+00	0.00E+00
TE133M	55.4-M	2.00E+07	1.96E+04	2.99E-04	0.00E+00	0.00E+00
TE133	12.5-M	1.65E+07	1.62E+04	5.01E-05	0.00E+00	0.00E+00
I133	20.8-H	3.60E+07	3.53E+04	1.63E+04	1.22E+01	0.00E+00
XE133M	2.23-D	1.21E+06	1.19E+03	1.04E+03	8.08E+01	0.00E+00
XE133	5.29-D	3.63E+07	3.56E+04	3.40E+04	1.16E+04	8.77E-02
CS133	STABLE	1.98E+04	2.59E+01	2.59E+01	2.60E+01	2.60E+01
TE134	42.-M	3.58E+07	3.51E+04	0.00E+00	0.00E+00	0.00E+00
I134M	3.6-M	5.94E+06	5.82E+03	0.00E+00	0.00E+00	0.00E+00
I134	52.6-M	4.01E+07	3.93E+04	1.03E-03	0.00E+00	0.00E+00
XE134	STABLE	2.23E+04	2.91E+01	2.91E+01	2.91E+01	2.91E+01
CS134	2.06-Y	1.90E+06	2.31E+03	2.31E+03	2.29E+03	2.11E+03
I135	6.59-H	3.68E+07	3.60E+04	2.88E+03	0.00E+00	0.00E+00
XE135M	15.3-M	8.73E+06	8.56E+03	4.41E+02	0.00E+00	0.00E+00
XE135	9.17-H	4.82E+06	4.73E+03	7.30E+03	1.10E-03	0.00E+00
CS135	STABLE	2.19E+04	2.87E+01	2.87E+01	2.87E+01	2.87E+01
I136	85.-S	1.95E+07	1.91E+04	0.00E+00	0.00E+00	0.00E+00
XE136	STABLE	1.93E+04	2.53E+01	2.53E+01	2.53E+01	2.53E+01
CS136	13.0-D	3.38E+05	3.31E+02	3.14E+02	1.94E+02	1.60E+00
XE137	3.84-M	3.52E+07	3.46E+04	0.00E+00	0.00E+00	0.00E+00
CS137	30.1-Y	1.69E+06	2.20E+03	2.20E+03	2.20E+03	2.19E+03
BA137M	2.55-M	1.61E+06	2.09E+03	2.08E+03	2.08E+03	2.07E+03
BA137	STABLE	1.05E+03	1.65E+00	1.65E+00	1.65E+00	1.66E+00
XE138	14.2-M	3.34E+07	3.28E+04	0.00E+00	0.00E+00	0.00E+00
CS138M	2.9-M	2.30E+06	2.26E+03	0.00E+00	0.00E+00	0.00E+00
CS138	32.2-M	3.47E+07	3.41E+04	0.00E+00	0.00E+00	0.00E+00
BA138	STABLE	1.99E+04	2.60E+01	2.60E+01	2.60E+01	2.60E+01

Table A-1. 600 MW(t) Core – "Design" Fuel Activit (Cont.)

Nuclide	Half-life	Core Equilibrium (Ci)	Average Power Element After 3 Years Operation			
			Initial (Ci)	1-Day Decay (Ci)	10-Day Decay (Ci)	100-Day Decay (Ci)
XE139	39.7-S	2.69E+07	2.64E+04	0.00E+00	0.00E+00	0.00E+00
CS139	9.3-M	3.28E+07	3.22E+04	0.00E+00	0.00E+00	0.00E+00
BA139	83.3-M	3.32E+07	3.25E+04	2.28E-01	0.00E+00	0.00E+00
LA139	STABLE	1.89E+04	2.47E+01	2.47E+01	2.47E+01	2.47E+01
XE140	13.6-S	1.95E+07	1.91E+04	0.00E+00	0.00E+00	0.00E+00
CS140	63.8-S	2.98E+07	2.92E+04	0.00E+00	0.00E+00	0.00E+00
BA140	12.8-D	3.26E+07	3.20E+04	3.03E+04	1.86E+04	1.42E+02
LA140	40.2-H	3.27E+07	3.20E+04	3.17E+04	2.13E+04	1.63E+02
CE140	STABLE	1.87E+04	2.45E+01	2.45E+01	2.45E+01	2.46E+01
BA141	18.3-M	3.01E+07	2.95E+04	0.00E+00	0.00E+00	0.00E+00
LA141	3.87-H	3.02E+07	2.96E+04	4.36E+02	0.00E+00	0.00E+00
CE141	32.5-D	3.02E+07	2.96E+04	2.91E+04	2.40E+04	3.53E+03
PR141	STABLE	1.74E+04	2.28E+01	2.28E+01	2.30E+01	2.37E+01
BA142	10.7-M	3.01E+07	2.95E+04	0.00E+00	0.00E+00	0.00E+00
LA142	92.4-M	3.06E+07	3.00E+04	6.90E-01	0.00E+00	0.00E+00
CE142	STABLE	1.78E+04	2.33E+01	2.33E+01	2.33E+01	2.33E+01
LA143	14.-M	3.07E+07	3.01E+04	0.00E+00	0.00E+00	0.00E+00
CE143	33.0-H	3.09E+07	3.03E+04	1.84E+04	1.97E+02	0.00E+00
PR143	13.58D	3.09E+07	3.03E+04	2.99E+04	2.02E+04	2.05E+02
ND143	STABLE	9.84E+03	1.13E+01	1.14E+01	1.15E+01	1.18E+01
CE144	284.-D	2.33E+07	2.57E+04	2.56E+04	2.50E+04	2.01E+04
PR144	17.3-M	2.33E+07	2.57E+04	2.56E+04	2.50E+04	2.01E+04
ND144	STABLE	1.43E+04	2.02E+01	2.02E+01	2.02E+01	2.02E+01
CE145	3.3-M	2.04E+07	2.00E+04	0.00E+00	0.00E+00	0.00E+00
PR145	5.98-H	2.04E+07	2.00E+04	1.25E+03	0.00E+00	0.00E+00
ND145	STABLE	1.21E+04	1.58E+01	1.58E+01	1.58E+01	1.58E+01
CE146	14.2-M	1.54E+07	1.51E+04	0.00E+00	0.00E+00	0.00E+00
PR146	24.2-M	1.55E+07	1.52E+04	0.00E+00	0.00E+00	0.00E+00
ND146	STABLE	9.27E+03	1.21E+01	1.21E+01	1.21E+01	1.21E+01
CE147	70.-S	1.21E+07	1.19E+04	0.00E+00	0.00E+00	0.00E+00
PR147	12.-M	1.23E+07	1.21E+04	0.00E+00	0.00E+00	0.00E+00

Table A-1. 600 MW(t) Core – "Design" Fuel Activit (Cont.)

Nuclide	Half-life	Core Equilibrium (Ci)	Average Power Element After 3 Years Operation			
			Initial (Ci)	1-Day Decay (Ci)	10-Day Decay (Ci)	100-Day Decay (Ci)
ND147	11.0-D	1.23E+07	1.21E+04	1.13E+04	6.43E+03	2.20E+01
PM147	2.62-Y	2.25E+06	2.37E+03	2.38E+03	2.42E+03	2.33E+03
SM147	STABLE	7.32E+03	9.65E+00	9.65E+00	9.60E+00	9.69E+00
PR148	2.0-M	1.03E+07	1.01E+04	0.00E+00	0.00E+00	0.00E+00
ND148	STABLE	6.28E+03	8.21E+00	8.21E+00	8.21E+00	8.21E+00
PM148M	41.3-D	5.12E+05	5.02E+02	4.93E+02	4.24E+02	9.36E+01
PM148	5.37-D	3.16E+06	3.10E+03	2.72E+03	8.52E+02	7.68E-03
PR149	2.3-M	7.85E+06	7.70E+03	0.00E+00	0.00E+00	0.00E+00
ND149	1.73-H	7.93E+06	7.77E+03	5.30E-01	0.00E+00	0.00E+00
PM149	53.1-H	7.75E+06	7.60E+03	5.75E+03	3.43E+02	0.00E+00
SM149	STABLE	1.68E+01	1.64E-02	2.11E-02	3.47E-02	3.56E-02
ND150	STABLE	3.99E+03	5.22E+00	5.22E+00	5.22E+00	5.22E+00
ND151	12.4-M	4.86E+06	4.76E+03	0.00E+00	0.00E+00	0.00E+00
PM151	28.4-H	4.87E+06	4.78E+03	2.68E+03	1.37E+01	0.00E+00
SM151	93.-Y	3.98E+03	3.90E+00	3.97E+00	4.07E+00	4.06E+00
EU151	STABLE	9.20E+01	9.02E-02	8.70E-02	8.29E-02	8.32E-02
ND152	11.5-M	3.82E+06	3.74E+03	0.00E+00	0.00E+00	0.00E+00
PM152	4.1-M	3.85E+06	3.78E+03	0.00E+00	0.00E+00	0.00E+00
SM152	STABLE	9.09E+02	9.79E-01	9.79E-01	9.79E-01	9.79E-01
EU152	13.-Y	1.32E+00	1.71E-03	1.71E-03	1.70E-03	1.68E-03
ND153	67.5-S	2.64E+06	2.59E+03	0.00E+00	0.00E+00	0.00E+00
PM153	5.4-M	2.85E+06	2.79E+03	0.00E+00	0.00E+00	0.00E+00
SM153	46.5-H	2.82E+06	2.76E+03	1.94E+03	7.74E+01	0.00E+00
EU153	STABLE	6.15E+02	6.52E-01	6.54E-01	6.58E-01	6.58E-01
ND154	7.73-D	1.67E+06	1.64E+03	1.50E+03	6.67E+02	2.08E-01
PM154	2.8-M	1.87E+06	1.84E+03	1.50E+03	6.67E+02	2.08E-01
SM154	STABLE	1.27E+03	1.65E+00	1.65E+00	1.65E+00	1.65E+00
EU154	8.6-Y	6.93E+04	8.88E+01	8.88E+01	8.87E+01	8.69E+01
SM155	22.2-M	1.26E+06	1.23E+03	0.00E+00	0.00E+00	0.00E+00
EU155	4.8-Y	2.22E+04	2.80E+01	2.80E+01	2.79E+01	2.70E+01
GD155	STABLE	9.99E+00	9.84E-03	9.84E-03	1.01E-02	1.24E-02

Table A-1. 600 MW(t) Core – "Design" Fuel Activit (Cont.)

Nuclide	Half-life	Core Equilibrium (Ci)	Average Power Element After 3 Years Operation			
			Initial (Ci)	1-Day Decay (Ci)	10-Day Decay (Ci)	100-Day Decay (Ci)
SM156	9.4-H	9.11E+05	8.93E+02	1.52E+02	1.85E-05	0.00E+00
EU156	15.2-D	8.49E+05	8.32E+02	8.14E+02	5.43E+02	8.95E+00
GD156	STABLE	5.51E+02	7.12E-01	7.12E-01	7.17E-01	7.27E-01
SM157	83.-S	7.07E+05	6.94E+02	0.00E+00	0.00E+00	0.00E+00
EU157	15.2-H	7.09E+05	6.95E+02	2.33E+02	1.23E-02	0.00E+00
GD157	STABLE	1.20E+00	1.18E-03	1.53E-03	1.71E-03	1.71E-03
	TOTALS	2.65E+09	2.61E+06	7.00E+05	3.93E+05	1.40E+05

Note: * Stable Nuclides are given in grams.

Table A-2. 600 MW(t) Core – "Maximum Expected" Fuel Activity

Nuclide	Half-life	Core Equilibrium (Ci)	Average Power Element After 3 Years Operation			
			Initial (Ci)	1-Day Decay (Ci)	10-Day Decay (Ci)	100-Day Decay (Ci)
H3	12.3-Y	3.32E+03	[4.12E+00]	[4.12E+00]	[4.11E+00]	[4.05E+00]
C14	5730-Y	1.18E+02	1.55E-01	1.55E-01	1.55E-01	1.55E-01
GE79	43.0-S	2.07E+05	2.03E+02	0.00E+00	0.00E+00	0.00E+00
AS79	9.0-M	2.24E+05	2.20E+02	0.00E+00	0.00E+00	0.00E+00
SE79M	3.89-M	2.24E+05	2.20E+02	0.00E+00	0.00E+00	0.00E+00
*SE79	STABLE	7.26E+01	9.50E-02	9.50E-02	9.50E-02	9.50E-02
SE80	STABLE	1.99E+02	2.60E-01	2.60E-01	2.60E-01	2.60E-01
SE81	18.5-M	9.17E+05	8.99E+02	0.00E+00	0.00E+00	0.00E+00
BR81	STABLE	3.05E+02	3.98E-01	3.98E-01	3.98E-01	3.98E-01
SE82	STABLE	4.77E+02	6.23E-01	6.23E-01	6.23E-01	6.23E-01
SE83M	70.-S	1.04E+06	1.02E+03	0.00E+00	0.00E+00	0.00E+00
SE83	22.5-M	1.15E+06	1.13E+03	0.00E+00	0.00E+00	0.00E+00
BR83	2.4-H	2.26E+06	2.22E+03	2.38E+00	0.00E+00	0.00E+00
KR83M	1.86-H	2.26E+06	2.22E+03	9.57E+00	0.00E+00	0.00E+00
KR83	STABLE	7.70E+02	1.01E+00	1.01E+00	1.01E+00	1.01E+00
SE84	3.3-M	3.84E+06	3.77E+03	0.00E+00	0.00E+00	0.00E+00
BR84	31.8-M	3.95E+06	3.88E+03	0.00E+00	0.00E+00	0.00E+00
KR84	STABLE	1.40E+03	1.83E+00	1.83E+00	1.83E+00	1.83E+00
BR85	2.87-M	5.20E+06	5.10E+03	0.00E+00	0.00E+00	0.00E+00
KR85M	4.48-H	5.21E+06	5.11E+03	1.26E+02	0.00E+00	0.00E+00
KR85	10.73Y	1.46E+05	1.88E+02	1.88E+02	1.88E+02	1.85E+02
RB85	STABLE	1.48E+03	1.95E+00	1.95E+00	1.95E+00	1.96E+00
KR86	STABLE	2.73E+03	3.56E+00	3.56E+00	3.56E+00	3.56E+00
KR87	76.-M	9.90E+06	9.70E+03	1.92E-02	0.00E+00	0.00E+00
RB87	STABLE	3.58E+03	4.68E+00	4.68E+00	4.68E+00	4.68E+00
KR88	2.8-H	1.38E+07	1.35E+04	3.56E+01	0.00E+00	0.00E+00
RB88	17.7-M	1.41E+07	1.39E+04	3.98E+01	0.00E+00	0.00E+00
SR88	STABLE	5.10E+03	6.67E+00	6.67E+00	6.67E+00	6.67E+00

Table A-2. 600 MW(t) Core – "Maximum Expected" Fuel Activit (Cont.)

Nuclide	Half-life	Core Equilibrium (Ci)	Average Power Element After 3 Years Operation			
			Initial (Ci)	1-Day Decay (Ci)	10-Day Decay (Ci)	100-Day Decay (Ci)
KR89	3.16-M	1.74E+07	1.71E+04	0.00E+00	0.00E+00	0.00E+00
RB89	15.2-M	1.86E+07	1.82E+04	0.00E+00	0.00E+00	0.00E+00
SR89	50.5-D	1.87E+07	1.83E+04	1.81E+04	1.60E+04	4.65E+03
Y89	STABLE	6.83E+03	8.93E+00	8.94E+00	9.01E+00	9.40E+00
KR90	32.3-S	1.88E+07	1.85E+04	0.00E+00	0.00E+00	0.00E+00
RB90M	4.28-M	5.18E+06	5.08E+03	0.00E+00	0.00E+00	0.00E+00
RB90	2.7-M	1.77E+07	1.73E+04	0.00E+00	0.00E+00	0.00E+00
SR90	29.-Y	1.12E+06	1.46E+03	1.46E+03	1.46E+03	1.45E+03
Y90	64.-H	1.12E+06	1.46E+03	1.46E+03	1.46E+03	1.45E+03
ZR90	STABLE	4.59E+02	7.17E-01	7.17E-01	7.17E-01	7.17E-01
KR91	9.0-S	1.25E+07	1.22E+04	0.00E+00	0.00E+00	0.00E+00
RB91	58.5-S	2.22E+07	2.17E+04	0.00E+00	0.00E+00	0.00E+00
SR91	9.48-H	2.36E+07	2.32E+04	4.01E+03	5.55E-04	0.00E+00
Y91	58.6-D	2.36E+07	2.32E+04	2.30E+04	2.07E+04	7.14E+03
ZR91	STABLE	8.81E+03	1.15E+01	1.15E+01	1.16E+01	1.22E+01
SR92	2.71-H	2.45E+07	2.41E+04	5.19E+01	0.00E+00	0.00E+00
Y92	3.53-H	2.47E+07	2.43E+04	7.61E+02	0.00E+00	0.00E+00
ZR92	STABLE	9.35E+03	1.22E+01	1.22E+01	1.22E+01	1.22E+01
SR93	7.5-M	2.71E+07	2.66E+04	0.00E+00	0.00E+00	0.00E+00
Y93	10.2-H	2.78E+07	2.72E+04	5.39E+03	2.27E-03	0.00E+00
ZR93	STABLE	1.06E+04	1.38E+01	1.39E+01	1.39E+01	1.39E+01
SR94	1.29-M	2.68E+07	2.63E+04	0.00E+00	0.00E+00	0.00E+00
Y94	19.0-M	2.89E+07	2.83E+04	0.00E+00	0.00E+00	0.00E+00
ZR94	STABLE	1.12E+04	1.46E+01	1.46E+01	1.46E+01	1.46E+01
Y95	10.5-M	2.97E+07	2.91E+04	0.00E+00	0.00E+00	0.00E+00
ZR95	65.5-D	3.01E+07	2.96E+04	2.93E+04	2.66E+04	1.03E+04
NB95M	3.61-D	2.82E+05	2.77E+02	2.80E+02	2.76E+02	1.09E+02
NB95	35.1-D	3.01E+07	2.96E+04	2.96E+04	2.92E+04	1.72E+04
MO95	STABLE	1.17E+04	1.54E+01	1.54E+01	1.54E+01	1.57E+01
Y96	6.0-S	2.82E+07	2.76E+04	0.00E+00	0.00E+00	0.00E+00

Table A-2. 600 MW(t) Core – "Maximum Expected" Fuel Activit (Cont.)

Nuclide	Half-life	Core Equilibrium (Ci)	Average Power Element After 3 Years Operation			
			Initial (Ci)	1-Day Decay (Ci)	10-Day Decay (Ci)	100-Day Decay (Ci)
ZR96	STABLE	1.18E+04	1.54E+01	1.54E+01	1.54E+01	1.54E+01
ZR97	16.8-H	2.94E+07	2.88E+04	1.07E+04	1.44E+00	0.00E+00
NB97	73.6-M	2.96E+07	2.90E+04	1.15E+04	1.56E+00	0.00E+00
MO97	STABLE	1.18E+04	1.54E+01	1.54E+01	1.54E+01	1.54E+01
NB98	51.0-M	2.04E+05	2.00E+02	6.34E-07	0.00E+00	0.00E+00
MO98	STABLE	1.20E+04	1.57E+01	1.57E+01	1.57E+01	1.57E+01
NB99M	2.5-M	1.11E+07	1.09E+04	0.00E+00	0.00E+00	0.00E+00
NB99	14.0-S	2.06E+07	2.02E+04	0.00E+00	0.00E+00	0.00E+00
MO99	66.2-H	3.20E+07	3.13E+04	2.44E+04	2.52E+03	0.00E+00
TC99M	6.02-H	2.81E+07	2.76E+04	2.34E+04	2.44E+03	0.00E+00
TC99	STABLE	1.30E+04	1.70E+01	1.70E+01	1.70E+01	1.70E+01
NB100M	7.0-S	1.64E+07	1.61E+04	0.00E+00	0.00E+00	0.00E+00
NB100	2.9-M	1.64E+07	1.61E+04	0.00E+00	0.00E+00	0.00E+00
MO100	STABLE	1.36E+04	1.78E+01	1.78E+01	1.78E+01	1.78E+01
MO101	14.6-M	2.81E+07	2.76E+04	0.00E+00	0.00E+00	0.00E+00
TC101	14.2-M	2.81E+07	2.76E+04	0.00E+00	0.00E+00	0.00E+00
RU101	STABLE	1.16E+04	1.52E+01	1.52E+01	1.52E+01	1.52E+01
MO102	11.1-M	2.57E+07	2.52E+04	0.00E+00	0.00E+00	0.00E+00
TC102M	4.3-M	2.57E+07	2.52E+04	0.00E+00	0.00E+00	0.00E+00
RU102	STABLE	1.08E+04	1.41E+01	1.41E+01	1.41E+01	1.41E+01
MO103	60.-S	2.29E+07	2.25E+04	0.00E+00	0.00E+00	0.00E+00
RU103	39.6-D	2.34E+07	2.29E+04	2.25E+04	1.92E+04	3.98E+03
RH103M	56.-M	2.31E+07	2.27E+04	2.23E+04	1.91E+04	3.95E+03
RH103	STABLE	9.87E+03	1.29E+01	1.29E+01	1.29E+01	1.29E+01
MO104	1.6-M	1.74E+07	1.71E+04	0.00E+00	0.00E+00	0.00E+00
TC104	18.-M	1.83E+07	1.79E+04	0.00E+00	0.00E+00	0.00E+00
RU104	STABLE	7.79E+03	1.02E+01	1.02E+01	1.02E+01	1.02E+01
TC105	8.0-M	1.42E+07	1.40E+04	0.00E+00	0.00E+00	0.00E+00
RU105	4.44-H	1.43E+07	1.40E+04	3.41E+02	0.00E+00	0.00E+00
RH105	35.5-H	1.16E+07	1.14E+04	8.32E+03	1.23E+02	0.00E+00
PD105	STABLE	6.16E+03	8.06E+00	8.06E+00	8.07E+00	8.07E+00

Table A-2. 600 MW(t) Core – "Maximum Expected" Fuel Activit (Cont.)

Nuclide	Half-life	Core Equilibrium (Ci)	Average Power Element After 3 Years Operation			
			Initial (Ci)	1-Day Decay (Ci)	10-Day Decay (Ci)	100-Day Decay (Ci)
RU106	369.-D	8.02E+06	9.12E+03	9.10E+03	8.95E+03	7.55E+03
PD106	STABLE	3.67E+03	5.28E+00	5.29E+00	5.33E+00	5.75E+00
RU107	4.2-M	8.11E+06	7.95E+03	0.00E+00	0.00E+00	0.00E+00
RH107	21.7-M	8.13E+06	7.97E+03	0.00E+00	0.00E+00	0.00E+00
PD107	STABLE	3.57E+03	4.66E+00	4.66E+00	4.66E+00	4.66E+00
RU108	4.5-M	5.28E+06	5.18E+03	0.00E+00	0.00E+00	0.00E+00
PD108	STABLE	2.14E+03	2.73E+00	2.73E+00	2.73E+00	2.73E+00
RH109	1.5-M	4.08E+06	4.00E+03	0.00E+00	0.00E+00	0.00E+00
PD109M	4.69-M	2.05E+06	2.01E+03	0.00E+00	0.00E+00	0.00E+00
PD109	13.5-H	4.09E+06	4.01E+03	1.17E+03	1.73E-02	0.00E+00
AG109	STABLE	9.70E+02	1.11E+00	1.12E+00	1.12E+00	1.12E+00
PD110	STABLE	7.09E+02	9.27E-01	9.27E-01	9.27E-01	9.27E-01
AG110M	252.-D	2.81E+04	3.06E+01	3.05E+01	2.97E+01	2.32E+01
RH111	63.-S	7.55E+05	7.40E+02	0.00E+00	0.00E+00	0.00E+00
PD111	22.-M	7.94E+05	7.79E+02	0.00E+00	0.00E+00	0.00E+00
AG111M	74.-S	7.97E+05	7.81E+02	0.00E+00	0.00E+00	0.00E+00
AG111	7.47-D	8.02E+05	7.86E+02	7.17E+02	3.11E+02	7.34E-02
CD111	STABLE	3.51E+02	4.56E-01	4.56E-01	4.59E-01	4.61E-01
PD112	20.1-H	3.66E+05	3.59E+02	1.57E+02	9.14E-02	0.00E+00
AG112	3.13-H	3.67E+05	3.60E+02	1.86E+02	1.08E-01	0.00E+00
PD113	1.5-M	2.20E+05	2.15E+02	0.00E+00	0.00E+00	0.00E+00
AG113	5.3-H	1.98E+05	1.94E+02	8.44E+00	0.00E+00	0.00E+00
CD113	STABLE	4.47E-01	4.38E-04	4.74E-04	4.75E-04	4.75E-04
SN119M	245.-D	1.44E+03	1.56E+00	1.55E+00	1.52E+00	1.17E+00
SN119	STABLE	5.39E+01	7.05E-02	7.05E-02	7.06E-02	7.06E-02
SN123	129.-D	2.08E+04	2.11E+01	2.10E+01	2.00E+01	1.23E+01
SB123	STABLE	6.54E+01	8.57E-02	8.58E-02	8.59E-02	8.68E-02
SN125	9.65-D	1.06E+05	1.04E+02	9.66E+01	5.06E+01	7.88E-02
SB125	2.73-Y	1.16E+05	1.44E+02	1.44E+02	1.43E+02	1.35E+02
TE125M	58.-D	2.62E+04	3.23E+01	3.23E+01	3.24E+01	3.16E+01
TE125	STABLE	6.48E+01	9.81E-02	9.82E-02	9.85E-02	1.05E-01

Table A-2. 600 MW(t) Core – "Maximum Expected" Fuel Activit (Cont.)

Nuclide	Half-life	Core Equilibrium (Ci)	Average Power Element After 3 Years Operation			
			Initial (Ci)	1-Day Decay (Ci)	10-Day Decay (Ci)	100-Day Decay (Ci)
SN126	STABLE	3.24E+02	4.24E-01	4.24E-01	4.24E-01	4.24E-01
SB126M	19.0-M	6.29E+05	6.16E+02	5.47E-03	5.47E-03	5.47E-03
SN127M	4.4-M	2.16E+05	2.12E+02	0.00E+00	0.00E+00	0.00E+00
SN127	2.12-H	9.85E+05	9.65E+02	3.77E-01	0.00E+00	0.00E+00
SB127	3.8-D	1.27E+06	1.24E+03	1.06E+03	2.04E+02	1.52E-05
TE127M	109.-D	1.99E+05	1.99E+02	1.99E+02	1.92E+02	1.09E+02
TE127	9.4-H	1.26E+06	1.24E+03	1.16E+03	3.80E+02	1.07E+02
I127	STABLE	6.59E+02	8.64E-01	8.64E-01	8.64E-01	8.64E-01
SN128	59.-M	2.19E+06	2.14E+03	9.63E-05	0.00E+00	0.00E+00
SB128M	10.4-M	2.16E+06	2.12E+03	1.17E-04	0.00E+00	0.00E+00
SB128	9.0-H	1.41E+05	1.38E+02	2.19E+01	1.31E-06	0.00E+00
TE128	STABLE	1.28E+03	1.68E+00	1.68E+00	1.68E+00	1.68E+00
SN129M	2.5-M	2.23E+06	2.18E+03	0.00E+00	0.00E+00	0.00E+00
SN129	7.5-M	1.63E+06	1.60E+03	0.00E+00	0.00E+00	0.00E+00
SB129	4.34-H	4.96E+06	4.86E+03	1.07E+02	0.00E+00	0.00E+00
TE129M	33.4-D	8.76E+05	8.59E+02	8.46E+02	7.02E+02	1.08E+02
TE129	70.-M	4.71E+06	4.62E+03	6.60E+02	4.47E+02	6.90E+01
I129	STABLE	2.66E+03	3.48E+00	3.48E+00	3.48E+00	3.49E+00
SN130	3.7-M	5.72E+06	5.61E+03	0.00E+00	0.00E+00	0.00E+00
SB130M	6.6-M	6.68E+06	6.55E+03	0.00E+00	0.00E+00	0.00E+00
SB130	37.-M	2.33E+06	2.29E+03	0.00E+00	0.00E+00	0.00E+00
TE130	STABLE	5.36E+03	7.01E+00	7.01E+00	7.01E+00	7.01E+00
SN131	63.-S	4.38E+06	4.30E+03	0.00E+00	0.00E+00	0.00E+00
SB131	23.-M	1.33E+07	1.30E+04	0.00E+00	0.00E+00	0.00E+00
TE131M	30.-H	3.07E+06	3.01E+03	1.74E+03	1.18E+01	0.00E+00
TE131	25.-M	1.29E+07	1.27E+04	3.17E+02	2.16E+00	0.00E+00
I131	8.04-D	1.65E+07	1.62E+04	1.50E+04	7.03E+03	3.00E+00
XE131M	12.0-D	2.31E+05	2.26E+02	2.21E+02	1.85E+02	2.03E+00
XE131	STABLE	8.85E+03	1.16E+01	1.16E+01	1.16E+01	1.17E+01
SN132	40.0-S	2.99E+06	2.93E+03	0.00E+00	0.00E+00	0.00E+00
SB132M	4.1-M	5.47E+06	5.36E+03	0.00E+00	0.00E+00	0.00E+00

Table A-2. 600 MW(t) Core – "Maximum Expected" Fuel Activit (Cont.)

Nuclide	Half-life	Core Equilibrium (Ci)	Average Power Element After 3 Years Operation			
			Initial (Ci)	1-Day Decay (Ci)	10-Day Decay (Ci)	100-Day Decay (Ci)
SB132	2.1-M	9.41E+06	9.23E+03	0.00E+00	0.00E+00	0.00E+00
TE132	78.-H	2.37E+07	2.32E+04	1.88E+04	2.75E+03	0.00E+00
I132	2.29-H	2.40E+07	2.36E+04	1.93E+04	2.84E+03	0.00E+00
XE132	STABLE	1.30E+04	1.70E+01	1.70E+01	1.70E+01	1.70E+01
SB133	2.4-M	1.08E+07	1.06E+04	0.00E+00	0.00E+00	0.00E+00
TE133M	55.4-M	1.90E+07	1.87E+04	2.83E-04	0.00E+00	0.00E+00
TE133	12.5-M	1.51E+07	1.48E+04	4.75E-05	0.00E+00	0.00E+00
I133	20.8-H	3.52E+07	3.45E+04	1.59E+04	1.19E+01	0.00E+00
XE133M	2.23-D	1.05E+06	1.03E+03	9.24E+02	7.34E+01	0.00E+00
XE133	5.29-D	3.53E+07	3.46E+04	3.31E+04	1.13E+04	8.52E-02
CS133	STABLE	1.93E+04	2.52E+01	2.52E+01	2.53E+01	2.54E+01
TE134	42.-M	3.20E+07	3.14E+04	0.00E+00	0.00E+00	0.00E+00
I134M	3.6-M	3.07E+06	3.01E+03	0.00E+00	0.00E+00	0.00E+00
I134	52.6-M	3.92E+07	3.85E+04	9.37E-04	0.00E+00	0.00E+00
XE134	STABLE	2.20E+04	2.88E+01	2.88E+01	2.88E+01	2.88E+01
CS134	2.06-Y	1.90E+06	2.31E+03	2.31E+03	2.29E+03	2.11E+03
I135	6.59-H	3.34E+07	3.27E+04	2.61E+03	0.00E+00	0.00E+00
XE135M	15.3-M	6.66E+06	6.53E+03	4.00E+02	0.00E+00	0.00E+00
XE135	9.17-H	4.40E+06	4.31E+03	6.62E+03	9.97E-04	0.00E+00
CS135	STABLE	2.00E+04	2.61E+01	2.61E+01	2.61E+01	2.61E+01
I136	85.-S	1.50E+07	1.47E+04	0.00E+00	0.00E+00	0.00E+00
XE136	STABLE	1.87E+04	2.44E+01	2.44E+01	2.44E+01	2.44E+01
CS136	13.0-D	3.38E+05	3.31E+02	3.14E+02	1.94E+02	1.60E+00
XE137	3.84-M	3.18E+07	3.12E+04	0.00E+00	0.00E+00	0.00E+00
CS137	30.1-Y	1.58E+06	2.06E+03	2.06E+03	2.06E+03	2.05E+03
BA137M	2.55-M	1.51E+06	1.96E+03	1.95E+03	1.95E+03	1.94E+03
BA137	STABLE	9.95E+02	1.55E+00	1.55E+00	1.55E+00	1.56E+00
XE138	14.2-M	3.14E+07	3.07E+04	0.00E+00	0.00E+00	0.00E+00
CS138M	2.9-M	1.28E+06	1.25E+03	0.00E+00	0.00E+00	0.00E+00
CS138	32.2-M	3.33E+07	3.26E+04	0.00E+00	0.00E+00	0.00E+00
BA138	STABLE	1.93E+04	2.52E+01	2.52E+01	2.52E+01	2.52E+01

Table A-2. 600 MW(t) Core – "Maximum Expected" Fuel Activit (Cont.)

Nuclide	Half-life	Core Equilibrium (Ci)	Average Power Element After 3 Years Operation			
			Initial (Ci)	1-Day Decay (Ci)	10-Day Decay (Ci)	100-Day Decay (Ci)
XE139	39.7-S	2.34E+07	2.29E+04	0.00E+00	0.00E+00	0.00E+00
CS139	9.3-M	3.11E+07	3.05E+04	0.00E+00	0.00E+00	0.00E+00
BA139	83.3-M	3.18E+07	3.12E+04	2.19E-01	0.00E+00	0.00E+00
LA139	STABLE	1.81E+04	2.37E+01	2.37E+01	2.37E+01	2.37E+01
XE140	13.6-S	1.60E+07	1.56E+04	0.00E+00	0.00E+00	0.00E+00
CS140	63.8-S	2.77E+07	2.72E+04	0.00E+00	0.00E+00	0.00E+00
BA140	12.8-D	3.14E+07	3.08E+04	2.92E+04	1.79E+04	1.36E+02
LA140	40.2-H	3.15E+07	3.09E+04	3.05E+04	2.06E+04	1.57E+02
CE140	STABLE	1.81E+04	2.36E+01	2.36E+01	2.36E+01	2.37E+01
BA141	18.3-M	2.87E+07	2.81E+04	0.00E+00	0.00E+00	0.00E+00
LA141	3.87-H	2.89E+07	2.84E+04	4.18E+02	0.00E+00	0.00E+00
CE141	32.5-D	2.89E+07	2.84E+04	2.79E+04	2.30E+04	3.38E+03
PR141	STABLE	1.67E+04	2.19E+01	2.19E+01	2.20E+01	2.27E+01
BA142	10.7-M	2.79E+07	2.73E+04	0.00E+00	0.00E+00	0.00E+00
LA142	92.4-M	2.88E+07	2.82E+04	6.48E-01	0.00E+00	0.00E+00
CE142	STABLE	1.68E+04	2.19E+01	2.19E+01	2.19E+01	2.19E+01
LA143	14.-M	2.78E+07	2.73E+04	0.00E+00	0.00E+00	0.00E+00
CE143	33.0-H	2.80E+07	2.74E+04	1.67E+04	1.78E+02	0.00E+00
PR143	13.58D	2.80E+07	2.74E+04	2.71E+04	1.83E+04	1.85E+02
ND143	STABLE	8.90E+03	1.03E+01	1.03E+01	1.04E+01	1.07E+01
CE144	284.-D	2.06E+07	2.27E+04	2.27E+04	2.22E+04	1.78E+04
PR144	17.3-M	2.06E+07	2.27E+04	2.27E+04	2.22E+04	1.78E+04
ND144	STABLE	1.27E+04	1.79E+01	1.79E+01	1.79E+01	1.79E+01
CE145	3.3-M	1.86E+07	1.83E+04	0.00E+00	0.00E+00	0.00E+00
PR145	5.98-H	1.87E+07	1.83E+04	1.14E+03	0.00E+00	0.00E+00
ND145	STABLE	1.11E+04	1.45E+01	1.45E+01	1.45E+01	1.45E+01
CE146	14.2-M	1.45E+07	1.42E+04	0.00E+00	0.00E+00	0.00E+00
PR146	24.2-M	1.46E+07	1.43E+04	0.00E+00	0.00E+00	0.00E+00
ND146	STABLE	8.75E+03	1.14E+01	1.14E+01	1.14E+01	1.14E+01
CE147	70.-S	1.09E+07	1.07E+04	0.00E+00	0.00E+00	0.00E+00
PR147	12.-M	1.14E+07	1.12E+04	0.00E+00	0.00E+00	0.00E+00

Table A-2. 600 MW(t) Core – "Maximum Expected" Fuel Activit (Cont.)

Nuclide	Half-life	Core Equilibrium (Ci)	Average Power Element After 3 Years Operation			
			Initial (Ci)	1-Day Decay (Ci)	10-Day Decay (Ci)	100-Day Decay (Ci)
ND147	11.0-D	1.14E+07	1.12E+04	1.05E+04	5.98E+03	2.05E+01
PM147	2.62-Y	2.09E+06	2.20E+03	2.21E+03	2.25E+03	2.17E+03
SM147	STABLE	6.80E+03	8.97E+00	8.97E+00	8.93E+00	9.01E+00
PR148	2.0-M	8.73E+06	8.56E+03	0.00E+00	0.00E+00	0.00E+00
ND148	STABLE	5.33E+03	6.97E+00	6.97E+00	6.97E+00	6.97E+00
PM148M	41.3-D	5.12E+05	5.02E+02	4.93E+02	4.24E+02	9.36E+01
PM148	5.37-D	3.16E+06	3.10E+03	2.72E+03	8.52E+02	7.68E-03
PR149	2.3-M	5.81E+06	5.70E+03	0.00E+00	0.00E+00	0.00E+00
ND149	1.73-H	6.03E+06	5.91E+03	4.03E-01	0.00E+00	0.00E+00
PM149	53.1-H	5.90E+06	5.78E+03	4.37E+03	2.61E+02	0.00E+00
SM149	STABLE	1.28E+01	1.25E-02	1.61E-02	2.64E-02	2.71E-02
ND150	STABLE	2.55E+03	3.33E+00	3.33E+00	3.33E+00	3.33E+00
ND151	12.4-M	2.93E+06	2.87E+03	0.00E+00	0.00E+00	0.00E+00
PM151	28.4-H	2.97E+06	2.91E+03	1.63E+03	8.38E+00	0.00E+00
SM151	93.-Y	2.43E+03	2.38E+00	2.42E+00	2.48E+00	2.48E+00
EU151	STABLE	5.61E+01	5.50E-02	5.30E-02	5.05E-02	5.07E-02
ND152	11.5-M	1.99E+06	1.95E+03	0.00E+00	0.00E+00	0.00E+00
PM152	4.1-M	2.05E+06	2.01E+03	0.00E+00	0.00E+00	0.00E+00
SM152	STABLE	4.95E+02	5.32E-01	5.32E-01	5.32E-01	5.32E-01
EU152	13.-Y	1.32E+00	1.71E-03	1.71E-03	1.70E-03	1.68E-03
ND153	67.5-S	1.10E+06	1.08E+03	0.00E+00	0.00E+00	0.00E+00
PM153	5.4-M	1.33E+06	1.30E+03	0.00E+00	0.00E+00	0.00E+00
SM153	46.5-H	1.32E+06	1.30E+03	9.07E+02	3.63E+01	0.00E+00
EU153	STABLE	2.88E+02	3.06E-01	3.07E-01	3.08E-01	3.09E-01
ND154	7.73-D	5.28E+05	5.18E+02	4.73E+02	2.11E+02	6.60E-02
PM154	2.8-M	6.80E+05	6.67E+02	4.74E+02	2.11E+02	6.60E-02
SM154	STABLE	5.18E+02	6.73E-01	6.73E-01	6.73E-01	6.73E-01
EU154	8.6-Y	6.93E+04	8.88E+01	8.88E+01	8.87E+01	8.69E+01
SM155	22.2-M	4.72E+05	4.63E+02	0.00E+00	0.00E+00	0.00E+00
EU155	4.8-Y	2.22E+04	2.80E+01	2.80E+01	2.79E+01	2.69E+01
GD155	STABLE	3.43E+00	3.41E-03	3.43E-03	3.66E-03	5.97E-03

Table A-2. 600 MW(t) Core – "Maximum Expected" Fuel Activit (Cont.)

Nuclide	Half-life	Core Equilibrium (Ci)	Average Power Element After 3 Years Operation			
			Initial (Ci)	1-Day Decay (Ci)	10-Day Decay (Ci)	100-Day Decay (Ci)
SM156	9.4-H	3.05E+05	2.99E+02	5.09E+01	6.18E-06	0.00E+00
EU156	15.2-D	2.86E+05	2.81E+02	2.75E+02	1.83E+02	3.02E+00
GD156	STABLE	1.86E+02	2.40E-01	2.40E-01	2.42E-01	2.45E-01
SM157	83.-S	1.92E+05	1.88E+02	0.00E+00	0.00E+00	0.00E+00
EU157	15.2-H	1.98E+05	1.94E+02	6.50E+01	3.42E-03	0.00E+00
GD157	STABLE	3.36E-01	3.29E-04	4.27E-04	4.77E-04	4.77E-04
	TOTALS	2.12E+09	2.09E+06	5.77E+05	3.16E+05	1.07E+05

Note: * Stable Nuclides are given in grams.

Table A-3. 600 MW(t) Core – "Design" Circuit Activity

Nuclide	Half-life	Circulating Activity (Ci)	Purification Sys. Activity (Ci)	Plateout Activity (Ci)		
				Initial	1-Day Decay	10-Day Decay
H3	12.3-Y	[2.40E-01]	[4.26E+03]	0.00E+00	0.00E+00	0.00E+00
C14	5730-Y	0.00E+00	0.00E+00	0.00E+00	0.00E+00	0.00E+00
GE79	43.0-S	9.51E-03	4.50E-06	9.94E-03	0.00E+00	0.00E+00
AS79	9.0-M	1.43E+01	1.42E-02	2.24E+01	0.00E+00	0.00E+00
SE79M	3.89-M	4.67E+00	5.74E-03	9.08E+00	0.00E+00	0.00E+00
*SE79	STABLE	4.02E-07	3.17E-04	5.62E-01	5.62E-01	5.62E-01
SE80	STABLE	1.02E-06	8.67E-04	1.32E+00	1.32E+00	1.32E+00
SE81	18.5-M	4.64E-01	6.49E-04	1.01E+00	0.00E+00	0.00E+00
BR81	STABLE	1.56E-06	1.33E-03	2.04E+00	2.04E+00	2.04E+00
SE82	STABLE	2.43E-06	2.08E-03	3.18E+00	3.18E+00	3.18E+00
SE83M	70.-S	2.68E-01	1.48E-04	2.88E-01	0.00E+00	0.00E+00
SE83	22.5-M	5.74E-01	8.99E-04	1.39E+00	0.00E+00	0.00E+00
BR83	2.4-H	7.67E-01	5.58E-03	8.61E+00	8.66E-03	0.00E+00
KR83M	1.86-H	1.20E+01	1.13E+00	0.00E+00	0.00E+00	0.00E+00
KR83	STABLE	1.25E-04	5.14E+00	0.00E+00	0.00E+00	0.00E+00
SE84	3.3-M	1.48E+00	1.06E-03	1.78E+00	0.00E+00	0.00E+00
BR84	31.8-M	2.38E+00	4.76E-03	7.49E+00	0.00E+00	0.00E+00
KR84	STABLE	2.24E-04	9.34E+00	0.00E+00	0.00E+00	0.00E+00
BR85	2.87-M	1.91E+00	1.33E-03	2.26E+00	0.00E+00	0.00E+00
KR85M	4.48-H	1.55E+01	7.74E+00	0.00E+00	0.00E+00	0.00E+00
KR85	10.73Y	2.53E-02	2.82E+02	0.00E+00	0.00E+00	0.00E+00
RB85	STABLE	3.23E-06	3.19E-03	4.22E+00	4.22E+00	4.22E+00
KR86	STABLE	4.32E-04	1.82E+01	0.00E+00	0.00E+00	0.00E+00
KR87	76.-M	1.91E+01	2.97E+00	0.00E+00	0.00E+00	0.00E+00
RB87	STABLE	7.67E-06	7.68E-02	1.00E+01	1.00E+01	1.00E+01
KR88	2.8-H	3.40E+01	1.17E+01	0.00E+00	0.00E+00	0.00E+00
RB88	17.7-M	4.04E+01	2.92E+01	8.58E+01	0.00E+00	0.00E+00
SR88	STABLE	3.30E-07	2.81E-01	8.67E-01	8.67E-01	8.67E-01

Table A-3. 600 MW(t) Core – "Design" Circuit Activity (Cont.)

Nuclide	Half-life	Circulating Activity (Ci)	Purification Sys. Activity (Ci)	Plateout Activity (Ci)		
				Initial	1-Day Decay	10-Day Decay
KR89	3.16-M	7.87E+00	5.08E-02	0.00E+00	0.00E+00	0.00E+00
RB89	15.2-M	1.05E+01	1.28E-01	2.06E+01	0.00E+00	0.00E+00
SR89	50.5-D	3.52E-03	1.31E-01	2.63E+01	2.60E+01	2.29E+01
Y89	STABLE	6.73E-09	5.72E-06	2.65E-01	2.65E-01	2.65E-01
KR90	32.3-S	3.53E+00	3.88E-03	0.00E+00	0.00E+00	0.00E+00
RB90M	4.28-M	9.59E-01	1.22E-03	1.22E+00	0.00E+00	0.00E+00
RB90	2.7-M	7.47E+00	9.20E-03	8.77E+00	0.00E+00	0.00E+00
SR90	29.-Y	1.59E-05	3.40E-03	1.25E+01	1.25E+01	1.25E+01
Y90	64.-H	2.20E-04	4.12E-03	1.26E+01	1.26E+01	1.25E+01
ZR90	STABLE	4.08E-10	3.45E-05	1.24E-01	1.24E-01	1.24E-01
KR91	9.0-S	1.24E+00	3.79E-04	0.00E+00	0.00E+00	0.00E+00
RB91	58.5-S	3.91E+00	1.47E-03	4.15E+00	0.00E+00	0.00E+00
SR91	9.48-H	1.36E-01	2.21E-03	5.29E+00	9.15E-01	1.27E-07
Y91	58.6-D	2.37E-04	7.42E-04	6.42E+00	6.37E+00	5.74E+00
ZR91	STABLE	8.64E-09	1.47E-05	7.51E-02	7.51E-02	7.52E-02
SR92	2.71-H	1.04E-01	7.70E-04	1.18E+00	2.54E-03	0.00E+00
Y92	3.53-H	8.95E-02	1.55E-03	2.37E+00	4.78E-02	0.00E+00
ZR92	STABLE	9.87E-09	2.34E-05	3.58E-02	3.58E-02	3.58E-02
SR93	7.5-M	8.82E-01	8.17E-04	1.30E+00	0.00E+00	0.00E+00
Y93	10.2-H	5.56E-02	1.69E-03	2.63E+00	5.19E-01	2.18E-07
ZR93	STABLE	1.08E-08	2.61E-05	4.03E-02	4.03E-02	4.03E-02
SR94	1.29-M	1.19E+00	6.74E-04	1.29E+00	0.00E+00	0.00E+00
Y94	19.0-M	1.17E+00	1.57E-03	2.67E+00	0.00E+00	0.00E+00
ZR94	STABLE	2.02E-08	2.55E-05	4.18E-02	4.18E-02	4.18E-02
Y95	10.5-M	8.57E-01	9.07E-04	1.43E+00	0.00E+00	0.00E+00
ZR95	65.5-D	3.85E-04	1.85E-03	2.87E+00	2.84E+00	2.59E+00
NB95M	3.61-D	4.10E-05	2.74E-05	4.23E-02	3.99E-02	2.91E-02
NB95	35.1-D	4.51E-04	9.48E-04	4.33E+00	4.30E+00	4.04E+00
MO95	STABLE	1.15E-08	1.97E-05	6.00E-02	6.00E-02	6.00E-02
Y96	6.0-S	1.34E+00	2.11E-04	1.35E+00	0.00E+00	0.00E+00
ZR96	STABLE	2.24E-08	1.21E-05	2.93E-02	2.93E-02	2.93E-02

Table A-3. 600 MW(t) Core – "Design" Circuit Activity (Cont.)

Nuclide	Half-life	Circulating Activity (Ci)	Purification Sys. Activity (Ci)	Plateout Activity (Ci)		
				Initial	1-Day Decay	10-Day Decay
ZR97	16.8-H	2.17E-02	9.23E-04	1.41E+00	5.24E-01	7.07E-05
NB97	73.6-M	2.54E-01	1.85E-03	2.83E+00	5.65E-01	7.62E-05
MO97	STABLE	1.36E-08	2.94E-05	4.50E-02	4.50E-02	4.50E-02
NB98	51.0-M	2.31E-03	6.37E-06	9.79E-03	3.10E-11	0.00E+00
MO98	STABLE	1.18E-08	1.01E-05	1.54E-02	1.54E-02	1.54E-02
NB99M	2.5-M	4.61E-01	3.10E-04	5.34E-01	0.00E+00	0.00E+00
NB99	14.0-S	9.72E-01	2.72E-04	9.87E-01	0.00E+00	0.00E+00
MO99	66.2-H	1.18E-02	1.59E-03	3.06E+00	2.37E+00	2.46E-01
TC99M	6.02-H	5.69E-02	8.83E-04	4.04E+00	2.37E+00	2.38E-01
TC99	STABLE	1.32E-08	2.04E-05	6.43E-02	6.43E-02	6.43E-02
NB100M	7.0-S	7.82E-01	1.38E-04	7.87E-01	0.00E+00	0.00E+00
NB100	2.9-M	6.65E-01	4.64E-04	7.87E-01	0.00E+00	0.00E+00
MO100	STABLE	1.89E-08	1.65E-05	2.60E-02	2.60E-02	2.60E-02
MO101	14.6-M	7.01E-01	8.64E-04	1.35E+00	0.00E+00	0.00E+00
TC101	14.2-M	1.08E+00	1.73E-03	2.70E+00	0.00E+00	0.00E+00
RU101	STABLE	2.06E-08	2.88E-05	4.47E-02	4.47E-02	4.47E-02
MO102	11.1-M	7.24E-01	7.85E-04	1.23E+00	0.00E+00	0.00E+00
TC102M	4.3-M	1.54E+00	1.54E-03	2.47E+00	0.00E+00	0.00E+00
RU102	STABLE	2.37E-08	2.62E-05	4.13E-02	4.13E-02	4.13E-02
MO103	60.-S	1.03E+00	5.45E-04	1.10E+00	0.00E+00	0.00E+00
RU103	39.6-D	5.96E-04	1.28E-03	2.22E+00	2.18E+00	1.86E+00
RH103M	56.-M	2.44E-01	1.99E-03	3.31E+00	2.16E+00	1.85E+00
RH103	STABLE	1.18E-08	8.27E-06	5.02E-02	5.02E-02	5.02E-02
MO104	1.6-M	7.58E-01	4.56E-04	8.35E-01	0.00E+00	0.00E+00
TC104	18.-M	7.63E-01	1.02E-03	1.71E+00	0.00E+00	0.00E+00
RU104	STABLE	1.43E-08	1.81E-05	2.94E-02	2.94E-02	2.94E-02
TC105	8.0-M	4.53E-01	4.30E-04	6.83E-01	0.00E+00	0.00E+00
RU105	4.44-H	6.37E-02	8.79E-04	1.37E+00	3.28E-02	0.00E+00
RH105	35.5-H	5.52E-03	1.33E-03	2.06E+00	1.41E+00	2.08E-02
PD105	STABLE	6.10E-09	5.16E-06	3.15E-02	3.15E-02	3.15E-02
RU106	369.-D	1.55E-05	3.42E-04	5.22E-01	5.21E-01	5.12E-01

Table A-3. 600 MW(t) Core – "Design" Circuit Activity (Cont.)

Nuclide	Half-life	Circulating Activity (Ci)	Purification Sys. Activity (Ci)	Plateout Activity (Ci)		
				Initial	1-Day Decay	10-Day Decay
PD106	STABLE	3.42E-09	7.81E-06	1.05E-02	1.05E-02	1.05E-02
RU107	4.2-M	3.07E-01	2.37E-04	3.89E-01	0.00E+00	0.00E+00
RH107	21.7-M	2.94E-01	4.89E-04	7.80E-01	0.00E+00	0.00E+00
PD107	STABLE	6.13E-09	8.70E-06	1.37E-02	1.37E-02	1.37E-02
RU108	4.5-M	1.97E-01	1.55E-04	2.54E-01	0.00E+00	0.00E+00
PD108	STABLE	2.36E-09	2.02E-06	3.08E-03	3.08E-03	3.08E-03
RH109	1.5-M	1.79E-01	1.06E-04	1.96E-01	0.00E+00	0.00E+00
PD109M	4.69-M	1.45E-01	1.13E-04	1.96E-01	0.00E+00	0.00E+00
PD109	13.5-H	8.24E-03	2.94E-04	4.90E-01	1.43E-01	2.12E-06
AG109	STABLE	1.86E-04	1.59E-01	2.43E+02	2.43E+02	2.43E+02
PD110	STABLE	6.99E-10	5.97E-07	9.12E-04	9.12E-04	9.12E-04
AG110M	252.-D	7.20E-03	1.08E-01	1.66E+02	1.65E+02	1.61E+02
RH111	63.-S	3.40E-02	1.82E-05	3.62E-02	0.00E+00	0.00E+00
PD111	22.-M	3.01E-02	4.28E-05	7.44E-02	0.00E+00	0.00E+00
AG111M	74.-S	6.32E-02	6.24E-05	1.12E-01	0.00E+00	0.00E+00
AG111	7.47-D	5.87E+00	2.63E+00	4.01E+03	3.66E+03	1.59E+03
CD111	STABLE	8.03E-07	3.25E-02	4.97E+01	4.97E+01	4.97E+01
PD112	20.1-H	2.27E-04	1.15E-05	1.76E-02	7.68E-03	4.47E-06
AG112	3.13-H	1.38E-03	2.30E-05	3.52E-02	9.17E-03	5.30E-06
PD113	1.5-M	9.62E-03	5.68E-06	1.05E-02	0.00E+00	0.00E+00
AG113	5.3-H	8.58E-04	1.13E-05	1.90E-02	8.24E-04	0.00E+00
CD113	STABLE	2.07E-07	1.77E-04	2.70E-01	2.70E-01	2.70E-01
SN119M	245.-D	3.61E-09	5.28E-08	8.07E-05	8.05E-05	7.84E-05
SN119	STABLE	5.29E-11	4.59E-08	7.00E-05	7.00E-05	7.00E-05
SN123	129.-D	8.79E-08	6.78E-07	1.04E-03	1.03E-03	9.81E-04
SB123	STABLE	4.11E-10	3.62E-07	5.49E-04	5.49E-04	5.49E-04
SN125	9.65-D	5.76E-06	3.33E-06	5.08E-03	4.73E-03	2.48E-03
SB125	2.73-Y	9.68E-07	6.10E-05	9.32E-02	9.31E-02	9.26E-02
TE125M	58.-D	1.05E-04	9.00E-04	5.64E-01	5.57E-01	5.01E-01
TE125	STABLE	9.21E-08	1.85E-04	1.28E-01	1.28E-01	1.28E-01
SN126	STABLE	3.18E-10	2.72E-07	4.15E-04	4.15E-04	4.15E-04

Table A-3. 600 MW(t) Core – "Design" Circuit Activity (Cont.)

Nuclide	Half-life	Circulating Activity (Ci)	Purification Sys. Activity (Ci)	Plateout Activity (Ci)		
				Initial	1-Day Decay	10-Day Decay
SB126M	19.0-M	1.37E-02	1.95E-05	3.02E-02	5.36E-06	5.36E-06
SN127M	4.4-M	8.12E-03	6.33E-06	1.04E-02	0.00E+00	0.00E+00
SN127	2.12-H	5.21E-03	3.09E-05	4.73E-02	1.85E-05	0.00E+00
SB127	3.8-D	1.16E-03	2.93E-04	4.48E-01	3.74E-01	7.25E-02
TE127M	109.-D	5.92E-04	3.86E-03	5.92E+00	5.89E+00	5.56E+00
TE127	9.4-H	6.03E-02	5.22E-03	8.15E+00	6.28E+00	5.47E+00
I127	STABLE	9.75E-07	4.11E-02	1.39E+00	1.39E+00	1.39E+00
SN128	59.-M	2.21E-02	6.83E-05	1.05E-01	4.72E-09	0.00E+00
SB128M	10.4-M	7.59E-02	1.34E-04	2.08E-01	5.72E-09	0.00E+00
SB128	9.0-H	1.94E-04	4.57E-06	6.99E-03	1.11E-03	6.61E-11
TE128	STABLE	1.90E-06	1.62E-03	2.48E+00	2.48E+00	2.48E+00
SN129M	2.5-M	9.22E-02	6.20E-05	1.07E-01	0.00E+00	0.00E+00
SN129	7.5-M	5.30E-02	4.91E-05	7.82E-02	0.00E+00	0.00E+00
SB129	4.34-H	2.19E-02	2.67E-04	4.23E-01	9.23E-03	0.00E+00
TE129M	33.4-D	4.63E-03	9.26E-03	1.42E+01	1.39E+01	1.15E+01
TE129	70.-M	5.39E-01	7.79E-03	1.21E+01	8.84E+00	7.33E+00
I129	STABLE	3.94E-06	1.66E-01	5.38E+00	5.38E+00	5.38E+00
SN130	3.7-M	2.22E-01	1.65E-04	2.75E-01	0.00E+00	0.00E+00
SB130M	6.6-M	3.67E-01	3.49E-04	5.68E-01	0.00E+00	0.00E+00
SB130	37.-M	4.01E-02	8.93E-05	1.40E-01	0.00E+00	0.00E+00
TE130	STABLE	7.93E-06	6.77E-03	1.03E+01	1.03E+01	1.03E+01
SN131	63.-S	1.97E-01	1.06E-04	2.10E-01	0.00E+00	0.00E+00
SB131	23.-M	3.39E-01	5.17E-04	8.47E-01	0.00E+00	0.00E+00
TE131M	30.-H	8.38E-02	6.33E-03	9.67E+00	5.55E+00	3.78E-02
TE131	25.-M	1.91E+00	3.10E-03	6.85E+00	1.01E+00	6.89E-03
I131	8.04-D	1.81E-01	4.22E+00	1.46E+02	1.34E+02	6.21E+01
XE131M	12.0-D	1.18E-01	2.23E+00	0.00E+00	0.00E+00	0.00E+00
XE131	STABLE	4.55E-04	1.71E+01	0.00E+00	0.00E+00	0.00E+00
SN132	40.0-S	1.38E-01	6.35E-05	1.44E-01	0.00E+00	0.00E+00
SB132M	4.1-M	2.63E-01	1.91E-04	3.34E-01	0.00E+00	0.00E+00
SB132	2.1-M	4.59E-01	2.88E-04	5.24E-01	0.00E+00	0.00E+00

Table A-3. 600 MW(t) Core – "Design" Circuit Activity (Cont.)

Nuclide	Half-life	Circulating Activity (Ci)	Purification Sys. Activity (Ci)	Plateout Activity (Ci)		
				Initial	1-Day Decay	10-Day Decay
TE132	78.-H	4.03E-01	7.83E-02	1.20E+02	9.70E+01	1.42E+01
I132	2.29-H	2.19E+00	6.80E-01	1.41E+02	9.99E+01	1.47E+01
XE132	STABLE	6.45E-04	2.51E+01	0.00E+00	0.00E+00	0.00E+00
SB133	2.4-M	4.50E-01	3.00E-04	5.19E-01	0.00E+00	0.00E+00
TE133M	55.4-M	2.34E+00	6.88E-03	1.06E+01	1.59E-07	0.00E+00
TE133	12.5-M	2.44E+00	3.49E-03	5.46E+00	2.67E-08	0.00E+00
I133	20.8-H	1.20E+00	2.93E+00	1.07E+02	4.82E+01	3.60E-02
XE133M	2.23-D	9.79E-01	3.91E+00	0.00E+00	0.00E+00	0.00E+00
XE133	5.29-D	2.01E+01	2.21E+02	0.00E+00	0.00E+00	0.00E+00
CS133	STABLE	3.99E-05	3.36E-02	5.21E+01	5.21E+01	5.21E+01
TE134	42.-M	4.19E+00	9.97E-03	1.54E+01	0.00E+00	0.00E+00
I134M	3.6-M	3.52E-01	2.59E-03	4.32E-01	0.00E+00	0.00E+00
I134	52.6-M	5.91E+00	5.35E-01	3.69E+01	5.62E-07	0.00E+00
XE134	STABLE	1.02E-03	4.25E+01	0.00E+00	0.00E+00	0.00E+00
CS134	2.06-Y	5.59E-03	2.52E-01	3.84E+02	3.84E+02	3.81E+02
I135	6.59-H	1.88E+00	1.52E+00	4.91E+01	3.92E+00	0.00E+00
XE135M	15.3-M	8.87E+00	2.82E-01	0.00E+00	0.00E+00	0.00E+00
XE135	9.17-H	2.76E+01	1.09E+01	0.00E+00	0.00E+00	0.00E+00
CS135	STABLE	4.16E-05	3.48E-02	5.42E+01	5.42E+01	5.42E+01
I136	85.-S	1.21E+00	3.52E-03	1.32E+00	0.00E+00	0.00E+00
XE136	STABLE	8.58E-04	3.60E+01	0.00E+00	0.00E+00	0.00E+00
CS136	13.0-D	2.84E-02	2.21E-02	3.38E+01	3.20E+01	1.98E+01
XE137	3.84-M	4.58E+00	3.60E-02	0.00E+00	0.00E+00	0.00E+00
CS137	30.1-Y	3.34E-03	1.66E+00	2.44E+03	2.44E+03	2.44E+03
BA137M	2.55-M	6.51E-02	1.57E+00	2.31E+03	2.31E+03	2.30E+03
BA137	STABLE	6.40E-09	1.01E-04	3.65E+01	3.65E+01	3.65E+01
XE138	14.2-M	8.50E+00	2.47E-01	0.00E+00	0.00E+00	0.00E+00
CS138M	2.9-M	5.18E-02	3.61E-05	6.13E-02	0.00E+00	0.00E+00
CS138	32.2-M	7.52E+00	6.18E-01	2.29E+01	0.00E+00	0.00E+00
BA138	STABLE	2.09E-07	1.04E-04	5.04E-01	5.04E-01	5.04E-01
XE139	39.7-S	1.40E+00	1.90E-03	0.00E+00	0.00E+00	0.00E+00

Table A-3. 600 MW(t) Core – "Design" Circuit Activity (Cont.)

Nuclide	Half-life	Circulating Activity (Ci)	Purification Sys. Activity (Ci)	Plateout Activity (Ci)		
				Initial	1-Day Decay	10-Day Decay
CS139	9.3-M	3.15E+00	5.70E-03	5.01E+00	0.00E+00	0.00E+00
BA139	83.3-M	7.44E-01	6.69E-03	6.53E+00	4.47E-05	0.00E+00
LA139	STABLE	2.65E-08	1.52E-05	1.22E-01	1.22E-01	1.22E-01
XE140	13.6-S	5.87E-01	2.72E-04	0.00E+00	0.00E+00	0.00E+00
CS140	63.8-S	2.62E+00	1.35E-03	2.80E+00	0.00E+00	0.00E+00
BA140	12.8-D	1.05E-02	7.68E-03	1.25E+01	1.18E+01	7.25E+00
LA140	40.2-H	9.87E-03	9.89E-04	1.40E+01	1.33E+01	8.34E+00
CE140	STABLE	1.78E-08	3.03E-05	2.37E-01	2.37E-01	2.37E-01
BA141	18.3-M	6.38E-01	8.86E-04	1.38E+00	0.00E+00	0.00E+00
LA141	3.87-H	1.29E-01	1.79E-03	2.77E+00	3.92E-02	0.00E+00
CE141	32.5-D	5.10E-04	2.70E-03	4.15E+00	4.08E+00	3.37E+00
PR141	STABLE	1.64E-08	1.40E-05	8.54E-02	8.54E-02	8.55E-02
BA142	10.7-M	7.98E-01	8.51E-04	1.34E+00	0.00E+00	0.00E+00
LA142	92.4-M	3.17E-01	1.75E-03	2.72E+00	5.91E-05	0.00E+00
CE142	STABLE	2.02E-08	4.12E-05	6.37E-02	6.37E-02	6.37E-02
LA143	14.-M	7.07E-01	8.54E-04	1.33E+00	0.00E+00	0.00E+00
CE143	33.0-H	1.62E-02	1.73E-03	2.68E+00	1.62E+00	1.74E-02
PR143	13.58D	1.09E-03	2.61E-03	4.02E+00	3.92E+00	2.59E+00
ND143	STABLE	1.60E-08	1.37E-05	8.34E-02	8.34E-02	8.34E-02
CE144	284.-D	4.66E-05	7.93E-04	1.21E+00	1.21E+00	1.18E+00
PR144	17.3-M	4.72E-01	1.57E-03	2.20E+00	1.21E+00	1.18E+00
ND144	STABLE	1.76E-08	3.70E-05	5.02E-02	5.02E-02	5.02E-02
CE145	3.3-M	7.40E-01	5.34E-04	8.95E-01	0.00E+00	0.00E+00
PR145	5.98-H	6.89E-02	1.12E-03	1.79E+00	1.11E-01	0.00E+00
ND145	STABLE	1.17E-08	2.71E-05	4.26E-02	4.26E-02	4.26E-02
CE146	14.2-M	3.67E-01	4.46E-04	6.97E-01	0.00E+00	0.00E+00
PR146	24.2-M	4.22E-01	9.00E-04	1.40E+00	0.00E+00	0.00E+00
ND146	STABLE	1.38E-08	2.17E-05	3.35E-02	3.35E-02	3.35E-02
CE147	70.-S	4.87E-01	2.69E-04	5.23E-01	0.00E+00	0.00E+00
PR147	12.-M	5.88E-01	6.19E-04	1.07E+00	0.00E+00	0.00E+00
ND147	11.0-D	1.13E-03	9.79E-04	1.62E+00	1.52E+00	8.63E-01

Table A-3. 600 MW(t) Core – "Design" Circuit Activity (Cont.)

Nuclide	Half-life	Circulating Activity (Ci)	Purification Sys. Activity (Ci)	Plateout Activity (Ci)		
				Initial	1-Day Decay	10-Day Decay
PM147	2.62-Y	6.30E-06	3.60E-04	2.17E+00	2.17E+00	2.16E+00
SM147	STABLE	4.26E-08	4.24E-05	9.05E-02	9.05E-02	9.05E-02
PR148	2.0-M	3.72E-01	2.36E-04	4.19E-01	0.00E+00	0.00E+00
ND148	STABLE	9.84E-09	8.29E-06	1.36E-02	1.36E-02	1.36E-02
PM148M	41.3-D	6.51E-06	1.61E-05	2.46E-02	2.41E-02	2.08E-02
PM148	5.37-D	3.09E-04	9.93E-05	1.52E-01	1.33E-01	4.17E-02
PR149	2.3-M	2.43E-01	1.60E-04	2.79E-01	0.00E+00	0.00E+00
ND149	1.73-H	7.03E-02	3.49E-04	5.68E-01	3.83E-05	0.00E+00
PM149	53.1-H	1.77E-03	5.39E-04	8.58E-01	6.41E-01	3.82E-02
SM149	STABLE	2.32E-08	1.98E-05	4.42E-02	4.42E-02	4.42E-02
ND150	STABLE	2.50E-09	2.14E-06	3.26E-03	3.26E-03	3.26E-03
ND151	12.4-M	7.88E-02	8.98E-05	1.41E-01	0.00E+00	0.00E+00
PM151	28.4-H	2.03E-03	1.83E-04	2.83E-01	1.58E-01	8.12E-04
SM151	93.-Y	2.95E-07	2.68E-04	4.11E-01	4.11E-01	4.11E-01
EU151	STABLE	1.32E-08	1.12E-05	2.49E-02	2.49E-02	2.49E-02
ND152	11.5-M	5.54E-02	6.10E-05	9.57E-02	0.00E+00	0.00E+00
PM152	4.1-M	1.22E-01	1.21E-04	1.94E-01	0.00E+00	0.00E+00
SM152	STABLE	9.79E-09	9.03E-06	1.40E-02	1.40E-02	1.40E-02
EU152	13.-Y	8.85E-12	2.39E-09	3.64E-06	3.64E-06	3.64E-06
ND153	67.5-S	4.93E-02	2.69E-05	5.28E-02	0.00E+00	0.00E+00
PM153	5.4-M	8.41E-02	6.62E-05	1.16E-01	0.00E+00	0.00E+00
SM153	46.5-H	8.33E-04	1.08E-04	1.81E-01	1.26E-01	5.05E-03
EU153	STABLE	5.26E-09	4.48E-06	9.85E-03	9.85E-03	9.85E-03
ND154	7.73-D	3.59E-05	1.66E-05	2.54E-02	2.32E-02	1.03E-02
PM154	2.8-M	2.77E-02	3.58E-05	5.80E-02	2.32E-02	1.03E-02
SM154	STABLE	3.70E-09	3.46E-06	5.34E-03	5.34E-03	5.34E-03
EU154	8.6-Y	4.78E-07	8.88E-05	1.36E-01	1.36E-01	1.35E-01
SM155	22.2-M	9.41E-03	1.46E-05	2.27E-02	0.00E+00	0.00E+00
EU155	4.8-Y	2.23E-07	3.18E-05	4.89E-02	4.89E-02	4.87E-02
GD155	STABLE	2.91E-10	8.24E-07	1.32E-03	1.32E-03	1.32E-03
SM156	9.4-H	4.00E-04	9.62E-06	1.47E-02	2.50E-03	3.04E-10

Table A-3. 600 MW(t) Core – "Design" Circuit Activity (Cont.)

Nuclide	Half-life	Circulating Activity (Ci)	Purification Sys. Activity (Ci)	Plateout Activity (Ci)		
				Initial	1-Day Decay	10-Day Decay
EU156	15.2-D	6.87E-05	7.18E-05	1.10E-01	1.05E-01	6.98E-02
GD156	STABLE	1.95E-10	1.39E-06	2.13E-03	2.13E-03	2.13E-03
SM157	83.-S	8.46E-03	4.89E-06	9.20E-03	0.00E+00	0.00E+00
EU157	15.2-H	3.06E-04	1.12E-05	1.88E-02	6.28E-03	3.31E-07
GD157	STABLE	1.30E-10	2.99E-07	4.86E-04	4.86E-04	4.86E-04
	TOTALS	3.29E+02	4.85E+03	1.04E+04	9.53E+03	7.10E+03

Note: * Stable Nuclides are given in grams.

Table A-4. 600 MW(t) Core – "Maximum Expected" Circuit Activity

Nuclide	Half-life	Circulating Activity (Ci)	Purification Sys. Activity (Ci)	Plateout Activity (Ci)		
				Initial	1-Day Decay	10-Day Decay
H3	12.3-Y	[6.00E-02]	[1.06E+03]	0.00E+00	0.00E+00	0.00E+00
C14	5730-Y	0.00E+00	0.00E+00	0.00E+00	0.00E+00	0.00E+00
GE79	43.0-S	3.07E-04	4.50E-07	9.94E-04	0.00E+00	0.00E+00
AS79	9.0-M	7.71E-02	1.42E-03	2.24E+00	0.00E+00	0.00E+00
SE79M	3.89-M	8.01E-03	1.43E-03	2.27E+00	0.00E+00	0.00E+00
*SE79	STABLE	1.89E-09	7.92E-05	1.41E-01	1.41E-01	1.41E-01
SE80	STABLE	5.16E-09	2.17E-04	3.31E-01	3.31E-01	3.31E-01
SE81	18.5-M	4.29E-03	1.62E-04	2.52E-01	0.00E+00	0.00E+00
BR81	STABLE	7.90E-09	3.33E-04	5.09E-01	5.09E-01	5.09E-01
SE82	STABLE	1.24E-08	5.20E-04	7.94E-01	7.94E-01	7.94E-01
SE83M	70.-S	1.55E-02	3.69E-05	7.19E-02	0.00E+00	0.00E+00
SE83	22.5-M	4.89E-03	2.25E-04	3.48E-01	0.00E+00	0.00E+00
BR83	2.4-H	3.89E-03	1.39E-03	2.15E+00	2.17E-03	0.00E+00
KR83M	1.86-H	3.00E+00	2.84E-01	0.00E+00	0.00E+00	0.00E+00
KR83	STABLE	3.11E-05	1.28E+00	0.00E+00	0.00E+00	0.00E+00
SE84	3.3-M	3.95E-02	2.66E-04	4.46E-01	0.00E+00	0.00E+00
BR84	31.8-M	1.46E-02	1.19E-03	1.87E+00	0.00E+00	0.00E+00
KR84	STABLE	5.60E-05	2.34E+00	0.00E+00	0.00E+00	0.00E+00
BR85	2.87-M	5.66E-02	3.32E-04	5.64E-01	0.00E+00	0.00E+00
KR85M	4.48-H	3.89E+00	1.93E+00	0.00E+00	0.00E+00	0.00E+00
KR85	10.73Y	6.32E-03	7.06E+01	0.00E+00	0.00E+00	0.00E+00
RB85	STABLE	6.57E-09	3.19E-04	4.22E-01	4.22E-01	4.22E-01
KR86	STABLE	1.08E-04	4.54E+00	0.00E+00	0.00E+00	0.00E+00
KR87	76.-M	4.77E+00	7.41E-01	0.00E+00	0.00E+00	0.00E+00
RB87	STABLE	1.56E-08	7.68E-03	1.00E+00	1.00E+00	1.00E+00
KR88	2.8-H	8.51E+00	2.92E+00	0.00E+00	0.00E+00	0.00E+00
RB88	17.7-M	1.52E-01	2.92E+00	8.58E+00	0.00E+00	0.00E+00
SR88	STABLE	8.81E-11	2.81E-02	8.67E-02	8.67E-02	8.67E-02

Table A-4. 600 MW(t) Core – "Maximum Expected" Circuit Activity (Cont.)

Nuclide	Half-life	Circulating Activity (Ci)	Purification Sys. Activity (Ci)	Plateout Activity (Ci)		
				Initial	1-Day Decay	10-Day Decay
KR89	3.16-M	1.97E+00	1.27E-02	0.00E+00	0.00E+00	0.00E+00
RB89	15.2-M	4.24E-02	1.28E-02	2.06E+00	0.00E+00	0.00E+00
SR89	50.5-D	2.72E-06	1.31E-02	2.63E+00	2.60E+00	2.29E+00
Y89	STABLE	1.36E-11	5.72E-07	2.65E-02	2.65E-02	2.65E-02
KR90	32.3-S	8.83E-01	9.71E-04	0.00E+00	0.00E+00	0.00E+00
RB90M	4.28-M	8.49E-03	1.22E-04	1.22E-01	0.00E+00	0.00E+00
RB90	2.7-M	9.24E-02	9.20E-04	8.77E-01	0.00E+00	0.00E+00
SR90	29.-Y	1.68E-08	3.40E-04	1.25E+00	1.25E+00	1.25E+00
Y90	64.-H	4.49E-07	4.12E-04	1.26E+00	1.26E+00	1.25E+00
ZR90	STABLE	8.25E-13	3.45E-06	1.24E-02	1.24E-02	1.24E-02
KR91	9.0-S	3.09E-01	9.47E-05	0.00E+00	0.00E+00	0.00E+00
RB91	58.5-S	1.03E-01	1.47E-04	4.15E-01	0.00E+00	0.00E+00
SR91	9.48-H	1.22E-04	2.21E-04	5.29E-01	9.15E-02	1.27E-08
Y91	58.6-D	4.31E-07	7.42E-05	6.42E-01	6.37E-01	5.74E-01
ZR91	STABLE	1.76E-11	1.47E-06	7.51E-03	7.51E-03	7.52E-03
SR92	2.71-H	2.32E-04	7.70E-05	1.18E-01	2.54E-04	0.00E+00
Y92	3.53-H	1.80E-04	1.55E-04	2.37E-01	4.78E-03	0.00E+00
ZR92	STABLE	1.87E-11	2.34E-06	3.58E-03	3.58E-03	3.58E-03
SR93	7.5-M	5.33E-03	8.17E-05	1.30E-01	0.00E+00	0.00E+00
Y93	10.2-H	7.26E-05	1.69E-04	2.63E-01	5.19E-02	2.18E-08
ZR93	STABLE	2.11E-11	2.61E-06	4.03E-03	4.03E-03	4.03E-03
SR94	1.29-M	2.56E-02	6.74E-05	1.29E-01	0.00E+00	0.00E+00
Y94	19.0-M	2.72E-03	1.57E-04	2.67E-01	0.00E+00	0.00E+00
ZR94	STABLE	2.27E-11	2.55E-06	4.18E-03	4.18E-03	4.18E-03
Y95	10.5-M	4.22E-03	9.07E-05	1.43E-01	0.00E+00	0.00E+00
ZR95	65.5-D	5.06E-07	1.85E-04	2.87E-01	2.84E-01	2.59E-01
NB95M	3.61-D	8.34E-08	2.74E-06	4.23E-03	3.99E-03	2.91E-03
NB95	35.1-D	9.16E-07	9.48E-05	4.33E-01	4.30E-01	4.04E-01
MO95	STABLE	2.34E-11	1.97E-06	6.00E-03	6.00E-03	6.00E-03
Y96	6.0-S	1.03E-01	2.11E-05	1.35E-01	0.00E+00	0.00E+00
ZR96	STABLE	4.04E-11	1.21E-06	2.93E-03	2.93E-03	2.93E-03

Table A-4. 600 MW(t) Core – "Maximum Expected" Circuit Activity (Cont.)

Nuclide	Half-life	Circulating Activity (Ci)	Purification Sys. Activity (Ci)	Plateout Activity (Ci)		
				Initial	1-Day Decay	10-Day Decay
ZR97	16.8-H	4.48E-05	9.23E-05	1.41E-01	5.24E-02	7.07E-06
NB97	73.6-M	6.15E-04	1.85E-04	2.83E-01	5.65E-02	7.62E-06
MO97	STABLE	2.35E-11	2.94E-06	4.50E-03	4.50E-03	4.50E-03
NB98	51.0-M	6.11E-06	6.37E-07	9.79E-04	3.10E-12	0.00E+00
MO98	STABLE	2.39E-11	1.01E-06	1.54E-03	1.54E-03	1.54E-03
NB99M	2.5-M	6.07E-03	3.10E-05	5.34E-02	0.00E+00	0.00E+00
NB99	14.0-S	5.71E-02	2.72E-05	9.87E-02	0.00E+00	0.00E+00
MO99	66.2-H	1.75E-05	1.59E-04	3.06E-01	2.37E-01	2.46E-02
TC99M	6.02-H	1.20E-04	8.83E-05	4.04E-01	2.37E-01	2.38E-02
TC99	STABLE	2.59E-11	2.04E-06	6.43E-03	6.43E-03	6.43E-03
NB100M	7.0-S	5.77E-02	1.38E-05	7.87E-02	0.00E+00	0.00E+00
NB100	2.9-M	7.83E-03	4.64E-05	7.87E-02	0.00E+00	0.00E+00
MO100	STABLE	2.85E-11	1.65E-06	2.60E-03	2.60E-03	2.60E-03
MO101	14.6-M	2.90E-03	8.64E-05	1.35E-01	0.00E+00	0.00E+00
TC101	14.2-M	3.04E-03	1.73E-04	2.70E-01	0.00E+00	0.00E+00
RU101	STABLE	2.37E-11	2.88E-06	4.47E-03	4.47E-03	4.47E-03
MO102	11.1-M	3.46E-03	7.85E-05	1.23E-01	0.00E+00	0.00E+00
TC102M	4.3-M	8.80E-03	1.54E-04	2.47E-01	0.00E+00	0.00E+00
RU102	STABLE	2.30E-11	2.62E-06	4.13E-03	4.13E-03	4.13E-03
MO103	60.-S	2.67E-02	5.45E-05	1.10E-01	0.00E+00	0.00E+00
RU103	39.6-D	7.80E-07	1.28E-04	2.22E-01	2.18E-01	1.86E-01
RH103M	56.-M	6.32E-04	1.99E-04	3.31E-01	2.16E-01	1.85E-01
RH103	STABLE	1.98E-11	8.27E-07	5.02E-03	5.02E-03	5.02E-03
MO104	1.6-M	1.39E-02	4.56E-05	8.35E-02	0.00E+00	0.00E+00
TC104	18.-M	1.78E-03	1.02E-04	1.71E-01	0.00E+00	0.00E+00
RU104	STABLE	1.58E-11	1.81E-06	2.94E-03	2.94E-03	2.94E-03
TC105	8.0-M	2.63E-03	4.30E-05	6.83E-02	0.00E+00	0.00E+00
RU105	4.44-H	8.57E-05	8.79E-05	1.37E-01	3.28E-03	0.00E+00
RH105	35.5-H	1.03E-05	1.33E-04	2.06E-01	1.41E-01	2.08E-03
PD105	STABLE	1.23E-11	5.16E-07	3.15E-03	3.15E-03	3.15E-03
RU106	369.-D	3.14E-08	3.42E-05	5.22E-02	5.21E-02	5.12E-02

Table A-4. 600 MW(t) Core – "Maximum Expected" Circuit Activity (Cont.)

Nuclide	Half-life	Circulating Activity (Ci)	Purification Sys. Activity (Ci)	Plateout Activity (Ci)		
				Initial	1-Day Decay	10-Day Decay
PD106	STABLE	6.95E-12	7.81E-07	1.05E-03	1.05E-03	1.05E-03
RU107	4.2-M	2.76E-03	2.37E-05	3.89E-02	0.00E+00	0.00E+00
RH107	21.7-M	6.08E-04	4.89E-05	7.80E-02	0.00E+00	0.00E+00
PD107	STABLE	7.22E-12	8.70E-07	1.37E-03	1.37E-03	1.37E-03
RU108	4.5-M	1.69E-03	1.55E-05	2.54E-02	0.00E+00	0.00E+00
PD108	STABLE	4.80E-12	2.02E-07	3.08E-04	3.08E-04	3.08E-04
RH109	1.5-M	3.44E-03	1.06E-05	1.96E-02	0.00E+00	0.00E+00
PD109M	4.69-M	7.38E-04	1.13E-05	1.96E-02	0.00E+00	0.00E+00
PD109	13.5-H	8.76E-06	2.94E-05	4.90E-02	1.43E-02	2.12E-07
AG109	STABLE	3.78E-07	1.59E-02	2.43E+01	2.43E+01	2.43E+01
PD110	STABLE	1.42E-12	5.97E-08	9.12E-05	9.12E-05	9.12E-05
AG110M	252.-D	1.46E-05	1.08E-02	1.66E+01	1.65E+01	1.61E+01
RH111	63.-S	8.47E-04	1.82E-06	3.62E-03	0.00E+00	0.00E+00
PD111	22.-M	6.69E-05	4.28E-06	7.44E-03	0.00E+00	0.00E+00
AG111M	74.-S	8.02E-04	6.24E-06	1.12E-02	0.00E+00	0.00E+00
AG111	7.47-D	1.19E-02	2.63E-01	4.01E+02	3.66E+02	1.59E+02
CD111	STABLE	1.52E-09	3.25E-03	4.97E+00	4.97E+00	4.97E+00
PD112	20.1-H	4.67E-07	1.15E-06	1.76E-03	7.68E-04	4.47E-07
AG112	3.13-H	3.00E-06	2.30E-06	3.52E-03	9.17E-04	5.30E-07
PD113	1.5-M	1.85E-04	5.68E-07	1.05E-03	0.00E+00	0.00E+00
AG113	5.3-H	1.12E-06	1.13E-06	1.90E-03	8.24E-05	0.00E+00
CD113	STABLE	4.20E-10	1.77E-05	2.70E-02	2.70E-02	2.70E-02
SN119M	245.-D	7.33E-12	5.28E-09	8.07E-06	8.05E-06	7.84E-06
SN119	STABLE	1.07E-13	4.59E-09	7.00E-06	7.00E-06	7.00E-06
SN123	129.-D	1.79E-10	6.78E-08	1.04E-04	1.03E-04	9.81E-05
SB123	STABLE	8.34E-13	3.62E-08	5.49E-05	5.49E-05	5.49E-05
SN125	9.65-D	1.17E-08	3.33E-07	5.08E-04	4.73E-04	2.48E-04
SB125	2.73-Y	1.97E-09	6.10E-06	9.32E-03	9.31E-03	9.26E-03
TE125M	58.-D	5.33E-07	2.25E-04	1.41E-01	1.39E-01	1.25E-01
TE125	STABLE	4.68E-10	4.63E-05	3.20E-02	3.20E-02	3.20E-02
SN126	STABLE	6.47E-13	2.72E-08	4.15E-05	4.15E-05	4.15E-05

Table A-4. 600 MW(t) Core – "Maximum Expected" Circuit Activity (Cont.)

Nuclide	Half-life	Circulating Activity (Ci)	Purification Sys. Activity (Ci)	Plateout Activity (Ci)		
				Initial	1-Day Decay	10-Day Decay
SB126M	19.0-M	5.00E-05	1.95E-06	3.02E-03	5.36E-07	5.36E-07
SN127M	4.4-M	7.04E-05	6.33E-07	1.04E-03	0.00E+00	0.00E+00
SN127	2.12-H	1.19E-05	3.09E-06	4.73E-03	1.85E-06	0.00E+00
SB127	3.8-D	2.29E-06	2.93E-05	4.48E-02	3.74E-02	7.25E-03
TE127M	109.-D	3.01E-06	9.65E-04	1.48E+00	1.47E+00	1.39E+00
TE127	9.4-H	3.14E-04	1.31E-03	2.04E+00	1.57E+00	1.37E+00
I127	STABLE	2.44E-07	1.03E-02	3.47E-01	3.47E-01	3.47E-01
SN128	59.-M	5.66E-05	6.83E-06	1.05E-02	4.72E-10	0.00E+00
SB128M	10.4-M	3.12E-04	1.34E-05	2.08E-02	5.72E-10	0.00E+00
SB128	9.0-H	4.02E-07	4.57E-07	6.99E-04	1.11E-04	6.61E-12
TE128	STABLE	9.64E-09	4.05E-04	6.19E-01	6.19E-01	6.19E-01
SN129M	2.5-M	1.21E-03	6.20E-06	1.07E-02	0.00E+00	0.00E+00
SN129	7.5-M	3.20E-04	4.91E-06	7.82E-03	0.00E+00	0.00E+00
SB129	4.34-H	3.11E-05	2.67E-05	4.23E-02	9.23E-04	0.00E+00
TE129M	33.4-D	2.35E-05	2.31E-03	3.54E+00	3.47E+00	2.88E+00
TE129	70.-M	3.32E-03	1.95E-03	3.02E+00	2.21E+00	1.83E+00
I129	STABLE	9.84E-07	4.14E-02	1.34E+00	1.34E+00	1.34E+00
SN130	3.7-M	2.19E-03	1.65E-05	2.75E-02	0.00E+00	0.00E+00
SB130M	6.6-M	1.57E-03	3.49E-05	5.68E-02	0.00E+00	0.00E+00
SB130	37.-M	9.80E-05	8.93E-06	1.40E-02	0.00E+00	0.00E+00
TE130	STABLE	4.03E-08	1.69E-03	2.59E+00	2.59E+00	2.59E+00
SN131	63.-S	4.92E-03	1.06E-05	2.10E-02	0.00E+00	0.00E+00
SB131	23.-M	9.42E-04	5.17E-05	8.47E-02	0.00E+00	0.00E+00
TE131M	30.-H	4.29E-04	1.58E-03	2.42E+00	1.39E+00	9.44E-03
TE131	25.-M	1.52E-02	7.74E-04	1.71E+00	2.53E-01	1.72E-03
I131	8.04-D	4.45E-02	1.05E+00	3.64E+01	3.35E+01	1.55E+01
XE131M	12.0-D	2.95E-02	5.59E-01	0.00E+00	0.00E+00	0.00E+00
XE131	STABLE	1.14E-04	4.27E+00	0.00E+00	0.00E+00	0.00E+00
SN132	40.0-S	4.66E-03	6.35E-06	1.44E-02	0.00E+00	0.00E+00
SB132M	4.1-M	2.07E-03	1.91E-05	3.34E-02	0.00E+00	0.00E+00
SB132	2.1-M	6.29E-03	2.88E-05	5.24E-02	0.00E+00	0.00E+00

Table A-4. 600 MW(t) Core – "Maximum Expected" Circuit Activity (Cont.)

Nuclide	Half-life	Circulating Activity (Ci)	Purification Sys. Activity (Ci)	Plateout Activity (Ci)		
				Initial	1-Day Decay	10-Day Decay
TE132	78.-H	2.05E-03	1.96E-02	3.00E+01	2.42E+01	3.56E+00
I132	2.29-H	5.37E-01	1.70E-01	3.52E+01	2.50E+01	3.66E+00
XE132	STABLE	1.61E-04	6.27E+00	0.00E+00	0.00E+00	0.00E+00
SB133	2.4-M	6.11E-03	3.00E-05	5.19E-02	0.00E+00	0.00E+00
TE133M	55.4-M	1.51E-02	1.72E-03	2.64E+00	3.97E-08	0.00E+00
TE133	12.5-M	2.49E-02	8.73E-04	1.36E+00	6.67E-09	0.00E+00
I133	20.8-H	2.88E-01	7.33E-01	2.67E+01	1.20E+01	9.01E-03
XE133M	2.23-D	2.45E-01	9.78E-01	0.00E+00	0.00E+00	0.00E+00
XE133	5.29-D	5.02E+00	5.52E+01	0.00E+00	0.00E+00	0.00E+00
CS133	STABLE	8.12E-08	3.36E-03	5.21E+00	5.21E+00	5.21E+00
TE134	42.-M	2.91E-02	2.49E-03	3.84E+00	0.00E+00	0.00E+00
I134M	3.6-M	8.79E-02	6.47E-04	1.08E-01	0.00E+00	0.00E+00
I134	52.6-M	1.24E+00	1.34E-01	9.21E+00	1.40E-07	0.00E+00
XE134	STABLE	2.56E-04	1.06E+01	0.00E+00	0.00E+00	0.00E+00
CS134	2.06-Y	1.14E-05	2.52E-02	3.84E+01	3.84E+01	3.81E+01
I135	6.59-H	4.71E-01	3.80E-01	1.23E+01	9.81E-01	0.00E+00
XE135M	15.3-M	2.22E+00	7.05E-02	0.00E+00	0.00E+00	0.00E+00
XE135	9.17-H	6.90E+00	2.73E+00	0.00E+00	0.00E+00	0.00E+00
CS135	STABLE	8.45E-08	3.48E-03	5.42E+00	5.42E+00	5.42E+00
I136	85.-S	3.04E-01	8.79E-04	3.31E-01	0.00E+00	0.00E+00
XE136	STABLE	2.14E-04	9.00E+00	0.00E+00	0.00E+00	0.00E+00
CS136	13.0-D	5.78E-05	2.21E-03	3.38E+00	3.20E+00	1.98E+00
XE137	3.84-M	1.15E+00	8.99E-03	0.00E+00	0.00E+00	0.00E+00
CS137	30.1-Y	6.78E-06	1.66E-01	2.44E+02	2.44E+02	2.44E+02
BA137M	2.55-M	8.10E-04	1.57E-01	2.31E+02	2.31E+02	2.30E+02
BA137	STABLE	1.17E-11	1.01E-05	3.65E+00	3.65E+00	3.65E+00
XE138	14.2-M	2.13E+00	6.17E-02	0.00E+00	0.00E+00	0.00E+00
CS138M	2.9-M	6.10E-04	3.61E-06	6.13E-03	0.00E+00	0.00E+00
CS138	32.2-M	2.25E-02	6.18E-02	2.29E+00	0.00E+00	0.00E+00
BA138	STABLE	2.52E-10	1.04E-05	5.04E-02	5.04E-02	5.04E-02
XE139	39.7-S	3.51E-01	4.75E-04	0.00E+00	0.00E+00	0.00E+00

Table A-4. 600 MW(t) Core – "Maximum Expected" Circuit Activity (Cont.)

Nuclide	Half-life	Circulating Activity (Ci)	Purification Sys. Activity (Ci)	Plateout Activity (Ci)		
				Initial	1-Day Decay	10-Day Decay
CS139	9.3-M	1.67E-02	5.70E-04	5.01E-01	0.00E+00	0.00E+00
BA139	83.3-M	6.49E-04	6.69E-04	6.53E-01	4.47E-06	0.00E+00
LA139	STABLE	3.63E-11	1.52E-06	1.22E-02	1.22E-02	1.22E-02
XE140	13.6-S	1.47E-01	6.80E-05	0.00E+00	0.00E+00	0.00E+00
CS140	63.8-S	6.47E-02	1.35E-04	2.80E-01	0.00E+00	0.00E+00
BA140	12.8-D	1.79E-05	7.68E-04	1.25E+00	1.18E+00	7.25E-01
LA140	40.2-H	2.00E-05	9.89E-05	1.40E+00	1.33E+00	8.34E-01
CE140	STABLE	3.60E-11	3.03E-06	2.37E-02	2.37E-02	2.37E-02
BA141	18.3-M	2.37E-03	8.86E-05	1.38E-01	0.00E+00	0.00E+00
LA141	3.87-H	1.94E-04	1.79E-04	2.77E-01	3.92E-03	0.00E+00
CE141	32.5-D	9.50E-07	2.70E-04	4.15E-01	4.08E-01	3.37E-01
PR141	STABLE	3.33E-11	1.40E-06	8.54E-03	8.54E-03	8.55E-03
BA142	10.7-M	3.89E-03	8.51E-05	1.34E-01	0.00E+00	0.00E+00
LA142	92.4-M	4.90E-04	1.75E-04	2.72E-01	5.91E-06	0.00E+00
CE142	STABLE	3.35E-11	4.12E-06	6.37E-03	6.37E-03	6.37E-03
LA143	14.-M	2.98E-03	8.54E-05	1.33E-01	0.00E+00	0.00E+00
CE143	33.0-H	2.22E-05	1.73E-04	2.68E-01	1.62E-01	1.74E-03
PR143	13.58D	2.20E-06	2.61E-04	4.02E-01	3.92E-01	2.59E-01
ND143	STABLE	3.25E-11	1.37E-06	8.34E-03	8.34E-03	8.34E-03
CE144	284.-D	9.47E-08	7.93E-05	1.21E-01	1.21E-01	1.18E-01
PR144	17.3-M	1.80E-03	1.57E-04	2.20E-01	1.21E-01	1.18E-01
ND144	STABLE	2.47E-11	3.70E-06	5.02E-03	5.02E-03	5.02E-03
CE145	3.3-M	7.92E-03	5.34E-05	8.95E-02	0.00E+00	0.00E+00
PR145	5.98-H	8.70E-05	1.12E-04	1.79E-01	1.11E-02	0.00E+00
ND145	STABLE	2.21E-11	2.71E-06	4.26E-03	4.26E-03	4.26E-03
CE146	14.2-M	1.54E-03	4.46E-05	6.97E-02	0.00E+00	0.00E+00
PR146	24.2-M	9.37E-04	9.00E-05	1.40E-01	0.00E+00	0.00E+00
ND146	STABLE	1.77E-11	2.17E-06	3.35E-03	3.35E-03	3.35E-03
CE147	70.-S	1.13E-02	2.69E-05	5.23E-02	0.00E+00	0.00E+00
PR147	12.-M	1.72E-03	6.19E-05	1.07E-01	0.00E+00	0.00E+00
ND147	11.0-D	1.15E-06	9.79E-05	1.62E-01	1.52E-01	8.63E-02

Table A-4. 600 MW(t) Core – "Maximum Expected" Circuit Activity (Cont.)

Nuclide	Half-life	Circulating Activity (Ci)	Purification Sys. Activity (Ci)	Plateout Activity (Ci)		
				Initial	1-Day Decay	10-Day Decay
PM147	2.62-Y	1.28E-08	3.60E-05	2.17E-01	2.17E-01	2.16E-01
SM147	STABLE	8.66E-11	4.24E-06	9.05E-03	9.05E-03	9.05E-03
PR148	2.0-M	5.78E-03	2.36E-05	4.19E-02	0.00E+00	0.00E+00
ND148	STABLE	1.21E-11	8.29E-07	1.36E-03	1.36E-03	1.36E-03
PM148M	41.3-D	1.32E-08	1.61E-06	2.46E-03	2.41E-03	2.08E-03
PM148	5.37-D	6.29E-07	9.93E-06	1.52E-02	1.33E-02	4.17E-03
PR149	2.3-M	3.41E-03	1.60E-05	2.79E-02	0.00E+00	0.00E+00
ND149	1.73-H	9.96E-05	3.49E-05	5.68E-02	3.83E-06	0.00E+00
PM149	53.1-H	2.92E-06	5.39E-05	8.58E-02	6.41E-02	3.82E-03
SM149	STABLE	4.71E-11	1.98E-06	4.42E-03	4.42E-03	4.42E-03
ND150	STABLE	5.09E-12	2.14E-07	3.26E-04	3.26E-04	3.26E-04
ND151	12.4-M	3.54E-04	8.98E-06	1.41E-02	0.00E+00	0.00E+00
PM151	28.4-H	2.75E-06	1.83E-05	2.83E-02	1.58E-02	8.12E-05
SM151	93.-Y	5.99E-10	2.68E-05	4.11E-02	4.11E-02	4.11E-02
EU151	STABLE	2.67E-11	1.12E-06	2.49E-03	2.49E-03	2.49E-03
ND152	11.5-M	2.59E-04	6.10E-06	9.57E-03	0.00E+00	0.00E+00
PM152	4.1-M	7.33E-04	1.21E-05	1.94E-02	0.00E+00	0.00E+00
SM152	STABLE	1.69E-11	9.03E-07	1.40E-03	1.40E-03	1.40E-03
EU152	13.-Y	1.80E-14	2.39E-10	3.64E-07	3.64E-07	3.64E-07
ND153	67.5-S	1.17E-03	2.69E-06	5.28E-03	0.00E+00	0.00E+00
PM153	5.4-M	4.22E-04	6.62E-06	1.16E-02	0.00E+00	0.00E+00
SM153	46.5-H	7.85E-07	1.08E-05	1.81E-02	1.26E-02	5.05E-04
EU153	STABLE	1.07E-11	4.48E-07	9.85E-04	9.85E-04	9.85E-04
ND154	7.73-D	7.30E-08	1.66E-06	2.54E-03	2.32E-03	1.03E-03
PM154	2.8-M	3.35E-04	3.58E-06	5.80E-03	2.32E-03	1.03E-03
SM154	STABLE	6.88E-12	3.46E-07	5.34E-04	5.34E-04	5.34E-04
EU154	8.6-Y	9.71E-10	8.88E-06	1.36E-02	1.36E-02	1.35E-02
SM155	22.2-M	3.22E-05	1.46E-06	2.27E-03	0.00E+00	0.00E+00
EU155	4.8-Y	3.38E-10	3.18E-06	4.89E-03	4.89E-03	4.87E-03
GD155	STABLE	5.90E-13	8.24E-08	1.32E-04	1.32E-04	1.32E-04
SM156	9.4-H	8.34E-07	9.62E-07	1.47E-03	2.50E-04	3.04E-11

Table A-4. 600 MW(t) Core – "Maximum Expected" Circuit Activity (Cont.)

Nuclide	Half-life	Circulating Activity (Ci)	Purification Sys. Activity (Ci)	Plateout Activity (Ci)		
				Initial	1-Day Decay	10-Day Decay
EU156	15.2-D	1.39E-07	7.18E-06	1.10E-02	1.05E-02	6.98E-03
GD156	STABLE	3.94E-13	1.39E-07	2.13E-04	2.13E-04	2.13E-04
SM157	83.-S	1.73E-04	4.89E-07	9.20E-04	0.00E+00	0.00E+00
EU157	15.2-H	3.97E-07	1.12E-06	1.88E-03	6.28E-04	3.31E-08
GD157	STABLE	2.56E-13	2.99E-08	4.86E-05	4.86E-05	4.86E-05
	TOTALS	4.58E+01	1.21E+03	1.15E+03	1.02E+03	7.28E+02

Note: * Stable Nuclides are given in grams.

APPENDIX B. TRITGO H-3 MASS BALANCE CALCULATIONS

The following example TRITGO output is for plant Configuration 3, steam generator loop (Section 8.2). Only the print times for 3-yr and 50-yr operation are included here.

600 MW(T)MHTGR TRITIUM ANALYSIS MYER'S ISOTHERM (TRITGO-V2)
10:40:50
22-APR-0

Reactor power (MWt)	600.00
Fission density (watts/cm**3)	6.60
Weight of helium (lbs)	10000.00
Helium pressure (atms)	69.08
Average He temperature (C)	770.00
He-3 abundance (fraction)	2.0000E-07
Helium replacement rate(/sec)	3.1700E-09
Helium purification rate(/sec)	2.3600E-05
Fuel Release Fraction	3.0000E-01
Mass of water in the secondary system (lbs)	2.0243E+05
Makeup rate of water in the system (lbs/day)	1.5500E+04

600 MW(T)MHTGR TRITIUM ANALYSIS MYER'S ISOTHERM (TRITGO-V2)

	CORE (TOP)	CORE (MID)	CORE (Bot)	REFLECTOR (TOP)
Weight (lbs)	8.2100E+04	1.1000E+05	8.2100E+04	5.5400E+04
Density (gm/cm3)	1.7400E+00	1.7400E+00	1.7400E+00	1.7400E+00
Surface Area (sq m/gm)	0.500	0.500	0.500	0.500
Region Temperature (oC)	686.000	908.000	996.000	490.000
Weight Fraction of Region With Channels and Holes	1.0000	1.0000	1.0000	1.0000
Width of Internal Annular Gap Between Rod Matrix and Graphite	0.0050	0.0050	0.0050	0.0050
Width of External Annular Gap Between Region Elements	0.040	0.040	0.040	0.040
H-3 Trapped in Solid (Fraction)	0.990	0.990	0.990	0.990
Fraction of Carbon in Solids	1.000	1.000	1.000	1.000

	REFLECTOR (BOTTOM)	FLOWDIST (PERMAN)	REFLECTOR (INNER)	REFLECTOR (OUTREP)
Weight (lbs)	3.4100E+04	1.7100E+04	2.8100E+05	4.1400E+05
Density (gm/cm3)	1.7400E+00	1.7400E+00	1.7400E+00	1.7400E+00
Surface Area (sq m/gm)	0.500	0.500	0.500	0.500
Region Temperature (oC)	944.000	947.000	561.000	586.000
Weight Fraction of Region With Channels and Holes	1.0000	1.0000	0.0000	0.0000
Width of Internal Annular Gap Between Rod Matrix and Graphite	0.0000	0.0000	0.0000	0.0000
Width of External Annular Gap Between Region Elements	0.040	0.040	0.040	0.040
H-3 Trapped in Solid (Fraction)	0.990	0.990	0.990	0.990
Fraction of Carbon in Solids	1.000	1.000	1.000	1.000

	REFLECTOR (OUTPER)	CORESUPPORT (STRUC)	CONTROL ROD (OPERA)
Weight (lbs)	3.2800E+05	2.2900E+05	7.4000E+03
Density (gm/cm3)	1.7400E+00	1.7400E+00	1.7400E+00
Surface Area (sq m/gm)	0.500	0.500	0.500
Region Temperature (oC)	551.000	919.000	630.000
Weight Fraction of Region With Channels and Holes	1.0000	0.0000	0.0000
Width of Internal Annular Gap Between Rod Matrix and Graphite	0.0000	0.0000	0.0000
Width of External Annular Gap Between Region Elements	0.040	0.040	0.050
H-3 Trapped in Solid (Fraction)	0.990	0.990	0.990
Fraction of Carbon in Solids	1.000	1.000	0.600

600 MW(T)MHTGR TRITIUM ANALYSIS MYER'S ISOTHERM (TRITGO-V2)

Name	Surface area m2	Thickness mm	Temperature Degrees C	Permeation Equation constants ACONST ppmv**.5-std m3/atm**.5-m2-h	BCONST K
STMGER-ECON	4.29E+02	3.81E+00	4.15E+02	6.102E+01	-6.249E+03
STMGER-EVAP	3.45E+02	3.81E+00	5.21E+02	6.102E+01	-6.249E+03
STMGER-SPHT1	1.08E+02	3.81E+00	5.76E+02	6.102E+01	-6.249E+03
STMGER-SPHT2	2.24E+02	3.81E+00	6.56E+02	6.102E+01	-6.249E+03

600 MW(T)MHTGR TRITIUM ANALYSIS MYER'S ISOTHERM (TRITGO-V2)

History lists--value of 1 in first column indicates end of list

Power history list

JX	month	day	year	rel power	start
1	1	1	108	0.900	14976.0

Chemical parameter list(hydrogen conc in ppm, and purification plant efficiency)

IX	month	day	year	H2(ppm)	GAM	start
1	1	1	108	10.000	1.000	14976.0

List of events indicated by code. 0=no printout,1= Printout provided for this point
9 = default value

KX	Month	day	year	code	start
0	1	1	108	1.0	14976.0
0	7	1	109	1.0	15523.0
0	1	1	111	1.0	16072.0
0	7	1	112	1.0	16619.0
0	1	1	114	1.0	17168.0
0	7	1	115	1.0	17714.0
0	1	1	117	1.0	18264.0
0	7	1	118	1.0	18810.0
0	1	1	120	1.0	19359.0
0	7	1	121	1.0	19906.0
0	1	1	123	1.0	20455.0
0	7	1	124	1.0	21002.0
0	1	1	126	1.0	21551.0
0	7	1	127	1.0	22097.0
0	1	1	129	1.0	22647.0
0	7	1	130	1.0	23193.0
0	1	1	132	1.0	23742.0
0	7	1	133	1.0	24289.0
0	1	1	135	1.0	24838.0
0	7	1	136	1.0	25385.0
0	1	1	138	1.0	25934.0
0	7	1	139	1.0	26480.0
0	1	1	141	1.0	27030.0
0	7	1	142	1.0	27576.0
0	1	1	144	1.0	28125.0
0	7	1	145	1.0	28672.0
0	1	1	147	1.0	29221.0
0	7	1	148	1.0	29768.0
0	1	1	150	1.0	30317.0
0	7	1	151	1.0	30863.0

```
 0     1      1    153   1.0    31413.0
 0     7      1    154   1.0    31959.0
 0     1      1    156   1.0    32508.0
 0     7      1    157   1.0    33055.0
 1     1      1    159   1.0    33604.0


Dates starting and stopping computation span

month   day   year   month   day   year       TBEGIN  TEND
          1           1         108           1           1         159
  1      1    108      1      1    159       14976.0 33604.0
```

600 MW(T)MHTGR TRITIUM ANALYSIS MYER'S ISOTHERM (TRITGO-V2)

Tritium generation and distribution in a high temperature gas cooled reactor

Full reactor power 600. MWth, 6.6Kw/l, Average gas temp 770. deg C, Pressure, 69.1 Atm

Purification rate 2.039040/Day
He amount 1.00E+04 lbs He makeup rate 2.74E-04/Day He-3 abundance 2.00E-07
Water 2.02E+05 lbs water makeup rate 0.08/Day Theo core flux-slow 8.08E+13, fast 2.57E+13

	CORE (TOP)	CORE (MID)	CORE (Bot)	REFLECTOR (TOP)
Weight (lbs)	8.2100E+04	1.1000E+05	8.2100E+04	5.5400E+04
Li Concentration (ppm)	0.036	0.036	0.036	0.036
Boron Concentration (ppm)	41.000	41.000	41.000	2.000
Be Concentration (ppm)	0.000	0.000	0.000	0.000
Assigned Fast Flux (n/cm2.s)	3.730E+13	3.730E+13	3.730E+13	3.730E+13
Assigned Slow Flux (n/cm2.s)	1.020E+12	1.020E+12	1.020E+12	1.020E+12
Effective Full Power Reaction Rates (1/sec)				
Li-6	4.158E-10	4.158E-10	4.158E-10	4.158E-10
Li-7	2.678E-13	2.678E-13	2.678E-13	2.678E-13
FB-10	5.043E-13	5.043E-13	5.043E-13	5.043E-13
SB-10	1.663E-09	1.663E-09	1.663E-09	1.663E-09
C-12	5.476E-15	5.476E-15	5.476E-15	5.476E-15
Be-9	6.162E-13	6.162E-13	6.162E-13	6.162E-13
He-3	2.326E-09	2.326E-09	2.326E-09	2.326E-09
Fuel	1.000E-04	1.000E-04	1.000E-04	1.000E-04
Arb	6.497E+05	6.497E+05	6.497E+05	6.497E+05
H-3	0.000E+00	0.000E+00	0.000E+00	0.000E+00
	0.000E+00	0.000E+00	0.000E+00	0.000E+00
Arbitrary release rate (Ci/day)	0.000E+00	0.000E+00	0.000E+00	0.000E+00
Fractional Fission Yield	1.000E-04	1.000E-04	1.000E-04	1.000E-04

Original Number of Atoms in Region

Li-6	8.630E+21	1.156E+22	8.630E+21	5.823E+21
Li-7	1.077E+23	1.443E+23	1.077E+23	7.266E+22
FB-10	1.666E+25	2.233E+25	1.666E+25	5.485E+23
SB-10	1.666E+25	2.233E+25	1.666E+25	5.485E+23
C-12	1.846E+30	2.473E+30	1.846E+30	1.245E+30
Be-9	0.000E+00	0.000E+00	0.000E+00	0.000E+00
He-3	2.554E+22	2.779E+22	1.930E+22	2.166E+22
Fuel	1.000E+00	1.000E+00	1.000E+00	0.000E+00
Arb	0.000E+00	0.000E+00	0.000E+00	0.000E+00
H-3	0.000E+00	0.000E+00	0.000E+00	0.000E+00
	0.000E+00	0.000E+00	0.000E+00	0.000E+00

	REFLECTOR (BOTTOM)	FLOWDIST (PERMAN)	REFLECTOR (INNER)	REFLECTOR (OUTREP)
Weight (lbs)	3.4100E+04	1.7100E+04	2.8100E+05	4.1400E+05
Li Concentration (ppm)	0.036	2.000	0.036	0.036
Boron Concentration (ppm)	2.000	2.000	2.000	2.000
Be Concentration (ppm)	0.000	0.000	0.000	0.000
Assigned Fast Flux (n/cm2.s)	3.730E+13	3.730E+13	1.000E+11	5.000E+12
Assigned Slow Flux (n/cm2.s)	1.020E+12	1.020E+12	5.000E+09	1.000E+11
Effective Full Power Reaction Rates (1/sec)				
Li-6	4.158E-10	4.158E-10	2.038E-12	4.076E-11
Li-7	2.678E-13	2.678E-13	7.180E-16	3.590E-14
FB-10	5.043E-13	5.043E-13	1.352E-15	6.760E-14
SB-10	1.663E-09	1.663E-09	8.153E-12	1.631E-10
C-12	5.476E-15	5.476E-15	1.468E-17	7.340E-16
Be-9	6.162E-13	6.162E-13	1.652E-15	8.260E-14
He-3	2.326E-09	2.326E-09	1.140E-11	2.280E-10
Fuel	1.000E-04	1.000E-04	1.000E-04	1.000E-04
Arb	6.497E+05	6.497E+05	3.185E+03	6.369E+04
H-3	0.000E+00	0.000E+00	0.000E+00	0.000E+00
	0.000E+00	0.000E+00	0.000E+00	0.000E+00
Arbitrary release rate (Ci/day)	0.000E+00	0.000E+00	0.000E+00	0.000E+00
Fractional Fission Yield	1.000E-04	1.000E-04	1.000E-04	1.000E-04

Original Number of Atoms in Region

Li-6	3.584E+21	9.986E+22	2.954E+22	4.352E+22
Li-7	4.472E+22	1.246E+24	3.685E+23	5.430E+23
FB-10	3.376E+23	1.693E+23	2.782E+24	4.099E+24
SB-10	3.376E+23	1.693E+23	2.782E+24	4.099E+24
C-12	7.666E+29	3.844E+29	6.317E+30	9.307E+30
Be-9	0.000E+00	0.000E+00	0.000E+00	0.000E+00
He-3	8.182E+21	4.093E+21	2.681E+20	7.670E+21
Fuel	0.000E+00	0.000E+00	0.000E+00	0.000E+00
Arb	0.000E+00	0.000E+00	0.000E+00	0.000E+00
H-3	0.000E+00	0.000E+00	0.000E+00	0.000E+00
	0.000E+00	0.000E+00	0.000E+00	0.000E+00

	REFLECTOR (OUTPER)	CORESUPPORT (STRUC)	CONTROL ROD (OPERA)
Weight (lbs)	3.2800E+05	2.2900E+05	7.4000E+03
Li Concentration (ppm)	2.000	2.000	0.000
Boron Concentration (ppm)	8.000	0.000	400000.000
Be Concentration (ppm)	0.000	0.000	0.000
Assigned Fast Flux (n/cm2.s)	1.000E+11	2.480E+13	2.480E+13
Assigned Slow Flux (n/cm2.s)	5.000E+09	6.800E+11	6.800E+11

Effective Full Power Reaction Rates (1/sec)

Li-6	2.038E-12	2.772E-10	2.772E-10
Li-7	7.180E-16	1.781E-13	1.781E-13
FB-10	1.352E-15	3.353E-13	3.353E-13
SB-10	8.153E-12	1.109E-09	1.109E-09
C-12	1.468E-17	3.641E-15	3.641E-15
Be-9	1.652E-15	4.097E-13	4.097E-13
He-3	1.140E-11	1.551E-09	1.551E-09
Fuel	1.000E-04	1.000E-04	1.000E-04
Arb	3.185E+03	4.331E+05	4.331E+05
H-3	0.000E+00	0.000E+00	0.000E+00
	0.000E+00	0.000E+00	0.000E+00
Arbitrary release rate (Ci/day)	0.000E+00	0.000E+00	0.000E+00
Fractional Fission Yield	1.000E-04	1.000E-04	1.000E-04

Original Number of Atoms in Region

Li-6	1.915E+24	1.337E+24	0.000E+00
Li-7	2.390E+25	1.669E+25	0.000E+00
FB-10	1.299E+25	0.000E+00	8.792E+27
SB-10	1.299E+25	0.000E+00	8.792E+27
C-12	7.374E+30	5.148E+30	9.982E+28
Be-9	0.000E+00	0.000E+00	0.000E+00
He-3	5.698E+20	2.079E+22	5.826E+20
Fuel	0.000E+00	0.000E+00	0.000E+00
Arb	0.000E+00	0.000E+00	0.000E+00
H-3	0.000E+00	0.000E+00	0.000E+00
	0.000E+00	0.000E+00	0.000E+00

600 MW(T)MHTGR TRITIUM ANALYSIS MYER'S ISOTHERM (TRITGO-V2)

During the period from 7 1 2009 to 1 1 2011 The power level was 0.90 and the purification plant efficiency was 1.00
The rate of permeation through the steam generator tubing was 2.3915E-07 sec-1

Cumulative tritium inventory in curies as of period end for production, and distribution sinks

Source -atoms	Tritium Production	Bound in Solids	Adsorbed on gr.surface	In primary Coolant	Leakage from Primary	Purif*n Plant	H2O in steam Generator	Blowdown+loss Steam generator
CORE (TOP)		Adsorption Ratio = 1.865E+07		Fraction of He-3(n,p)T recoils bound in solid = 0.40993				
Arb	**********	**********	**********	0.0000E+00	0.0000E+00	0.0000E+00	0.0000E+00	0.0000E+00	0.0000E+00
Fuel	1.0000E+00	2.1272E+03	1.4890E+03	6.3812E+02	3.4224E-05	4.9916E-06	3.7161E-02	9.1160E-06	2.7633E-04
He-3	2.5281E+22	1.3328E+01	5.4635E+00	7.8639E+00	4.2176E-07	6.1620E-08	4.5875E-04	1.1235E-07	3.4094E-06
FB-10	1.4991E+25	3.0214E+01	2.9912E+01	3.0212E-01	1.6204E-08	2.3989E-09	1.7859E-05	4.3188E-09	1.3220E-07
SB-10	1.4991E+25	5.8367E-01	5.7784E-01	5.8364E-03	3.1302E-10	3.8392E-11	2.8582E-07	8.2421E-11	2.2459E-09
Li-7	1.7798E+24	4.1128E-01	4.0717E-01	4.1127E-03	2.2057E-10	2.0557E-11	1.5304E-07	5.8235E-11	1.3364E-09
C-12	1.8457E+30	3.0234E-03	2.9931E-03	3.0232E-05	1.6214E-12	1.7620E-13	1.3118E-09	4.2167E-13	1.0715E-11
Be-9	6.4638E+23	2.3474E-03	2.3239E-03	2.3473E-05	1.2589E-12	6.2303E-14	4.6383E-10	3.2357E-13	4.3767E-12
Li-6	8.4179E+21	1.3433E+01	1.3298E+01	1.3432E-01	7.2039E-09	1.0546E-09	7.8511E-06	1.9192E-09	5.8316E-08
Region totals				6.4643E+02	3.4670E-05	5.0567E-06	3.7646E-02	9.2347E-06	2.7993E-04
CORE (MID)		Adsorption Ratio = 1.865E+07		Fraction of He-3(n,p)T recoils bound in solid = 0.42365				
Arb	**********	**********	**********	0.0000E+00	0.0000E+00	0.0000E+00	0.0000E+00	0.0000E+00	0.0000E+00
Fuel	1.0000E+00	2.8501E+03	1.9950E+03	8.5497E+02	4.5855E-05	6.6880E-06	4.9791E-02	1.2214E-05	3.7024E-04
He-3	2.7505E+22	1.4501E+01	6.1432E+00	8.3569E+00	4.4821E-07	6.5486E-08	4.8753E-04	1.1939E-07	3.6233E-06
FB-10	2.0086E+25	4.0482E+01	4.0077E+01	4.0479E-01	2.1711E-08	3.2141E-09	2.3929E-05	5.7866E-09	1.7713E-07
SB-10	2.0086E+25	7.8202E-01	7.7420E-01	7.8198E-03	4.1941E-10	5.1440E-11	3.8296E-07	1.1043E-10	3.0091E-09
Li-7	2.3847E+24	5.5105E-01	5.4554E-01	5.5103E-03	2.9554E-10	2.7544E-11	2.0506E-07	7.8027E-11	1.7906E-09
C-12	2.4730E+30	4.0508E-03	4.0103E-03	4.0506E-05	2.1725E-12	2.3608E-13	1.7576E-09	5.6497E-13	1.4357E-11
Be-9	8.6604E+23	3.1451E-03	3.1136E-03	3.1450E-05	1.6868E-12	8.3477E-14	6.2147E-10	4.3354E-13	5.8641E-12
Li-6	1.1279E+22	1.7998E+01	1.7818E+01	1.7996E-01	9.6522E-09	1.4130E-09	1.0519E-05	2.5714E-09	7.8135E-08
Region totals				8.6393E+02	4.6335E-05	6.7582E-06	5.0313E-02	1.2342E-05	3.7413E-04
CORE (Bot)		Adsorption Ratio = 1.863E+07		Fraction of He-3(n,p)T recoils bound in solid = 0.42903				
Arb	**********	**********	**********	0.0000E+00	0.0000E+00	0.0000E+00	0.0000E+00	0.0000E+00	0.0000E+00
Fuel	1.0000E+00	2.1272E+03	1.4890E+03	6.3812E+02	3.4259E-05	4.9967E-06	3.7199E-02	9.1253E-06	2.7661E-04
He-3	1.9106E+22	1.0072E+01	4.3213E+00	5.7506E+00	3.0874E-07	4.5108E-08	3.3582E-04	8.2241E-08	2.4958E-06
FB-10	1.4991E+25	3.0214E+01	2.9912E+01	3.0212E-01	1.6220E-08	2.4013E-09	1.7877E-05	4.3233E-09	1.3233E-07
SB-10	1.4991E+25	5.8367E-01	5.7784E-01	5.8364E-03	3.1334E-10	3.8431E-11	2.8611E-07	8.2505E-11	2.2482E-09
Li-7	1.7798E+24	4.1128E-01	4.0717E-01	4.1127E-03	2.2080E-10	2.0578E-11	1.5320E-07	5.8295E-11	1.3378E-09
C-12	1.8457E+30	3.0234E-03	2.9931E-03	3.0232E-05	1.6231E-12	1.7638E-13	1.3131E-09	4.2210E-13	1.0726E-11
Be-9	6.4638E+23	2.3474E-03	2.3239E-03	2.3473E-05	1.2602E-12	6.2367E-14	4.6431E-10	3.2390E-13	4.3812E-12
Li-6	8.4179E+21	1.3433E+01	1.3298E+01	1.3432E-01	7.2113E-09	1.0557E-09	7.8592E-06	1.9211E-09	5.8376E-08
Region totals				6.4432E+02	3.4592E-05	5.0453E-06	3.7561E-02	9.2140E-06	2.7930E-04

REFLECTOR (TOP) Adsorption Ratio = 0.000E+00 Fraction of He-3(n,p)T recoils bound in solid = 0.39754

Arb	**********	**********	**********	0.0000E+00	0.0000E+00	0.0000E+00	0.0000E+00	0.0000E+00	0.0000E+00
He-3	2.1441E+22	1.1303E+01	4.4936E+00	0.0000E+00	3.2638E-03	9.0937E-04	6.7701E+00	8.7905E-04	3.4696E-02
FB-10	4.8473E+23	9.8551E-01	9.7566E-01	0.0000E+00	4.4660E-06	1.3162E-06	9.7990E-03	1.2048E-06	4.9104E-05
SB-10	4.8473E+23	1.9038E-02	1.8847E-02	0.0000E+00	1.7436E-07	2.5414E-08	1.8920E-04	4.5878E-08	9.2772E-07
Li-7	1.3642E+23	8.8731E-02	8.7843E-02	0.0000E+00	4.9295E-07	1.1838E-07	8.8133E-04	1.3276E-07	5.2269E-06
C-12	1.2455E+30	2.0401E-03	2.0197E-03	0.0000E+00	2.8865E-08	2.7217E-09	2.0263E-05	7.4139E-09	9.9781E-08
Be-9	5.0869E+23	2.3760E-03	2.3522E-03	0.0000E+00	4.3050E-08	3.1533E-09	2.3476E-05	1.1321E-08	2.2657E-07
Li-6	5.6580E+21	9.0441E+00	8.9537E+00	0.0000E+00	4.2907E-05	1.2078E-05	8.9916E-02	1.1560E-05	4.5917E-04
Region totals				0.0000E+00	3.3119E-03	9.2292E-04	6.8709E+00	8.9202E-04	3.5210E-02

REFLECTOR (BOTTOM) Adsorption Ratio = 1.864E+07 Fraction of He-3(n,p)T recoils bound in solid = 0.41797

Arb	**********	**********	**********	0.0000E+00	0.0000E+00	0.0000E+00	0.0000E+00	0.0000E+00	0.0000E+00
He-3	8.0994E+21	4.2699E+00	1.7847E+00	2.4851E+00	1.3330E-07	1.9475E-08	1.4499E-04	3.5507E-08	1.0775E-06
FB-10	2.9836E+23	6.0661E-01	6.0054E-01	6.0657E-03	3.2535E-10	4.8384E-11	3.6021E-07	8.6727E-11	2.6627E-09
SB-10	2.9836E+23	1.1718E-02	1.1601E-02	1.1718E-04	6.2851E-12	7.7506E-13	5.7702E-09	1.6553E-12	4.5306E-11
Li-7	8.3971E+22	5.4616E-02	5.4070E-02	5.4613E-04	2.9293E-11	3.9195E-12	2.9180E-08	7.7869E-12	2.2301E-10
C-12	7.6662E+29	1.2558E-03	1.2432E-03	1.2557E-05	6.7353E-13	7.3191E-14	5.4489E-10	1.7516E-13	4.4511E-12
Be-9	3.1311E+23	1.4625E-03	1.4478E-03	1.4624E-05	7.8442E-13	3.8820E-14	2.8901E-10	2.0161E-13	2.7270E-12
Li-6	3.4826E+21	5.5669E+00	5.5112E+00	5.5666E-02	2.9858E-09	4.3757E-10	3.2576E-06	7.9545E-10	2.4189E-08
Region totals				2.5475E+00	1.3664E-07	1.9966E-08	1.4864E-04	3.6399E-08	1.1047E-06

FLOWDIST (PERMAN) Adsorption Ratio = 1.864E+07 Fraction of He-3(n,p)T recoils bound in solid = 0.41815

Arb	**********	**********	**********	0.0000E+00	0.0000E+00	0.0000E+00	0.0000E+00	0.0000E+00	0.0000E+00
He-3	4.0516E+21	2.1360E+00	8.9315E-01	1.2427E+00	6.6659E-08	9.7392E-09	7.2506E-05	1.7757E-08	5.3886E-07
FB-10	1.4693E+23	3.0141E-01	2.9839E-01	3.0139E-03	1.6166E-10	2.4151E-11	1.7980E-07	4.3098E-11	1.3272E-09
SB-10	1.4693E+23	5.8223E-03	5.7641E-03	5.8220E-05	3.1229E-12	3.8724E-13	2.8829E-09	8.2263E-13	2.2619E-11
Li-7	1.2683E+24	1.2721E+00	1.2594E+00	1.2720E-02	6.8230E-10	9.9278E-11	7.3910E-07	1.8173E-10	5.5000E-09
C-12	3.8444E+29	6.2972E-04	6.2342E-04	6.2969E-06	3.3776E-13	3.6703E-14	2.7325E-10	8.7836E-14	2.2321E-12
Be-9	1.7940E+23	9.7783E-04	9.6805E-04	9.7781E-06	5.2449E-13	2.5956E-14	1.9324E-10	1.3480E-13	1.8234E-12
Li-6	9.6388E+22	1.5469E+02	1.5315E+02	1.5468E+00	8.2971E-08	1.2175E-08	9.0639E-05	2.2105E-08	6.7275E-07
Region totals				2.8054E+00	1.5048E-07	2.2038E-08	1.6407E-04	4.0088E-08	1.2185E-06

REFLECTOR (INNER) Adsorption Ratio = 0.000E+00 Fraction of He-3(n,p)T recoils bound in solid = 0.68204

Arb	**********	**********	**********	0.0000E+00	0.0000E+00	0.0000E+00	0.0000E+00	0.0000E+00	0.0000E+00
He-3	2.6540E+20	1.3991E-01	9.5427E-02	0.0000E+00	2.1322E-05	5.9408E-06	4.4228E-02	5.7427E-06	2.2666E-04
FB-10	2.7805E+24	1.4266E-02	1.4124E-02	0.0000E+00	6.8676E-08	1.9051E-08	1.4183E-04	1.8495E-08	7.2849E-07
SB-10	2.7805E+24	1.3349E-06	1.3215E-06	0.0000E+00	1.2685E-11	1.7817E-12	1.3264E-08	3.3350E-12	6.6677E-11
Li-7	3.7024E+23	1.0049E-03	9.9490E-04	0.0000E+00	4.8436E-09	1.3420E-09	9.9906E-06	1.3044E-09	5.1371E-08
C-12	6.3173E+30	3.6638E-10	3.6272E-10	0.0000E+00	5.1890E-15	4.8878E-16	3.6389E-12	1.3326E-15	1.7921E-14
Be-9	6.9175E+21	4.2714E-10	4.2287E-10	0.0000E+00	7.7617E-15	5.6688E-16	4.2203E-12	2.0406E-15	4.0725E-14
Li-6	2.9533E+22	2.2839E-01	2.2611E-01	0.0000E+00	1.0997E-06	3.0498E-07	2.2705E-03	2.9615E-07	1.1664E-05
Region totals				0.0000E+00	2.2495E-05	6.2662E-06	4.6650E-02	6.0587E-06	2.3910E-04

REFLECTOR (OUTREP)			Adsorption Ratio = 0.000E+00	Fraction of He-3(n,p)T recoils bound in solid = 0.68388					
Arb	**********	**********	**********	0.0000E+00	0.0000E+00	0.0000E+00	0.0000E+00	0.0000E+00	0.0000E+00
He-3	7.5926E+21	4.0028E+00	2.7374E+00	0.0000E+00	6.0646E-04	1.6898E-04	1.2580E+00	1.6334E-04	6.4470E-03
FB-10	4.0495E+24	1.0447E+00	1.0343E+00	0.0000E+00	5.0010E-06	1.3951E-06	1.0386E-02	1.3470E-06	5.3226E-05
SB-10	4.0495E+24	1.9573E-03	1.9377E-03	0.0000E+00	1.8535E-08	2.6124E-09	1.9449E-05	4.8735E-09	9.7541E-08
Li-7	5.9251E+23	7.5465E-02	7.4710E-02	0.0000E+00	3.7004E-07	1.0076E-07	7.5016E-04	9.9656E-08	3.9245E-06
C-12	9.3074E+30	2.6966E-05	2.6696E-05	0.0000E+00	3.8203E-10	3.5975E-11	2.6782E-07	9.8112E-11	1.3188E-09
Be-9	5.0958E+23	3.1448E-05	3.1133E-05	0.0000E+00	5.7130E-10	4.1736E-11	3.1072E-07	1.5020E-10	2.9984E-09
Li-6	4.3388E+22	6.7199E+00	6.6527E+00	0.0000E+00	3.2310E-05	8.9735E-06	6.6806E-02	8.7018E-06	3.4298E-04
Region totals				0.0000E+00	6.4416E-04	1.7945E-04	1.3360E+00	1.7350E-04	6.8472E-03

REFLECTOR (OUTPER)			Adsorption Ratio = 0.000E+00	Fraction of He-3(n,p)T recoils bound in solid = 0.39442					
Arb	**********	**********	**********	0.0000E+00	0.0000E+00	0.0000E+00	0.0000E+00	0.0000E+00	0.0000E+00
He-3	5.6401E+20	2.9734E-01	1.1728E-01	0.0000E+00	8.6300E-05	2.4045E-05	1.7901E-01	2.3244E-05	9.1741E-04
FB-10	1.2981E+25	6.6607E-02	6.5941E-02	0.0000E+00	3.2062E-07	8.8945E-08	6.6217E-04	8.6347E-08	3.4011E-06
SB-10	1.2981E+25	6.2322E-06	6.1699E-06	0.0000E+00	5.9221E-11	8.3183E-12	6.1928E-08	1.5570E-11	3.1129E-10
Li-7	2.3908E+25	6.5108E-02	6.4457E-02	0.0000E+00	3.1354E-07	8.6943E-08	6.4727E-04	8.4439E-08	3.3254E-06
C-12	7.3740E+30	4.2766E-10	4.2338E-10	0.0000E+00	6.0569E-15	5.7053E-16	4.2475E-12	1.5555E-15	2.0918E-14
Be-9	9.2256E+21	6.6477E-10	6.5812E-10	0.0000E+00	1.2080E-14	8.8225E-16	6.5682E-12	3.1759E-15	6.3383E-14
Li-6	1.9151E+24	1.4810E+01	1.4662E+01	0.0000E+00	7.1310E-05	1.9777E-05	1.4724E-01	1.9204E-05	7.5634E-04
Region totals				0.0000E+00	1.5824E-04	4.3999E-05	3.2756E-01	4.2619E-05	1.6805E-03

CORESUPPORT (STRUC)			Adsorption Ratio = 1.864E+07	Fraction of He-3(n,p)T recoils bound in solid = 0.70837					
Arb	**********	**********	**********	0.0000E+00	0.0000E+00	0.0000E+00	0.0000E+00	0.0000E+00	0.0000E+00
He-3	2.0581E+22	1.0850E+01	7.6859E+00	3.1640E+00	1.6970E-07	2.4794E-08	1.8459E-04	4.5205E-08	1.3718E-06
FB-10	0.0000E+00	0.0000E+00	0.0000E+00	0.0000E+00	0.0000E+00	0.0000E+00	0.0000E+00	0.0000E+00	0.0000E+00
SB-10	0.0000E+00	0.0000E+00	0.0000E+00	0.0000E+00	0.0000E+00	0.0000E+00	0.0000E+00	0.0000E+00	0.0000E+00
Li-7	1.6685E+25	1.1272E+01	1.1159E+01	1.1271E-01	6.0453E-09	8.8172E-10	6.5642E-06	1.6103E-09	4.8811E-08
C-12	5.1483E+30	2.4890E-03	2.4641E-03	2.4889E-05	1.3349E-12	1.4504E-13	1.0798E-09	3.4714E-13	8.8212E-12
Be-9	1.5974E+24	3.8669E-03	3.8282E-03	3.8668E-05	2.0739E-12	1.0259E-13	7.6373E-10	5.3302E-13	7.2063E-12
Li-6	1.3061E+24	1.3894E+03	1.3756E+03	1.3894E+01	7.4518E-07	1.0912E-07	8.1241E-04	1.9852E-07	6.0336E-06
Region totals				1.7170E+01	9.2093E-07	1.3480E-07	1.0036E-03	2.4533E-07	7.4543E-06

CONTROL ROD (OPERA)			Adsorption Ratio = 0.000E+00	Fraction of He-3(n,p)T recoils bound in solid = 0.62760					
Arb	**********	**********	**********	0.0000E+00	0.0000E+00	0.0000E+00	0.0000E+00	0.0000E+00	0.0000E+00
He-3	5.7668E+20	3.0402E-01	1.9080E-01	0.0000E+00	5.4263E-05	1.5119E-05	1.1256E-01	1.4615E-05	5.7684E-04
FB-10	7.9991E+27	1.0658E+04	1.0551E+04	0.0000E+00	4.9000E-02	1.4234E-02	1.0597E+02	1.3211E-02	5.3230E-01
SB-10	7.9991E+27	1.3670E+02	1.3534E+02	0.0000E+00	1.2602E-03	1.8249E-04	1.3586E+00	3.3150E-04	6.6783E-03
Li-7	7.9276E+26	1.4286E+02	1.4143E+02	0.0000E+00	1.3175E-03	1.8976E-04	1.4127E+00	3.5482E-04	1.3961E-02
C-12	9.9818E+28	4.8258E-05	4.7776E-05	0.0000E+00	6.8311E-10	6.4380E-11	4.7930E-07	1.7545E-10	2.3602E-09
Be-9	3.0970E+22	7.4973E-05	7.4224E-05	0.0000E+00	1.3598E-09	9.9502E-11	7.4077E-07	3.5754E-10	7.1490E-09
Li-6	5.3646E+17	7.3220E-05	7.2488E-05	0.0000E+00	6.7137E-10	9.7262E-11	7.2410E-07	1.8086E-10	7.1568E-09
Region totals				0.0000E+00	5.1632E-02	1.4621E-02	1.0885E+02	1.3912E-02	5.5352E-01
Total curies				2.1772E+03	5.5885E-02	1.5791E-02	1.1756E+02	1.5057E-02	5.9844E-01
Average activity			**********	2.9316E+00	2.2005E-06	**********	**********	1.6398E-04	**********
of given region				uCi/g C	uCi/SCC He			uCi/g H2O	

600 MW(T)MHTGR TRITIUM ANALYSIS MYER'S ISOTHERM (TRITGO-V2)

During the period from 7 1 2057 to 1 1 2059 The power level was 0.90 and the purification plant efficiency was 1.00
The rate of permeation through the steam generator tubing was 2.3915E-07 sec-1

Cumulative tritium inventory in curies as of period end for production, and distribution sinks

Source -atoms	Tritium Production	Bound in Solids	Adsorbed on gr.surface	In primary Coolant	Leakage from Primary	Purif*n Plant	H2O in steam Generator	Blowdown+loss Steam generator
CORE (TOP)		Adsorption Ratio = 1.865E+07		Fraction of He-3(n,p)T recoils bound in solid = 0.40993				
Arb	**********	**********	**********	0.0000E+00	0.0000E+00	0.0000E+00	0.0000E+00	0.0000E+00	0.0000E+00
Fuel	1.0000E+00	1.2867E+04	9.0071E+03	3.8579E+03	2.0691E-04	3.0354E-04	2.2598E+00	5.5715E-05	2.2838E-02
He-3	2.4579E+22	7.8197E+01	3.2056E+01	4.6114E+01	2.4732E-06	3.6408E-06	2.7105E-02	6.6598E-07	2.7393E-04
FB-10	1.4528E+25	1.7429E+02	1.7255E+02	1.7419E+00	9.3423E-08	1.3737E-07	1.0227E-03	2.5158E-08	1.0335E-05
SB-10	1.4528E+25	3.3664E+00	3.3327E+00	3.3644E-02	1.8044E-09	2.6073E-09	1.9411E-05	4.8494E-10	1.9618E-07
Li-7	2.2430E+24	7.1487E+00	7.0773E+00	7.1446E-02	3.8318E-09	5.4943E-09	4.0904E-05	1.0318E-09	4.1346E-07
C-12	1.8457E+30	1.8281E-02	1.8098E-02	1.8270E-04	9.7987E-12	1.4010E-11	1.0430E-07	2.6283E-12	1.0542E-09
Be-9	8.6175E+23	5.3742E-02	5.3205E-02	5.3712E-04	2.8807E-11	4.0416E-11	3.0089E-07	7.7413E-12	3.0413E-09
Li-6	8.3651E+21	8.0375E+01	7.9571E+01	8.0327E-01	4.3081E-08	6.3233E-08	4.7076E-04	1.1601E-08	4.7576E-06
Region totals				3.9067E+03	2.0952E-04	3.0739E-04	2.2884E+00	5.6420E-05	2.3127E-02
CORE (MID)		Adsorption Ratio = 1.865E+07		Fraction of He-3(n,p)T recoils bound in solid = 0.42365				
Arb	**********	**********	**********	0.0000E+00	0.0000E+00	0.0000E+00	0.0000E+00	0.0000E+00	0.0000E+00
Fuel	1.0000E+00	1.7240E+04	1.2068E+04	5.1689E+03	2.7723E-04	4.0670E-04	3.0278E+00	7.4651E-05	3.0599E-02
He-3	2.6742E+22	8.5078E+01	3.6043E+01	4.9006E+01	2.6284E-06	3.8692E-06	2.8806E-02	7.0775E-07	2.9111E-04
FB-10	1.9465E+25	2.3352E+02	2.3119E+02	2.3339E+00	1.2517E-07	1.8405E-07	1.3702E-03	3.3709E-08	1.3847E-05
SB-10	1.9465E+25	4.5104E+00	4.4653E+00	4.5078E-02	2.4177E-09	3.4934E-09	2.6008E-05	6.4975E-10	2.6285E-07
Li-7	3.0052E+24	9.5781E+00	9.4823E+00	9.5726E-02	5.1341E-09	7.3616E-09	5.4805E-05	1.3825E-09	5.5397E-07
C-12	2.4730E+30	2.4493E-02	2.4248E-02	2.4479E-04	1.3129E-11	1.8771E-11	1.3975E-07	3.5216E-12	1.4124E-09
Be-9	1.1546E+24	7.2005E-02	7.1285E-02	7.1965E-04	3.8597E-11	5.4152E-11	4.0315E-07	1.0372E-11	4.0750E-09
Li-6	1.1208E+22	1.0769E+02	1.0661E+02	1.0762E+00	5.7723E-08	8.4724E-08	6.3075E-04	1.5544E-08	6.3745E-06
Region totals				5.2215E+03	2.8005E-04	4.1084E-04	3.0587E+00	7.5410E-05	3.0911E-02
CORE (Bot)		Adsorption Ratio = 1.863E+07		Fraction of He-3(n,p)T recoils bound in solid = 0.42903				
Arb	**********	**********	**********	0.0000E+00	0.0000E+00	0.0000E+00	0.0000E+00	0.0000E+00	0.0000E+00
Fuel	1.0000E+00	1.2867E+04	9.0071E+03	3.8579E+03	2.0712E-04	3.0385E-04	2.2621E+00	5.5773E-05	2.2861E-02
He-3	1.8575E+22	5.9096E+01	2.5354E+01	3.3722E+01	1.8105E-06	2.6652E-06	1.9842E-02	4.8751E-07	2.0052E-04
FB-10	1.4528E+25	1.7429E+02	1.7255E+02	1.7419E+00	9.3519E-08	1.3751E-07	1.0237E-03	2.5184E-08	1.0346E-05
SB-10	1.4528E+25	3.3664E+00	3.3327E+00	3.3644E-02	1.8063E-09	2.6100E-09	1.9431E-05	4.8544E-10	1.9638E-07
Li-7	2.2430E+24	7.1487E+00	7.0773E+00	7.1446E-02	3.8358E-09	5.4999E-09	4.0946E-05	1.0329E-09	4.1388E-07
C-12	1.8457E+30	1.8281E-02	1.8098E-02	1.8270E-04	9.8088E-12	1.4024E-11	1.0441E-07	2.6310E-12	1.0552E-09
Be-9	8.6175E+23	5.3742E-02	5.3205E-02	5.3712E-04	2.8837E-11	4.0458E-11	3.0120E-07	7.7492E-12	3.0445E-09
Li-6	8.3651E+21	8.0375E+01	7.9571E+01	8.0327E-01	4.3126E-08	6.3298E-08	4.7124E-04	1.1613E-08	4.7624E-06
Region totals				3.8943E+03	2.0907E-04	3.0672E-04	2.2835E+00	5.6299E-05	2.3077E-02

REFLECTOR (TOP) Adsorption Ratio = 0.000E+00 Fraction of He-3(n,p)T recoils bound in solid = 0.39754

Arb	**********	**********	**********	0.0000E+00	0.0000E+00	0.0000E+00	0.0000E+00	0.0000E+00	0.0000E+00
He-3	2.0846E+22	6.6320E+01	2.6365E+01	0.0000E+00	3.1732E-03	5.3121E-03	3.9548E+01	8.5457E-04	3.9771E-01
FB-10	4.2392E+23	5.1049E+00	5.0538E+00	0.0000E+00	3.9057E-06	6.7872E-06	5.0529E-02	1.0536E-06	5.0774E-04
SB-10	4.2392E+23	9.8598E-02	9.7612E-02	0.0000E+00	1.5249E-07	1.3108E-07	9.7587E-04	4.0123E-08	9.7863E-06
Li-7	1.9721E+23	1.0079E+00	9.9787E-01	0.0000E+00	8.1226E-07	1.3401E-06	9.9764E-03	2.1875E-07	1.0064E-04
C-12	1.2455E+30	1.2336E-02	1.2212E-02	0.0000E+00	2.8865E-08	1.6398E-08	1.2208E-04	7.4139E-09	1.2232E-06
Be-9	1.1624E+24	1.0692E-01	1.0585E-01	0.0000E+00	1.7240E-07	1.4213E-07	1.0581E-03	4.5336E-08	1.0677E-05
Li-6	5.5354E+21	5.3059E+01	5.2528E+01	0.0000E+00	4.1846E-05	7.0543E-05	5.2518E-01	1.1274E-05	5.2815E-03
Region totals				0.0000E+00	3.2201E-03	5.3911E-03	4.0136E+01	8.6721E-04	4.0363E-01

REFLECTOR (BOTTOM) Adsorption Ratio = 1.864E+07 Fraction of He-3(n,p)T recoils bound in solid = 0.41797

Arb	**********	**********	**********	0.0000E+00	0.0000E+00	0.0000E+00	0.0000E+00	0.0000E+00	0.0000E+00
He-3	7.8746E+21	2.5053E+01	1.0471E+01	1.4573E+01	7.8166E-07	1.1507E-06	8.5666E-03	2.1048E-07	8.6575E-05
FB-10	2.6093E+23	3.1422E+00	3.1108E+00	3.1403E-02	1.6844E-09	2.4957E-09	1.8580E-05	4.5360E-10	1.8777E-07
SB-10	2.6093E+23	6.0689E-02	6.0082E-02	6.0653E-04	3.2533E-11	4.7377E-11	3.5271E-07	8.7435E-12	3.5647E-09
Li-7	1.2139E+23	6.2041E-01	6.1421E-01	6.2006E-03	3.3259E-10	4.7513E-10	3.5373E-06	8.9555E-11	3.5751E-08
C-12	7.6662E+29	7.5928E-03	7.5169E-03	7.5884E-05	4.0703E-12	5.8196E-12	4.3326E-08	1.0918E-12	4.3789E-10
Be-9	7.1546E+23	6.5810E-02	6.5152E-02	6.5774E-04	3.5280E-11	4.7884E-11	3.5649E-07	9.4801E-12	3.6030E-09
Li-6	3.4071E+21	3.2659E+01	3.2332E+01	3.2640E-01	1.7507E-08	2.5722E-08	1.9149E-04	4.7143E-09	1.9352E-06
Region totals				1.4938E+01	8.0125E-07	1.1795E-06	8.7810E-03	2.1576E-07	8.8742E-05

FLOWDIST (PERMAN) Adsorption Ratio = 1.864E+07 Fraction of He-3(n,p)T recoils bound in solid = 0.41815

Arb	**********	**********	**********	0.0000E+00	0.0000E+00	0.0000E+00	0.0000E+00	0.0000E+00	0.0000E+00
He-3	3.9392E+21	1.2532E+01	5.2403E+00	7.2875E+00	3.9090E-07	5.7544E-07	4.2840E-03	1.0526E-07	4.3295E-05
FB-10	1.5208E+22	4.2816E-01	4.2388E-01	4.2776E-03	2.2944E-10	5.3937E-10	4.0155E-06	6.1861E-11	4.0599E-08
SB-10	1.5208E+22	8.2691E-03	8.1864E-03	8.2614E-05	4.4313E-12	1.0304E-11	7.6715E-08	1.1937E-12	7.7581E-10
Li-7	1.3995E+24	8.4603E+00	8.3757E+00	8.4553E-02	4.5353E-09	6.5424E-09	4.8707E-05	1.2212E-09	4.9223E-07
C-12	3.8444E+29	3.8075E-03	3.7695E-03	3.8053E-05	2.0411E-12	2.9184E-12	2.1727E-08	5.4750E-13	2.1959E-10
Be-9	3.0478E+24	2.6852E-01	2.6583E-01	2.6841E-03	1.4397E-10	1.4717E-10	1.0957E-06	3.8628E-11	1.1064E-08
Li-6	5.5803E+22	6.3319E+02	6.2686E+02	6.3277E+00	3.3941E-07	5.5951E-07	4.1654E-03	9.1426E-08	4.2104E-05
Region totals				1.3707E+01	7.3522E-07	1.1422E-06	8.5034E-03	1.9801E-07	8.5944E-05

REFLECTOR (INNER) Adsorption Ratio = 0.000E+00 Fraction of He-3(n,p)T recoils bound in solid = 0.68204

Arb	**********	**********	**********	0.0000E+00	0.0000E+00	0.0000E+00	0.0000E+00	0.0000E+00	0.0000E+00
He-3	2.5803E+20	8.2091E-01	5.5989E-01	0.0000E+00	2.0730E-05	3.4703E-05	2.5836E-01	5.5828E-06	2.5982E-03
FB-10	2.7783E+24	8.6221E-02	8.5359E-02	0.0000E+00	6.8623E-08	1.1463E-07	8.5343E-04	1.8481E-08	8.5840E-06
SB-10	2.7783E+24	8.0658E-06	7.9851E-06	0.0000E+00	1.2675E-11	1.0723E-11	7.9830E-08	3.3323E-12	8.0135E-10
Li-7	3.7241E+23	6.1190E-03	6.0578E-03	0.0000E+00	4.8721E-09	8.1355E-09	6.0567E-05	1.3121E-09	6.0922E-07
C-12	6.3173E+30	2.2147E-09	2.1926E-09	0.0000E+00	5.1890E-15	2.9441E-15	2.1918E-11	1.3326E-15	2.1961E-13
Be-9	1.5808E+22	1.9222E-08	1.9030E-08	0.0000E+00	3.1086E-14	2.5553E-14	1.9024E-10	8.1728E-15	1.9196E-12
Li-6	2.9527E+22	1.3812E+00	1.3674E+00	0.0000E+00	1.0995E-06	1.8364E-06	1.3671E-02	2.9609E-07	1.3751E-04
Region totals				0.0000E+00	2.1903E-05	3.6663E-05	2.7295E-01	5.8987E-06	2.7449E-03

REFLECTOR (OUTREP) Adsorption Ratio = 0.000E+00 Fraction of He-3(n,p)T recoils bound in solid = 0.68388

Arb	**********	**********	**********	0.0000E+00	0.0000E+00	0.0000E+00	0.0000E+00	0.0000E+00	0.0000E+00
He-3	7.3819E+21	2.3485E+01	1.6061E+01	0.0000E+00	5.8963E-04	9.8708E-04	7.3486E+00	1.5879E-04	7.3901E-02
FB-10	3.9878E+24	6.2113E+00	6.1492E+00	0.0000E+00	4.9248E-06	8.2582E-06	6.1480E-02	1.3265E-06	6.1833E-04
SB-10	3.9878E+24	1.1634E-02	1.1518E-02	0.0000E+00	1.8253E-08	1.5467E-08	1.1515E-04	4.7992E-09	1.1558E-06
Li-7	6.5420E+23	5.1415E-01	5.0901E-01	0.0000E+00	4.1078E-07	6.8357E-07	5.0891E-03	1.1063E-07	5.1222E-05
C-12	9.3074E+30	1.6305E-04	1.6142E-04	0.0000E+00	3.8203E-10	2.1674E-10	1.6136E-06	9.8112E-11	1.6167E-08
Be-9	1.1645E+24	1.4152E-03	1.4011E-03	0.0000E+00	2.2880E-09	1.8813E-09	1.4006E-05	6.0156E-10	1.4133E-07
Li-6	4.3232E+22	4.0480E+01	4.0076E+01	0.0000E+00	3.2193E-05	5.3820E-05	4.0068E-01	8.6700E-06	4.0300E-03
Region totals				0.0000E+00	6.2718E-04	1.0499E-03	7.8160E+00	1.6890E-04	7.8602E-02

REFLECTOR (OUTPER) Adsorption Ratio = 0.000E+00 Fraction of He-3(n,p)T recoils bound in solid = 0.39442

Arb	**********	**********	**********	0.0000E+00	0.0000E+00	0.0000E+00	0.0000E+00	0.0000E+00	0.0000E+00
He-3	5.4836E+20	1.7446E+00	6.8810E-01	0.0000E+00	8.3905E-05	1.4046E-04	1.0457E+00	2.2596E-05	1.0516E-02
FB-10	1.2838E+25	3.9967E-01	3.9568E-01	0.0000E+00	3.1708E-07	5.3138E-07	3.9560E-03	8.5392E-08	3.9789E-05
SB-10	1.2838E+25	3.7388E-05	3.7014E-05	0.0000E+00	5.8566E-11	4.9705E-11	3.7004E-07	1.5398E-11	3.7145E-09
Li-7	2.4052E+25	3.9555E-01	3.9160E-01	0.0000E+00	3.1543E-07	5.2590E-07	3.9152E-03	8.4946E-08	3.9381E-05
C-12	7.3740E+30	2.5852E-09	2.5593E-09	0.0000E+00	6.0569E-15	3.4366E-15	2.5584E-11	1.5555E-15	2.5634E-13
Be-9	1.5680E+23	1.8261E-07	1.8078E-07	0.0000E+00	3.9926E-13	2.4274E-13	1.8071E-09	1.0497E-13	1.8208E-11
Li-6	1.9098E+24	8.9408E+01	8.8514E+01	0.0000E+00	7.1112E-05	1.1887E-04	8.8497E-01	1.9151E-05	8.9012E-03
Region totals				0.0000E+00	1.5565E-04	2.6039E-04	1.9385E+00	4.1918E-05	1.9497E-02

CORESUPPORT (STRUC) Adsorption Ratio = 1.864E+07 Fraction of He-3(n,p)T recoils bound in solid = 0.70837

Arb	**********	**********	**********	0.0000E+00	0.0000E+00	0.0000E+00	0.0000E+00	0.0000E+00	0.0000E+00
He-3	2.0010E+22	6.3660E+01	4.5095E+01	1.8554E+01	9.9514E-07	1.4650E-06	1.0906E-02	2.6797E-07	1.1022E-04
FB-10	0.0000E+00	0.0000E+00	0.0000E+00	0.0000E+00	0.0000E+00	0.0000E+00	0.0000E+00	0.0000E+00	0.0000E+00
SB-10	0.0000E+00	0.0000E+00	0.0000E+00	0.0000E+00	0.0000E+00	0.0000E+00	0.0000E+00	0.0000E+00	0.0000E+00
Li-7	1.6681E+25	6.8172E+01	6.7491E+01	6.8132E-01	3.6542E-08	5.3610E-08	3.9912E-04	9.8399E-09	4.0335E-06
C-12	5.1483E+30	1.5050E-02	1.4899E-02	1.5041E-04	8.0670E-12	1.1534E-11	8.5868E-08	2.1638E-12	8.6786E-10
Be-9	2.7142E+25	1.0620E+00	1.0514E+00	1.0615E-02	5.6935E-10	5.8199E-10	4.3328E-06	1.5276E-10	4.3754E-08
Li-6	9.0214E+23	6.4462E+03	6.3817E+03	6.4420E+01	3.4551E-06	5.4848E-06	4.0833E-02	9.3060E-07	4.1272E-04
Region totals				8.3667E+01	4.4874E-06	7.0040E-06	5.2143E-02	1.2086E-06	5.2702E-04

CONTROL ROD (OPERA) Adsorption Ratio = 0.000E+00 Fraction of He-3(n,p)T recoils bound in solid = 0.62760

Arb	**********	**********	**********	0.0000E+00	0.0000E+00	0.0000E+00	0.0000E+00	0.0000E+00	0.0000E+00
He-3	5.6068E+20	1.7838E+00	1.1195E+00	0.0000E+00	5.2757E-05	8.8319E-05	6.5751E-01	1.4208E-05	6.6123E-03
FB-10	1.7635E+27	2.3404E+04	2.3170E+04	0.0000E+00	1.0802E-02	3.1120E-02	2.3168E+02	2.9124E-03	2.3098E+00
SB-10	1.7635E+27	3.0013E+02	2.9713E+02	0.0000E+00	2.7782E-04	3.9907E-04	2.9710E+00	7.3082E-05	2.9586E-02
Li-7	7.0254E+27	2.3189E+04	2.2957E+04	0.0000E+00	2.2575E-02	3.0829E-02	2.2951E+02	6.0797E-03	2.3197E+00
C-12	9.9818E+28	2.9179E-04	2.8887E-04	0.0000E+00	6.8311E-10	3.8788E-10	2.8877E-06	1.7545E-10	2.8933E-08
Be-9	5.2624E+23	2.0590E-02	2.0384E-02	0.0000E+00	4.4929E-08	2.7370E-08	2.0377E-04	1.1814E-08	2.0530E-06
Li-6	1.3720E+20	4.8293E-01	4.7810E-01	0.0000E+00	6.4915E-07	6.4201E-07	4.7796E-03	1.7487E-07	4.8259E-05
Region totals				0.0000E+00	3.3709E-02	6.2437E-02	4.6483E+02	9.0796E-03	4.6658E+00
Total curies				1.3135E+04	3.8439E-02	7.0209E-02	5.2269E+02	1.0353E-02	5.2481E+00

Average activity of given region	**********	1.7686E+01 uCi/g C	1.5135E-06 uCi/SCC He	**********	**********	1.1275E-04 uCi/g H2O	**********

GENERAL ATOMICS
P.O. BOX 85608 SAN DIEGO, CA 92186-5608 (858) 455-3000